Examination of the Effect of PEG-Rich Matrices in Multi Drug Resistance-Associated Protein (MRP) and Multi Drug Resistance (MDR) Substrates Transport Utilizing the CaCo-2 Cell Model

By

Nilmarie Santos-Román

Thesis submitted in partial fulfillment
of the requirements for the degree in

DOCTOR OF PHILOSOPHY
In
Chemical Engineering

UNIVERSITY OF PUERTO RICO
MAYAGÜEZ CAMPUS
2008

Approved by:

_____	_____
Madeline Torres-Lugo, PhD Chair, graduate committee	Date
_____	_____
Carlos M. Rinaldi, PhD Member, graduate committee	Date
_____	_____
David Suleiman Rosado, PhD Member, graduate committee Chair, Chemical Engineering Department	Date
_____	_____
Juan Lopéz-Garriga, PhD Member, graduate committee	Date
_____	_____
Vivian Navas, PhD Representative, graduate studies	Date

ABSTRACT

Multidrug resistance (MDR) is responsible for the low absorption of a very wide range of drugs and has been recognized as one of the major hurdles in drug absorption. Crosslinked poly(ethylene glycol) based morphologies are being proposed as multidrug resistance (MDR1) and multidrug resistance associated protein (MRP) inhibitors with the added advantage that these can be tailored for controlled drug delivery applications. For this purpose, three design variables were studied; the PEG tethered chain length, crosslinker length, and particle size. Results demonstrated that the length of the tethered chain has an important role on the properties of the hydrogel, specifically swelling ratio, correlation length, and diffusion mechanism. As the length of the tethered chain increased, the diffusion mechanism changed from almost Fickian to relaxation controlled. The hydrogels were considere not cytotoxic after appropriate wash protocol was established, thus cytotoxic effect can be dismissed. Also, the hydrogels demonstrated that they have MRP inhibitory effects by successfully enhancing the transport of fluorescein sodium salt (FLUO) up to 250%. The transport enhancement appears to be dependent on the hydrogel morphology as well (crosslinker and tethered chain length). Temperature effect experiments seem to confirm that this transport enhancement is due to an active interaction with the MRP proteins, since no effect was observed at 4°C. Polymers also demonstrated to have transport enhancement of the MDR1 substrate Rhodamine 123 (RHO) of up to 350%. This effect was found to be dependent on the length of the tethered chain as well as the concentration of the suspension. These observations suggest a possible competitive action. The potency of the hydrogel inhibition appears to be greater than the known inhibitors verapamil, genistein, and probenecid, but similar to the linear PEG-300 morphology. Contrary to the expected results a reduction in particle size did not produce an increase in transport enhancement, possibly due to direct interaction effects. Finally, no correlation was observed between membrane fluidity and transport enhancement, suggesting other mechanisms are present. Therefore, we can conclude that PEG based

hydrogels are potential candidates for controlled drug delivery devices that could be used in conjuntio with the inhibition of MRP and MDR1 proteins.

RESUMEN

La resistencia múltiple a medicamentos es responsable por la baja absorción de una amplia gama de medicamentos y esta reconocida como una de las barreras de absorción. Morfologías basadas en poli(glicol de etileno) (PEG) entrecruzado están siendo propuestas como inhibidores de las proteínas asociadas a la resistencia de medicamentos (MDR1 y MRP) con la ventaja adicional de que estas pueden ser diseñadas para aplicaciones de liberación controlada de medicamentos. Con este propósito, tres variables de control fueron estudiadas, el largo de las ramificaciones de PEG, el largo del entrecuzante y el tamaño de partículas. Los resultados demostraron que el largo de las ramificaciones tienen un rol importante en las propiedades de la gel hidrofílica, especialmente en la razón de hinchamiento, el largo de correlación, y el mecanismo de difusión. El mecanismo de difusión cambió de casi Fickiano a controlado por la relajación de las cadenas con un aumento en el largo de las ramificaciones. Las geles demonstraron no tener efecto cytotóxico luego de implantar el protocolo de lavado, por lo tanto los efectos cytotóxicos pueden ser descartados. También, las geles hidrofílicas demostraron tener propiedad inhibitorias de las proteínas MRP al aumentar el transporte de la sal de sodio de fluoresceína (FLUO) hasta 250%. Este aumento en transporte aparenta ser también función de la estructura del gel (largo de raminificaciones y de entrecruzante). Los experimentos de efectos de temperatura aparentan confirmar que este aumento en transporte es debido a una interacción interactiva, pues el efecto no fue observado a 4 ºC. Los polímeros también demostraron aumento en el transporte de Rhodamina 123, un substrato de MDR1, de hasta 350%. Los resultados demuestran que este efecto es función del largo de las ramificaciones y la concentración de las suspensiones. Estas observaciones sugieren una posible interacción competitiva. Al comparar los efectos de inhibición de estos polímeros con los inhibidores conocidos verapamil, genisteina, y probenecid, se encontró que los polímeros sobrepasan en potencia a estos inhibidores, pero similar a la morfología lineal de PEG-300. Contrario a los resultados esperados, reducir el

tamaño de partícula no resultó en un aumento en los efectos de inhibición. Finalmente, no se encontró una correlación en los efectos de fluidez de membrana y el aumento en transporte, sugiriendo que otros mecanismos están presentes. Por lo tanto, podemos concluir que geles hidrofílicas con base de poli(glicol de etileno) son posibles candidatos para liberación controlada de medicamentos y a la vez inhibir las proteínas de resistencia múltiple a medicamentos MDR1 y MRP.

To the Holy Spirit
The guide and the light in all
of our life journeys

To my family
To my husband Nelson
I could not have done this without your support.
To my daughters Alejandra and Isabel
All the sacrifices were proudly made for your behalf

Acknowledgments

This has been a long journey that has taken six years to complete. It would be unjust to say that this fruit lays on my shoulders alone. There have been numerous people that have helped in one way or another that deserve my most sincere thanks.

First and foremost I must thank my family, without your ongoing support this task would have never been completed. Nelson, you are the wind beneath my wings. Your ongoing support and your patience with me, my experiments, and my crazy schedule has made all this possible. There was never a doubt in your mind that I could do this and your emotional support was always there when most needed. It is such an honor to have such a wonderful husband and friend.

Alejandra and Isabel my two beautiful daughters, all this was done for you. Seeing you grow and the time we have spent together has validated that this decision was worth the effort. Just a smile from your lips gave me the strength to keep going. I just feel sorry that mommy has made you jump around so much, but you never complained. One day when you two are older, we will sit down and talk about this experience and maybe have a laugh.

Carmen y José (Mom and Dad), I cannot count the ways and the times you have given me your unwavering support. Whether it was helping me, the girls, or both you were always there to give a lending hand with no expectations. I would need more than one lifetime to pay you back all that you

have given me. José (broher), Jai (sister), Francisco y Héctor thanks for supporting me trough the distance.

Iris, Nelson padre, Viviana, Rafy, Thamara, Adita, Paco, Janet, Sory, Alejandro, Mariana, and Gabito, thanks. I sincerely think I am such a lucky girl for having such a wonderful second family, thank you for welcoming me. My daughters are blessed for being born into this beautiful family. Your support has been magnificent and most welcomed. Please accept my most sincere thanks.

Dr. Madeline Torres-Lugo, my thesis advisor, a much appreciated thanks. They say one of the most important decisions during your doctorate is the selection of your thesis advisor. I am glad to say that I have chosen an excellent one, my experience has been enriching. I hope we can continue our relationship for years to come. Dr. Carlos Rinaldi, Dr. Juan Lopéz-Garriga, Dr. Vivian Navas, Dr. David Suleiman, my thesis committee, thank you for your time and your support

Angelines, Celimar, Héctor, Janet, Magda, Margarita, Lorena, and Vanessa, my lab partners, we have gone through thick and thin in this journey together. Celimar and Hector we have seen the ups and downs of the lab together but you always helped me see the humor in things. Janet, thank you all your technical and emotional support. You have sincerely help me think like biologist. I can't thank you enough. Lorena, a special thanks. We have been through so much together, but we always came afloat trough each other's support. Your not only my lab partner, you are my friend. Adriana, Jimmy, and

David, my undergraduate students, thank you. It was your initial support that kept this work going. I cannot thank you enough.

Amayla, Irma, Griselle, Bismark, and Manuel my support team at UPR Río Piedras, thank you. It was most enriching working with such a diverse group of people. This has helped view the thesis with a different perspective. I learned so much from all of you and I most indebted. José Almodovar (Tito), Microscopy technician, thank you for all your help in setting up the FRAP experiments. Without your help this work would not have been completed.

Finally, I must thank all the institutions that have provided me financial support throughout the years, these are: National Institute of Health, Chemical Engineering Department, Merck Sharp and Dohme, Compañía de Fomento Industrial, IDeA Network of Biomedical Research Excellence, and Alliance for Graduate Education and the Professoriate. Without your support I could not have been able to continue as a graduate student.

Table of Contents

List of Tables

List of Figures

List of Appendixes

1. INTRODUCTION

Drug delivery is a complex feat where numerous factors must be taken into consideration. Some of these factors include patient compliance, comfort, drug absorption and disposition, and last but not least, economics. Each of these has their own set of issues that influence the decision-making related to a potential pharmaceutical product. This work focuses on one of the major hurdles encountered during drug absorption, drug resistance.

Classical approach attributed poor drug absorption to two main roadblocks. The first one is physico-chemical problems, for example poor solubility in the gastrointestinal fluids or inability to diffuse through the intestinal membrane. The second was first-pass hepatic metabolism (1). Recently, researchers have learned of a third roadblock, known as multidrug resistance (MDR). It can be defined as the efflux of drugs from the cell due to active interactions with an ATP-binding cassette (ABC) protein.

A wide span of drugs are affected by multidrug resistance (as illustrated in Table 1), therefore the phenomenon has an effect on a wide range of diseases as well. Among the MDR substrates one can find antibiotics, antifungals, antiarrhythmics, calcium channel blockers, chemotherapeutics, inmunosuppressants, and hormones to name a few. From these, for example, antiarrhythmics, calmodulin antagonists, and calcium channel blockers are used in the treatment of heart associated conditions. Heart disease is one of the most common afflictions, with 79.4 million Americans suffering from some

form of cardiovascular disease according the American Heart Association (2004 statistics). It is also the number one cause of death in United States (36.6% of all deaths). The use of multidrug inhibitors along with heart disease prescription can have a huge impact on the pharmaceutical industry, as well as in the lives of those affected by the disease. For example MDR inhibition can potentially improve drug absorption, which may result in a decrease in the amount of the active ingredient in a given formulation. This in turn would have the effect of lowering treatment cost and reduce potential drug side effects. The economic factor should not be taken lightly since in 2002 Americans spent $12 billion on prescription drugs to treat high blood pressure. Finally, these are lifelong treatments, meaning that the cost reductions will affect us for years to come.

Secondly, multidrug resistance affects cancer treatment as well. Cancer is the second leading cause of death in America causing 22.9% of all deaths. The impact of MDR on cancer is heightened by the fact that cancer tumors tend to overexpress these proteins, either intrinsically, or induced by treatment (2, 3). This is especially true in remission cases, in which chemotherapy is most likely to fail unless combined with some other type of treatment. Also, the economic factor of cancer therapy should not be disregarded, due to the monumental costs of these treatments. Finally, the possibility of reducing the side effects of chemotherapy could have huge impacts on patient compliance due to devastating side effects of the treatments, which include hair loss,

nausea and vomiting, fatigue, an increased chance of bruising and bleeding and getting an infection.

Antibiotics also merit our attention. Due to the increased use of antibiotics by consumers, more and more bacteria are becoming resistant to these treatments. Therefore, new and stronger antibiotics must be developed routinely. According to the US Food and Drug Administration an increasing number of diseases have become resistant to antibiotic treatment including tuberculosis, gonorrhea, malaria, and childhood ear infections. Also, about 70% of the bacteria that causes infections in hospitals are resistant to at least one of the most commonly used antibiotics used to treat them. Some are resistant to all approved drugs and must be treated with experimental and potentially harmful drugs. The problem has become aggravated by the indiscriminate use of antibiotics by most patients. Even though antibiotics are only useful for bacterial infections, most patient still request antibiotic prescriptions for mostly viral infections such as the cold and flu. Doctors oblige, against their common sense, to keep the clientele content. Also, not using the antibiotic treatment as prescribed may add to the problem. It is of outmost importance that the patient takes the full dose regimen.

Recently, it has been observed that cells that have been in contact with linear morphologies of poly(ethylene glycol) (PEG) based polymers have exhibited an enhanced drug transport for known multidrug resistance associated protein (MRP) and multidrug resitance (MDR) substrates. Poly(ethylene glycol) (PEG) is a linear or branched neutral polymer. This

polymer has been widely used in a variety of biological applications for its unique properties, for example non-immunogenicity, nonantigenicity, and non-toxicicity (4, 5). Its use has been reported in topical, ophthalmic, oral and rectal pharmaceutical formulations (6). Several morphologies have been proven to enhance transport of P-glycoprotein (P-gp) (also known as MDR1) substrates such as pluronic block copolymers, linear PEG of several chain lengths, PMAA-g-PEG hydrogels, co-polymers containing PEG in their structure, and several polyethoxylated surfactants (7-12)

However, at this point the effect of crosslinked PEG hydrogels and their role in multidrug resistance has not been studied. The advantage of using crosslinked morphologies is that they can be used to design controlled drug delivery devices. Controlled drug delivery in turn can be defined as a system that delivers an active ingredient in a controlled fashion for an extended period of time or might localize or target drug action. The scenarios in which controlled drug delivery can be used are numerous. For example, bulk hydrogels containing the active ingredient can be located near a tumor to provide treatment for cancer. This setup provides localization of the chemotherapeutic agent, thus reducing dosage and adverse effects. It goes without saying that it also improves the patient quality of life. Another scenario can be the use of hydrogels for targeted oral delivery in oral formulations. If used in conjunction with an anionic monomer, like methacrylic acid, the hydrogel could be used to protect the active ingredient from the harsh pH of the stomach releasing the drug in the more benign pH of the small intestine. These

are just two examples of how controlled drug delivery can be used in conjunction with MDR/MRP inhibition to improve drug administration.

In order to design such devices, the first order of action is to understand the design variables and how they affect drug release and inhibition of both MDR and MRP proteins. This work focuses on understanding such details. For these purposes, PEG hydrogels were characterized for important drug delivery properties such as swelling, correlation length, partition coefficient and release profile of a model molecule. The colon adenocarcinoma cell line Caco-2 was used to study the cytotoxic effects of hydrogels, transport enhancement effects of known MDR and MRP substrates and inhibitors, and membrane fluidity effects.

Table 1.1: Partial list of multidrug resistance (MDR) and multidrug resistance-associated protein (MRP) substrates (13).

Pharmacological category	Examples
Antiarrhythmic	Amiodearone, lidocaine, quinidine
Antibiotics and antifungals	Cefoperazone, cefriazone, erythromycin, itraconazole, ketoconozole, aureobasidin A
Antimalaria and antiparasites	Chloroquine, emetine, hydroxychloroquine, quinacrine, quinine
Calcium channel blockers	Bepridil, diltriazem, felodipine, nifedipine, nisoldipine, nitredipine, tiapamil, verapamil
Calmodulin antagonist	Chlorpromazine, trifluoperazine
Cancer Chemotherapeutics	Actinomycin D, colchicines, daunorubicin, doxorubicin, etoposide, mitomycin C, mithramycin, podophyllotoxin, puromycin, taxol, toptecan, treamterene, vinblastine, vincristine
Fluorescent dyes	BCECF-AM, Fluro-2, Fura-2, Rhodamine 123, Hoechst 33342
HIV protease inhibitors	Ininavir, nelfinavir, ritonavir, saquinavir
Hormones	Aldosterone, clomiphene, cortisol, deoxycorticosterone, dexamethosone, predinisone, progesterone analogs, tamoxifen, hydrocortisone, testoterone
Immunosuppressants	Cyclosporin A, cyclosporin H, tacrolimus, sirolimus
Indole alkaloids	Reserpine, yohimbine
Local anaesthetics	Bupivacaine
Surfactants/solvents	Cremophor-EL, triton X-100, Tween 80
Toxic peptides	N-Acetyl-leucyl-leucinal, gramicidine D, Valinomycin
Tricyclic antidepressants	Desipramine, trazadone
Miscellaneous	Components of grape and citrus fruit juice, ethidium bromide, GF 120918, ivermectin, MS-209, liposomes, LY335979, quercetin, SDZ 833 (valspodar), terfindine, tumor necrosis factor, Vitamin A

1.1 References

1 L. Z. Benet, Cummins, C. L., "The drug efflux-metabolism: biochemical aspects," *Advanced Drug Delivery Reviews*, vol. 50, pp. 3-11, 2001.

2 J. H. Goldie, "Drug resistance in cancer: A perspective," *Cancer Metastasis Reviews*, vol. 20, 2001.

3 R. Krishna and L. D. Mayer, "Multidrug resistance (MDR) in cancer Mechanisms, reversal using modulators of MDR and the role of MDR modulators in influencing the pharmacokinetiscs of anticancer drugs," *European Journal of Pharmaceutical Sciences*, vol. 11, pp. 265-283, 2000.

4 J. M. Harris, *Poly(ethylene glycol) Chemistry. Topics in Applied Chemistry*: New York Plenum Press, 1992.

5 J. M. Harris, Zalipsky, S., *Poly(ethylene glycol) Chemistry and Biological Applications.*, vol. 680. Washington, DC: American Chemical Society, 1997.

6 R. C. Rowe, P. J. Sheskey, and S. C. Owen, *Handbook of Pharmaceutical Excipients*, Fifth Edition ed. London: Pharmaceutical Press and American Pharmacist Association, 2006.

7 E. Batrakova, S. Li, W. Elmquist, D. Miller, V. Alakhov, and A. Kabanov, "Mechanism of sensitization of MDR cancer cells by Pluronic block copolymers: Selective energy depletion," *British Journal of Cancer*, vol. 85, pp. 1987–1997, 2001.

8 E. D. Hugger, Novak, B. L., Burton, P. S., Audus, K. L., Borchardt, R. T., "A Comparison of Commonly Used Polyethoxylated Pharmaceutical Excipients on Their Ability to Inhibit P-glycoprotein Activity In Vitro.," *Journal of Pharmaceutical Science*, vol. 91, pp. 1991-2002, 2002.

9 M. Torres-Lugo, "Physicochemical Behavior and Cellular Interactions of Novel Oral Calcitocin Delivery Systems," in *Chemical Engineering Department*, vol. PhD. West Lafayette, IN: Purdue University, 2001.

10 B. M. Johnson, W. N. Charman, and C. J. H. Porter, "An In Vitro Examination of the Impact of Polyethylene Glycol 400, Pluronic P85, and Vitamin E d-a-Tocopheryl Polyethylene Glycol 1000 Succinate on PGlycoprotein Efflux and Enterocyte-Based Metabolism in Excised Rat Intestine," *AAPS PharmSci*, vol. 4, pp. 1-13, 2002.

11 S. W. Wang, J. Monagle, C. McNulty, D. Putnam, and H. Chen, "Determination of P-glycoprotein Inhibition Excipients and Their Combinations Using an Integrated High-Throughput Process," *Journal of Pharmaceutical Sciences*, vol. 93, pp. 2755-2767, 2004.

12 E. S. Lee, K. Naa, and Y. H. Baea, "Doxorubicin loaded pH-sensitive polymeric micelles for reversal of resistant MCF-7 tumor," *Journal of Controlled Release*, vol. 103, pp. 405–418, 2005.

13 M. V. S. Varma, Y. Ashokraj, C. S. Dey, and R. Panchagnula, "P-glycoprotein inhibitors and their screening: a perspective from

bioavailability enhancement," *Pharmaceutical Research*, vol. 48, pp. 347-359, 2003.

2. BACKGROUND

2.1 Multidrug Resistance Structure, Location and Expression

The multidrug resistance (MDR) phenomenon was first discovered in the 1970's. During the late 1980's and early 1990's the scientific community recognized its protagonist role in drug disposition (1, 2). Since then, numerous publications have emerged on the subject. MDR is defined as the active efflux of a molecule by interaction with a member of the ATP-binding cassette (ABC) protein superfamily. The ABC is a group of proteins consisting of transporters, ion channels and receptors. They are further subdivided into subfamilies according to general sequence and structural homology of the proteins (3). To date, more than 100 ABC transporters have been identified between prokaryotes and human (4). In humans alone, 48 ABC genes have been identified, the function and expression of these genes are summarized in table 2.1. Due to the ubiquitous nature of these proteins, they are associated with the cell natural defense mechanism against potentially harmful xenobiotics (1).

The first of these proteins to be discovered was the p-glycoprotein also known as P-gp, MDR1 or ABCB1. It is a 170-180 kDa integral protein and a member of the MDR/TAP (the transporter associated with antigen processing) subfamily. It is glycosylated at the first extracellular loop (4). P-gp is comprised of 1280 amino acids divided in 12 transmembrane (TM) domains that are arranged in α-helix configurations (1, 2). The TM's domains are separated in two homologous parts, which are joined by a nucleotide-binding domain (NBD)

located in the cytoplasm, as depicted in figure 2.1. As all MDR proteins, Pgp has an ATP-binding region that consists roughly of 90-100 amino acids. This region includes a Walker A and B motif, a linker or dodecapeptide region (also known as Walker C) which is located between the two Walker motifs and some homologous regions upstream and downstream as depicted in figure 2.2 (5). Other members of the MDR/TAP subfamily include MDR3 (ABCB4), the bile salt export pump (BSEP, or Sister Pgp (SPgp)), 1 (TAP1) and TAP2 (3).

Numerous attempts have been made to find a common denominator between the P-gp substrates. At first the P-gp substrates were described as hydrophobic, amphiphatic molecules with a planar ring system with a molecular weight higher than 400 g/mol and a positive charge at pH 7.4 (1). Substrates include chemotherapeutic drugs, antibiotics, antivirals, calcium channel blockers as well as plant chemicals (3, 6). However, not all P-gp substrates conform to this description. For example, digoxin is neutral, atorvastine is negatively charged, and methotrexate is hydrophilic. A study done by Seeling (7) utilizing a statistical analysis for over one hundred compounds known to interact with P-gp helps in filling that gap. The recognition elements where divided in two, one consisting of two electron donor groups with a spatial separation of 2.5 ± 0.3 Å and the second of three electron donor groups with a spatial separation of 4.6 ± 0.6 Å. Furthermore, the binding to P-gp increases with the strength and concentration of the electron donor groups. Interestingly, a high percentage of amino acids with hydrogen donor capabilities has been found in the transmembrane domains relevant to substrate recognition (7). The

substrates of the MRPs are usually organic anions (8). Finally the substrate specifity of breast cancer reistance protein (BCRP) is similar to that of P-gp (2).

P-gp is expressed in numerous tissues including intestine, liver, kidney, and blood brain barrier (2, 3). It is localized in the apical side of the cell or mucosa, as depicted in figure 2.3 (3, 9). Due to this location, its role is attributed to efflux of xenobiotics into the intestinal lumen, bile, urine and blood (3).

The multidrug resistance associated proteins (MRP) are other members of the ABC's family known as the MRP/CFTR subfamily. Its members include MRP1, MRP2, MRP3, MRP4, MRP5, MRP6, MRP7, MRP8, MRP9, the cystic fibrosis transmembrane conductance regulator (CFTR), and the sulfonylurea receptors 1 and 2 (SUR1 and SUR2) (3). It is a 190 kDa integral protein comprised of 1531 amino acids; which posses only 15% homology with P-gp (2). There are two major differences between the MRPs and the MDRs. The first being the deletion of 13 amino acids located between the Walker A and B motif of the NBD1. This deletion alters the spacing between the Walker A and B motif and may affect the folding and activity of this domain (8). The second difference is that they are usually larger than other ABC transporters (10). Most of them have 5 extra TM domanis on the N-terminus as for example MRP1, MRP2, MRP3, MRP6 and MRP7. Others lack these extra TMs domains, making their structure more similar to that of P-gp; including MRP 4, MRP5 and MRP8, as depicted in figure 1 (3, 10).

Table 2.1: Function, expression and gene locus of ATP binding cassette (ABC) transporters (3, 10-12)

Gene	Alias	Gene locus	Expression	Function
ABCBA1	ABC1, TGD, HGLDT 1, CERP	9q31.1	Ubiquitous	Cholesterol efflux onto high density lipoprotein
ABCBA2	ABC2	9q34	Brain	Drug resistance
ABCBA3	ABC3, ABCC	16p13.3	Lung	
ABCBA4	ABC10 , ABCR, STGD1 , RT19, FFM	1p22.1-p21	Rod photorecepto rs	N-retinylidiene-phosphatidylethanolamine efflux
ABCBA5	ABC13	17q24	Muscle, heart, testis	
ABCBA6		17q24	Liver	
ABCBA7	ABCX	19p13.3	Spleen, thymus	
ABCBA8		17q24	Ovary	
ABCBA9		17q24	Heart	
ABCBA10		17q24	Muscle, heart	
ABCBA12		2q34	Stomach	
ABCBA13		7p11-q11	Low in all tissues	
ABCB1	ABCB2 0, MDR1, PGY1, Pgp, P-170	7p21	Adrenal, kidney, brain	Multidrug resistance
ABCB2	ABC17 , TAP1, PSF1, RING4	6p21	Ubiquitous	Peptide Transport
ABCB3	ABC18i , TAP2, PSF1, RING1 1	6p21	Ubiquitous	Peptide Transport
ABCB4	ABC21 , MDR2	7q21.1	Liver	Phosphatidylcholine transport

	(MDR3), PGY3, PFIC3			
ABCB5	ABC19	7p14	Ubiquitous	
ABCB6	ABC14, MTABC3	2q36	Mitochondria	Iron transport
ABCB7	ABC7, ATM1P	Xq12-q13	Mitochondria	Fe/S cluster transport
ABCB8	ABC22, MABC1	7q36	Mitochondria	
ABCB9	ABC23	12q24	Hear, brain	
ABCB10	MTABC2	1q42	Mitochondria	
ABCB11	ABC16, SPgp, BSEP, PGY4	2q24	Liver	Bile salts transport
ABCC1	ABC29, MRP1, GS-X	16p13.1	Intestine, brain, kidney, lung, testis	Drug resistance
ABCC2	ABC30, MRP2, cMOAT, cMRP	10q24	Liver, intestine and kidney tubules	Organic anion efflux
ABCC3	ABC31, MRP3, cMOAT2, MOATD, MLP2	17q21.3	Liver, intestine, lung	Drug resistance
ABCC4	ABC32 MRP4, MOAT-B	13q32	Prostate	Nucleosid transport
ABCC5	ABC33, MRP5, MOATC, pABC1	16p13.1	Ubiquitous	Nucleosid transport

	1			
ABCC6	ABC34, MRP6, MOATE, MLP1, ARA	7q31.1	Kidney, liver	
CFTR	ABC35, ABCC7	7q31.2	Exocrine tissues	Choride ion trasport
ABCC8	ABC36, SUR1, MRP8, PHHI, HI, HRINS	11p15.1	Pancreas	Sulfonyl urea receptor
ABCC9	ABC37, SUR2	12p12.1	Heart Muscle	
ABCC10	ABC26, MRP7	6p21	Low in all tissues	
ABCC11		16q11q12	Low in all tissues	
ABCC12		16q11q12	Low in all tissues	
ABCD1	ABC42, ALD, ALDP, AMN	Xq28	Peroxisomes	Very long chain fatty acid transport
ABCD2	ABC39, ALDL1, ALDR, ALDRP	12q11-q12	Peroxisomes	
ABCD3	ABC43, PXMP1, PMP70	1p22-p21	Peroxisomes	
ABCD4	ABC41, PMP1L, PMP69, P70R	14q24.3	Peroxisomes	
ABCE1	ABC38, OABP,	4q31	Ovary, testis, spleen	Oligoadenylate binding protein

	RNS41, RL1, RNAse LI			
ABCF1	ABC50	6p21.33	Ubiquitous	
ABCF2	ABC28	7q36	Ubiquitous	
ABCF3	ABC25	3q25	Ubiquitous	
ABCG1	ABC8, White	21q22.3	Ubiquitous	Cholesterol transport?
ABCG2	ABCP, BCRP, MXR	4q22	Placenta, intestine	Toxin efflux, drug resistance
ABCG4	ABC15, BCRP1, MXR1, ABCP1, White 2	11q23	Liver	
ABCG5	White 3	2p21	Liver, intestine	Sterol transport
ABCG8		2p21	Liver, intestine	Sterol transport

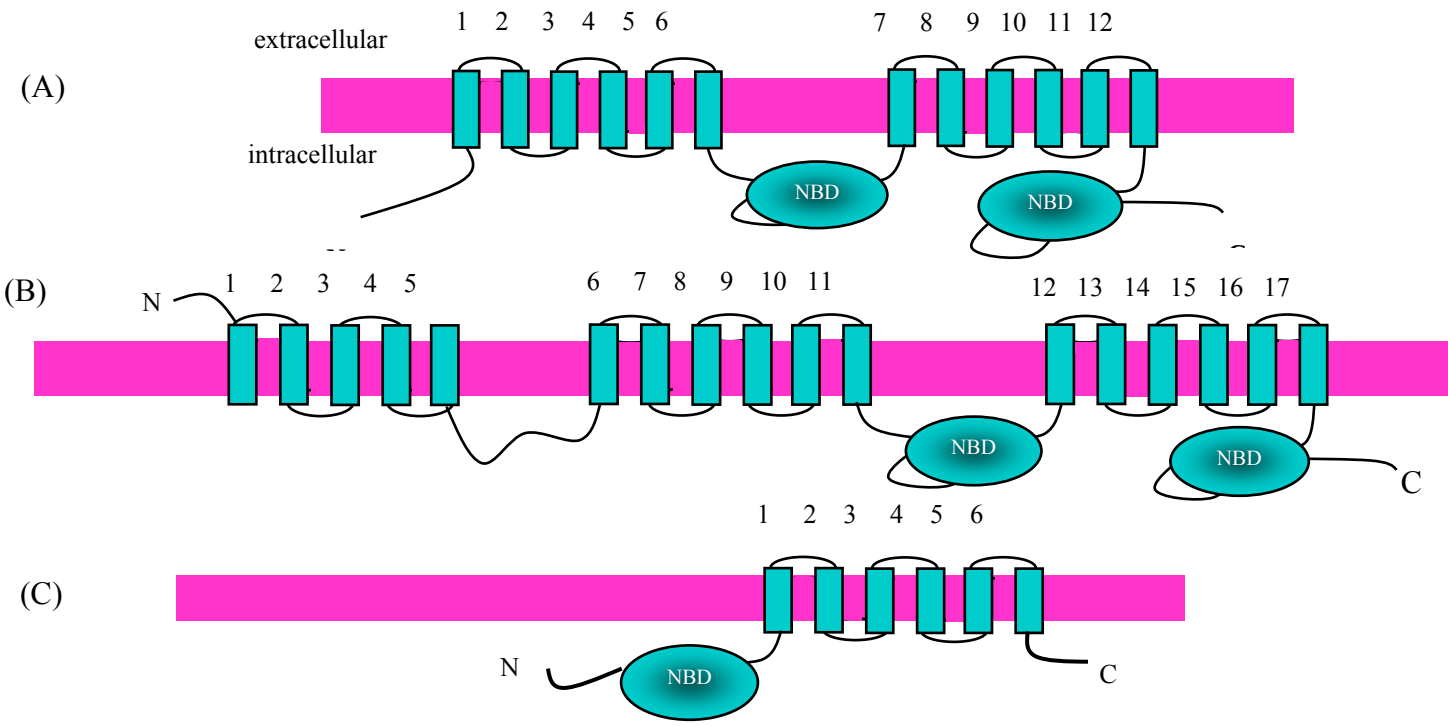

Figure 2.1: Multi drug resistance (MDR) and multi drug resistance associated protein structures (MRP) (A) MDR1, MDR3, bile salt export pump (BSEP) (siter P-gp (SPgp)), MRP 4-5 & 8, (B) MRP1-3, MRP 6-7, (C) breast cancer resistance protein (BCRP) (mitoxantrone resistance protein (MXR)). NBD denotes nucleotide binding domain (3, 13)

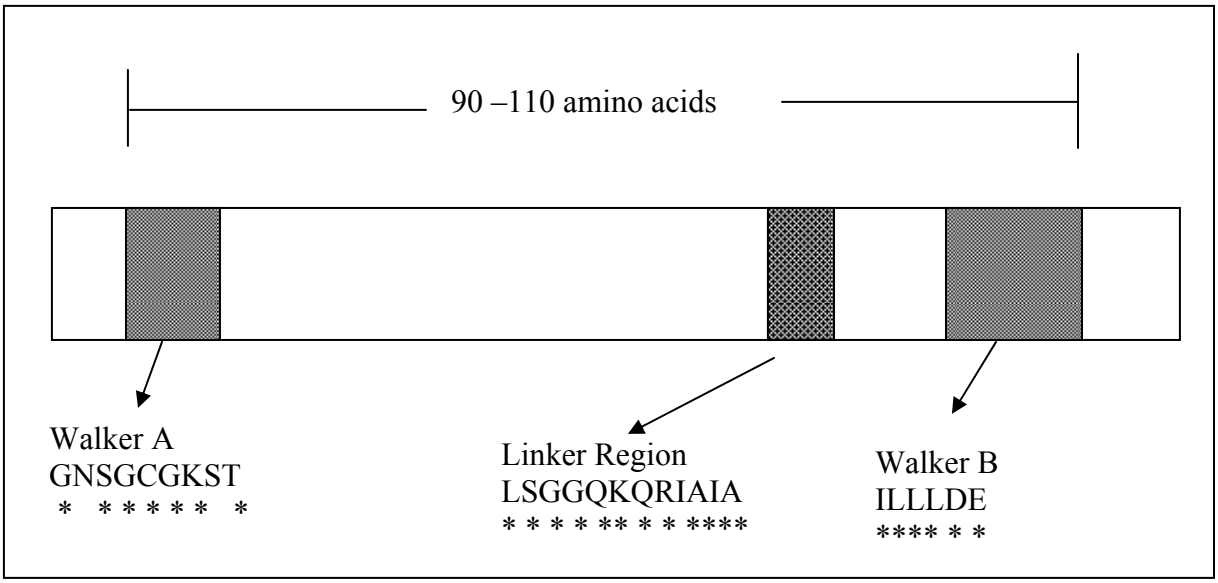

Figure 2.2: Schematic representation of the ATP-binding region. The most conserved amino acids of each region are written in the lower part using the protein single code (5).

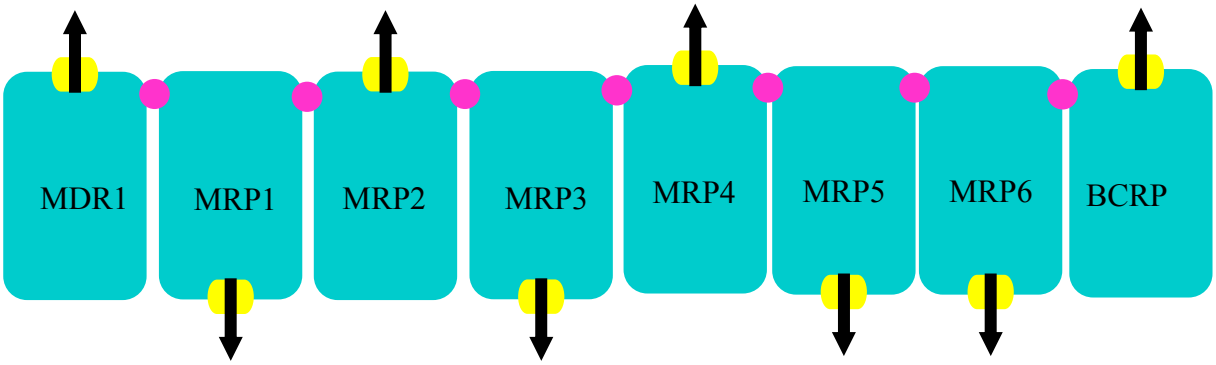

Figure 2.3: Cellular location of multidrug resistance 1 (MDR1), Multidrug resistance associated proteins 1-6 (MRP1-6) and breast cancer resistance protein (BCRP) (3, 9)

These proteins only have less than 40% homology to MRP1 (2). However, they show more homology to other members of the MRP/CFTR subfamily than to P-gp. More importantly, the extra TM domain is not required for transport activity (10).

The substrate specificity of MRP is not well defined, it has been attributed to organic anions (2). MRP1, MRP3, MRP5 and MRP6 are located in the basolateral side of the cell (or lumen) (3, 9, 14). The ubiquitous expression of MRP1 and its localization on the basolateral membrane suggests that it contributes to the organism defense by extruding the xenobiotics into the blood (3). MRP2 and MRP 4 are located on the apical side of cell (3, 9, 14). Due to its expression in the liver and its location in the apical membrane MRP2, is thought to have a detoxification role by transporting the substrates into the bile. The expression and substrate interaction of these proteins are summarized in Table 2.1.

Finally, the breast cancer resistance protein (BCRP) belongs to the ABC subfamily known as White (3). It is also known as mitoxantrone resistance protein (MXR) (2, 3). BCRP is a 72.1 kDa integral protein comprised of 655 amino acids (2, 15). It is considered a half transporter because it has only one TM domain and one nucleotide binding domain in the N-terminus as depicted in figure 1 (2, 3). The substrate specificity of BCRP resembles that of P-gp but with different efficiency (2). It is expressed in numerous tissues and it is located in the apical side of the cell membrane as its homologous P-gp.

2.2 Multidrug Resistance: Mechanism of Action

The mechanism of action of the efflux proteins is not yet well understood. There are three main models that explain the function of the proteins to a certain extent: 1) pore model, 2) flippase model, and 3) hydrophobic vacuum cleaner (HVC) model (refer to figure 4). In the pore model, the drugs associated with P-gp in the cytoplasm are transported out of the cell through a protein channel. In the flippase model, the drugs are embedded in the inner leaflet of the cell bilayer membrane. They bind to P-gp within the membrane. Finally, they are "flipped" to the outer leaflet from which they passively diffuse into the extracellular fluid. Last, the HVC model is a combination of the previous two.

This last model has been the best received within the scientific community (6). A recent publication by Rosenberg (16), supports the HVC model. Electron crystallography data showed that in the absence of adenosine triphosphate (ATP) the two transmembrane domains form a single barrel 5-6 nm in diameter and approximately 5nm deep with a central pore that is open to the extracellular surface covering most of the membrane depth. After ATP binding, the transmembrane domains then form three domains, each of 2-3 nm in diameter and 5-6 nm deep. The central pore opens and could allow access to drugs from the lipid bilayer to the central pore of the ABC transporter protein (6). Further evidence which supports the HVC model lies in the fact that biochemical data supports that the drug binds at the transmembrane domains TM4, TM5, TM6, TM10, TM11, and TM12 (2, 17, 18).

Other evidence that seems to support the HVC model, has to do with the relationship between the plasma membrane and the P-gp substrates. First of all, P-gp substrates are able to partition into the cell membrane (19). This piece of data correlates well with the fact that the drug-binding sites appear to be within the TM's domains. There is also evidence that supports that P-gp structure and function is very dependent on its lipid environment, further suggesting that the efflux process occurs in the lipid phase.

Also, it is important to note that the multidrug resistance phenomenon is considered an active transport, especially due to its ability to transport substrates against a concentration gradient. Therefore, energy in the form of adenosine tri-phosphate (ATP) is consumed during the efflux process. One molecule is effluxed at the expense of two molecules of ATP. The catalytic process can be summarized as follows. The drug and the nucleotide (ATP) bind at their particular domains. Then, ATP hydrolyses to Adenosine di-phosphate (ADP) and gives the necessary energy to efflux the drug. The ADP is released from the binding site and the first catalytic cycle is completed. Then, a conformational change reduces the affinity for the substrate and the nucleotide. The second catalytic cycles starts with the hydrolysis of a second ATP molecule. The energy released is used to reorient the protein into its native form (2, 6).

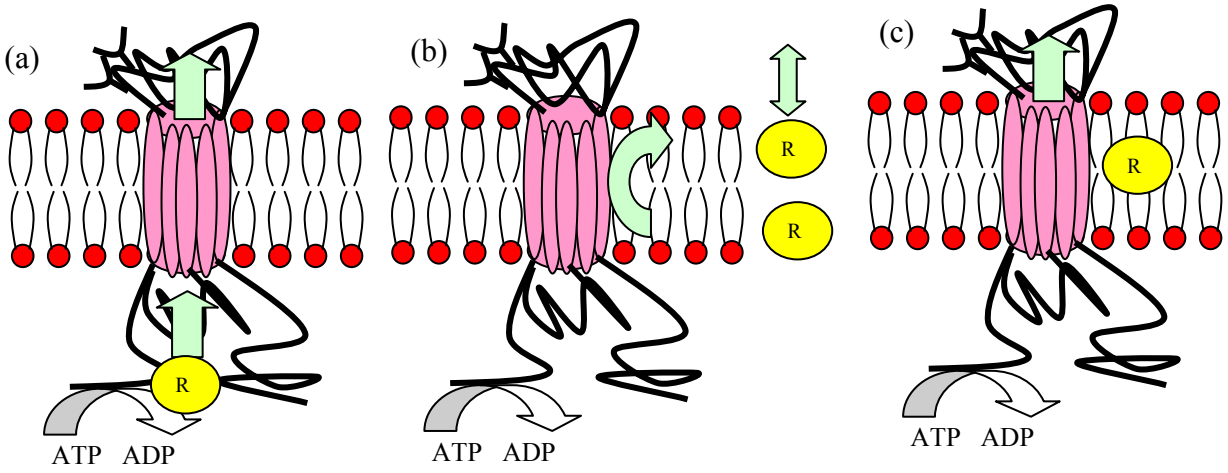

Figure 2.4: Graphical representation of the models that explain the possible efflux mechanism of P-gp a) pore model, b) flippase model, c) hydrophobic vacuum cleaner model (6). R denotes the protein substrate.

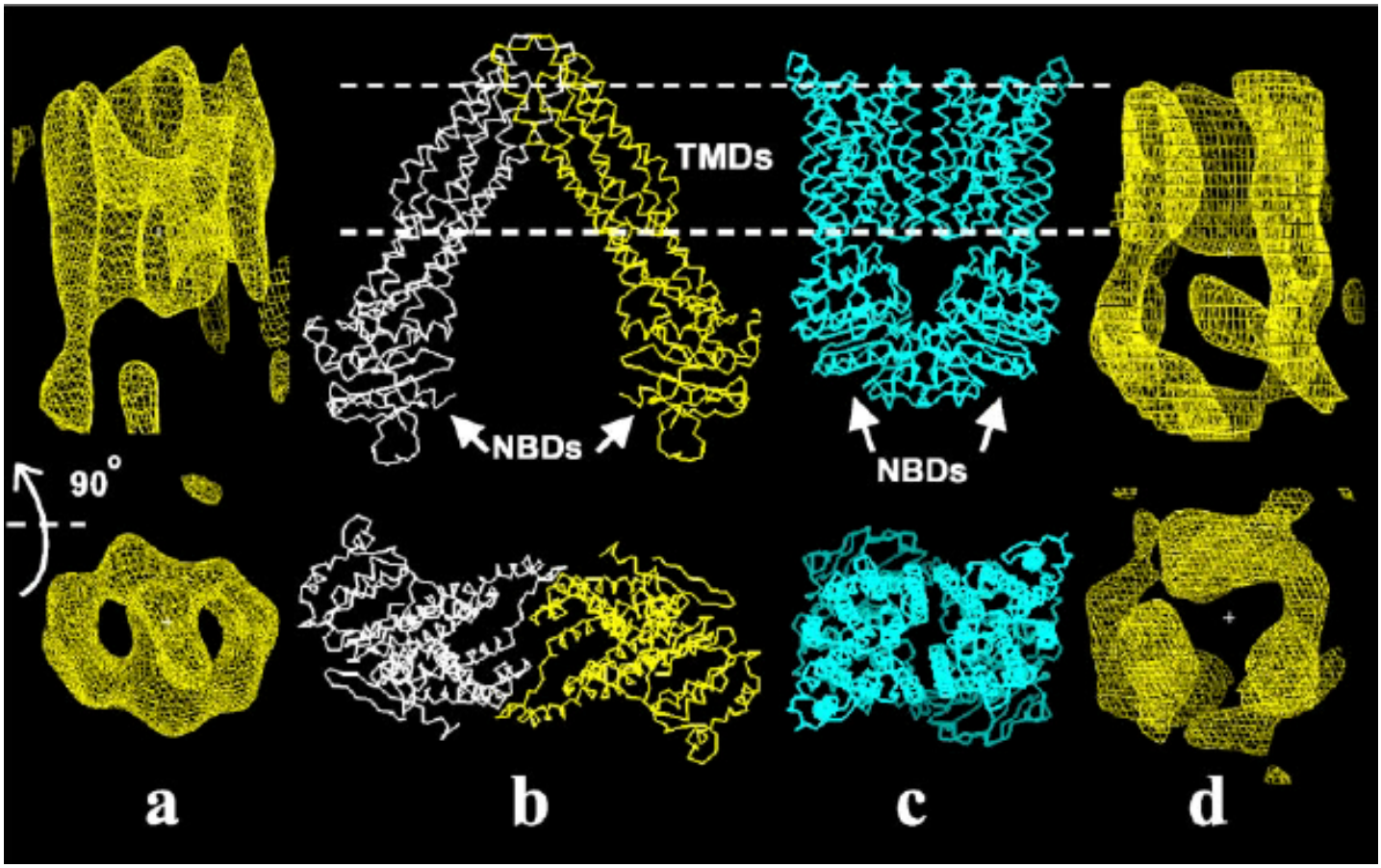

Figure 2.5: Three-dimensional computer schematic of MDR1 in the absence of nucleotide an in the absence of nucleotide (a) and (b) and in the presence of nucleotide (c) and (d), top and side view (16).

2.3 Clinical Significance of Multidrug Resistance

The ABC transporters have a significant role on drug disposition, mainly drug absorption (reducing absorption). Since the substrates for these transporters are so varied and span so many diseases, its role cannot be belittled. Recent data suggests that the inhibition of these proteins has an impact on drug bioavailability, which can be defined as the extent to which the drug reaches the systemic circulation. The bioavailabity of HIV-1 protease inhibitors indinavir, nelfinavir and saquinavir were 2 to 5 times higher in MDR knock out mice when compared to wild type in a study by Kim (20). Also, when grapefruit juice (a flavonoid known as an MDR modulator) was administered in conjunction with talinolol the following pharmacological effects were observed: doubled C_{max}, enhanced pharmokinetical area under the curve (AUC), reduced t_{max}, and unaltered $t_{1/2}$ (1). Bogman studied the effect of D-tocopheryl polyethylene glycol 1000 succinate (TPGS) on talinolol on healthy male non-smokers. TPGS increased the $AUC_{0-\infty}$ by 39%, C_{max} by 100%; t_{max} and $t_{1/2}$ were unaltered (21). Finally, Varma summarizes the pharmokinetic effects of several MDR modulators on corresponding substrates. Effects such as increased absorption rate, increased AUC, increased peak concentration, decrease in clearance and increase in C_{max} were observed (6).

The link between multidrug resistance and human disease was first made when it was recognized that cancer drug resistance was associated with P-gp. The intrinsic or treatment induced drug resistance in cancer is one of the reasons why chemotherapy alone can rarely be used to cure cancer (22, 23).

Some scientists believe that the appropriate route to reduce drug resistance in cancer is not to inhibit its function; but to find ways to reduce or eliminate the expression of multidrug resistant genes in cancer (2). This observation stems from the fact that thus far attempts to use MDR inhibitors to improve chemotherapeutic response *in vivo* have not yielded the expected results (2, 24). However, most of these trials were performed using first generation inhibitors whereas experiments with more potent second generation inhibitors have yielded much better results (24). However, the ABC transporters are not only associated with cancer; it has been discovered that many inherited human diseases are related to defects on ABC transporters (5). In fact, 14 ABC genes mutations have been directly related to human disease (4). For example cystic fibrosis is related to a defected CFTR gene, other diseases are summarized on table 2.2 (5). These discoveries have prompted the scientific community to take a more scrutinized look at the ABC transporters and their effects on human disease.

Multidrug resistance in bacteria is another problem that affects public health. Bacterial infection is the cause of a significant amount of human diseases. MDR in bacteria has prompted the need of new more potent and potentially harmful antibiotics. It has also aided in the proliferation of diseases that were previously under control like tuberculosis, gonorrhea, and childhood ear infections. However, multidrug resistance development in bacteria appears to be unstoppable, mostly because it is part of the evolution process of the organism (26). Consequently, new therapeutic protocols should be developed

regarding the treatment of bacterial infection (27). For example, new methods should be developed for the early diagnosis of the multidrug resistance phenotype on bacteria. Also, the use of inhibitors in conjunction with the antibiotic treatment should be addressed (27). These strategies become more important nowadays because the development of new antimicrobial drugs has become stagnant in recent years.

Table 2.2: Relationship between ABC transporters and human diseases (5, 25)

Disease	ABC Transporter
Cancer	ABCB1 (MDR1), ABCC1 (MRP1), ABCG2 (MXR)
Cystic fibrosis	ABCC7 (CFTR)
Stargardt disease and age-related macular degeneration	ABCA4 (ABCR)
Tangier disease and familial HDL deficiency	ABCA1 (ABC1)
Progressive familial intrahepatic cholestasis	ABCB11 (SPGP), ABCB4 (MDR2)
Dubin–Johnson syndrome	ABCC2 (MRP2)
Pseudoxanthoma elasticum	ABCC6 (MRP6)
Persistent hypoglycemia of infancy	ABCC8 (SUR1), ABCC9 (SUR2)
Sideroblastic anemia and ataxia	ABCB7 (ABC7)
Adrenoleukodystrophy	ABCD1 (ALD)
Sitosterolemia	ABCG5, ABCG8
Multiple Sclerosis	ABCB2 (TAP2)
Diabetes Mellitus	ABCB2 (TAP1) allele
Immune deficiency	ABCB2 (TAP1), ABCB3 (TAP2)

In summary, the multidrug resistance phenomenon is a real clinical problem that can be observed during many aspects of human disease discovery and treatment. The impact of MDR on therapeutic treatment varies

from reduction in bioavailability and effectiveness of treatment, to proliferation of diseases and finally to direct association with some disorders. Therefore, this problem must be taken seriously and the scientific community must find ways to reduce its impact. The therapeutic strategies of MDR substrates must be readdressed and the use of inhibitor conjunction therapy should be considered. Also, more studies regarding the human genome and the causes of multidrug resistance in cancer tissues and bacteria are needed. Lastly, potential interactions between drug and the multidrug resistance proteins should be considered during the drug discovery process.

2.4 Previous work

After the multidrug resistance phenomenon was connected to human disease, it became evident that inhibition was a potential solution to the problem. The first inhibitor to be discovered was verapamil (VER) in 1981 (28). Verapamil is a calcium channel blocker used for the treatment of arrhythmia and hypertension. Tsuruo used nontoxic doses of verapamil in conjunction with vincristine in the P388 leukemia cell line and the vincristine resistant subline P388/VCR. It was also used in mice that were carriers of the same leukemia cell line. Results indicated that mice treated with the vincristine/ verapamil mixture had a life span increase of 40-50% as compared to the mice given only vincristine. Also, verapamil had little influence in the influx of vincristine into the P388, but show dramatic effects on the efflux of the drug. Cells previously treated with vincristine retained more than 70% of the drug after being

incubated for 1 hour with verapamil. In contrast, cells that were not incubated with verapamil lost about 95% of the drug. Verapamil is an example of first generation inhibitors, and is one of the most frequent MDR inhibitors used in the literature. These modulators were not designed with a suppression function in mind. Rather they were designed for other pharmacological uses, but later it was discovered that they posses MDR inhibitory abilities as well. Other examples include the immunosuppressant, Cyclosporin A (CsA), the anti-hypertensive resrpine, and the antiestrogen tamoxifen (6, 29). The use of these compounds is limited by their toxicity because usually high doses are required to achieve inhibition.

Due to the high toxicity of the first generation modulators, scientists developed new chemicals that were based on their first generation counterparts but were engineered to have higher P-gp affinity with no pharmacological activity. These modulators are commonly known as second generation. One of the first to be studied was the non-immunosuppressant analog of Cyclosporin A SDZ PSC 833 (PSC, Vaslpodar) in 1991, shortly after the discovery of Cyclosporin A as a modulator in 1987 (4, 30). Various cytostatic agents were studied coupled with SDZ PSC 833 in the P388 leukemia cell line and the multidrug resistant subline MDR-P388 and in mice that were carriers of the same leukemia cell line. The *in vitro* results showed a 10-fold increase of activity of PSC as compared to CsA, it also showed more activity than verapamil. *In vivo* the life prolongation of the mice was significantly improved when using a PSC/ Vinblasitne (VBL) regime as compared to VBL alone, even

though the VBL dose was lower in the combination therapy. Other examples of second generation inhibitors include, the structural analogs of verapamil: dexverapamil, emopamil, gallopamil, and Ro11-2933(6, 29). These inhibitors demonstrated to be effective in P-gp reversal *in vitro* at much lower concentrations, thus eliminating the cytotoxicity issue.

However, drug-drug interactions were encountered during their use, hindering their potential for therapeutic uses. There were also some issues regarding the effects on the pharmacokinetis and biodistribution properties of the active ingredient (29). Therefore, third generation inhibitors were developed based on the structure-activity relationships targeted to specific MDR mechanisms. Among these modulators the first one to be tested was LY335979 (developed by Eli Lilly), also called zosuquidar trihydrochloride (31). This modulator was capable of fully reversing MDR *in vitro* on five different multidrug resistant cell lines. The doses required for inhibition were extremely low, ranging from 12 to 100 nM. The mechanism for inhibition was assessed as competitive binding. *In vivo* a combination therapy of LY225979/ Doxorubicin was successful in improving the survival rate of P388 infected mice. Furthermore, this modulator showed no effect on the pharmacokinetics (specifically AUC) of doxorubicin and etoposide in contrast to CsA and VER. In general third generation agents have proven to be potent inhibitors at very low doses (usually nanomolar). Other examples include, the diarylimidazole OC144093, and the diketopiperazine XR9576 (6, 29). These agents appear to

be well tolerated in combination therapies with chemotherapeutic drugs, however no clinical trials have been performed (29).

Specific MRP modulators have also been investigated. The first one to be discovered was difloxacin in 1995 (4). However, one of the most studied inhibitors is probenecid whose inhibitory properties were discovered in 1997 (32). Probenecid is a uricosuric agent used in the treatment of gout. It is also used to increase the serum concentration of certain antibiotics. Probenecid was effective in increasing the accumulation and reversing the resistance of daunorubicin and vincristine in HL60/AR and H69/AR MRP overexpressing cell lines. Probenecid had no effect on the MDR1 overexpressing cell lines HL60/TAX and P388/ ADR. For more details on other inhibitors of MDR1, MRP and BCRP please refer to table 4.

In general, there are three mechanisms to inhibit P-gp that have been identified. The first involves locking of the drug binding site by competitive, non-competitive or allosteric means. This is the most common type of inhibition. It has been proposed that the mechanism of interaction of these inhibitors is that the inhibitor is “flipped” by P-gp and then “flops” back into the inner leaflet of the membrane. This creates a large difference between the rate of efflux of the substrate and the inhibitor, preventing the efflux of the substrate. The second involves the interference with the ATP hydrolysis. Among these modulators, one can find steroids and flavonoids (4). The binding site of steroids is located in the vincinity of the AP binding site (33). Flavonoids on the other have are considered bifunctional with interactions in the ATP and the

steroid binding site (34). One example of such flavonoids is genistein, an isoflavone derived from soy. Genistein has been reported to enhance the accumulation and reduce efflux of P-gp, MRP and BCRP substrates (35-38). This mechanism requires lower doses to produce inhibition effects. However, the mechanisms are not well understood.

The last is due to alteration of the integrity of the cell membrane. Under this category, surfactants are emerging as a different class of inhibitors. The hypothesis is that they change the fluidity of the cell membrane, thus facilitating the influx of substrates (6). The cellular membrane is composed of a double lipid bilayer of phospholipids. Membrane fluidity is related to the spatial arrangement of these phospholipidis (39). However, there are contradictory findings. Researchers have classified surfactants as active or inactive depending on their inhibition effects. Only non-ionic polyethoxylated surfactants are considered active. There is at least one report of decreased membrane fluidity with an inhibition effect, contrary to the observation of other researchers. Furthermore, it is not clear if other events like inhibitor-protein interactions are taking place as well (40, 41).

Table 2.3: List of inhibitors of P-glycoprotein, multidrug resistance associated protein and breast cancer resistance protein known to date (4).

Protein	Year	Inhibitor
P-gp	2004	Benzyl-,phenethyl-, and alpha-naphtyl isothiocyanates, diallyl sulfide, PK 11195, small scFv recombinant Pgp antibody fragment
	2003	Amooranin, etrandrine, fagchinoline, ginsenoside Rg, KR30031, methylenedioxyethylamphetamine, protopanaxatriol ginsenosides, saquinavir, siRNA of mdr1 gene, tRA 98006
	2002	3,5-dibenzoyl,-1,4-dihydropyridines, PKC412, pyronaridine, sinensetin
	2001	Agosterol A, haloperidol and dihydrohaloperidol, SB203580, tropane alkaloid ester, SNF4435C and D, tea polyphenol, trans-N,N'-bis(3,4-dimethoxybenzyl)-N-solanesyl-1,2-diaminocyclo hexane (N-5228)
	2000	Astemizole, atorvastatin, 7-O-benzoylpyripyropene A, 5-O-benzolylated taxinine k, clarithromycin and YM17K (3,4'-dideoxy mycaminosyl tylonolide hydrochloride) cyclopamine and tomatidine, 3,5-diacetyl-1,4-dihydropyridines, 7,8-dihydroxy-3benzepine, doxorubicin-gallium-transferrin conjugate, macrolide antibiotics (josamycin, tamolarizine). nelfinavir, norverapamil, ontogen (ONT-093, formely OC-144-093), R101933, taxuspine C, 2'-desacetoxyaustrospicatine and 2-desacetoxytaxinine, V-104
	1999	D-alpha-tocopheryl polyethylene glycol 1000 succinate, anti-MDR1 ribozymes, AR-2, carvedilol, erythromycin, ketoconazole, kopsiflorine, nomegestrol, PAK-200S, pluronic block copolymer, reversin, ritonavir rosemary extract, TTD, XR9576(2)
	1998	Ardeemins, AV200, 5-O-benzoylated taxuspine C, bromocriptine, dipyridamole, droloxifene, imidazothiazole derivatives (N276-12, N276-14, N276-17), oxalyl bis(N-phenyl)hydroxamic acid, tetrandine and fangchinoline, tiamulin, XR9051
	1997	Biricodar (VX-710, Incel), cyproheptadine
	1996	CL 329,753, indole-3-carbinol, itraconazole, LY335979, medroxyprogesterone, mefloquine, mifepristone (RU-486), reserpine
	1995	Azelastine and flezelastine, B9209-005, dexniguldipine (B8509-035), dexverapamil, epidermal growth factor (EGF), insulin-like growth factor I (IGF-1), quercetin
	1994	MS-209, pentoxifylline, Ro11-2933 (DMDP), RU486
	1993	Dilantin, GF120918, meperidine, pentazocine, and methadone, Pgp monoclonal antibodies and antisense oligonucleotide, tamoxifen and toremifene
	1992	Staurosporine and NA-382
	1991	Biperidil, SDZ PSC 833
	1990	Cremophor EL
	1989	Cefoperazone, cetriaxone, phenothiazine, YM534
	1987	Diltiazem, cyclosporine A
	1986	Aamiodarone
	1984	Quinidine
	1981	Verapamil

MRP	2004	Benzyl-,phenethyl-,and alpha-naphtyl isothiocyanates
	2003	TRA 98006
	2001	Agosterol A
	2000	5-O-benzoylated taxinine k, 4-deaceoxyagosterol A, doxorubicin-gallium-transferrin conjugate, V-104, pluronic block copolymer, quinoline-based drugs (cholorquine, quinine, quinidine, and primaquine)
	1999	Dipyridamole, erythromycin and ofloxacin, mifepristone (RU-486), MS-209, rifampicin
	1998	Biricodar (VX-710; Incel), imidazothiazole derivatives (N276-12, N-276-14, N-276-17), NSAIDs (indomethacin, sulindac, tolmetin, acemetacin, zomepirac, and mefenamic acid), ONO-1078, quercetin
	1997	Indomethacin, probenecid
	1996	Acrolein and chloroacetaldehyde, d,1-buthionin-(S,R)-sulfoximine, itraconazol, PAK-104P
	1995	Difloxacin, MK571
BCRP	2004	Chrysin and biochanin A, genistein and naligenin, Imatinib mesylate (Gleevec, ST1571)
	2003	Estrone, diethylstilbestrol and TAG-139, tRA 98006
	2002	Ko143
	1999	GF120918
	1998	Fumitremorgin C

Polyethoxylated morphologies have emerged as MDR inhibitors as well. One of the first studies was developed by Batrakova and coworkers were they observed that linear pluronic block copolymers (poly(ethylene oxide)-*block*-poly(propylene oxide)-*block*-poly(ethylene oxide) $EO_{m/2}$-PO_n-$EO_{m/2}$) can inhibit p-gp function as well as MRP efflux pumps. Furthermore they demonstrated that the extent of the effect was strongly dependent on the molecular structure of the copolymer, in particular the length of the EO (hydrophilic chain) and PO (hydrophobic chain). However, it was unlikely that altering the hydrophobicity of the copolymer will help increase the selectivity of the polymer towards inhibition of MRP versus P-gp. In addition, it was observed that these polymers do not only alter the accumulation of drug in the cell, but they also affected the

intracellular location of the drug. Finally, the effect was also dependent on the concentration of the polymers. Finally, it was observed that the internal ATP of the cell was reduced and the membrane fluidity was increased with the addition of these polymers. It was hypothesized that the polymers are internalized into the cell interfering with the mitochondria thus reducing ATP. The inhibition mechanism proposed for these polymer is a dual action of ATP reduction by mitochondria interaction and increase membrane fluidiztion (42-45).

The effects of lineal PEG morphologies of varying lengths have also been studied. PEG of low chain lengths (PEG-4, PEG-8, PEG-20, PEG-75, PEG-150, PEG-200) did not show a transport enhancement of P-gp substrates. However, the concentrations (0.5% (w/v)) at which these experiments were performed was low as compared to other investigators (46-48). PEGs of chain length of 300 and 400 have shown a transport enhancement of P-gp substrates at concentrations as low as 1% (w/v) (47-49), no studies have been done on MRP substrates. The effect of PEG 400 was observed wether the excipient was added at the basal or the apical side of the experiment, suggesting internalization of the polymer in accordance to Batrakova's findings (45, 49-51). There was an increase in membrane fluidity for cells treated with PEG-300; however, there was not a concentration dependent relationship between inhibition and changes in fluidity. Concentrations as low as 2.5% (v/v) produced an inhibition effect, while membrane fluidity changes were not observed for concentrations lower than 15% (v/v) (48). Therefore, the effect of membrane fluidization and P-gp inhibition merits further examination.

Finally, the role of methoxypolyethylene glycol-block-polycaprolactone diblock copolymers has been studied. These polymers exhibited an accumulation enhancement of the P-gp substrate rhodamine 123 that was concentration dependent. The enhancement increased up to a critical point after which the enhancement was reduced. Furthermore, there was a marked effect of the morphology of the copolymers and the accumulation of the substrate. Increasing lengths of polycaprolactone reduced the accumulation enhancement of the substrates (52). Also transport experiments using these copolymers showed that these polymers were capable of reducing the efflux of rhodamine 123, although no significant transport enhancement was observed. The proposed mechanism for the accumulation enhancement was P-gp inhibition and polymer membrane interactions (53).

2.6 References

1. J. Sun, Z. G. He, G. Cheng, S. J. Wang, X. H. Hao, and M. J. Zou. Multidrug resistance P-glycoprotein: crucial significance in drug disposition and interaction. *Medical Science Monitor* **10**: RA5-14 (2004).
2. T. Litman, T. E. Druley, W. D. Stein, and S. E. Bates. From MDR to MXR: new understanding of multidrug resistance systems, their properties and clinical significance. *Cellular and Molecular Life Sciences* **58**: (2001).
3. L. M. S. Chan, S. Lowes, and B. H. Hirst. The ABCs of Drug Transport in Intestine and Liver: Efflux Proteins Limiting Drug Absorption and Bioavailability. *European Journal of Pharmaceutical Sciences* **21**: 25-51 (2004).
4. C.-H. Choi. ABC transporters as multidrug resistance mechanisms and the development of chemosensitizers for their reversal. *Cancer Cell International* **5**: 30 (2005).
5. M. M. Gottesman and S. V. Ambudkar. Overview: ABC Transporters and Human Disease. *Journal of Bioenergetics and Biomembranes* **33**: 453-458 (2001).
6. M. V. S. Varma, Y. Ashokraj, C. S. Dey, and R. Panchagnula. P-glycoprotein inhibitors and their screening: a perspective from bioavailability enhancement. *Pharmaceutical Research* **48**: 347-359 (2003).
7. A. Seeling. A General Pattern for Substrate Recognition by P-gp. *European Journal of Biochemistry* **251**: 252-261 (1998).
8. D. R. Hipfner, R. G. Deeley, and S. P. C. Cole. Structural, mechanistic and clinical aspects of MRP1. *Biochimica et Biophysica Acta* **1461**: 359-376 (1999).
9. W. Lo¨scherand H. Potschka. Blood-Brain Barrier Active Efflux Transporters: ATP-Binding Cassette Gene Family. *NeuroRx: The Journal of the American Society for Experimental NeuroTherapeutics* **Vol. 2**: 86–98 (2005).
10. P. Borst, R. Evers, M. Kool, and J. Wijnholds. A Famaily of Drug Transporters: the Multidrug Resitance-Associated Proteins. *Journal of the National Cancer Institute* **92**: 1295-1302 (2000).
11. M. Dean, Y. Hamon, and G. Chimini. The human ATP-binding cassette (ABC) transporter superfamily. *Journal of Lipid Research* **42**: 1007-1017 (2001).
12. T. Efferth. The Human ATP-Binding Cassette Transporter Genes: From the Bench to the Bedside. *Current Molecular Medicine* **1**: 45-65 (2001).
13. M. A. Al-Nasassrah, F. Podczeck, and J. M. Newton. The effect of an increase in chain length on the mechanical properties of polyethylene

glycols. *European Journal of Pharmaceutics and Biopharmaceutics* **46**: 31-38 (1998).
14. C. J. Endres, P. Hsiao, F. S. Chung, and J. D. Unadkat. The Role of Transporters in Drug Interactions. *European Journal of Pharmaceutical Sciences* **27**: 501-517 (2006).
15. Y. Sugimoto, S. Tsukahara, E. Ishikawa, and J. Mitsuhashi. Breast cancer resistance protein: Molecular target for anticancer drug resistance and pharmacokinetics/pharmacodynamics. *Cancer Science* **96**: 457–465 (2005).
16. M. F. Rosenberg, A. B. Kamis, R. Callaghan, C. F. Higgins, and R. C. Ford. Three-Dimensional Structures of the Mammalian Multidrug Resistance P-glycoprotein Demonstrate Major Conformational Changes in the Transmembrane Domains upon Nucleotide Binding. *Journal of Biological Chemistry* **278**: 8294-8299 (2003).
17. T. W. Looand D. M. Clark. Identification of Residues the Drug-binding Site of Human P-glycoprotein Using a Thiol-reactive Substrate. *Journal of Biological Chemistry* **272**: 31945–31948 (1997).
18. T. W. Looand D. M. Clarke. Identification of Residues in the Drug-binding Domain of Human P-glycoprotein: Analysis of Transmembrane Segment 11 by Cystein-Scanning Mutagenesis and Inhibition by Dibromobimane. *Journal of Biological Chemistry* **274**: 35388–35392 (1999).
19. J. Ferte. Analysis of the tangled relationships between P-glycoprotein-mediated multidrug resistance and the lipid phase of the cell membrane. *European Journal of Biochemistry* **267**: 277-294 (2000).
20. B. Kimand N. A. Peppas. Synthesis and characterization of pH-sensitive glycopolymers for oral drug delivery systems. *Journal of Biomaterial Science Polymer Edition* **13**: 1271–1281 (2002).
21. K. Bogman, Y. Zysset, L. Degen, G. Hopfgartner, H. Gutmann, J. Alsenz, and J. Drewe. P-glycoprotein and surfactants: Effect on intestinal talinolol absorption. *Clinical Pharmacology & Therapeutics* **77**: 24-32 (2005).
22. I. F. Tannock. Tumor physiology and drug resistance. *Cancer and Metastasis Reviews* **20**: 123–132 (2001).
23. R. S. Kerbel. Molecular and physiologic mechanisms of drug resistance in cancer: An overview. *Cancer and Metastasis Reviews* **20**: 1–2 (2001.).
24. V. S. Donnenberg, PhDand A. D. Donnenberg, PhD. Multiple Drug Resistance in Cancer Revisited: The Cancer Stem Cell Hypothesis. *Journal of Clinical Pharmacology* **45**: 872-877 (2005).
25. T. Akao, M. Hanada, Y. Sakashita, K. Sato, M. Morita, and T. Imanaka. Efflux of baicalin, a flavone glucuronide of Scutellariae Radix, on Caco-2 cells through multidrug resistace-associated protein 2. *Journal of Pharmacy and Pharmacology* **59**: 87-93 (2007).
26. P. Courvalin. Antimicrobial Drug Resistance:"Prediction Is Very Difficult, Especially about the Future". *Emerging Infectious Diseases* **11**: 1503-1506 (2005).

27. J. M. Pages, M. Masi, and J. Barbe. Inhibitors of efflux pumps in Gram-negative bacteria. *Trends in Molecular Medicine* **11**: 382-389 (2005).
28. T. Tsuruo, H. Iida, S. Tsukagoshi, and Y. Sakurai. Overcoming of Vincristine Resistance in P388 Leukemia in Vivo and in Vitro through Enhanced Cytotoxicity of Vincristine and Vinblastine by Verapamil. *Cancer Research* **41**: 1967-1972 (1981).
29. R. Krishnaand L. D. Mayer. Multidrug resistance (MDR) in cancer Mechanisms, reversal using modulators of MDR and the role of MDR modulators in influencing the pharmacokinetiscs of anticancer drugs. *European Journal of Pharmaceutical Sciences* **11**: 265-283 (2000).
30. D. Boesch, C. Gaveriaux, B. Jachez, A. Pourtier-Manzanedo, P. Bellinger, and F. Loor. In Vivo Circumvention of P-Glycoprotein-mediated Multidrug Resistance of Tumor Cells with SDZ PSC 833. *Cancer Research* **51**: 4226-4233 (1991).
31. A. H. Dantzig, R. L. Shepard, J. Cao, K. L. Law, W. J. Ehlhardt, Todd M. Baughman, T. F. Bumol, and J. J. Starling. Reversal of P-Glycoprotein-mediated Multidrug Resistance by a Potent Cyclopropyldibenzosuberane Modulator, LY335979. *Cancer Research* 4171-4179 (1996).
32. S. Gollapudi, C. Kim, B. Tran, S. Sangha, and S. Gupta. Probenecid reverses multidrug resistance in multidrug resistance-associated protein-overexpressing HL60/AR and H69/AR cells but not in P-glycoprotein-overexpressing HL60/Tax and P388/ADR cells. *Cancer Chemotherapy Pharmacology* **40**: 150-158 (1997).
33. G. Dayan, J.-M. Jault, H. Baubichon-Cortay, L. G. Baggetto, J.-M. Renoir, E.-E. Baulieu, P. Gros, and A. D. Pietro. Binding of Steroid Modulators to Recombinant Cytosolic Domain from Mouse P-Glycoprotein in Close Proximity to the ATP Site. *Biochemistry* **36**: 15208-15215 (1997).
34. G. Conseil, H. Baubichon-Cortay, G. Dayan, J.-M. Jault, D. Barron, and A. D. Pietro. Flavonoids: A class of modulators with bifunctional interactions at vicinal ATP- and steroid-binding sites on mouse P-glycoprotein. *Proceedings of the Natural Academy of Science USA* **95**: 9831–9836 (1998).
35. C. Versantvoort, T. Rhodes, and P. Twentyman. Acceleration of MRP associated efflux of Rhodamine 123 by genistein and related compounds. *British Journal of Cancer* **74**: 1949-54 (1996).
36. S. Zhang, X. Yang, and M. E. Morris. Combined Effects of Multiple Flavonoids on Breast Cancer Resistance Protein (ABCG2)- Mediated Transport. *Pharmaceutical Research* **21**: 1263-1274.
37. A. F. Castroand G. A. Altenberg. Inhibition of Drug Transport by Genistein in Multidrug-Resistant Cells Expressing P-Glycoprotein. *Biochemical Pharmacology* **53**: 89-93 (1997).
38. S. Dallas, L. Schlichter, and R. Bendayan. Multidrug Resistance Protein (MRP) 4- and MRP 5-Mediated Efflux of 9-(2-Phosphonylmethoxyethyl)adenine by Microglia. *Journal of Pharmacology And Experimental Therapeutics* **309**: Vol. 309, No. 3 (2004).

39. K. B. Kostoand W. M. Deen. Hindered Convection of Macromolecules in Hydrogels. *Biophysical Jorunal* 277-286 (2005).
40. M. Nerurkar, P. S. Burton, and R. T. Borchardt. The Use of Surfactants to Enhance the Permeability of Peptides Through Caco-2 Cells by Inhibition of an Apically Polarized Efflux System. *Pharmaceutical Research* **13**: 528-534 (1996).
41. P. K. Dudeja, K. M. Anderson, J. S. Harris, L. Buckingham, and J. S. Coon. Reversal of Multidrug Resistance Phenotype by Surfactants: Relationship to Membrane Lipid Fluidity. *Archives of Biochemistry and Biophysics* **319**: 309-315 (1995).
42. D. W. Miller, Bratakovaand K. E. V., A. V. Inhibition of Multidrug Resistance Associated Protein (MRP) Functional Activity with Pluronic Block Copolymers. *Pharmaceutical Research* **16**: 396-401 (1999).
43. E. V. Batrakova, H. Han, V. Yu, D. W. Miller, and A. V. Kabanov. Effects of Pluronic Block Copolymers on Drug Absorption in Caco-2 Cell Monolayers. *Pharmaceutical Research* **15**: 850-855 (1998).
44. E. V. Batrakova, S. Li, D. W. Miller, and A. V. Kabanov. Pluronic P85 Increases Permeability of a Broad Spectrum of Drugs in Polarized BBMEC and Caco-2 Cell Monolayer. *Pharmaceutical Research* **16**: 1366-1372 (1999).
45. E. Batrakova, S. Li, W. Elmquist, D. Miller, V. Alakhov, and A. Kabanov. Mechanism of sensitization of MDR cancer cells by Pluronic block copolymers: Selective energy depletion. *British Journal of Cancer* **85**: 1987–1997 (2001).
46. S. W. Wang, J. Monagle, C. McNulty, D. Putnam, and H. Chen. Determination of P-glycoprotein Inhibition Excipients and Their Combinations Using an Integrated High-Throughput Process. *Journal of Pharmaceutical Sciences* **93**: 2755-2767 (2004).
47. E. D. Hugger, Novak, B. L., Burton, P. S., Audus, K. L., Borchardt, R. T. A Comparison of Commonly Used Polyethoxylated Pharmaceutical Excipients on Their Ability to Inhibit P-glycoprotein Activity In Vitro. *Journal of Pharmaceutical Science* **91**: 1991-2002 (2002).
48. E. D. Hugger, K. L. Audus, and R. T. Borchardt. Effects of Poly(ethylene glycol) on Efflux Transporter Activity in Caco-2 Cell Monolayers. *Journal of Pharmaceutical Science* **91**: 1980-1990 (2002).
49. B. M. Johnson, W. N. Charman, and C. J. H. Porter. An In Vitro Examination of the Impact of Polyethylene Glycol 400, Pluronic P85, and Vitamin E d-a-Tocopheryl Polyethylene Glycol 1000 Succinate on PGlycoprotein Efflux and Enterocyte-Based Metabolism in Excised Rat Intestine. *AAPS PharmSci* **4**: 1-13 (2002).
50. E. V. Batrakova, S. Li, Y. Li, V. Y. Alakhov, and A. V. Kabanov. Effect of Pluronic P85 on ATPase Activity of Drug Efflux Transporters. *Pharmaceutical Research* **21**: 2226-2233 (2004).
51. E. V. Batrakova, S. Li, S. V. Vinogradov, V. Y. Alakhov, Donald W. Miller, and A. V. Kabanov. Mechanism of Pluronic Effect on P-Glycoprotein Efflux System in Blood-Brain Barrier: Contributions of

Energy Depletion and Membrane Fluidization. *The Journal of Pharmacology and Experimental Therapeutics* **299**: 483-493 (2001).

52. J. Zastre, J. Jackson, M. Bajwa, R. Liggins, F. Iqbal, and H. Burta. Enhanced cellular accumulation of a P-glycoprotein substrate, rhodamine-123, by caco-2 cells using low molecular weight methoxypolyethylene glycol-block-polycaprolactone diblock copolymers. *European Journal of Pharmaceutics and Biopharmaceutics* **54**: 299–309 (2002).
53. J. Zastre, J. Jackson, and H. Burt. Evidence for Modulation of P-glycoprotein–Mediated Efflux by Methoxypolyethylene Glycol-block-PolycaprolactoneAmphiphilic Diblock Copolymers. *Pharmaceutical Research* **21**: 1489-1497 (2004).

3.0 OBJECTIVES

Understanding the effects that polyethylene glycol morphologies have on the transport of MDR and MRP substrates is of outmost importance. It will allow researchers to design drug delivery devices that will be more effective and at the same time reduce adverse effects to the patients. Therefore, the main goal of this work is to investigate the effects of polyethylene glycol morphologies in the transport of MDR and MRP substrates. To achieve these goals the following specific objectives have been outlined:

i. Determine the optimum polymerization conditions for poly(ethylene glycol) hydrogels
    a. Crosslinked poly(ethylene glycol) microparticles using poly(ethylene glycol) monomehacrylate of 200, 400 and 1000 g/mol and poly(ethylene glycol) dimethacrylate of 600 and 1000 g/mol.
    b. Crosslinked ply(ethylene glycol) submicron spheres using poly(ethylene glycol) monomethacrylate of 400 and 1000 g/mol and poly(ethylene glycol) dimethacrylate of 400 g/mol.
ii. Characterize the polymers for properties important to drug delivery applications: swelling, partition coefficient, correlation length and release properties (i.e. contribution for diffusion fickian or not, diffusion coefficient)
iii. Investigate the cytotoxic effects of the polymers on the cell monolayer to understand the conditions at which the polymer will not have toxic effects on the cell monolayers

iv. Investigate the transport mechanism of Fluorescein sodium salt (FLUO) , an MRP substrate and Rhodamine 123 (R123), an MDR substrate in the presence and absence of these crosslinked PEG polymers to asses the inhibition effects of the various morphologies

v. Investigate the transport mechanism of the known MRP substrate FLUO in the presence and absence of known MRP inhibitors genistein and probenecid

vi. Investigate the transport mechanism of the known MDR substrate Rhodamine 123 in the presence and absence of known MDR inhibitors genistein and verapamil

vii. Investigate the transport mechanism of the known MDR and MRP substrates R123 and FLUO on the presence and absence of the lineal PEG 300 g/mol morphology

    a. Perform experiments apical to basolateral and vice versa
    b. Perform experiments at different temperatures (4 ºC and 37 ºC)
    c. Perform experiments at different concentrations of the polymer

viii. Investigate the effect of the hydrogels on the membrane fluidity using fluorescence recovery after photobleaching (FRAP)

4.0 SYNTHESIS AND CHARACTERIZATION OF POLY(ETHYLENE GLYCOL) HYDROGELS FOR CONTROLLED DRUG DELIVERY OF MDR AND MRP SUBSTRATES

4.1 Introduction

Poly(ethylene glycol) (PEG) is a linear or branched neutral polymer with the form

$$HO\text{-}(CH_2CH_2O)_n\text{-}CH_2\text{-}CH_2\text{-}OH \qquad [4.1]$$

It is a common excipient used in the pharmaceutical industry under the common names Carbowax, Carbowax Sentry, Lipoxol, Lutrol E, PEG, Pluriol E, polyoxyethylene glycol. The most common uses for PEG are ointment base, plasticizer, solvent, suppository base, and tablet and capsule lubricant (1).

As previously mentioned, poly(ethylene glycol) based morphologies have received the attention of several investigators because it has shown MDR and MRP inhibitory properties. However, no research has been done regarding the inhibitory properties of crosslinked PEG based hydrogel morphologies. The advantage of using crosslinked polymer systems as opposed to lineal polymers is that these can be tailored for controlled drug delivery applications. This work focuses on the use of PEG-rich hydrogel morphologies for controlled drug delivery devices that will inhibit MDR and MRP efflux pump and aiding the absorption of its substrates.

These morphologies are called PEG-rich hydrogels because their structure includes the incorporation of PEG tethered chains as seen in figure 4.1. These chains increase the amount of PEG moieties within the structure potentially maximizing its inhibitory effect. During the synthesis of such morphologies, there are three variables that can be controlled, the length of the tethered chain, the length of the crosslinker and the particle size. Each of these variables has a particular impact on the structural and drug release properties of the hydrogel as well as on the possible inhibitory effects.

The length of the tethered chain plays a role on the structure of the hydrogel (the structure of the hydrogel in turn impacts the release profile of the drug), as it also provides PEG moieties that will later interact with the MDR and MRP proteins. The crosslinker length also has an impact on the structure of the hydrogel (such as the amorphous or glassy state and the structural strength of the polymer) as well as the availability of the PEG tethered chains to the surface. Finally, by reducing the particle size one can maximize the surface area, thus providing more availability of the functional groups that can later have an impact on the efflux pump inhibition.

It is therefore, very important that all these factors are well understood because this will lead to the rational design of future controlled drug delivery devices. Since the morphologies described herein are very well understood in the literature it is not necessary to perform a detailed characterization. Therefore, the characterization was reduced to the essential properties needed

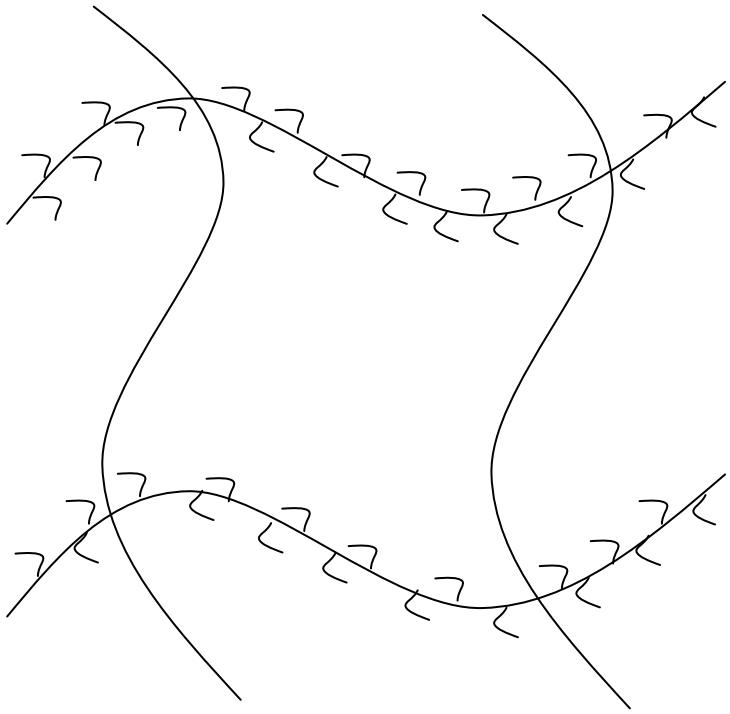

Figure 4.1: Graphical representation of the tethered chains formed by the poly(ethylene glycol) monomethyl ether monomer

to understand the substrate release of swelling controlled devices. These properties include the swelling ratio, the correlation length, and the partition coefficient, and the release profile of a model drug. This information later coupled with the inhibitory effect will be employed for the rational design of a controlled drug delivery apparatus, which is beyond the scope of this thesis.

4.2 Background

The unique properties of linear PEG have prompted its use in biological applications. For example PEG excludes other polymers from its presence in aqueous solution. Therefore, it can be used for protein rejection and formation of two-phase systems with other polymers. It also provides the polymer with non-immunogenicity and nonantigenicity. The polymer is also non-toxic and does not harm active proteins or cells. However, it interacts with cell membranes. It is subject to chemical modification and attachment to other molecules and surfaces. On the other hand, when attached, it has little effect on their chemistry, but controls their solubility and increases their size. Therefore, linear PEG may be used to improve water solubility. Also, PEG binding can improve solubility in organic solvents. It is amphiphilic (able to solubilize in both organic and aqueous solvents) and its solubility and partitioning patterns can be altered by attachment of hydrophobic tails. PEG forms hydrogen bonding on the hydroxyl group, and conserve molecule activity. It does not denature proteins or hinder the approach of other small molecules. Finally, PEG can form complexes with metal cations (2).

There are hundreds of examples of the biological applications of the different PEG based morphologies in the literature. PEG has been used in all possible morphologies available from lineal, branched, crosslinked, interpenetrated polymer networks (IPN), stars and dendrimers. It applications are as varied as the possible morphology configurations. Some examples include: drug delivery (3, 4), proteins modification (pegylation) (5, 6), gene delivery (7), MDR and MRP inhibition (8, 9), imprinting (10), mucoadhesion (11), modification of other hydrogels (12, 13), surface immobilization (14-16), and bioactive molecule carriers (17).

Lineal PEG is generally considered nontoxic. It is included in the FDA Inactive Ingredients Guide, the Canadian List of Acceptable Non-medicinal Ingredients and the nonparatenteral medicines licensed in the UK (1). Nevertheless, fatal poisoning with PEG has been reported in human burn patients who were treated with PEG-based anti-microbial creams (18). The effects included hyperosmolarity, metabolic acidosis, and renal failure. The cream contained a mixture of three fractions of PEG with average molecular weights of 300, 1000 and 4000 g/mol. Later it was found that PEG of molecular weights less than 400 g/mol may be oxidized *in vivo* into toxic diacids. Oral toxicity studies showed no adverse reproductive or tetratogenic effects on Chinese hamsters. Also, subcutaneous and intravenous studies showed no serious tissue damage on rats (18, 19).

Metabolism studies of PEG showed that high molecular weight PEGs (>1000 daltons) are minimally absorbed from the gastrointestinal tract. Renal clearance studies on rats suggest that PEG up to a molecular weight of 4000 is excreted by glomerular filtration without participation of the renal tubules. Finally, high molecular weight PEG's are retained in the blood for a longer period than low molecular weight PEGs, and urinary clearance decreases with increasing molecular weight (19).

The recommended daily dosage of PEG is 10mg/kg body weight (1). The maximum recommended concentration for parenteral products is 30% (v/v) (1). Other animal toxicity data is listed in table 4.1.

Table 4.1: Animal toxicity data reported as 50% lethal dose (LD_{50}) for various lineal PEG morphologies. IV denotes the intravenous route, while IP denotes the intraperitoneal route (1).

PEG	LD_{50} (g/kg)								
	Guinea pig (oral)	Mouse (IP)	Mouse (IV)	Mouse (oral)	Rabbit (oral)	Rabbit (IV)	Rat (IP)	Rat (IV)	Rat (oral)
PEG 200	---	7.5	---	34	19.9	---	---	---	28.0
PEG 300	19.6	---	---	---	17.3	---	---	---	27.5
PEG 400	15.7	10.0	8.6	28.9	26.8	---	9.7	7.3	---
PEG 600	---	---	---	47.0	---	---	---	---	38.1
PEG 1000	---	20	---	---	---	---	15.6	---	32
PEG 1500	28.9	---	---	---	28.9	8.0	17.7	---	44.2
PEG 4000	50.9	---	16.0	---	76.0	---	11.6	---	50.0
PEG 6000	50.0	---	---	---	---	---	6.8	---	---

In summary, PEG is a unique polymer with several properties that make it an ideal material for biological applications. It has been used in numerous applications and in diverse morphologies. This work focuses on the use of PEG as crosslinked hydrogel morphologies and on the effects of the variables of control during the hydrogel synthesis on both the hydrogel structure and the inhibition of the MDR and MRP proteins. Therefore, it is important to elaborate on the hydrogel structural parameters that where evaluated.

The structural parameters chosen for evaluation must be able to describe the type of controlled release expected from these materials. The materials used for controlled drug delivery devices are classified according to the mechanism of drug release. One important category is swelling controlled devices. These devices are prepared by the incorporation of a drug into the polymer matrix (usually in the glassy state) in a dissolved or dispersed phase. Once the polymer is put into contact with a thermodynamically compatible liquid, it swells. The drug is then released as the polymer imbibes the surrounding fluid displacing its contents on the relaxing hydrogel. The most important properties of a hydrogel needed to design a swelling controlled delivery device are the swelling ratio, the correlation length, the partition coefficient, and the release profile of a model drug.

One of the defining characteristics of hydrogels is their capacity to swell or imbibe water. It is this characteristic that makes them suitable for controlled release applications. The swelling mechanism begins by water molecules that enter the matrix and hydrate the most polar, hydrophilic groups (primary bound

water). As these groups become hydrated, the network swells and exposes hydrophobic groups that also interact with the water molecules. This is known as hydrophobically-bound water or secondary bound water. The primary and secondary bound water combine to form total bound water. At this point, the network will imbibe more water due to the osmotic driving force of the network chains. This phenomenon is counterbalanced by the covalent or physical crosslinks of the network, leading to an equilibrium swelling (20). The capacity of the hydrogel to swell can be characterized using the volume-swelling ratio.

$$Q = \frac{V_{gel}}{V_p} \qquad [4.2]$$

where V_{gel} and V_p are the volume of the swollen polymer and the dry hydrogel respectivel7 (21).

The volume of the polymer was calculated using the following expression

$$V = \frac{W_a - W_h}{\rho_h} \qquad [4.3]$$

Where V is the volume of the polymer, W_a and W_h is the weight of the polymer in air and heptane respectively and ρ_h is the density of heptane (0.68 g/cm^3) (20, 22).

The swelling behavior of a hydrogel is closely related to its mesh size. The distance between two cross-links in turn can quantify the mesh size or correlation length (ξ). The Peppas-Merrill equation has been successfully used to predict the distance between crosslinks. This equation is a modification of

the Flory-Rehner analysis that describes gels as neutral with tetra-functional junctions and polymer chains that exhibit Gaussian behavior (20, 23)

To understand the rational behind the calculations for mesh size, first it is important to understand the thermodynamics of swelling. According to Flory-Renher a hydrogel immersed in fluid and in equilibrium with its surroundings is subject to two opposing forces: (i) the thermodynamic force of mixing, and (ii) the retractive force of the polymer chains (24). This can be expressed mathematically by the following expression (25):

$$\Delta G_{Total} = \Delta G_{Elastic} + \Delta G_{Mixing} \qquad [4.4]$$

where ΔG_{Total} is the Gibbs free energy of the system, $\Delta G_{Elastic}$ is the contribution due elastic retractive forces of the hydrogel and ΔG_{Mixing} is the contribution due to spontaneous mixing of fluid and hydrogel chains. At equilibrium this two forces are equal.

Differentiating equation (4.4) with respect to the total number of solvent molecules and maintaining temperature and pressure constant yields (25):

$$\mu_1 - \mu_{1.0} = \Delta\mu_{Elastic} + \Delta\mu_{Mixing} \qquad [4.5]$$

here μ_1 is the chemical potential of the solvent in the polymer gel, $\mu_{1,0}$ is the chemical potential of the pure solvent, $\Delta\mu_{Elastic}$ and $\Delta\mu_{Mixing}$ is the chemical potential of the penetrating solvent due to elastic retractive forces and spontaneous mixing respectively. Again at equilibrium these two chemical potential must balance each other.

The chemical potential of mixing can be solved using heat and entropy of mixing. The elastic chemical potential can be solved using rubber elasticity

theory. The molecular weight between crosslinks of a neutral hydrogel in the absence of solvent can be derived from equating these two chemical potentials as follows (25):

$$\frac{1}{\overline{M}_c} = \frac{2}{\overline{M}_n} - \frac{(\overline{\upsilon}/V_1)\left[\ln(1-\upsilon_{2,s}) + \upsilon_{2,s} + \chi_1 \upsilon_{2,s}^2\right]}{\upsilon_{2,s}^{1/3} - \frac{\upsilon_{2,s}}{2}} \qquad [4.6]$$

In this equation $\overline{M}_c$ is the average molecular weight between crosslinks, $\overline{M}_n$ is the average molecular weight of the uncrosslinked polymer, $\overline{\upsilon}$ is the specific volume of the polymer (0.898 cm^3/g for PEG), V_1 is the molar volume of water (18.1 cm^3/mol), $v_{2,s}$ is the swelled polymer volume fraction and is given by [4.8] and X_1 is the Flory polymer-water interaction parameter (0.55 for PEG).

Peppas and Merrill modified this equation for hydrogels prepared in the presence of water. The addition of water changes the chemical potential due to elastic forces rendering the following equation (25):

$$\frac{1}{\overline{M}_c} = \frac{2}{\overline{M}_n} - \frac{(\overline{\upsilon}/V_1)\left[\ln(1-\upsilon_{2,s}) + \upsilon_{2,s} + \chi_1 \upsilon_{2,s}^2\right]}{\upsilon_{2,r}\left(\left(\frac{v_{2,s}}{v_{2,r}}\right)^{1/3} - \frac{1}{2}\left(\frac{v_{2,r}}{v_{2,s}}\right)\right)} \qquad [4.7]$$

here $v_{2,r}$ is the relaxed polymer volume fraction and is given by (4.9)

$$v_{2,s} = \frac{V_p}{V_s} \qquad [4.8] \qquad v_{2,r} = \frac{V_p}{V_{g,s}} \qquad [4.9]$$

Where V_p is the volume of the dry polymer, $V_{g,s}$ is the volume of the polymer immediately after crosslinking, but prior to swelling, and V_s is the volume of the swollen polymer (20, 21).

The average molecular weight of the uncrosslinked polymer can be calculated using kinetic data for the free radical polymerization of the polymer as described below.

$$M_n = \frac{M_0 k_p [M]}{\left(f k_d k_t [I]\right)^{1/2}} \qquad [4.10]$$

In this equation M_0 is the molecular weight of the monomer unit, k_p is the kinetic propagagion constant (670L/mol/s), k_d is the initiator decay constant (0.0165 s^{-1}), k_t is the kinetic termination constant (2.1E6 L/mol/s), f is the initiator efficiency (0.5), [M] and [I] are the monomer and initiator concentrations respectively (20, 21).

Once the molecular weight of the polymer between crosslinks is known the end-to-end distance of the polymer in the unperturbed state can be calculated from the following relationship:

$$\left(r_0^2\right)^{1/2} = \left(\frac{2C_n \overline{M}_c}{M_0}\right)^{1/2} l \qquad [4.12]$$

In this equation C_n is the characteristic ratio of the polymer (3.8 for PEG), l is the length along the polymer chains (1.54 Å for a carbon-carbon bond). Finally the mesh size can be calculated from (20, 21) :

$$\xi = v_{2,s}^{-1/3} \left(r_0^2 \right)^{1/2} \qquad [4.13]$$

The partition coefficient is closely related to the mesh size or correlation length because the mesh size gives an approximate idea of how many particles can enter (partition) between the spaces or cavities created by the hydrogel. It can also provide information regarding possible interaction that might be present between polymer and substrate. It can calculated from the following expression

$$K = \frac{C_m}{C_s} \qquad [4.14]$$

Where C_m and C_s are the concentration of the model molecule in the membrane and the solution respectively (23). This equation can be rearranged into measurable properties as follows

$$\mathrm{K} = \frac{\mathrm{C}_0 - \mathrm{C}_\mathrm{e}}{\mathrm{C}_\mathrm{e}} \frac{\mathrm{V}_\mathrm{s}}{\mathrm{V}_\mathrm{m}} \qquad [4.15]$$

In this equation C_0 is the initial concentration of the solute in the solution while C_e is the equilibrium concentration. V_s and V_m are the volume of the solution and the membrane respectively.

Finally, the release profile of a model drug through a hydrogel provides valuable information regarding the rate of release of the drug and the predominant drug release mechanism present. The semi-empirical equation known as the power law has become the gold standard for hydrogel release analysis. This equation is based in the Berens and Hopfenberg phenomenological equation that states that the solute diffusion from a hydroel is due to the summation of two different mechanisms: (i) Fickian diffusion, and (ii) the relaxation of the hydrogel chains (26). It was first introduced for the diffusional parameters of glassy polymer powders. Later Korsmeyer successfully applied the model for controlled delivery systems developing what is commonly known in the literature as the exponential model (27). Finally, Ritger realized an in depth analysis of the model for different geometries and size distributions (28). The exponential model reads as follows:

$$\frac{M_t}{M_\infty} = K_1 t^{1/2} + K_2 t \quad \text{for } 0 < \frac{M_t}{M_\infty} < 0.6 \qquad [4.16]$$

where M_t is the cumulative mass released at time t, M_∞ is the total mass incorporated, K_1 and K_2 are constants for the Fickian and non-Fickian behavior, respectively (3, 29). This equation can be rewritten in a more general (power law) form to give:

$$\frac{M_t}{M_\infty} = Kt^n \quad \text{for } 0 < \frac{M_t}{M_\infty} < 0.6 \qquad [4.17]$$

where n is the diffusional exponent. Fickian diffusion will dominate for n=0.5, relaxation of the chains will dominate for n=1 and for 1>n>0.5 the diffusion is said to be anomalous. This equation is only valid for one-dimensional release of planar systems. However for thin disks whose aspect ratio ($2r/\delta$) (δ is the thickness of the disk) is greater than 50 this assumption is still applicable (28).

If the diffusion is dominated solely by Fickian contributions then Fick's second law of diffusion applies (3, 30).

$$\frac{\partial C}{\partial t} = \frac{\partial}{\partial x}\left\{D\frac{\partial C}{\partial x}\right\} \qquad [4.18]$$

where C is the concentration of the solute, δ is distance, D is the diffusion coefficient, and t is time.

The boundary conditions are as follows

$t = 0$	$-l/2 < x < l/2$	$C = C_1$
$t > 0$	$x = \pm l/2$	$C = C_0$

An approximate solution of this equation given in trigonometric series is (28)

$$\frac{M_t}{M_\infty} = 1 - \sum_{n=0}^{\infty} \frac{8}{(2n+1)^2} \exp\left[-D \frac{(2n+1)^2 \pi^2}{\delta^2} t \right] \qquad [4.19]$$

An alternate solution in the form of the error function series is as follows (28):

$$\frac{M_t}{M_\infty} = 4\left[\frac{Dt}{l^2}\right]^{1/2}\left[\frac{1}{\pi^{1/2}} + 2\sum_{n=1}^{\infty}(-1)^n \, ierfc\,\frac{nl}{2\sqrt{Dt}}\right] \qquad [4.20]$$

Therefore the short time approximation (i.e. small values of the dimensionless time $4Dt/l^2$) is given by (3, 30):

$$\frac{M_t}{M_\infty} = 4\left[\frac{Dt}{\pi\delta^2}\right]^{1/2} \qquad [4.21]$$

Therefore, the Fickian diffusion coefficient of the hydrogel can be found by comparing equations [4.16] and [4.21]. This short time approximation is valid for M_t/M_∞ values smaller than 60%. This number was obtained by comparing the solutions of the approximate solution [4.19] and the short time approximation [4.20] (28). Technically as long as the function of M_t/M_∞ against $t^{1/2}$ is lineal the correlation is still valid.

If the transport is dominated by pure relaxation of the chains, more commonly known as Case II transport then the following differential equation can be written (30):

$$\frac{dM_t}{dt} = K_0 A \qquad [4.22]$$

where K_0 is the Case II relaxation constant and is the A cross sectional area. This model assumes that the phenomenon follows first order kinetics.

The amount of solute released from the swollen region at any time t can be obtained from the following mass balance (30):

$$M_t = C_0 A\left(\frac{l}{2} - X\right) \qquad [4.23]$$

where C_0 is the initial concentration of solute in the hydrogel;

Substituting [4.23] into [4.22] and solving for X we obtain the following expression (30):

$$M_t = \left(\frac{2C_0 A}{l}\right)\left(\frac{2k_0}{C_0 l}t\right) \qquad [4.24]$$

The term $2C_0A/l$ denotes the solute release at long times or M_∞. Therefore equation (24) can be rewritten as follows:

$$\frac{M_t}{M_\infty} = \frac{2K_0}{C_0\delta}t \qquad [4.25]$$

Again the Case II relaxation constant of the hydrogel can be obtained by comparing equations [4.16] and [4.25].

To summarize poly(ethylene glycol) hydrogels are excellent materials for drug delivery applications. They are nontoxic, resemble biological tissues and are capable of drug delivery due to the relaxation of the chains. The most important control variables during the hydrogel synthesis are the length of the tethered chain and the crosslinker chain and finally the particle size. These variables have an impact on the structural parameters of the hydrogel that can be assessed by studying the hydrogel swelling ratio, correlation length, partition coefficient and release of a model drug.

4.3 Experimental

4.3.1 Materials

The monomer poly(ethylene)glycol monomethacrylate (PEGMA) with PEG chains of 200, 400 and 1000 g/mol, and the cross linker poly(ethylene) glycol dimetachrylate (PEGDMA) with chains of 400, 600 and 1000 g/mol were purchased from Polysciences, Inc (Warrington, PA) (structure on Figure 4.2). The photo-initiator, 1-hydroxyciclohexylphenyl ketone (see structure on Figure 4.2), the model substrate Fluorescein sodium salt, and the phosphate buffered saline (PBS) (pH = 7.4) were obtained from Aldrich Chemical Co. (Milwaukee, WI). The thermal initiator azobisisobutyronitrile (AIBN) and the surfactants Sodium Duoceyl Sulfate (SDS) and Tween 80 were also obtained from Aldrich Chemical Co. (Milwaukee, WI). Finally, the solvents, ethanol and heptane were purchased from Fisher Scientific (Hampton, NH).

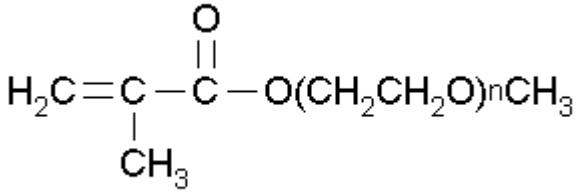

Polyethylene Glycol Monomethylehter Methacrylate
(PEGMA)

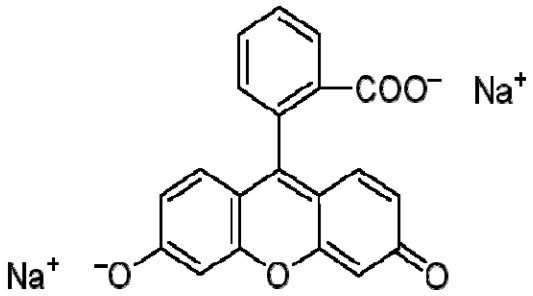

Fluorescein Sodium

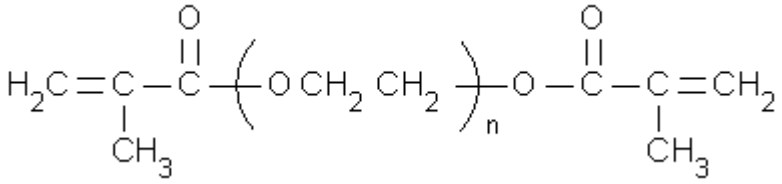

Polyethylene Glycol Dimethylehter Dimethacrylate
(PEGDMA)

Figure 4.2: Molecular structure of Fluorescein Sodium Salt, Polyethylene Glycol Monomethylether Methacrylate, and Polyethylene Glycol Dimethylether Dimethacrylate

4.3.2 Methods

Hydrogel Preparation

Hydrogels were synthesized by free radical solution polymerization according to M. Torres-Lugo (3). PEG rich hydrogel networks were synthesized using monomers with tethered PEG of various lengths. Polymerization of tethered chains of Poly(ethylene glycol) monomethyl ether monomethacrylate (PEGMA) (MW= 200, 400, 1000 g/mol) was performed using poly (ethylene glycol) dimethacrylate (PEGDMA) (MW=600, 1000 g/mol) as the crosslinker. The pre-polymeric solution was prepared by mixing a monomer/crosslinker combination of a 1:1 molar ratio of monomer to crosslinker in a 50 % (w/w) ethanol/water solution with 0.1% of 1-hydroxycyclohexy phenyl ketone as the initiator. The monomer/crosslinker combinations that were studied are summarized in table 4.2. The pre-polymeric solution was later purged using 99.998% pure nitrogen atmosphere provided by Balston Analyatical Gas System 76-92 (Parker-Balston, Haverhill, MA) for 20 minutes. The nitrogen purge was used to reduce the amount of oxygen in the solution, because oxygen acts a free radical scavenger. The pre-polymeric solution was then transferred by capillary action between two microscopes slides separated by Teflon® spacers (0.030 in.). Later the solution was exposed to an UV source (EXFO, Acticure, Ontario, Canada) with an intensity of approximately 30-40 mW/cm^2, measured with an UV radiometer, under a nitrogen environment. The polymers were then washed for a week in

deionized water, and finally dried for a week at 32^{o} C in a vacuum oven (Cole Palmer, Vernon Hills, IL). From now on the convention used to refer to the polymers will be PEGMA MW /PEGDMA MW.

Table 4.2: Selected poly(ethylene glycol) hydrogels for synthesis and characterization

		Monomer length (g/mol)		
		200	400	600
Crosslinker length (g/mol)	400		X[Ŧ]	X[Ŧ]
	600	X	X	X
	1000	X	X	X

[Ŧ] Submicron spheres

Submicron spheres synthesis

The surfactant solution was prepared by adding 99% (w/w) Tween 80 solution 0.045g/L and 1% (w/w) 0.245 g/L Sodium Duoceyl Sulfate (SDS) solution. The surfactant solution was filtered using a 0.2 μm filter before use. The prepolymeric solution was prepared by mixing 98% (w/w) surfactant solution and 2% (w/w) monomer/crosslinker. The monomer/crosslinker portion consisted of 50:50 by weight poly(ethylene glycol) monomethyl ether (monomer) and poly(ethylene glycol) dimethacrylate (crosslinker) and 1% azobisisobutyronitrile (AIBN, heat activated initiator). The pre-polymeric solution was purged in Argon atmosphere for 30 minutes. The solution was then transferred to a silicone oil bath kept at 80 ºC (AIBN is activated at temperatures above 60 ºC) and let cure for 90 minutes. After polymerization was completed, the particle size of the polymer dispersion was analyzed using dynamic light scattering (DLS). In short a 1 mL sample of the polymer dispersion was placed on a glass cuvette. The cuvette was then placed in the DLS sample chamber. The DLS analyzed the particle size at room temperature taking an average of 5 different measurements. The polymer suspension was dialyzed in water using 10^6 kDa MWCO (molecular weight cut off) dialysis membrane (Spectra Por, Rancho Dominguez, CA). The water was changed three times a day for a period of 5 days. After dialysis was completed, the particle size distribution was reanalyzed. The yield of the solution was assessed by gravimetric analysis. In essence, a predetermined volume of the solution was weighted and let dry in vacuum oven for 48 hours. The dried

polymer spheres were re-weighted and the mg/mL concentration of the polymeric solution was compared to that of the pre-polymeric solution.

Hydrogel Swelling Ratio

Polymers were prepared as described in the hydrogel preparation section. After the polymerization was completed, the polymer slide was cut with a 9/16-inch diameter mold. The polymer discs were washed with deionized water for 3 days with 2 changes per day. The polymer discs were transferred to a dessicator and let dry for 2 days. The polymer discs were placed in a vacuum oven for 1day. The volume of the dry polymer disc was measured by taking the weight of the polymer disc in air and in heptane solvent using a density kit coupled to the Voyager analytical balance (Ohaus, Pine Brook, NJ). The polymer discs were then transferred to 10 mL of Phosphate Buffered Saline at 7.4 pH and 25 ºC for 24 hours. The volume of the swollen polymer disc was measured as described above.

Hydrogel Correlation Length

Polymers were prepared as described in the hydrogel preparation section. After the polymerization was completed the polymer slide was cut with a 9/16-inch diameter mold. Immediately after cutting, the weight of the polymer disc in air and in heptane solvent was measured using a density kit coupled to the Voyager (Ohaus, Pine Brook, NJ) (in order to measure the volume of the relaxed hydrogel). The polymer discs were washed with deionized water for 3 days with 2 changes per day. The polymer discs were transferred to a

desiccator and let dry for 2 days. The polymer discs were placed in a vacuum oven for 1day. At this point the volume of the dry polymer disc was measured as described above. The polymer discs were transferred to 10 mL of phosphate buffered saline at 7.4 pH and 25 ºC for 24 hours. The volume of the swollen polymer disc was measured.

Model Substrate Partition Coefficient

Polymers discs equilibrated in 10 mL of phosphate buffered saline at 5.7 and 7.5 pH and 37 C for 24 hours. The volume of the swollen polymer disc was measured as described above. The polymer was transferred to a 10 μg/mL of fluorescein sodium salt in phosphate buffered saline solution prepared at one of the two pH's mentioned above and allowed to equilibrate for 48 hours. Samples from the equilibrium solutions were taken, diluted to a 1:4 ratio and then fluorescence was measured using a Gemini EM Spectra Max (Molecular Devices, Sunyvale, CA) 460 Abs and 515 Em.

Model Substrate Release Profiles

Polymer discs with fluorescein sodium salt incorporated from the partition coefficient experiment were allowed to air dry for 1 day, followed by 1 day in the vacuum oven. The dried polymer discs were transferred to 5 mL of Phosphate Buffered Saline at 7.4 pH that was pre-warmed at 37 ^{o}C and place in the G4 Environmental Incubator Shaker (New Brunswick Scientific, Edison, NJ) at 37 ^{o}C and 50 RPM. At predetermined time intervals, the polymer discs were placed into 5 mL of fresh buffer. The fluorescence of the samples was

measured using a Gemini EM Spectra Max (Molecular Devices, Sunyvale, CA) 460 Abs and 515 Em.

4.4 Results and Discussion

Crosslinked PEG based hydrogels have been proposed for controlled drug delivery applications. All polymers were translucent solids of a flexible nature. Also, as expected, as the length of the tethered chain increased the hydrogels became more rubbery in nature. Finally, the polymers that had monomers with a larger PEG graft chain as compared to the crosslinker could not be polymerized. The only exception was the combination of PEGMA1000/PEGDMA600. This morphology was very brittle. This could be due to localized stress in the hydrogel structure due to the size of the tethered chain (see figure 4.1).

Experiments at the cellular level (which will be discussed with greater detail in the following section) suggested no advantage of the crosslinked hydrogel structures as compared to the lineal morphologies. Therefore it was decided to increase the surface area (i. e. Interactions) by reducing the particle size of the hydrogel. This was achieved by synthesizing the polymer via dispersion polymerization using techniques described by Torres-Lugo (31). This technique yields hydrogel spheres dispersions in the particle range of the hundreds of nanometers. These hydrogel morphologies were useful for the investigation of possible membrane fluidity effects between the polymer and the cellular membrane that will be discussed later in the manuscript.

Hydrogels submicron spheres were first attempted using the PEGDMA 1000 and 600 g/mol crosslinkers to no avail. The resulting dispersions were translucid in nature and the submicronsphere phase could not be observed at plain sight. Upon analysis with the DLS, the particle size of the polymer dispersion was similar to that of the solvent. However, when the monomer/crosslinker percentage was increased to 5% (w/w) using the PEGDMA 1000 crosslinker, the resulting gel dispersion had a consistency similar to that of hair styling gel. The gel was also transluscent in color. From these observations it can be concluded that the solution that consisted of 2% (w/w) monomer/crosslinker was polymerized succesfully, but the submicron spheres were transluscent and could not be observed at plain sight. It was noticed that structures that had more steric hindrance tended to be opaque while structures that were looser were transluscent. It is possible that more compact structures suffered an increase in the refraction index due to the crosslinking, while looser structures could retain an index similar to that of the lineal morphology. Since the refraction index of lineal PEG (1.46) is similar to that of water (1.33), this might explain why they were not observable with the DLS. Similar results were observed when PEGDMA 600 crosslinker was used. Therefore, submicron spheres of PEGMA 1000/PEGDMA 400 and PEGMA 400/PEGDMA 400 were successfully synthesized. The PEGMA 200/PEGDMA 400 had results similar to those synthesized using the PEGDMA 1000 and 600 croslinkers. The particle size distribution is fairly narrow and monodisperse as can be observed on figure 4.3. The difference in particle size between the

PEGMA 400 and 1000 submicron spheres could be due to the fact that the latter has less steric hindrance that could promote particle growth. The particle size decreased and the particle size distribution becomes narrower after dialysis as observed in figure 4.3 and table 4.3. Most likely this is due to the elimination of oligomer chains that were partially crosslinked. As expected, the suspensions provided a good yield (above 50%).

Table 4.3: Particle size, concentration and yield of PEGMA/PEGDMA submicron spheres

Hydrogel	Particle Size before dialysis (nm)	Particle Size after dialysis (nm)	Final Concentration (mg/mL)	Yield (%)
PEGMA 1000/ PEGDMA 400	617.2	525.6	15.2	76
PEGMA 400/ PEGDMA 400	217	128.7	12.5	62

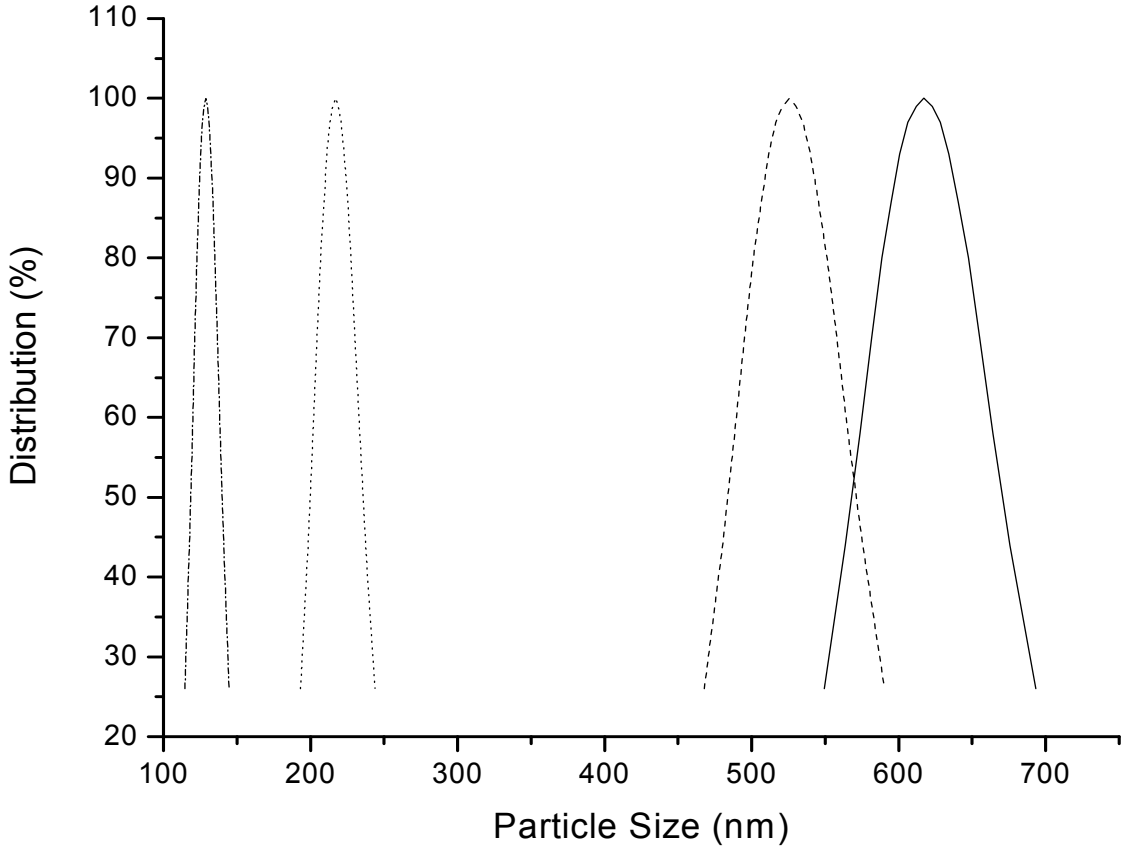

Figure 4.3: Particle size distribution of PEGMA 1000/PEGDMA 400 and PEGMA 400/ PEGDMA 400 sub-micron spheres before and after dialysis as analyzed by dynamic light scattering. The distribution was reported using the number count of particles. ——PEGMA 1000/ PEGDMA 4000 before dialysis, .----- PEGMA 1000 / PEGDMA 4000 after dialysis, ····· PEGMA 400/ PEGDMA 4000 before dialysis, –·– PEGMA 400/ PEGDMA 4000 after dialysis

Equilibrium Volume Swelling Ratio

Swellable hydrogels are premier candidates for controlled drug delivery applications. First, their ability to imbibe waters makes them resemble natural tissues and makes them more biocompatible. Second, they can be used for swelling-controlled delivery devices (20). It is evident that structural parameters associated with the swelling behavior of the gel must be characterized. Since poly(ethylene glycol) is a neutral polymer no pH interaction was expected in the swelling behavior, therefore all experiments were performed at the neutral pH of 7.4.

These hydrogels showed moderate swelling, common in poly(ethylene glycol) hydrogels with an effect of the tethered chain and the crosslinker chain length as evidenced in figure 4.4. There is evidence that lineal chains of PEG imbibe water and swell, which explains the effect of tethered chain length on the swelling of the hydrogels (2, 32). Jo et. al. (33) has presented evidence that short chains of PEG are capable of water uptake. Oligo(Poly(Ethylene Glycol) fumarate macromers were synthesized and characterized. These oligomers were capable of swelling ratios between 5.7 and 16 (swelling ratio reported as grams of water drawn by 1 gram of dry polymer). The swelling increase was only dependent on the molecular weight of the PEG chain.

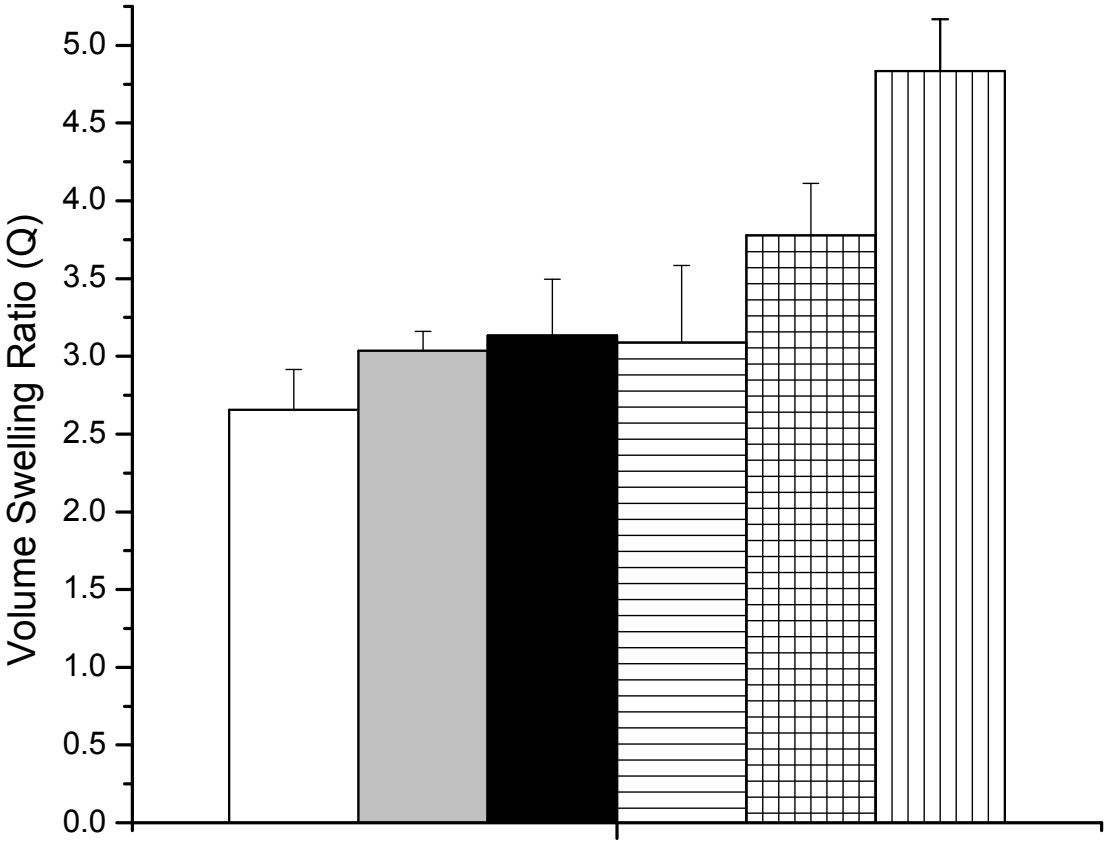

Figure 4.4: The equilibrium swelling ratio of various PEG morphologies at 25 °C and PBS at 7.4 pH. ☐ PEGMA 200/PEGDMA 600, ▩ PEGMA 200/PEGDMA 1000, ■ PEGMA 400/PEGDMA 600, ▤ PEGMA 400/PEGDMA 1000, ▦ PEGMA 1000/PEGDMA 600, and ▥ PEGMA 1000/PEGDMA 1000. Each bar represents an average of 6 observations ± one std. dev.

These hydrogels were characterized by the presence of PEG tethered chains on their structure. The characterization data indicated that these chains greatly affected the behavior of these hydrogels. The incorporation of grafts into a hydrogel and the length of such grafts have been shown to affect the kinetics of polymerization and the structure of the polymer network as observed by Ward (34). The propagation of the gel becomes more diffusion controlled as the length of the graft increases. Also, the structure becomes more heterogeneous with numerous microgel regions as the length of the graft is increased. Also, tethered chains can be used to specifically tailor the gel surface structure, the gel/gel adhesion strength, the equilibrium gel distance and the interface structure as evidenced by Huang (35).

The special interaction of PEG with water appears to lay in its ability to form hydrates in the hydroxyl termination groups as evidenced by Graham (36). Moreover, the interaction of PEG with water seems to be dependent on the chain length of the polymer (19). Many investigators have reported a molecular weight dependency with swelling behavior of PEG hydrogels (32, 37, 38). In a study by Sukumar the swelling of lineal morphologies of PEG and star hydrogels increased with increasing molecular weight (32). Also, in a research by Padmavathi poly(ethylene glycol) diacrylate (PEGDA) hydrogels, the swelling behavior of the hydrogels also increased with the increased molecular weight of the monomer unit (38). The fact that the effect of the chain length was slight may be related to the relatively short chains used by Padmavathi from 200 to 1,000g/mol. Sukumar used chain lengths ranging from 1,000 to

20,0000 g/mol and Padmavathi from 200 to 3,400 g/mol. Crosslinked copolymers composed of poly(metracrylic acid) (PMAA) and PEG tethered chains also showed an increase swelling ratio with increasing PEG tethered chain length (39). However, dynamic swelling studies with shorter PEG chain showed that the copolymers with larger content of PEG had a larger swelling ratio at the early stages of swelling (40). Finally, due to the modest swelling behavior exhibited by PEG hydrogels and the lack of functionality of the polymer major changes in swelling behavior are not expected.

To summarize, it can be concluded that the PEG-rich hydrogels were able to swell at proportions that are comparable with similar structures found in the literature. The composition of the hydrogel had an impact on the swelling capacity of the hydrogel with both the crosslinker length and the tethered chain length contributing to the swelling effect. However, the contribution of the tethered chain is more notable than the crosslinker. This is expected because the tethered chain is responsible for the increase of PEG moieties on the hydrogel structure. The changes were not statistically different due to the modest swelling exhibited by neutral PEG. However, the positive lineal trend cannot be negated and there is a statistical difference between the two morphologies located at the two extremes.

Correlation Length.

The correlation length of an hydrogel indicates the distance between two adjacent crosslinks or tie-points (20). It can also be related to the pore or mesh size of the hydrogel as depicted in figure 4.5. It is a very useful characteristic of the polymer and it can be used to generalize the average size of the particles that can be incorporated into the gel. There are two theories that are used in the literature to characterize the correlation length of a hydrogel. The first one is based in the thermodynamic analysis of Flory-Renher and its subsequent modifications (41). This method has the advantage that the experiments required are fairly simply and no special equipment is needed. The data from this model has been successfully used in the literature with good correlations. The disadvantage of this model is that the analysis of ionic polymers of polymers that form interpolymer complexes becomes much more complex. The complexity arises due to the fact that the model must now consider the interactions between fixed and mobile ions in the gels as well as between mobile ions in the solvent. The second theory is based on rubber elasticity theory (42). This model has the advantage that the analysis of ionic polymers is simplified. However, a tensile testing system is required to calculate the correlation length.

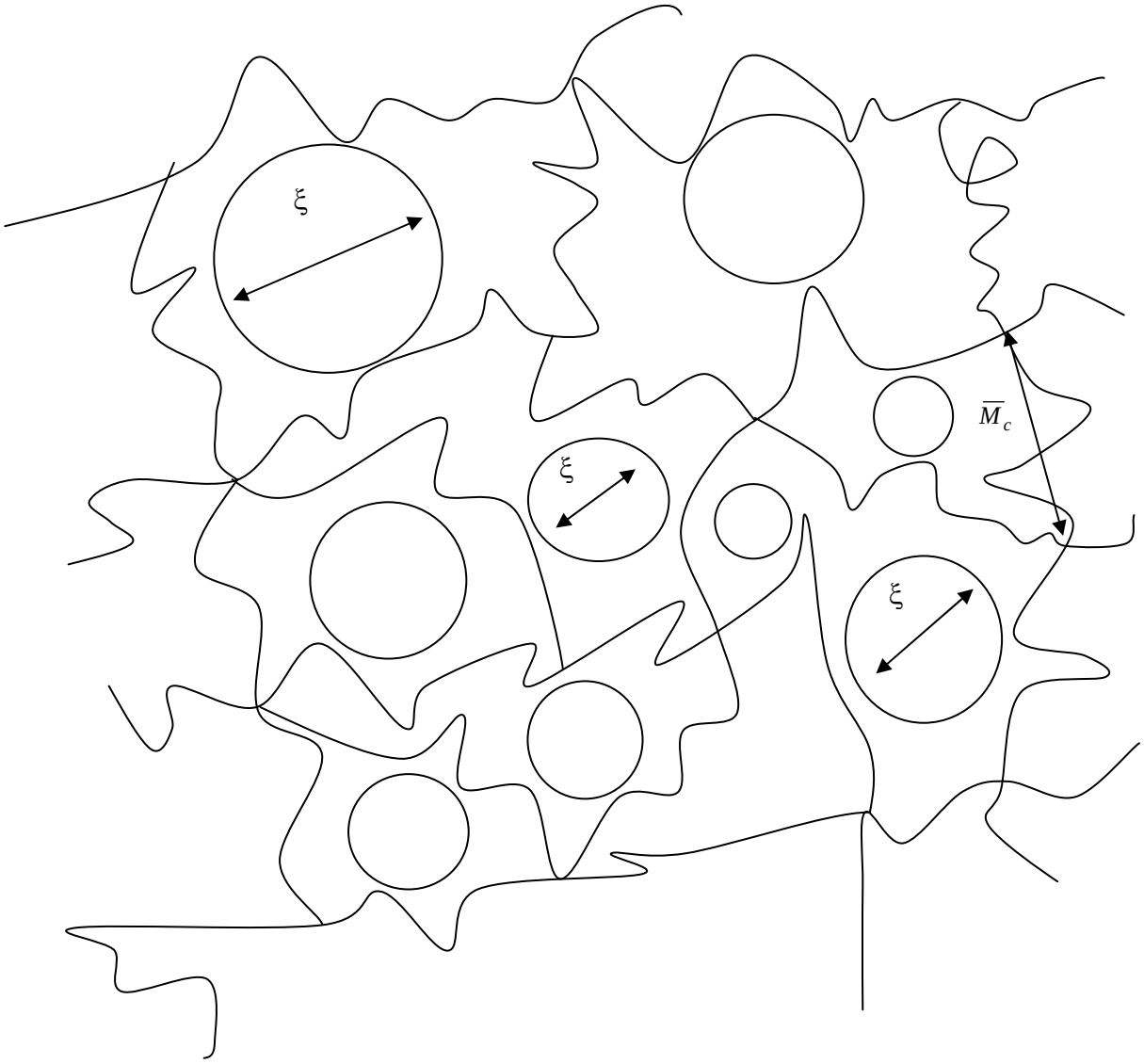

Figure 4.5: Physical interpretation of the correlation length (ξ) and the molecular weight between crosslinks $\overline{M}_c$

Since PEG is a neutral polymer, the thermodynamic model was chosen to calculate the correlation length due to the simplicity of the experiments. Figure 4.6 summarizes the correlation length of the various morphologies. There is no apparent correlation between correlation length and the hydrogel morphology, as would be expected observing the hydrogel swelling data. This may be due to model constraints.

The correlation length is closely tied to the swelling behavior of the polymer by the molecular weight between crosslinks (M_c) and the Flory-Rehner theory. Specifically, M_c represents the stretching of the chains and it is solvent dependent (38). So the tendencies of the correlation length of the hydrogels should mimics the ones observed for swelling. These observations are supported by previous research in which similar tendencies were reported (32, 38). However, the model does not take into account the presence of tethered chains in the backbone polymer as acknowledged by Torres-Lugo (3). Torres-Lugo investigated the swelling behavior of PMAA-g-PEG hydrogels and in that case the effect was not as marked as in the PEG hydrogels in question. PMAA hydrogels exhibited high levels of swelling, while PEG hydrogels have low to moderate swelling; for these low swelling hydrogels the effect of the tethered chain appears to be heightened.

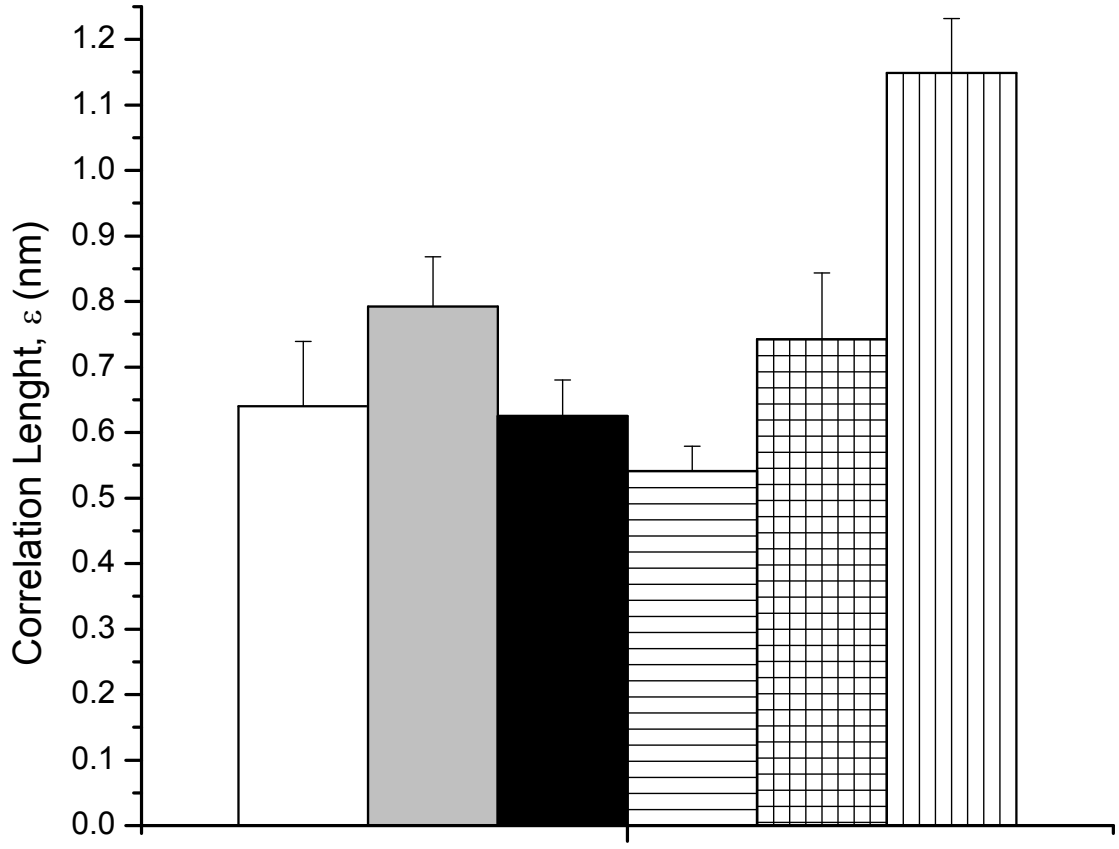

Figure 4.6: Correlation length of various PEG hydrogels at 25C and PBS at 7.4 pH. ☐ PEGMA 200/PEGDMA 600, ▒ PEGMA 200/PEGDMA 1000, ■ PEGMA 400/PEGDMA 600, ▤ PEGMA 400/PEGDMA 1000, ▦ PEGMA 1000/PEGDMA 600, and ▥ PEGMA 1000/PEGDMA 1000. Each bar represents an average of 6 observations ± one std. dev

Another factor that must be taken into consideration is the possibility of entanglements forming and their effect on the M_c. It is important to note that these structures are characterized by the relatively large amount of dangling chains that are more prone to entanglements. Finally, the structure of the hydrogel network may also play a part due to the heterogeneity of the crosslinked regions of these type of hydrogels (34).

To summarize, contrary to expected results there was no observable correlation between the correlation length and the structural parameters of the hydrogel. This was probably due to the fact that the thermodynamic model used to determine the correlation length of the hydrogels does not take into consideration the presence of tethered chains. This serves as further evidence of the impact that these tethered chains can have on the properties of the hydrogel. Since PEG is a hydrogel that experiences moderate swelling, these effects are heightened.

Partition Coefficient of Model Substrate Fluorescein Sodium Salt

The partition coefficient (K_D) is defined as the ratio of concentration of a solute in the two phases of a mixture of immiscible solvents at equilibrium (43). It is a very useful metric with many uses cited in the literature. For example, it has been used to analyze the separation of an impurity from a solvent by analyzing the countercurrent distribution of the solute. It's use has also been reported to analyze the equilibrium constant of reactions. It can also be used to characterize the hydrophilic-lipophilic balance of a system, among others (43). It's use in biomaterials and biomedicine science is related to the dissolution and partitioning of drugs. The partition coefficient data can provide valuable information regarding possible interactions between the drug and the solute. It can also play an important role in the subsequent release of the drug and absorption and distribution in the host.

Figure 4.7 shows the partition coefficient for the PEG hydrogels. The partition of the model substrate fluorescein sodium salt showed the same trend as the mesh size, again probably due to tethered chain effects. Also an interaction was observed at pH's above the pKa of the salt (6.5) probably due to electrostatic repulsion of the salt and the partially negative oxygen present in the ether groups of the chain or the end metharcrylate group. Details of the chemical structures of fluorescein sodium salt and the poly(ethylene glycol) monomer and crosslinker can be seen in figure 4.2.

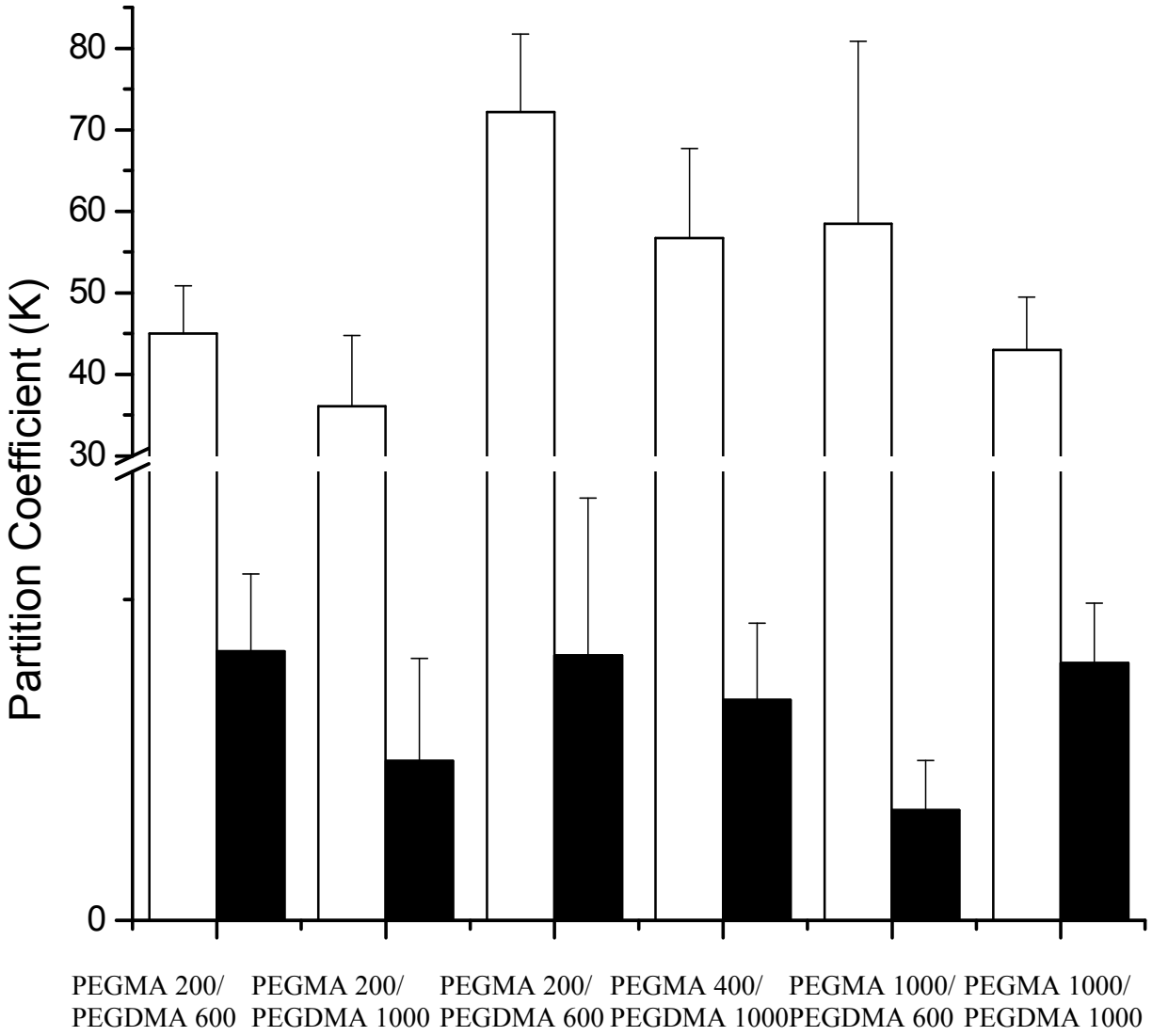

Figure 4.7: Partition coefficient of a 10 μg/mL solution of fluorescein sodium salt in phosphate buffered saline at 25 C in various PEG morphologies at □ 5.7 and ■ 7.5 pH

To better understand the pH variation observed in the partition coefficient, it is important to further explain this phenomenon. Entropic and enthalpic effects influence the partition coefficient of a drug into a hydrogel. An inactive partition is due to the drug dissolving into the hydrogel and locating a free-volume to reside in. On the other hand, active partition is due to attractive or repulsive interactions between drug and the hydrogel. Therefore, it can be stated that the partition coefficient provides affinity information of the drug-hydrogel complex. That said it comes as no surprise that as the pH increases above the pKa the salt becomes ionized providing electrostatic repulsive forces between the salt and the partially positive charged oxygen atoms. Other investigators have observed the effect of repulsive forces on the partitioning of substrates into hydrogels. Fere (44) studied the effects of pH and total polymer concentration on the partition coefficient of lysozyme and bovine serum albumin (BSA) on PEG-water-dextran systems. They concluded that the partition coefficient is a function of both the total polymer concentration and the pH. Huglin studied the effects of the potassium thiocyanate salt on the properties of hydrogels composed of the zwitterionic monomer N,N-dimethyl-N-[(methacryloyloxy)ethyl]-N-(3-sulfopropyl) ammonium betaine (SPE) and the cationic monomer 2-hydroxyethyl methacrylate (HEMA) (45). They concluded that partition coefficient was influenced by the salt concentration (which influenced the repulsion forces) and the monomer composition.

To summarize it can be observed that there is no correlation between the structural parameters of the hydrogel and the partition coefficient a pattern that emulates what was previously observed in the correlation length. This observation further demonstrates the impact that the tethered chains have on the hydrogel characteristics, specially for moderate swelling hydrogels like poly(ethylene glycol). Also there was a strong dependence of partition coefficient and pH providing evidence of electrostatic interaction between the fluorescein sodium salt ions and the partially negative charges of the oxygen atoms. Nevetheless there was an acceptable partition of the dye into the hydrogel, making it suitable for drug release applications.

Release of Model Substrate Fluorescein Sodium Salt

The release of a solute from a swellable material is controlled by two mechanisms; either the rate of relaxation of the polymer chains during the transition from a glassy to a rubbery state or the diffusion of the drug through the rubbery polymer dominates (46). The fundamental solution of this system is very complex due to the numerous phenomena occurring. The differential equations that describe the problem are described below. The transport of the solvent is modeled by (46):

$$\frac{\partial c_1}{\partial t} = \frac{\partial}{\partial x}\left(D_1 \frac{\partial c_1}{\partial x} \right) \qquad [4.26]$$

or by

$$\frac{\partial c_1}{\partial t} = \frac{\partial}{\partial x}\left(D_1 \frac{\partial c_1}{\partial x} - \upsilon c_1 \right) \qquad [4.27]$$

The drug transport is modeled by:

$$\frac{\partial c_2}{\partial t} = \frac{\partial}{\partial x}\left(D_2 \frac{\partial c_2}{\partial x} \right) \qquad [4.28]$$

In the previous equations D_1 and D_2 are the diffusion coefficients of the solvent and the solute respectively, and $c_1$and c_2 are the concentrations of the solvent and the solute respectively, υ is the convective velocity of water, t is time and x is position. Usually D_1 and D_2 are functions of c_1 and sometimes c_2. Therefore, the problem consists of coupled differential equations with moving boundary conditions. The solution is usually attained using numerical methods.

In an attempt to simplify the solution of the release profiles of swellable hydrogels several alternatives have been proposed. For example various dimensionless numbers have been proposed to explain the phenomena. Among them the most important is the Deborah number (De) proposed by Vrentas (47).

$$De = \frac{\lambda}{\theta} \qquad [4.29]$$

here, λ is the relaxation time and θ is the diffusion time. If De >>1 the transport is completely relaxation controlled, if De << 1 it is completely diffusion control. Finally, if De ~1 anomalous diffusion behavior is observed. Several phenomelogical models have been proposed. Among them the power law model analyzed in depth by Ritger (28) and first used in controlled release polymers by Korsmeyer (27) is the most relevant. This was the method chosen to analyze the release profiles of fluorescein sodium salt from the various hydrogel. The advantage of this model is that is very simple to use and provides remarkable adjustment to the theoretical data.

Figure 4.8 shows an amplification of the release of fluorescein sodium salt up to 10 hours. This data shows and increase in the rate of release of fluorescein sodium salt with increasing tethered chain length. Upon further observation of the graph follows a curved pattern resembling an S, this indicative of anomalous release dynamics. This is corroborated by fitting data to equation [4.17]. According to table 4.4 most of the hydrogels have an n value indicative of anomalous behavior with the exception of PEGMA 1000/PEGDMA 1000 whose behavior most closely resembles super case II dynamics.

The release of Fluorescein sodium salt model substrate from PEG hydrogels showed a direct effect from the length of the tethered chain to the release mechanism of the model substrate, as observed in Table 6. As the length of the tethered chain is increased, the mechanism changes from almost Fickian to Case II transport. This suggests that these chains are having a whipping effect in helping the release of the substrate. It is expected that these chains provide more mobility to the hydrogel because they are only attached to the network at one end. This mobility of the tethered chain is not expected to be restricted by the repulsive force of crosslinking, hence providing an increased diffusion profile. The only exception is the PEGMA 1000/ PEGDMA 600 morphology.

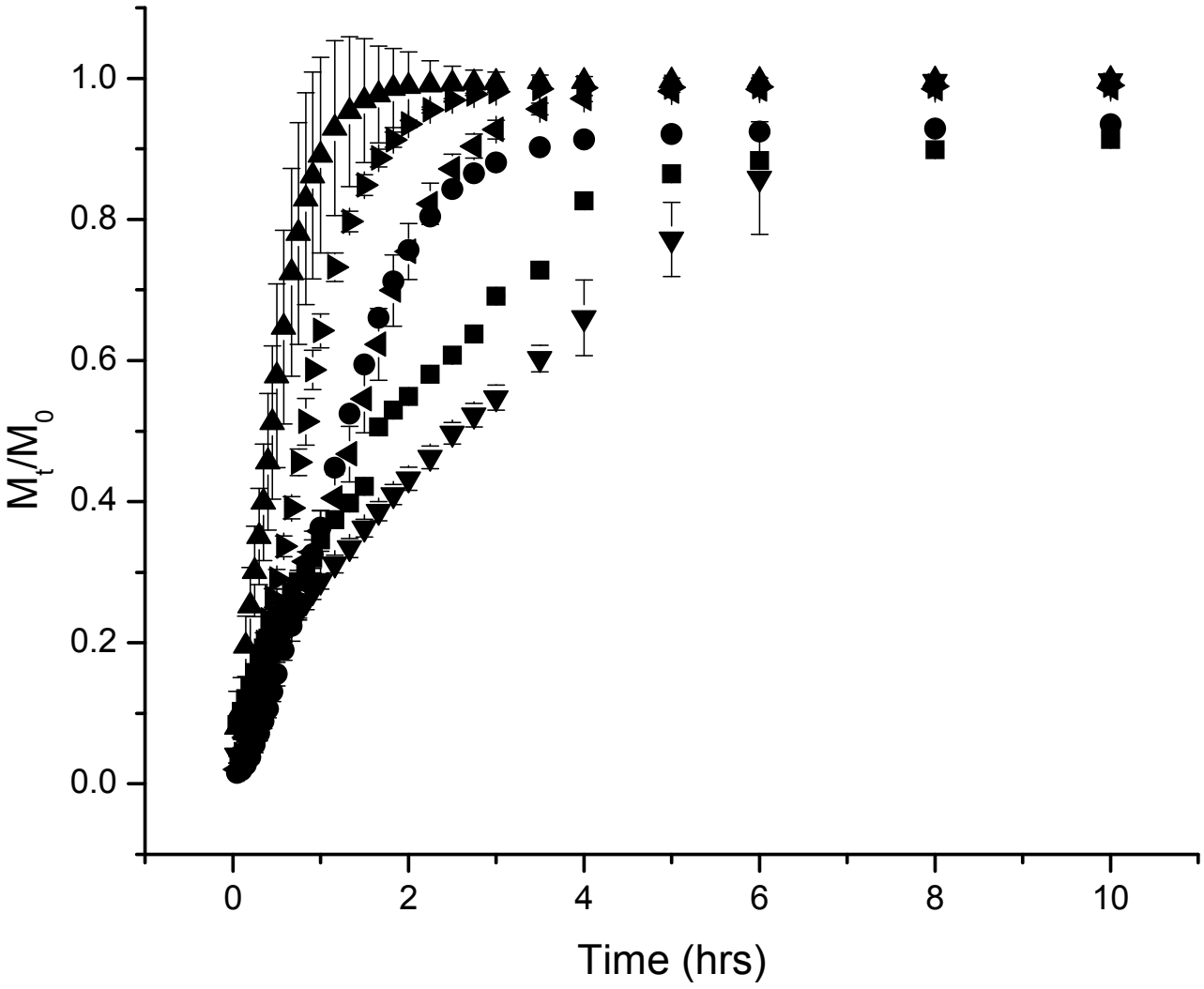

Figure 4.8: Release dynamics of fluorescein sodium salt into phosphate buffered solution at 37 C, 7.4 pH and 50 RPM, up to 10 hours of release. ■PEGMA 200/PEGDMA 600, ▼ PEGMA 200/PEGDMA 1000, ● PEGMA 400/PEGDMA 600, ◀ PEGMA 400/ PEGDMA 1000, ▲PEGMA 1000/PEGDMA 600, and ▶PEGMA 1000/PEGDMA 1000. Each point represents an average of 3 observations ± one std. dev.

Table 4.4: Fluorescein sodium salt diffusion parameters from various PEG hydrogels into phosphate buffered solution at 37 ºC, 7.4 pH and 50 RPM, using 95% confidence interval statistics

Hydrogel	n	D $*10^9$ (cm/s)	k_0 10^5 (mg*cm/s)
PEGMA 200/PEGDMA 600	0.60 ± 0.014	1.68 ± 0.022	0.50 ± 0.06
PEGMA 400/PEGDMA 600	0.79 ± 0.034	91.06 ± 1.35	3.68 ± 0.45
PEGMA 1000/PEGDMA 600	0.69 ± 0.015	28.19 ± 0.25	2.05 ± 0.19
PEGMA 200/PEGDMA 1000	0.59 ± 0.0026	2.45 ± 0.04	0.6 ± 0.08
PEGMA 400/PEGDMA 1000	0.88 ± 0.015	34.28 ± 0.059	2.25 ± 0.09
PEGMA 1000/PEGDMA 1000	1.14 ± 0.017	158 ± 0.063	4.85 ± 0.10

However, this morphology suffers from serious steric hindrance constraints that could block the free movement of the tethered chains therefore minimizing their effect. The reduced crosslinker length could be acting as a repulsion force that could result in less mobility of the tethered chains. This phenomenon is observed in numerous instances as this morphology also suffers from a reduced correlation length and partition coefficient.

Hydrogels whose structure lacked the presence of PEG dangling chains the release of a solute has been mostly due to Fickian contributions, although some relaxation controlled effects are observed (48, 49). The tethered chain effect was observed by other investigators, for example El-Sherbiny (50) using graft copolymers and hydrogels based on poly(ethylene glycol) and chitosan. As the extent of grafted poly(ethylene glycol) was increased, higher percentages of drug were released. However, copolymers based in PMAA and PEG did not show a correlation between the diffusion properties and the length

of the PEG tethered chain (39). PMAA hydrogels are characterized by high swelling ratios and relaxation controlled release profiles. The results suggest that the relaxations contributions due to the PMAA are stronger than those due to PEG. Therefore the effects due to the length of the PEG tethered chains was not observed.

In summary, the release profile of fluorescein sodium salt was strongly affected by the structural parameters of the hydrogel. In particular the length of the tethered chain appeared to be providing a whipping effect that resulted in an increased release profile. Therefore, the structure of the hydrogel is an important parameter that is crucial to its characteristics and must be taken into consideration during the hydrogel design. It is important to stress that these effects are easily observable on the PEG hydrogels due to its low swelling capability that heightens the effects of the tethered chains.

4.5 Conclusions

New hydrogel morphologies based on poly(ethylene glycol) have been synthesized and characterized. These morphologies were created with the objective of using them to design controlled drug delivery devices that are capable of inhibiting the MDR and MRP proteins. Therefore, these devices will have the potential of improving the bioavailability of the MDR and MRP substrates. Two design controlled variables were studied: (i) the length of the PEG tethered chain, and (ii) the length of the crosslinker length. The hydrogels were characterized for several properties that are important in the design of

swellable controlled delivery devices such as, swelling ratio, correlation length, partition coefficient, and release profile of a model drug.

These hydrogel morphologies are characterized by the presence of PEG tethered chains in their structure. These chains have proven to play a major role in the molecular structure of the hydrogel network. It affected all the major properties like the swelling ratio, correlation length and most importantly the release of the model drug. During the release of the model drug, the PEG tethered chains appeared to have a whipping effect that aided in the release of the model drug. It is important to note that the effect of these tethered chains is easily observed in these hydrogels due to the limited swelling behavior of the hydrogel. Studies performed with hydrogels with greater swelling capacity fail to observe the contributions of the tethered chains to the molecular structure of the hydrogel network.

These hydrogels have a moderate swelling behavior as expected, which does not make them particularly attractive for controlled drug delivery devices. However, the swelling behavior can be modified by co-polymerizing with hydrogels that have a larger swelling ratio behavior like for example poly(methacrylate acid) (PMAA). PMAA is particularly interesting because it has calcium chelating properties that can aid in the transport of ionic drugs and it has demonstrated pH sensitive swelling behavior as well. The MDR inhibiting properties of PEG provides a strategically advantage over other hydrogel. Therefore, PEG-rich hydrogel can be construed as potential candidates for controlled drug delivery devices of MDR and MRP drug substrates.

4.6 References

1. R. C. Rowe, P. J. Sheskey, and S. C. Owen. *Handbook of Pharmaceutical Excipients*, Pharmaceutical Press and American Pharmacist Association, London, 2006.
2. J. M. Harris. *Poly(ethylene glycol) Chemistry. Topics in Applied Chemistry*, New York Plenum Press, 1992.
3. M. Torres-Lugo and N. Peppas. Molecular Design and in Vitro Studies of Novel pH Sensitive Hydrogels for Oral Delivery of Calcitonin. *Macromolecules* **32**: 6646-651 (1999).
4. S. S. Vinogradov, T. K. Bronich, and A. V. Kabanov. Nanosized cationic hydrogels for drug delivery: preparation, properties and interactions with cells. *Advanced Drug Delivery Reviews* **54**: 135-147 (2002).
5. C. Monfardini, O. Schiavon, P. Calicet, M. Morpurgo, J. M. Harris, and F. M. Veronese. A Branched Monomethoxypoly(ethylene glycol) for Protein Modification. *Bioconjugate Chemistry* **6**: (1995).
6. M. Miralles, J. McGinity, and A. Martin. Combined water-soluble carriers for coprecipitates of tolbutamide. *Journal of Pharmaceutical Science* **71**: 302-304 (1982).
7. C.-W. Changa, D. Choib, W. J. Kima, J. W. Yockmana, L. V. Christensena, Y.-H. Kimc, and S. W. Kima. Non-ionic amphiphilic biodegradable PEG–PLGA–PEG copolymer enhances gene delivery efficiency in rat skeletal muscle. *Journal of Controlled Release* **118**: 245-253 (2007).
8. E. V. Batrakova, S. Li, D. W. Miller, and A. V. Kabanov. Pluronic P85 Increases Permeability of a Broad Spectrum of Drugs in Polarized BBMEC and Caco-2 Cell Monolayer. *Pharmaceutical Research* **16**: 1366-1372 (1999).
9. E. Batrakova, S. Li, W. Elmquist, D. Miller, V. Alakhov, and A. Kabanov. Mechanism of sensitization of MDR cancer cells by Pluronic block copolymers: Selective energy depletion. *British Journal of Cancer* **85**: 1987–1997 (2001).
10. U. G. Spizzirri and N. A. Peppas. Structural Analysis and Diffusional Behavior of Molecularly Imprinted Polymer Networks for Cholesterol Recognition. *Chemistry of Materials* **17**: 6719-6727 (2005).
11. A. D. Ascentiis, J. L. deGrazia, C. N. Bowman, P. Colombo, and N. A. Peppas. Mucoadhesion of poly(2-hydroxyethyl methacrylate) is improved when linear poly(ethylene oxide) chains are added to the polymer network. *Journal of Controlled Release* **33**: 197-201 (1995).
12. J. Hao and X. Deng. Semi-interpenetrating networks of bacterial poly(3-hydroxybutyrate) with net-poly(ethylene glycol). *Polymer* **42**: 4091-4097 (2001).

13. S. S. Kim, Y. M. Lee, and C. S. Cho. Synthesis and properties of semi-interpenetrating polymer networks composed of b-chitin and poly (ethylene glycol) macromer. *Polymer* **36**: 4497-4501 (1995).
14. R. C. Hedden and B. J. Bauer. Structure and Dimensions of PAMAM/PEG Dendrimer-Star Polymers. *Macromolecules* **36**: 1829-1835 (2003).
15. R. C. Hedden, B. J. Bauer, A. P. Smith, F. Gröhn, and E. Amis. Templating of inorganic nanoparticles by PMAM/PEG dendrimer-star polymers. *Polymer* **43**: 5473-5481 (2002).
16. E. W. Merrill. Poly(ethylene oxide) star molecules: synthesis, characterization and applications in medicine and biology. *Journal of Biomaterial Science Polymer Edition* **5**: 1-11 (1993).
17. Y. H. Choe, C. D. Conover, D. Wu, M. Royzen, Y. Gervacio, V. Borowski, M. Mehlig, and R. B. Greenwald. Anticancer drug delivery systems: multi-loaded N4-acyl poly(ethylene glycol) prodrugs of ara-C. II Efficacy in ascites and solid tumors. *Journal of Controlled Release* **79**: 55-70 (2002).
18. Anonymous. Topical PEG in burn oinments. *FDA Drug Bulletin* 25-26 (1982).
19. J. M. Harris, Zalipsky, S. *Poly(ethylene glycol) Chemistry and Biological Applications.*, American Chemical Society, Washington, DC, 1997.
20. N. A. Peppas, Y. Huang, M. Torres-Lugo, J. H. Ward, and J. Zhang. Physicochemical Foundations and Structural Design of Hydrogels in Medicine and Biology. *Annual Reviews of Biomedical Engineering* **2**: 9-29 (2000).
21. C. M. Hassan, F. J. D. III, and N. A. Peppas. Dynamic Behavior of Glucose-Responsive Poly(methacrylic acid-g-ethylene glycol) Hydrogels. *Macromolecules* **30**: 6166-6173 (1997).
22. J. M. Brake, M. K. Daschner, and N. L. Abbott. Formation and Characterization of Phospholipid Monolayers Spontaneously Assembled at Interfaces between Aqueous Phases and Thermotropic Liquid Crystals. *Langmuir* **21**: 2218-2228 (2005).
23. J. Zhang and N. A. Peppas. Synthesis and Characterization of pH- and Temperature-Sensitive Poly(methacrylic acid)/Poly(N-isopropylacrylamide) Interpenetrating Polymeric Networks. *Macromolecules* **33**: 102-107 (2000).
24. P. J. Flory. Statistical Mechanics of Swelling of Network Structures. *Journal of Chemical Physics* **18**: 108-111 (1950).
25. N. A. Peppas, P. Buresa, W. Leobandunga, and H. Ichikawa. Hydrogels in pharmaceutical formulations. *European Journal of Pharmaceutics and Biopharmaceutics* **50**: 27-46 (2000).
26. A. R. Berens and H. B. Hopfenberg. Diffusion and Relaxation in Glassy Polymer Powders:2. Separation of Diffusion and Relaxation Parameters. *Polymer* **19**: 489-496 (1978).

27. R. W. Korsmeyer and N. A. Peppas. Effect of the Morphology of Hydrophilic Polymeric Matrices on the Diffusion and Release of Water Soluble Drugs. *Journal of Membrane Science* **9**: 211-227 (1981).
28. P. L. Ritger and N. A. Peppas. A simple equation for description of solute release I. fickian and non-fickian release from non-swellable devices in the form of slabs, spheres, cylinders or discs. *Journal of Controlled Release* **5**: 23-36 (1987).
29. N. A. Peppasand L. Brannon-Peppas. Water Diflbsion and Sorption in amorphous macromolecular Systems and Foods. *Journal of Food Engineering* **22**: 189-210 (1994).
30. N. A. Peppas and L. Brannon-Peppas. Water Diflfusion and Sorption in Amorphous Macromolecular Systems and Foods. *Journal of Food Engineering* **22**: 189-210 (1994).
31. M. Torres-Lugo. Physicochemical Behavior and Cellular Interactions of Novel Oral Calcitocin Delivery Systems, *Chemical Engineering Department*, Vol. PhD, Purdue University, West Lafayette, IN, 2001.
32. V. S. Sukumar and S. T. Lopina. Network Model for the Swelling Properties of End-Linked Linear and Star Poly(ethylene oxide) Hydrogels. *Macromolecules* **35**: 10189-10192 (2002).
33. S. Jo, H. Shin, A. K. Shung, J. P. Fisher, and A. G. Mikos. Synthesis and Characterization of Oligo(poly(ethylene glycol) fumarate) Macromer. *Macromolecules* **34**: 2839-2844 (2001).
34. J. H. Ward, K. Furman, and N. A. Peppas. Effect of Monomer Type and Dangling End Size on Polymer Network Synthesis. *Journal of Applied Polymer Science* **89**: 3506–3519 (2003).
35. Y. Huang, I. Szleifera, and N. A. Peppas. Gel–gel adhesion by tethered polymers. *Journal of Chemical Physics* **114**: 3809-3816 (2001).
36. N. B. Graham, N. E. Nwachuku, and P. J. Walsh. Interaction of poly(ethylene oxide) with solvents: 1 Preparation and swelling of a crosslinked poly(ethylene oxide) Hydrogel. *Polymer* **23**: 1345 (1982).
37. M. Iza, G. Stoianovici, J. Viora, J. L. Grossiord, and G. Couarraze. Hydrogels of poly(ethylene glycol): mechanical characterization and release of a model drug. *Journal of Controlled Release* **52**: 41 (1998).
38. N. C. Padmavathi and P. R. Chatterji*. Structural Characteristics and Swelling Behavior of Poly(ethylene glycol) Diacrylate Hydrogels. *Macromolecules* **29**: 1976-1979 (1996).
39. B. Kim and N. A. Peppas. Poly(Ethylene Glycol)-Containing Hydrogels for Oral Proteins Delivery Applications. *Biomedical Microdevices* **5**: 333-341 (2003).
40. L. Serra, J. Domenech, and N. A. Peppas. Design of poly(ethylene glycol)-tethered copolymers as novel mucoadhesive drug delivery systems. *European Journal of Pharmaceutics and Biopharmaceutics* **63**: 11–18 (2006).
41. P. J. Flory and J. John Rehner. Statistical Mechanics of Crosslinked Polymer Networks: II Swelling. *Journal of Chemical Physics* **11**: 521-526 (1943).

42. A. M. Lowman and N. A. Peppas. Molecular analysis of interpolymer complexation in graft copolymer networks. *Polymer* **41**: 73–80 (2000).
43. A. Leo, C. Hansch, and D. Elkins. Partition coefficients and their uses. *Chemical Reviews* **71**: 525 - 616 (1971).
44. L. Fele and M. Fermeglia. Partition Coefficients of Proteins in Poly(ethylene glycol) + Dextran+ Water at 298 K. *J. Chem. Eng. Data* 331-334 (1996).
45. M. B. Hughlinand J. M. Rego. Influence of a Salt on the Properties of Hydrogels of 2-Hydroxyethyl Methacrylate with a Sulfobetaine Comonomer. *Macromolecules* **26**: 3118-3126 (1993).
46. B. Narasimhan and N. Peppas. *Controlled Drug Delivery*, ACS Symposium Series, Washington DC, 1997.
47. J. S. Vrentas, C. M. Jarzebskil, and J. L. Duda. A Deborah Number for Diffusion in Polymer-Solvent Systems. *AlChE Journal* **21**: 894-905 (1975).
48. A. W. Watkins and K. S. Anseth. Investigation of Molecular Transport and Distributions in Poly(ethylene glycol) Hydrogels with Confocal Laser Scanning Microscopy. *Macromolecules* **38**: 1326-1334 (2005).
49. G. V. N. Rathna. Hydrogels of Modified Ethylenediaminetetraacetic Dianhydride Gelatin Conjugated with Poly(ethylene glycol) Dialdehyde as a Drug-Release Matrix. *Journal of Applied Polymer Science* **91**: 1059–1067 (2004).
50. I. M. El-Sherbiny, E. M. Abdel-Bary, and D. R. K. Harding1. Swelling Characteristics and In Vitro Drug Release Study with pH- and Thermally Sensitive Hydrogels Based on Modified Chitosan. *Journal of Applied Polymer Science* **102**: 977–985 (2006).

5.0 The Use of Caco-2 Cell Model to Study the Effects of PEG-Rich Matrices on the Transport of MDR and MRP Substrates

5.1 Introduction

These days drugs need to be subjected to rigorous characterization before they can be approved for human use. The aim of these trials is to provide in depth information regarding the structure, biochemistry, mechanism of action, toxicity, and dosage information before human clinical trials can commence. Information such as the toxicity and mechanism of action are typically obtained from animal experiments. In recent years, the use of mammalian cell culture *in vitro* has emerged as alternative to animal testing. This technique has been well received amongst the scientific community because it offers several advantages: 1) rapid evaluation of drug transport and behavior; 2) detailed examination of the possible mechanisms of drug transport under a controlled environment; 3) complete assessment of possible delivery carriers; 4) use of human cells rather than animals; and 5) reduced time and expenses (1). Cell culture cannot completely substitute animal experimentation because some data like possible interactions, clearance mechanisms, and fatal doses can only be obtained from animals.

The Caco-2 cell model is currently one of the best characterized and most commonly used cell system for modeling drug transport. This model uses human colon adenocarcinoma clones which exhibit many characteristics of the human small intestinal epithelium. However, they have been reported to retain

some of the characteristics of the colonic epithelium, specifically the tight junctions (2). The model offers several advantages as compared to other cell lines such as: 1) the ability to differentiate spontaneously; 2) reach confluence in 6-8 days; 3) forms tight junctions; 4) form brush border enzymes with comparable activity to the ones found in the small intestine; 5) expression of several active and ion transport mechanisms, including MDR1 and MRP's; 6) development of mircrovilli; 7) mature intact cell monolayers characterized by a discreet transepithelial electrical resistance (TEER), 8) ability to use pharmacological agents to probe the mechanistic of uptake and transport at the molecular level, 9) allows studies that separate the overall transport process into the individual uptake and efflux steps and 10) good correlation with oral absorption *in vivo* (1, 3-5).

Among the advantages of the Caco-2 cell model there are several that are of particular interest for the assessment of multidrug resistance mechanisms. The formation of tight junctions is important to reduce paracellular permeation and promote transcellular permeation and MDR interactions. This cellular property can be easily verified using TEER measurements. Most important Caco-2 cells have been characterized and demonstrated to express most of the multidrug resistance associated proteins including MDR1, and MRP1-6 (6, 7). Also, the protein expression correlates well with *in vivo* data, which allows for possible extrapolation of results. This allows the study of several transport mechanism and possible interactions using one cell line, as opposed to other cell lines such as MCF-7 and MCDK-II.

Finally, the historical data of Caco-2 cell model for multidrug resistance transport interaction is unsurpassed by any other cell line.

The disadvantages of this model is that properties of these monolayers tends to vary within laboratories due to external factors like passage number, time in culture, extracellular support (filter), and cell culture medium (2), as best described in table 5.1. Also, this cell line lacks the ability to produce mucus, which is present in the intestinal epithelium. The disadvantages of the model can be easily overcome. For example, since the variability of the model is well known the external factors must be maintained as constant as possible. Finally, since the main objective of this work is to study the interactions between the poly(ethylene glycol) and the MDR and MRP proteins, the lack of mucus layer of the model is not regarded as significant.

Table 5.1: Factors that affect transport measurements of CaCo-2 cell model (2).

Factor	Parameter affected
Source of cells, passage number	Intactness of monolayer, expression of endogenous transporters
Incubation medium for cell growth and maintenance	Time to confluency, expression of endogenous transporters
Type of transport unit	Cost, amount of test compound needed, adsorption
Composition and porosity of filter in transport unit	Adsorption, free diffusion of solutes
Use of extracellular matrix coating on filter	Characteristics of monolayer and matrix secreted by cells
Length of time cells grown on filters	Maturity of monolayer, tight junctions
Size of transport unit filter (area in cm^2)	Number of cells needed, cost of unit, amount of test compound needed, amount of transport measured
Buffer volume in apical and basolateral chambers	Amount of test compound needed, dilution factor which impacts analytics
Composition of transport buffer	Cost, efficiency, ease of use, analysis, experimental flexibility
PH of transport buffer	Experimental flexibility
Time and temperature	Experimental flexibility
Mixing or stirring apparatus	Unstirred boundary layer effects

5.2 Background

5.2.1 Analysis of Drug Resistance using Mammalian Cell Culture Models

In general, three mechanisms to inhibit multidrug resistance proteins have been identified. The first involves the blocking of the drug binding site by competitive, non-competitive or allosteric means. This is the most common type of inhibition. It has been proposed that the mechanism of interaction of these inhibitors is that the inhibitor is "flipped" by MDR1 and then "flops" back into the inner leaflet of the membrane. This creates a large difference between the rate of efflux of the substrate and the inhibitor, preventing the efflux of the substrate. The second involves the interference with the ATP hydrolysis. This mechanism requires lower doses to produce inhibition effects; but, the mechanics are not well understood. The last is due to alteration of the integrity of the cell membrane. The cellular membrane is composed of a bilayer of phospholipids. Membrane fluidity is related to the spatial arrangement of these phospholipidis (8). Under this category, surfactants are emerging as a different class of inhibitors. The hypothesis is that they change the fluidity of the cell membrane, thus facilitating the influx of substrates. There are contradictory findings regarding this area. Researchers have classified surfactants as active or inactive depending on their inhibition effects. So far only non-ionic polyethoxylated surfactants are considered active (10-13). There is at least one report of decreased membrane fluidity with an inhibition effect, contrary to

the observation by other researchers (11). Furthermore, it is not clear if other events like inhibitor-protein interactions are taking place as well (10, 11).

Several *in-vivo*, *in-situ* and *in-vitro* techniques are available to screen substances for their ability to inhibit multidrug resitance proteins. The most commonly used are transport assays. This technique uses cell cultured monolayers. The ratio of the permeability of known substrates in the basolateral (B) to apical (A) direction and the apical to basolateral direction is compared in the presence and absence of inhibitors. Due to the concentration dependence of active efflux, B-A permeability decreases while A-B permeability increases until the ratio approaches unity as the dose of the inhibitor is increased. This metric is known as the efflux ratio and is usually used specifically for MDR1 inhibition. Calculating the concentration that gives 50% of the maximum inhibition of a known MDR1 substrate (IC50) can be used to evaluate the potency of an inhibitor. The relative potency of inhibitors can be assessed by competitive assays performed using know specific inhibitors [for example LY335979 for MDR1(14)]. An alternative to assess the potency of the inhibitor is to conduct drug accumulation assays. In this case, the amount of substrate taken up by the cell is compared in the presence and absence of inhibitors. To have a better understanding of transport due to active efflux, drug efflux assays are recommended. Here the cells, cell monolayers, membrane vesicles, or MDR1 reconstituted proteoliposomes are preloaded with the substrate and the transport to the surrounding medium is studied.

A drug accumulation assay that has received much attention lately involves the use of calcein acetomethyl ester (calcein AM (9)). This compound is non-fluorescent, lipophilic and diffuses into the cytoplasm. Once, inside the cell it is converted into calcein that is hydrophilic and fluorescent. Calcein AM is efflux by MDR1 and MRP and the concentration of fluorescent calcein inside the cell decreases. The concentration of calcein inside the cell can be used to quantify the potency of the inhibitor.

Another alternative is to perform ATPase assay, which can be performed using cell membranes, cultured cells, and membrane vesicles. ATPase activity is determined as the difference of ATP consumed in the presence and absence of inhibitors. Vandate is used as a marker for complete multidrug resistance inhibition because it completely abolishes ATPase activity by trapping ADP and forming the ternary complex ADP·Vi (ADP/vanadate induced) in one of the nucleotide biding domains (9, 15). Quantifying ATP, ADP or inorganic phosphate is used to measures ATPase activity. There are several disadvantages associated with this method. For example, it indirectly estimates efflux transport, and does not provide data on the kinetics of drug transport or inhibition. Finally, it is difficult to distinguish between modulator and inhibitors because typically, inhibitors do not activate ATPase while modulators do (9).

On this particular work, transport experiments were chosen to assess the possible inhibitory effects of PEG-rich hydrogels. This technique provides a direct measurement of drug efflux contrary to what can be expected from ATPase or Calcein AM assays. It also provides flexibility to perform these

experiments with varying conditions like direction of transport, temperature and inhibitor concentrations. This flexibility allows for a better understanding of the inhibition effects and can provide hints as of possible mechanisms that might be taking place.

5.2.2 Epithelial Cells

Transport through Caco-2 cell monolayers was chosen as the experimental set up to determine the possible inhibitory effects of poly(ethylene glycol) rich hydrogels. In order to understand the inhibition phenomenon it is important to understand the physiological aspects of the cell. To this end, this section will focus on the description of their morphology, structure, and role within the human body.

The human body is composed of over 200 different cell types. These cells are organized into tissues that in turn form organs. A group of organs form a body system. The four major tissue categories are epithelial, muscle, connective, and nerve (16). Epithelial cells and tissues comprise about 60% of the human body (17). By definition, these cells are those that cover the internal and external surfaces of the body. Epithelial cells almost always rest on a bed of connective tissue. A schematic representation of a typical epithelial cell can be observed in figure 5.1.

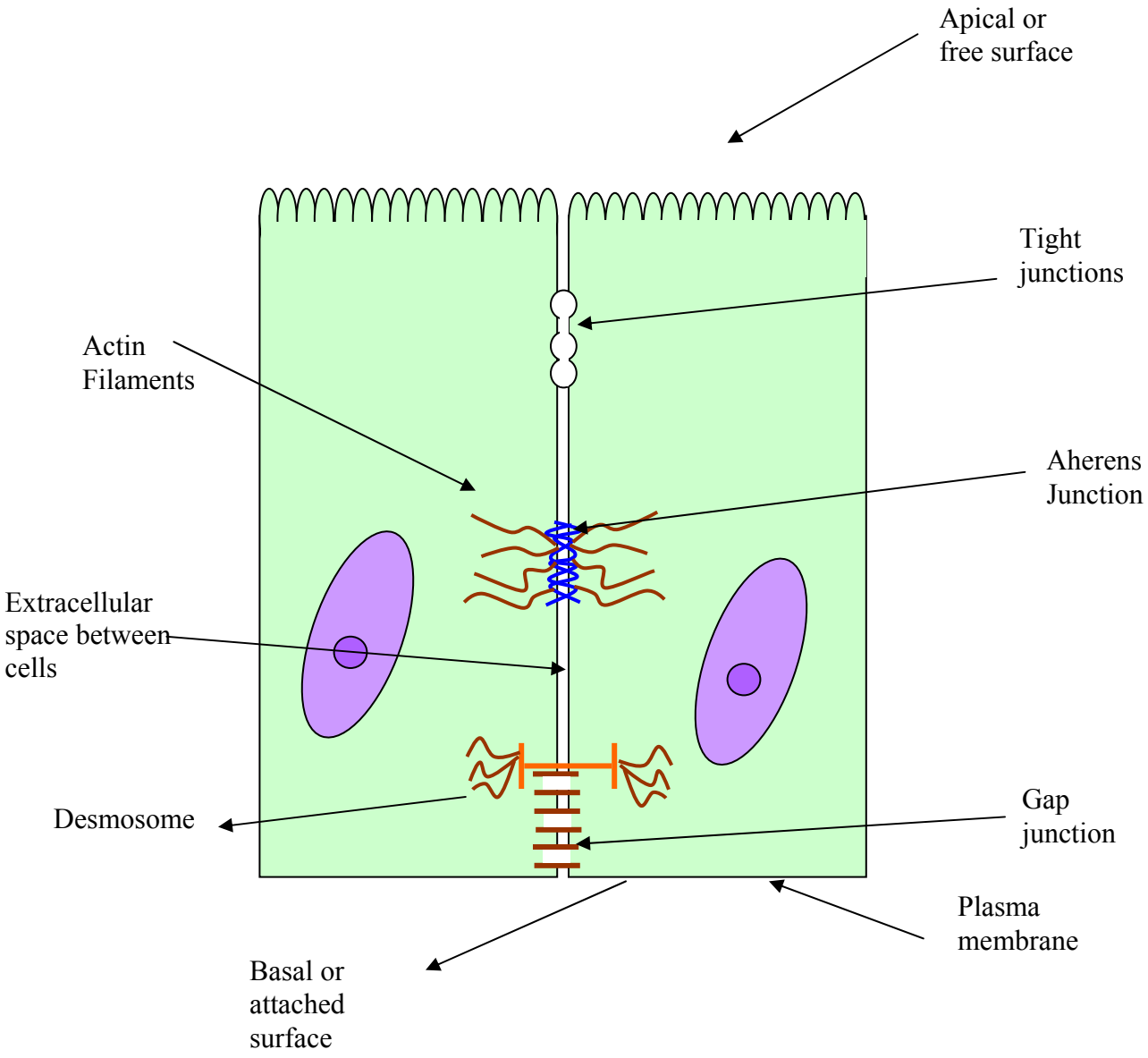

Figure 5.1: Schematic representation of an epithelial cell. Epithelial cells are composed of numerous structures including tight junctions, adherens junctions, desmosome, plasma membrane, gap junctions, and apical and basal surfaces (18).

Epithelial cells can be classified according to their structure, arrangement and, function. The structure of these cells can be classified as columnar, cuboidal, polygonal, irregular, squamous, and ciliated. They can be arranged in transitional to pseudo-stratified and stratified structures. They can also be arranged as monolayers. Finally, their functions can be protective, absorptive or secretory (17). Caco-2 cells are classified as absorptive columnar cells arranged in monolayers. It is important to note that Caco-2 cells have microvilli, which is an important structure for their absorptive function. The most common epithelial barriers for drug transport in the human body are: 1) intestinal and rectal mucosa; 2) buccal and sublingual mucosa; 3) nasal mucosa; 4) keratyoncytes of the epidermis; and 5) corneal cells (1). Table 5.2 summarizes the classification structure for these cells (17).

Table 5.2: Classification according to function, arrangement and structure of the most common epithelial cell barriers for drug transport (17).

Route	Function	Arrangement	Structure
Corneal	protective	stratified	polygonal squamous
Nasal	Absorptive Secret protective	Stratified Pseudo-stratified	Squamous Ciliated
Pulmonary			
(i)bronchi bronchioles	Protective Secrete	Pseudo-stratified	Ciliated Goblet Cuboidal Clara
(ii) alveoli	absorptive	monolayer	squamous
Buccal	protective	stratified	Squamous
Small Intestine	Absorptive Secret Endocrine M-cells	monolayer	Columnar paneth
Large Intestine	Absorptive Secrete	monolayer	Columnar
Vaginal	protective	stratified	squamous
Skin	protective	stratified	squamous

5.2.3 Passive transport across epithelial cells

Once the structure and function of the Caco-2 cells is well understood the next step is to understand the mechanism for drug transport across these cell monolayers. Transport across epithelial cells can occur by two main mechanisms. The first is passive transport, which occurs in favor of the concentration gradient (downhill). The second is active transport, which can occur against the concentration gradient (uphill), and requires energy to occur (3). The transport routes are summarized in figure 5.2.

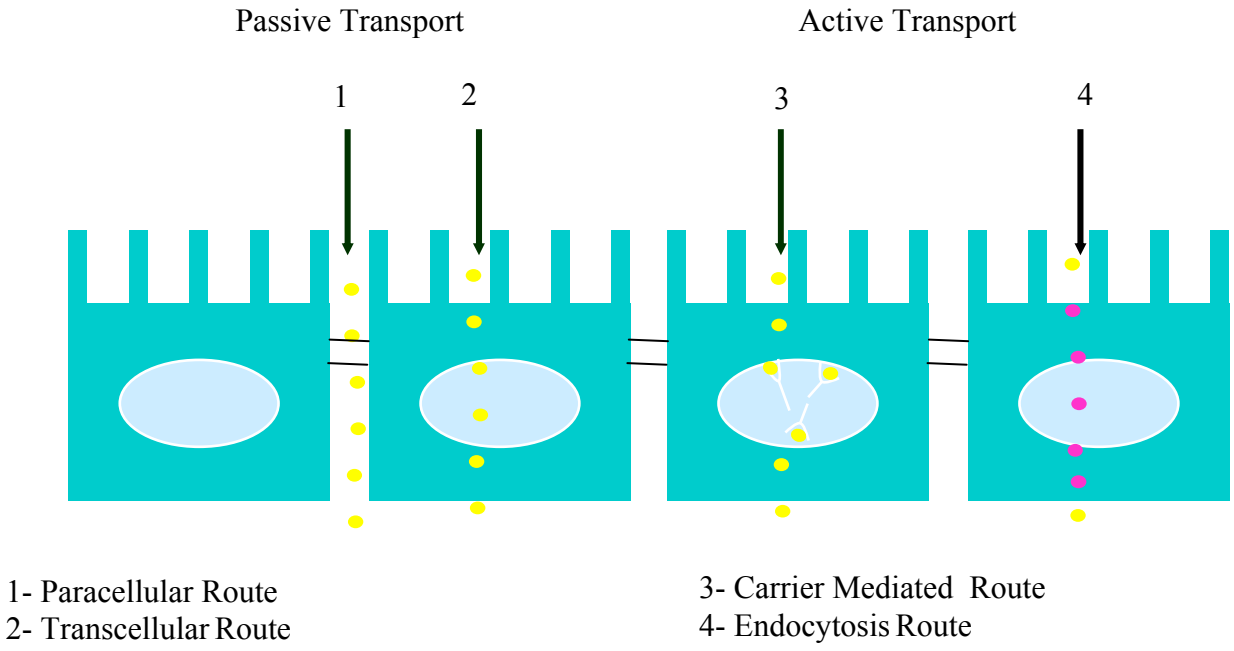

Figure 5.2: Transport routes for epithelial cells. Transport is classified as passive either paracellular or transcellular or active as carrier mediated or endocytosis.

There are two major pathways for passive transport. The first is the transcellular route. In this case the molecules are solubilized in the cell membrane and transported. Therefore, only small highly hydrophobic molecules can be absorbed through this route (3). In some cases, a channel protein within the cell membrane can aid passive transport through the cell membrane; this process is known as facilitated diffusion. Channel proteins usually form an aqueous pore that extends across the plasma membrane thus assisting in the movement of molecules. Mostly, these proteins are involved in the transport of ions; in that case the electrical potential difference across the membrane also plays a role in transport (19).

The second is the paracellular route, which is the transport of molecules between the aqueous spaces between the cells. The paracellular pathway accounts for about 8% of the available area for transport (20). Usually, small hydrophilic molecules are absorbed through this route, such as amino acids and monosaccharide. The transcellular route is regulated by a two distinct set of proteins; one is located in the apical side of the cell while the other is on the basolateral side. In order to maintain a polarized transport direction, these proteins must not be allowed to migrate from apical to basolateral and viceversa. Therefore, the space between cells must be tightly sealed. These seals are called tight junctions. The cells may also alter their seal to allow the passage of certain solutes and/or water.

As described above, the connections between cells mediate the paracellular route. Therefore, it is important to understand its role as a transport

barrier. The epithelial cells are joined together by four different junctions including adherens junctions, gap junctions, desmosones, and tight junctions (TJ) (please refer back to figure 5.2). The adherens junctions provide mechanical attachment between the cells. They are composed of cadherins (transmembrane protein), cateins, and actin filaments. The gap junctions are intracellular channels of 1.5-2 nm in diameter that permit the passage between cells of ions and small molecules. Desmosones are localized patches that hold two cells tightly together (16).

The tight junctions (TJ) have two functions, they prevent the transport of ions or molecules trough the aqueous space between the cells, and they block the movement of integral membrane proteins. The TJ respond to a series of physiological, pathological and pharmacological stimuli (21-23). Its structure is depicted in figure 5.3.

The TJs are composed of a series of proteins including: occludin, zonula occludens -1, and -2 (ZO-1/ZO-2), claudins and junctional adhesion molecule (see fig. 20). Occludin is composed of four transmembrane domains, two extracellular domains and a long cytoplasmic tail with the N and C terminus located in the cytoplasm and loops projecting into the paracellular space. The loops from the occludin may interact with the loops from the neighboring cell or other molecules to promote a seal. It can be independently regulated without affecting other TJ proteins and at least one of the extracellular loops is important to paracellular permeability (23, 24). ZO-1 and ZO-2 belong to the membrane associated guanylate kinase (MAGUK) family of proteins.

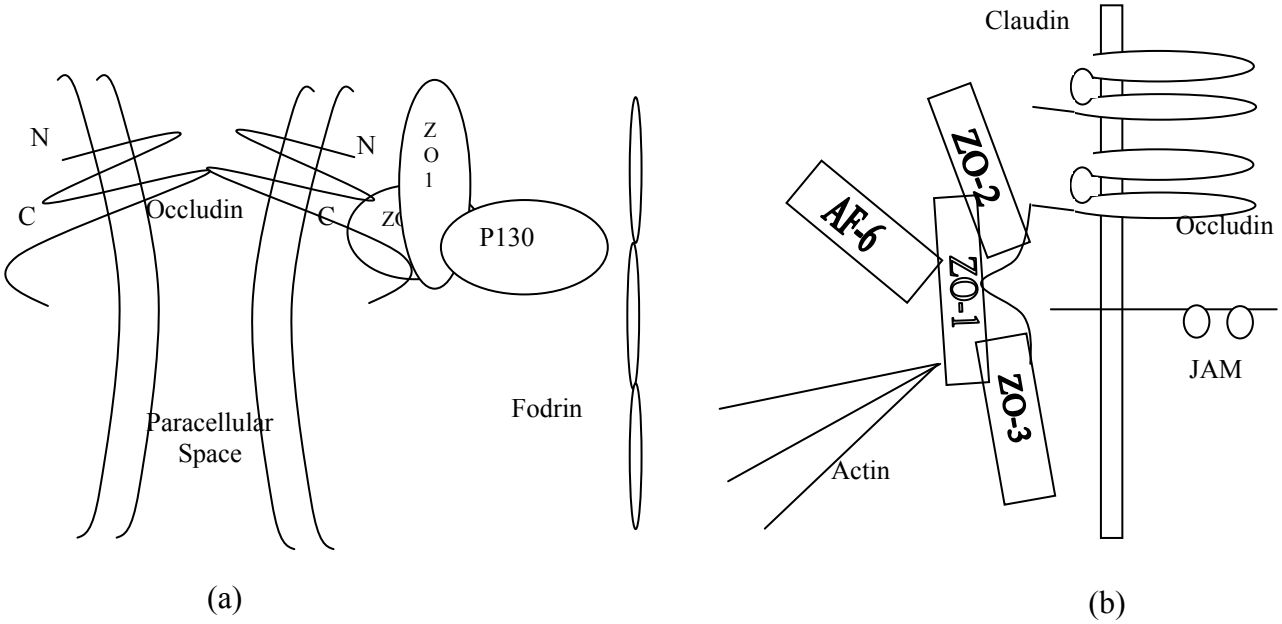

Figure 5.3: Tight junctions structure (a) and the known interactions of the tight junction proteins (b) [29-30]. (24, 25)

ZO-1 is found in TJ; it is also found in filtration slits of glomerular epithelial cells and in some cadherins junctions. ZO-2 is only found in TJ. The MAGUK family has a PDZ domain (named for the three proteins were the domain was first recognized: PSD-95, Dlg and ZO-1) that appears to interact with the C-terminus of transmembrane proteins. This is thought to be the mechanism of interaction of ZO-1 and occluding. ZO-1 has multiple phosphorylation sites for tyrosine and serine/threonine phosphorylation (23, 24).

Claudins are a multigene family of transmembrane proteins with two extracellular domains. All claudins C-terminus tail end with a Y-V motif. This is a known PDZ binding motif, therefore the claudins have a capability to interact with cytoplasmic proteins. Specifically, the claudins interact with ZO-1, ZO-2 and ZO-3. (23, 24). The junction associated molecule (JAM) is a member of the Immunoglobin (Ig) superfamily, and it may play a role in transmigration of leukocytes trough the junctional zone during an immune reaction.

The extracellular Ca^{2+} is involved in the homotypic interactions of E-cadherin required for the formation of junctional complex. Intracellular Ca^{2+} is critical for the biogenesis of TJ. Localized Ca^{2+} depletion is very well known to cause opening of the TJ (23). This process is also reversible and important for the movement of ZO-1 from intracellular sites to the plasma membrane (23, 24, 26). TJs also respond to ATP depletion or phosphorylation events. During an ATP depletion event, the ZO-1 remains in the lateral membrane and becomes less soluble due to tight association with cytoskeletal proteins like frodin,

therefore opening the tight junction. After, ATP is repleated the ZO-1 becomes more soluble, no longer associates with fodrin and other cytoskeletal proteins and the TJ integrity is reestrablished (24, 27, 28). This phenomenom is summarized in figure 5.4.

The integrity of the TJ can be measured by two methods, the first is the use of paracellular markers and the second is the measure of the transepithelial electrical resistance (TEER). Paracellular markers typically include molecules of varying molecular weight that are expected to be transported trough the paracellular route; the most commonly used include mannitol, insulin, and PEG 4000. The TEER is the resistance measured across the apical and basolateral chambers of the cultured cells. This resistance is associated with the degree of opening of the TJ. Typically values close to 100 Ω/cm^2 are considered open, while values raging from 300-400 Ω/cm^2 are considered closed (23, 25-28).

5.2.4 Active transport across epithelial cells

As explained in the previous section, the other major mechanism for drug transport is active or energy dependent transport. There are two major pathways for active transport. The first is endocytosis, in this mechanism, the membrane invaginates and is ruptured and forms a vesicle that allows the transport of the molecule until the vesicle breaks open and the contents is release into the cell (3, 8). The reverse process is called exocytosis.

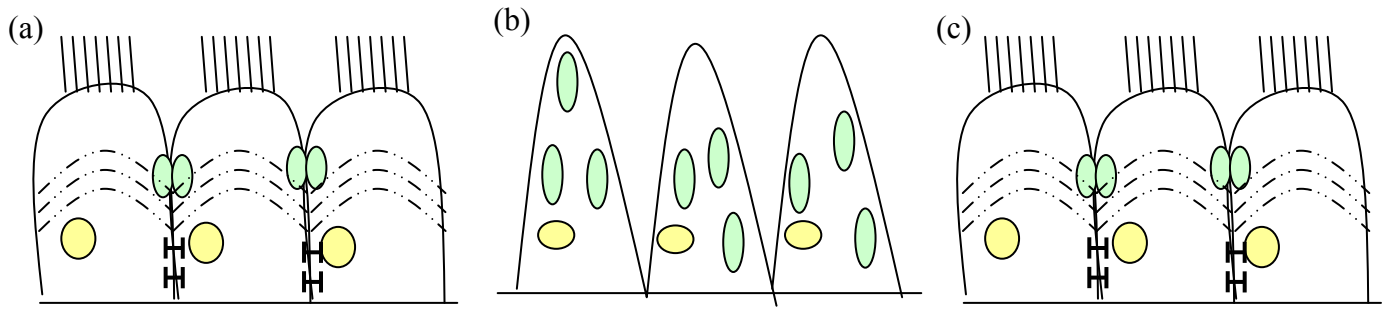

Figure 5.4: Tight junction opening due to Ca^{2+} depletion, (a) cells with normal calcium level, (b) upon depletion of calcium the tight junction opens and the ZO-1 becomes more soluble, (c) upon reestablishment of normal calcium level, the ZO-1 becomes less soluble moves to the lateral membrane and tight junction integrity is reestablished.

In some cases a receptor may be involved and the receptor-ligand complex is engulfed in the vesicle, this process is called receptor-mediated endocytosis. The cell sometimes will re-deposit the receptor in the plasma membreane after edocytosis has concluded. This process is called trancytosis. Two other varieties are distinguished due to their size. The first is phagocytosis (cellular eating) that involves the uptake of large molecules such as microorganisms and dead cells via large vesicles called phagosomes (order of > 250 nm). Specialized cells called phagocytes carry out this process. The second is pynocytosis (cellular drinking) that involves the uptake of fluid and solutes trough small pinocyitic vesicles (order of 100 nm) (19).

The second pathway is the carrier mediated. The carrier protein (also called carrier, permeases, transporter or pump) undergoes reversible conformational changes after the solute is bound to it, therefore assisting in transport. These proteins can have one or multiple specific binding site that allows the conformational changes. Therefore, they act very similar to an enzyme-substrate reaction, with the difference that the substrate does not suffer any covalent modifications. The carrier proteins become saturated at which point the rate of transport becomes a maximum, referred as V_{max} (please refer to figure 5.5). They also have a characteristic binding constant known as K_m (19).

These carriers have three distinct mechanism of action. The first is coupled carriers. In this case the transport of one substrate is tied to that of another. This mechanism can be further divided in two.

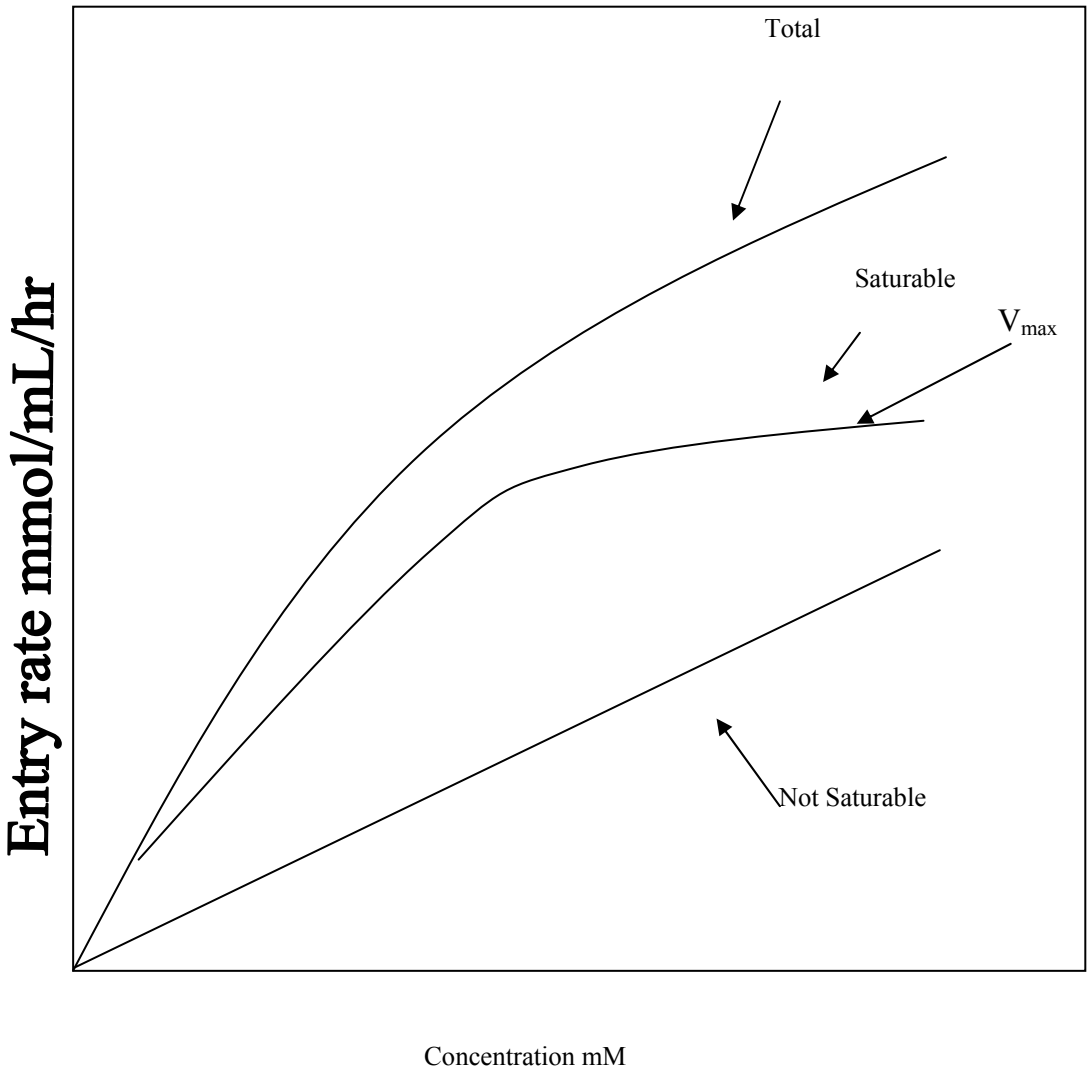

Figure 5.5: The illustration depicts the behavior of saturable (carrier-mediated), non-saturable (passive diffusion) and total transport process.

A symporter refers to a pump that can produce simultaneous transport of two substrates in the same direction, while an anitporter produces the transport of a second substrate in the opposite direction. The energy required for this mechanism is provided by the free energy released during the movement of an inorganic ion down an electrochemical gradient. The second is ATP-driven where the transport of the substrate is coupled to ATP hydrolysis. ABC transporters are classified as ATP-driven. The last one is the light-driven where the transported is tied to a light energy source. These pumps are typically found in bacteria (19).

Several carrier proteins have been studied; among them specifically important are the many ion transporters of the cells like Na^+, Na^+-K^+, H^+, and Ca^{2+}. For example, the H^+ and Na^+ pumps are consider crucial in maintaining the cytosolic pH at 7.2. The Na^+-K^+ pump, pumps Na^+ out of the cell while it pumps K^+ out of the cell, because the protein hydrolyzes ATP during the process it is considered to have ATPase activity. It also plays a major role in maintaining cell volume during osmotic events. Cells require a steep concentration gradient of Ca^+ and large amounts of it are removed from the cell by the Ca^+ pump, therefore it is also considered to have ATPase activity (19). The ABC transporters are also considered carrier proteins due to their ATP dependent movement of molecules. This family of carrier proteins is quite possibly the largest in existence due to its span across several species including mammals, bacteria, yeast, and protozoa (the protist *Plasmodium falciparum* that causes malaria (29)).

Often, molecule transport occurs by a combination of processes. For example, very hydrophilic drugs may be transported partly by the transcellular route. The larger surface area of the cell membrane can compensate for the difference in partitioning between the cell membrane and the extracellular fluid. Also, transport can be carried out partly by the carrier mediated and passive routes. Since the carrier-mediated pathway is saturable the contribution of the passive route will increase with increasing dose. In the case of p-glycoproteins that mediate transport to the mucosal direction, the saturation of the carrier can result in an increased absorption of the drug. The endocytosis route has low capacity and is seldom used in drug administration applications, the transcellular route is the preferred route (4). Endocytosis is observed in the absorption of vitamins and other essential nutrients.

5.2.5 Mathematical Models to Estimate Transport through Cell Monolayers

It is clear from the discussion of sections 5.2.3 and 5.2.4, that drug transport occurs through a combination of mechanisms. Therefore, a comprehensive model for drug transport trough cell monolayers should account for all possible scenarios. Upon literature review, it is evident that no single model accounts for all possible scenarios. One must be careful to understand the assumptions of the model to fully comprehend if it accurately describes the complexity of the *in-vivo* situation.

To choose an appropriate model to estimate cellular transport, we must first examine the experimental setup. Since the model molecules chosen to

study are substrates of the MDR1 (P-gp) or the MRP pumps, one can expect carrier-mediated transport to be present. Endocytosis is seldom used for drug transport, therefore its contributions are deemed negligible. The contributions due to paracellular transport are expected to be minimal. This is expected because the Caco-2 cell monolayers have very rigid tight junctions and the area available for transport is very small in comparison to the transcellular pathway.

Since no model can accurately describe all possible contributions, Cogburn suggested a more realistic approach, where a series of experiments, i.e. effect of temperature, concentration, and direction taken as a whole can accurately predict the transport pathway (30). Cogburn's approach is qualitative, but can provide a better description of the transport pathway than the quantitative models. Active transport like the one observed during drug resistance efflux is affected by a number of external effects. For example, at low temperatures the cell metabolism is significantly reduced rendering active transport contributions negligible. Active transport can also be assed by analyzing the concentration dependent data. Since this type of transport is saturable usually a plateau can be observed, as depicted in figure 5.6. Finally, due to the discrete location of the ABC pumps transport effects are expected depending on the direction of movement. Using, this approach one can have a better idea if carrier-mediated transport due to MDR and MRP interactions is present.

The main goal of this research is to investigate if poly(ethylene glycol) rich hydrogel have inhibitory effects on the MDR and MRP proteins. To

investigate this hypothesis only the net flux of the MDR substrate across the cell monolayer is needed. Therefore, the net flux was obtained using the well-known Fick's law, which has become the standard in the literature.

$$\frac{dC_A}{dt} = \frac{P_{eff} A C_0}{V_b} \qquad [5.1]$$

This equation can be rewritten as:

$$\frac{C_A}{C_0} = \frac{AP_{eff}t}{V_b} \qquad [5.2]$$

Here C_A is the concentration of the receiving well, C_0 is the concentration of the donor well, A is the area of transport, V_b is the volume of the receiving well and t is time. Fick's first law model assumes that the apparent permeability is independent of time, concentration and area. It also assumes, that the initial concentration was constant, therefore sink conditions were maintained (4). To maintain sink conditions, data was collected for changes in initial concentration of less than ten percent.

The advantage of this model is that is simple and does not depend on the approximation of other parameters in order to provide permeability coefficients. Also, since is the standard in the literature, it can be used for comparison basis with the literature database. The disadvantage is that it does

not provide information regarding the individual contributions of the different transport pathways, but as stated before the predominant transport route for these experiments is the active transport due to ABC transporter interactions.

It is important to keep in mind that the effective permeability measurement factors in other barriers of transport contributions as well. The apparent permeability is assumed to depend lineally on these resistances to transport (31):

$$\frac{1}{P_{eff}} = \frac{1}{P_c} + \frac{1}{P_f} + \frac{1}{P_{BL}} \qquad [5.3]$$

where P_c represents the permeability of the cell monolayer, P_f the permeability of the filter support and P_{BL} is the permeability of the aqueous boundary layer.

The boundary layer will have a significant effect on the transport of molecules specially if it thickness becomes significant due to lack of mixing. Even though there is an aqueous boundary/mucus layer in the *in-vivo* situation; the layer is thicker in unstirred *in-vitro* models than *in-vivo*. Large molecules will be most affected by boundary layer effects, as their transport tends to be slower. It is also important to note that two boundary layers are formed, one in the donor side of the well and another in the receiving side (3, 31). The expression that correlates these quantities is written below:

$$\frac{1}{P_{BL}} = \frac{1}{P_{BLD}} + \frac{1}{P_{BLR}} = \frac{P_{BLD} + P_{BLR}}{P_{BLD}P_{BLR}} \quad [5.4]$$

where P_{BLD} and P_{BLR} are the boundary layer permeabilities in the donor and receiving sides of the well, respectively (31). It has been observed that for the case of the cell monolayer/Transwell® system placed on a rotating platform device, the boundary layer thickness was unequal due to asymmetry in the hydrodynamic conditions(31).

There are several approaches to estimate the boundary layer and filter permeability coefficient. For example, the approach described by Adson (31) defines the boundary layer permeability as:

$$P_{BL} = \frac{D}{h} = k_D v^x \quad [5.5]$$

where D is the diffusion coefficient (cm^2/s), h the effective thickness of the boundary layer (cm), k_D a constant descriptive of the diffusivity of the permeant kinematic viscosity, unit conversion and geometric factors, v the stirring parameter (rpm). Equation [5.4] may be rewritten as:

$$\frac{1}{P_{BL}} = \frac{1}{k_{BLD}v^x} + \frac{1}{k_{BLR}v^z} = \frac{1}{K_{BL}v^n} \quad [5.6]$$

where k_{BLD} and k_{BLR} are constants descriptive of the diffusivity of the permeant kinematic viscosity in the donor and receiving wells respectively, $x \neq z$ and $k_{BLD} \neq k_{BLR}$, $K_{BL}v^n$ is an operational expression of P_{BL} where the empirical constant

K_{BL} and the nth power are found experimentally. With this expression [5.3] may be rewritten as:

$$\frac{1}{P_{app}} = \frac{1}{P_c} + \frac{1}{P_f} + \frac{1}{K_{BL} v^n} \qquad [5.7]$$

where $\left(\frac{1}{P_c} + \frac{1}{P_f}\right)$ and $\frac{1}{K_{BL}}$ may be found from a linear regression of $\frac{1}{P_{app}}$ versus $\frac{1}{v^n}$ (31).

The filter permeability can be defined as:

$$P_f = \frac{\varepsilon_f D[F(r/R_F)]}{h_f} \qquad [5.8]$$

where ε_f is the porosity, D is the diffusivity in the bulk solution, R_f is the channel radius, h_f is the filter thickness. $F[(r/R_F)]$ is the dimensionless molecular sieving function of Renkin (31) described as:

$$F\left(\frac{r}{R_F}\right) = \left(1 - \frac{r}{R_F}\right)^2 \left[1 - 2.104\left(\frac{r}{R_F}\right) + 2.09\left(\frac{r}{R_F}\right)^3 - 0.95\left(\frac{r}{R_F}\right)^5\right] \qquad [5.9]$$

A major disadvantage of this model is that is based on two empirical constants. Specifically, the nth power is not well defined. For the system studied by Adson, an nth power of 0.8 was used, even though theory will predict a range of 0.3 to 0.5. The explanation for the high value was attributed to the asymmetry in hydrodynamic conditions.

Karlsson (32) followed a more simplistic approach:

$$\frac{v}{P_{app}} = \frac{1}{K} + \left(\frac{1}{P_c} + \frac{1}{P_f} \right) v \qquad [5.10]$$

where v is the stirring rate, this equation can be solved using a linear regression of $\frac{v}{P_{app}}$ versus v (30).

In this model P_{BL} and P_f are defined as follows:

$$\frac{1}{P_{BL}} = \frac{1}{Kv} \qquad [5.11]$$

$$\frac{1}{P_f} = \frac{h_f}{n\pi r_p^2 D_{aq}} \qquad [5.12]$$

where h_f is the thickness (pore length), n is the number of pores per unit area, r_p is the pore radius, and D_{aq} is the aqueous diffusion coefficient, that can be estimated using the Stoke-Einstein equation (32).

Since this work is only concerned with general tendencies in the apparent permeability of the substrate, Fick's second law of diffusion was chosen to estimate this value due to the simplicity of the equation (i.e. experiment). Also this model does not rely on the estimation of external values to estimate the permeability. It is important to note that due to the fact that the cell monolayer is assembled in the horizontal position and no stirring is used the boundary layer does provide a significant barrier to transport. To reduce this boundary layer there were two alternatives, but none of them were plausible. The first was to provide adequate stirring. The large particle size of the hydrogels and the high concentrations used during experimentation could

produce tears in the cell monolayer and artificially alter the transport values. The second was to use a vertical assembly of the cell monolayer, like the one provided by Ussing Cambers® (Warner Instruments, Hamdem, CT). However, these hydrogels are expected to interact intimately with the cell monolayer due to direct contact and this arrangement can reduce those interactions. Since, all other variables during the experiments are kept constant, it is expected that any changes in the apparent permeability be only due to variations in the cell permeability.

5.3 Experimental

5.3.1 Materials

The monomer poly(ethylene)glycol monomethacrylate (PEGMA) with PEG chains of 200, 400 and 1000 g/mol, the cross linker poly(ethylene) glycol dimetachrylate (PEGDMA) with chains of 400, 600 and 1000 g/mol, and the lineal poly(ethylene glycol) with molecular weight of 300 g/mol (PEG-300) were purchased from Polysciences, Inc (Warrington, PA). The photo-initiator, 1-hydroxyciclohexyl phenyl ketone, the MRP substrate fluorescein sodium salt (FLUO) (33), the MDR1 substrate Rhodamine 123 (RHO 123) (33), the MRP inhibitors Probenecid (Prob), the MDR1 and MRP inhibitor genistein (Gen), the MDR1 inhibitor Verapamil (Ver), and the phosphate buffered saline (PBS) (pH = 7.4) were obtained from Aldrich Chemical Co. (Milwaukee, WI). Finally, the solvent, ethanol was purchased from Fisher Scientific (Hampton, NH), and used as received.

The Caco-2 cell line (HBT-37) was purchased from the American Type Culture Collection (Manassas, VA). Dulbecco's modified eagle's medium (DMEM) and hanks balanced salt solution (HBSS) were obtained from Sigma-Aldrich (St Louis, MO), supplemented with fetal bovine serum, and L-glutamine from Invitrogen (Carlsbad, California), and penicillin/strepromycin antibiotics, and amphotericin B antimycotic from Sigma-Aldrich (St Louis, MO).

5.3.2 Methods

Cell Culture

Cells were cultured in Dulbecco's modified Eagle's medium (DMEM) (Sigma, St Louis, MO), supplemented with 10% fetal bovine serum (Invitrogen, Carlsbad, California), 1% L-glutamine (Invitrogen, Carlsbad, California), 100µg/ml penicillin, 100µg/ml streptomycin, and 250 µg/mL amphotericin B (Sigma, St Louis, MO). The medium was changed every 3 days. The cells were transferred weekly after trypsinization in 0.25% trypsin with 0.02% ethylenediaminetetraacetic acid (EDTA) (Sigma, St Louis, MO) and grown in culture flasks of 75 $cm^{2.}$ Flasks with cells were kept in a CO_2 Water Jacketed Incubator (Nuaire, Plymouth, MN) in a humidified atmosphere of 5% CO_2 in air. For experiments, cells were used between cell passage number 20-60.

Preparation of Hydrogel Microparticles Suspensions

The PEGMA/PEGDMA hydrogel films were synthesized as described in section 4.3.2 and micronized to a particle size of 90-106 μm using a mortar and pistil using the appropriate sieves. The resulting microparticles were dialyzed in deionized water using a dialysis membrane of 10^6 Da molecular weight cut off (MWCO) (Spectra Por, Rancho Dominguez, CA) for 3 days with 2 changes per day. The washed polymer microparticles were allowed to air dry for 7 days, followed by 7 days of drying in a vacuum oven at 32^o C. The hydrogel suspensions were prepared by adding the appropriate polymer weight to the HBSS volume. The resulting suspension was then allowed to equilibrate with HBSS for 24 hours by dialysis using a membrane with a 30,000 Da MWCO (Spectra Por, Rancho Dominguez, CA).

Cytotoxic Evaluation of Polymers

Caco-2 cells were seeded in 96 well plates suitable for cell culture and spectrofluorometric analysis (Corning Inc, Corning, NY) at a concentration range of 14,000 to 10,000 cells/cm^2. Incubation media was changed every other day until cells reached confluence. Once cells reached confluence, the cells were washed twice with HBSS, then 200 μL of a polymer/HBSS suspension or suspension supernatant (the suspension supernatant was obtained after a 24 hour equilibration of the hydrogel microparticles and the HBSS solution) was added at the following polymer concentrations: 20, 10, 5,

and 1 mg/ mL and incubated for 2 or 48 hours. The effect of filtering and autoclaving the supernatant solution was also studied. Supernatant were filtered using a 2 μm filter (Fisher Scientific, Pittsburgh, PA).

The effect of microparticles suspensions prepared (as is) without the dialysis washing procedure was also studied. HBSS was used as negative control while sodium hypochlorite at a concentration 1% (v/v) was used as a positive control. During the 48 hour experiments the suspension liquid used was DMEM without phenol red in order to minimize cell death due to lack of nutrients. Next, the cells were washed twice with HBSS and a solution consisting of 2 μL of Cell Titer Blue™ (Promega, Madison, WI) in 100 μL of HBSS was added and incubated for 1 hour. Finally, the cell viability was evaluated using Spectra Max Gemini EM fluorometer (Sunnydale, CA) by reading the fluorescence at Ex 579nm/ Em584 nm.

The Cell Titer Blue™ cell viability assay contains highly purified resazurin. Viable cells retain the ability to reduce resazurin into resorufin. Resazurin is dark blue and has negligible intrinsic fluorescence, while resorufin is pink and highly fluorescent.

Transport of Model Substrates or Inhibitors

The polymer suspensions at a concentration of 20 or 10 mg/mL were prepared by further dialysis in a 10 μg/ml (FLUO) or 10μM (RHO 123) solution for 1 day with 3 changes per day and later diluted to their final concentrations. The submicron spheres were dialyzed at the resulting concentration after

polymerization in the appropriate fluorescein sodium salt or rhodamine 123 solutions. Fluorescein sodium salt solutions for the transport studies were used at a final concentration of 2µg/ml in HBSS, while Rhodamine 123 was used at a final concentration of 10 µM. Verapamil and probenecid were used at final concentration of 100 µM, while genistein was used at a final concentration of 37 µM.

The experiment combination consisted of a set of controls (either FLUO or RHO 123) and an experimental set composed of polymer suspension or inhibitor plus FLUO or RHO 123. The TEER of the monolayers was monitored before and after the experiments to ensure monolayer integrity using an EVON volt-ohm meter (World Precision Instruments, Sarasota, FL) with chopstick electrodes. A TEER value of 300-400 ohm/cm^2 was considered indicative of cell membrane integrity. Cells were also visually inspected to ensure the integrity of the cell monolayer. Monolayers that were damaged were discarded.

Transport experiments were performed using Transwells® plates (4.71 cm / well, pore size 0.4um) (Costar®, Corning Inc., Corning, NY) at a cell density of 5.25 x 10^4 cells/ cm^2. The plates were cultivated in DMEM for 21-25 days. The culture media was changed every 3 to 4 days. At this point, the cells were washed twice with HBSS and allowed to equilibrate for 2 hours. Next, the experimental combination A 200µl sample was taken from the receiving well and replenished with fresh HBSS (the dilution factor was accounted for during calculations) at 30, 60, 90, 120, and 150 minutes intervals. Finally, the samples were read at Ex 544nm/Em612 (FLUO) or Ex

507nm/Em529 (RHO 123) in a Spectra Max Gemini EM fluorometer (Sunnydale, CA).

5.4 Results and Discussion

Cytotoxic Effects

Poly(ethylene glycol) hydrogels with varying tethered chain length and crosslinker lengths were designed as possible MDR and MRP inhibitors. These morphologies were also selected because they are suitable for controlled drug delivery applications, thus providing an added edge to their function. The previous chapter detailed the characterization of such hydrogels providing evidence that they are excellent candidates for such usage. This chapter will detail the information regarding their effects on the transport of MDR and MRP substrates and their possible inhibitory effects. However, before these effects can be investigated it is important to determine any possible cytotoxic effects that these morphologies may have on the cell monoloyers. It is crucial that the hydrogels do not have any toxic effects on the cells during the course of the experiments. A harmful effect of the polymers on the cultured cells could lead to erroneous conclusions.

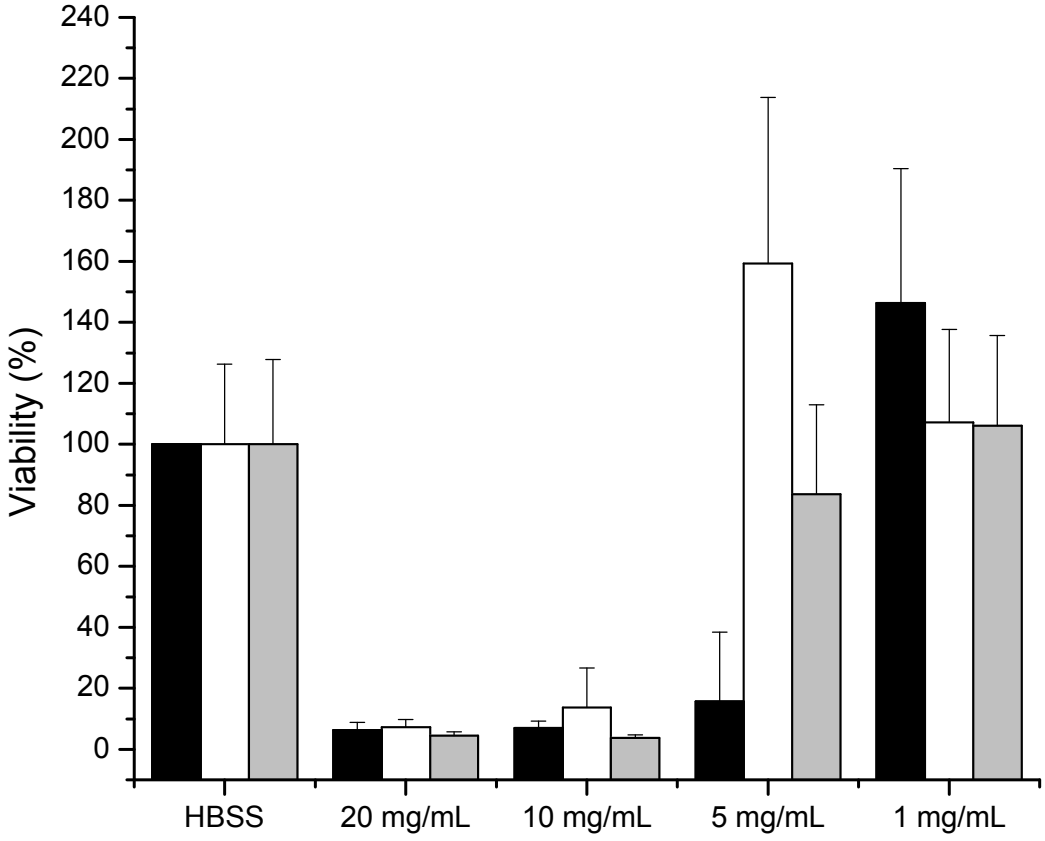

Figure 5.6: Cell viability effects of diverse PEG hydrogel morphologies microparticles of 106-90 μm particle size suspended on HBSS; ■ PEGMA 400/ PEGDMA 1000, □ PEGMA 1000/ PEGDMA 600, and ▨ PEGMA 400/ PEGDMA 600. Cells were subjected to a 2 hour contact exposure at a 37 ° C atmosphere. Each bar represents an average of n=16 wells ± stdv. Cell passage number was 27.

The first protocol of hydrogel suspension preparation to be evaluated was the use of the hydrogel suspension as is, with no washing procedure. The results (figure 5.6) revealed that for polymer suspensions of concentrations greater than 5 mg/mL the effects were toxic without regards of the used morphology. In order to understand the nature of the toxic effects, the supernatants of the solutions were collected and analyzed for cytotoxicity (please refer to figures 5.7 and 5.8, the same protocol was used to generate both figures, supernatant was obtain after a 24 hour equilibration period of the hydrogel/HBSS suspension). The micronization effect was studied by analyzing the cytotoxicity of the supernatant as a function of filtration and autoclaving; the filtered used had a 2 μm pore size. It is well known that the polymerization conversion rarely reaches 100%; and the monomer is known for its toxic effects. The process of micronization may facilitate the release of unreacted monomer, therefore allowing it's leaching into the solvent. Results indicated that the filtered supernatants still had similar toxic effects than the polymer suspensions, suggesting that a toxic substance was leaching from the polymer into the buffer and causing the toxic effects.

To verify that possible toxic substance were leaching out of the hydrogel microparticles, the polymer supernatants were also autoclaved at 121 °C and 1 atm for 20 minutes. Although, cytotoxicity was improved after autoclaving of the supernatant, the toxicity remained at unacceptable levels.

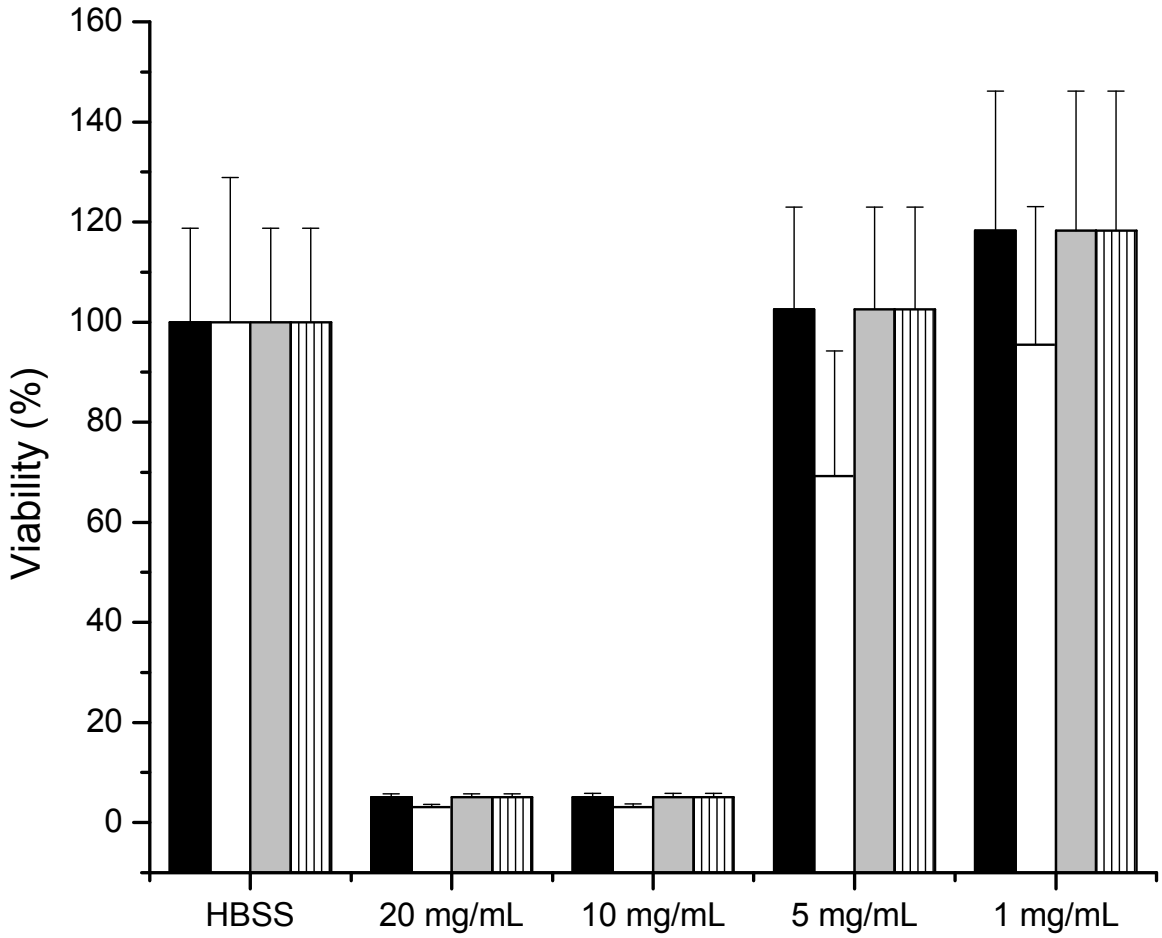

Figure 5.7: Comparison of cell viability effects of the filtered versus the unfiltered supernatants of diverse 106-90 μm PEG microparticles originating from diverse hydrogel morphologies of particle size suspended on HBSS; ■PEGMA 1000/ PEGDMA 1000 filtered, □ PEGMA 1000/ PEGDMA 1000 not filtered, ▭ PEGMA 400/ PEGDMA 1000 filtered, and ▥ PEGMA 400/PEGDMA 1000 not filtered. Cells were subjected to a 2 hour contact exposure at 37 ° C. Each bar represents an average of n=16 wells ± stdv. Cell passage number was 28.

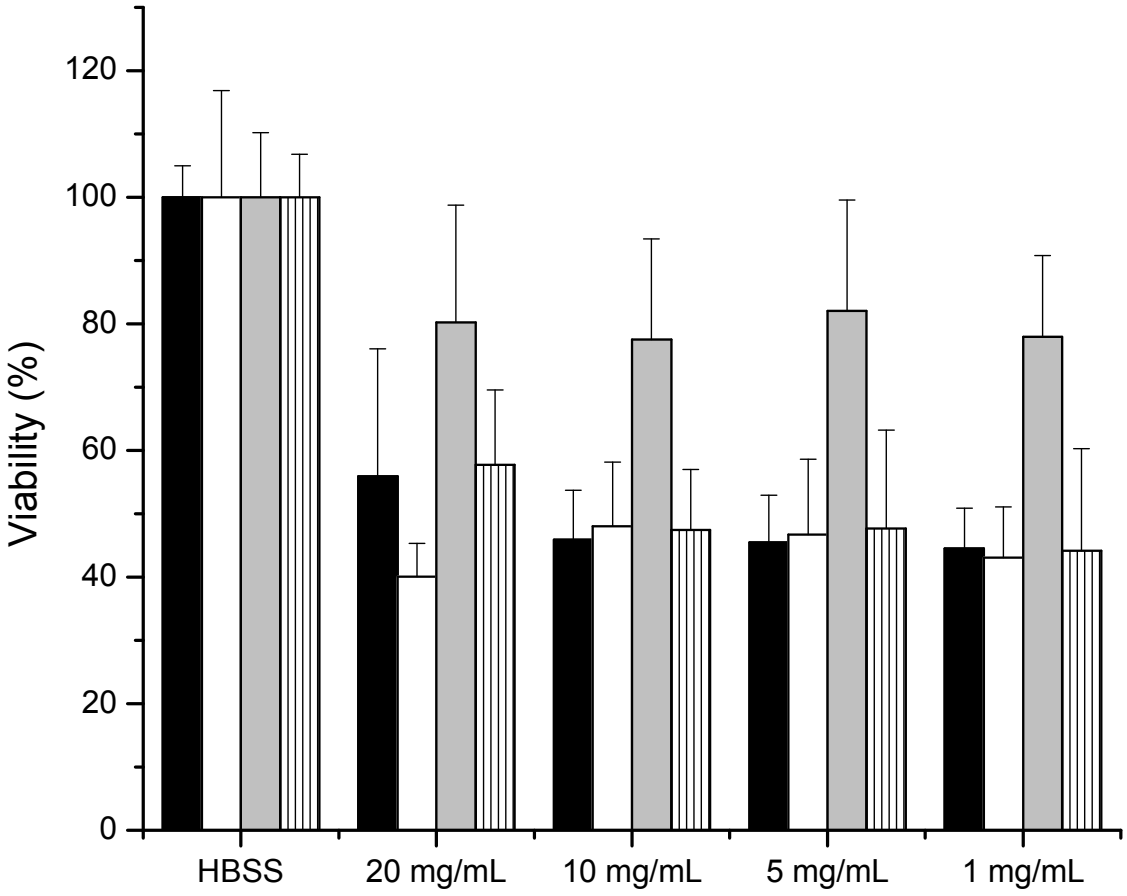

Figure 5.8: Comparison of cell viability effects of the autoclaved filtered versus unfiltered supernatants of diverse 106-90 μm PEG microparticles originating from diverse hydrogel morphologies of particle size suspended on HBSS; ■PEGMA 1000/ PEGDMA 1000 autoclaved and non filtered, □ PEGMA 1000/ PEGDMA 1000 autoclaved and filtered, ▨ PEGMA 400/ PEGDMA 1000 autoclaved and non filtered, and ▥ PEGMA 400/ PEGDMA 1000 autoclaved and filtered. Cells were subjected to a 2 hour contact exposure at 37 ° C. Each bar represents an average of n=16 wells ± stdv. Cell passage number was 29.

The results suggests that during autoclaving procedure some of the toxic components may become degraded, but not enough as to render the hydrogel suspension non toxic. Autoclaving for longer times was not recommended because it posed a danger for polymer degradation or oxidation and therefore it was no further pursued. Therefore, it was recommended to wash the polymer microparticles with dialysis membranes prior to performing the experiments.

The results of washing the hydrogel suspensions (using the dialysis procedure explained earlier) on the 2 and 48 hour cytotoxicity of the Caco-2 cells is summarized in figures 5.9 and 5.10. The washing procedure had a dramatic effect on the cell vialibility. Using this protocol it was possible to maintain cell viability even at the high polymer concentration of 20 mg/mL. The cell viability was retained still during 48 hour experiments.

In conclusion washing the hydrogel suspension using a 10^6 Da dialysis membrane is necessary to remove toxic substances remaining after the polymerization reaction. This is true for all hydrogels.

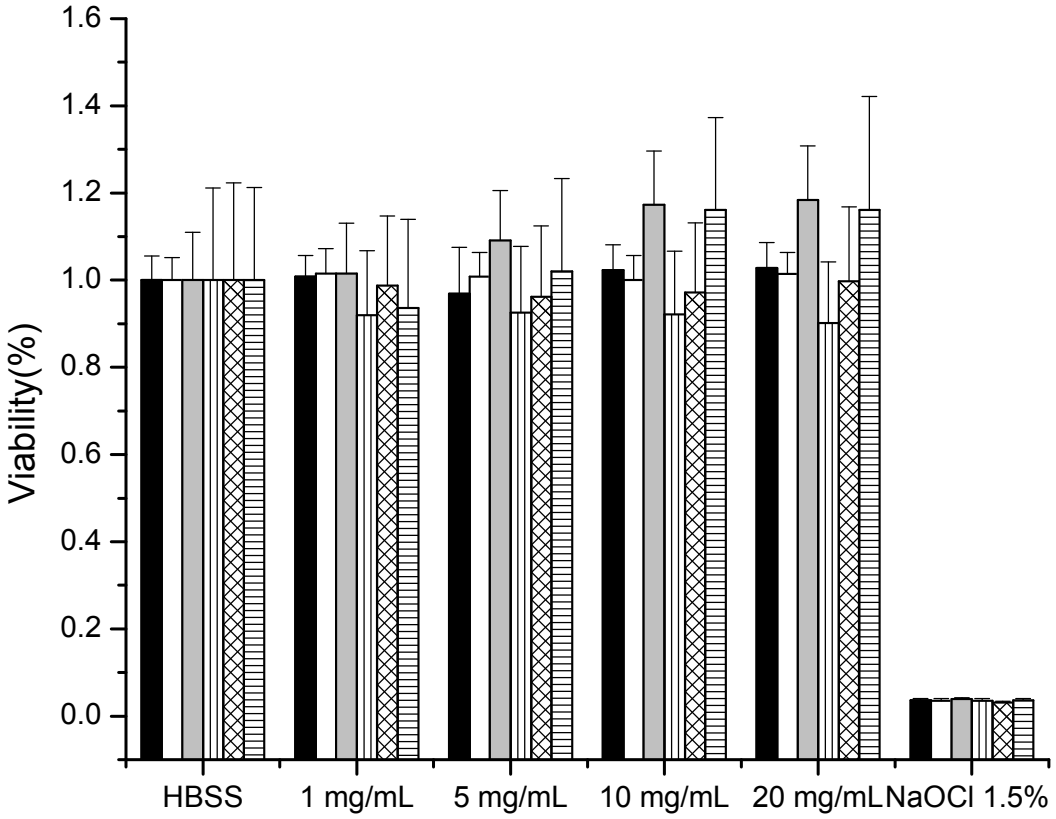

Figure 5.9: Cell viability effects of diverse PEG hydrogel morphologies microparticles of 106-90 μm particle size suspended on HBSS; ■ PEGMA 200/ PEGDMA 600, □ PEGMA 200/ PEGDMA 1000, ▒ PEGMA 400/ PEGDMA 600, ▥ PEGMA 400/ PEGDMA 1000, ▩ PEGMA 1000/ PEGDMA 600, and ▤ PEGMA 1000/ PEGDMA 1000. Cells were subjected to a 2 hour contact exposure at 37 ° C. Each bar represents an average of n=16 wells ± stdv. Cell passage number was 30-40.

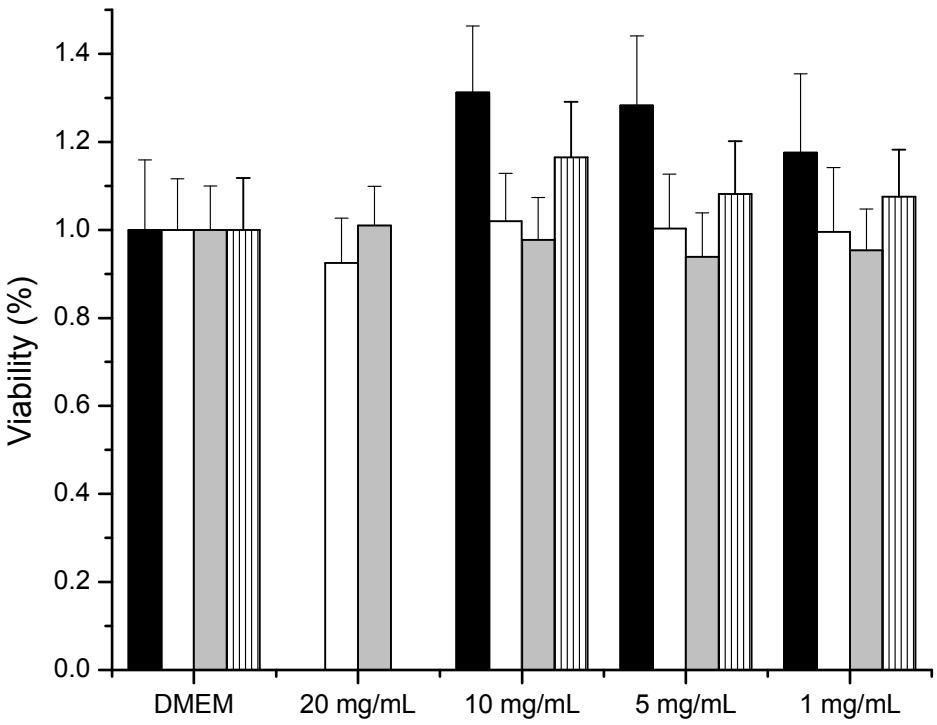

Figure 5.10: Cell viability effects of diverse PEG hydrogel morphologies microparticles of 106-90 μm particle size suspended on HBSS; ■ PEGMA 400/ PEGDMA 400, □ PEGMA 400/ PEGDMA 600, ▒ PEGMA 400/ PEGDMA 1000, and ▥ PEGMA 1000/ PEGDMA 400. Cells were subjected to a 48 hour contact exposure at 37 ° C. Each bar represents an average of n=16 wells ± stdv. Cell passage number was 60-70.

Transport effects of the MRP substrate fluorescein sodium salt (FLUO)

Once the protocol for hydrogel preparation was well established, the effects of theses morphologies on the transport of the MRP substrate, fluorescein sodium salt, through Caco-2 cell monolayers were ready to be conducted. Fluorescein sodium salt was selected as an MRP substrate. There are several advantages for using fluorescein sodium salt as opposed to other available MRP substrates. First, it is a fluorescent probe, therefore concentration analysis is simplified, as opposed to liquid chromatography. Fluorescent spectroscopy has several advantages over UV or radiation spectroscopy, which are also simplify the detection techniques. As compared to radiation spectroscopy, both techniques offer similar sensitivity; but fluorescent probes are not hazardous and they do not decay over time. Fluorescent spectroscopy offers approximately 1000 times the sensitivity of UV spectroscopy (34). Second, it is economical making it more attractive than other fluorescent MRP substrates available like fluo-3 acetyloxymethyl ester (35).

The movement of fluorescein sodium salt across the cell monolayers could be attributed to two different mechanisms; (i) passive diffusion (driven by a concentration gradient) across the transport barrier, and (ii) active transport (energy dependent), like MRP efflux. Often, both of the transport mechanisms are present at the same time. The transport of substrates across a cell model monolayer has been successfully calculated using Ficks first law of diffusion, equation [5.2]. Isolation of the multiple transport mechanisms can be difficult

and often a number of carefully planned different sets of trials are required. This manuscript is concerned with possible active transport interactions due to MRP efflux. Transport experiments were performed in the apical to basolateral (A-BL) direction and vice versa (BL-A) and at 37 and 4 °C. PEG hydrogel transport effects were compared to the known inhibitors probenecid and genistein, and also the lineal PEG morphology with a molecular weight of 300 g/mol (PEG-300).

Results indicated that at 37 °C the transport of fluorescein sodium salt was enhanced by the presence of the PEG hydrogel, as observed in figure 5.11. The transport enhancement was observed in both the AB and BA directions. This is consistent with the fact that MRP proteins are present in both apical and basolateral membranes (36, 37). Moreover, the transport enhancement appears to be dependent on the hydrogel morphology. In general, morphologies with the larger crosslinker length of 1000 g/mol show a significantly lower enhancement than their 600-g/mol counterparts.

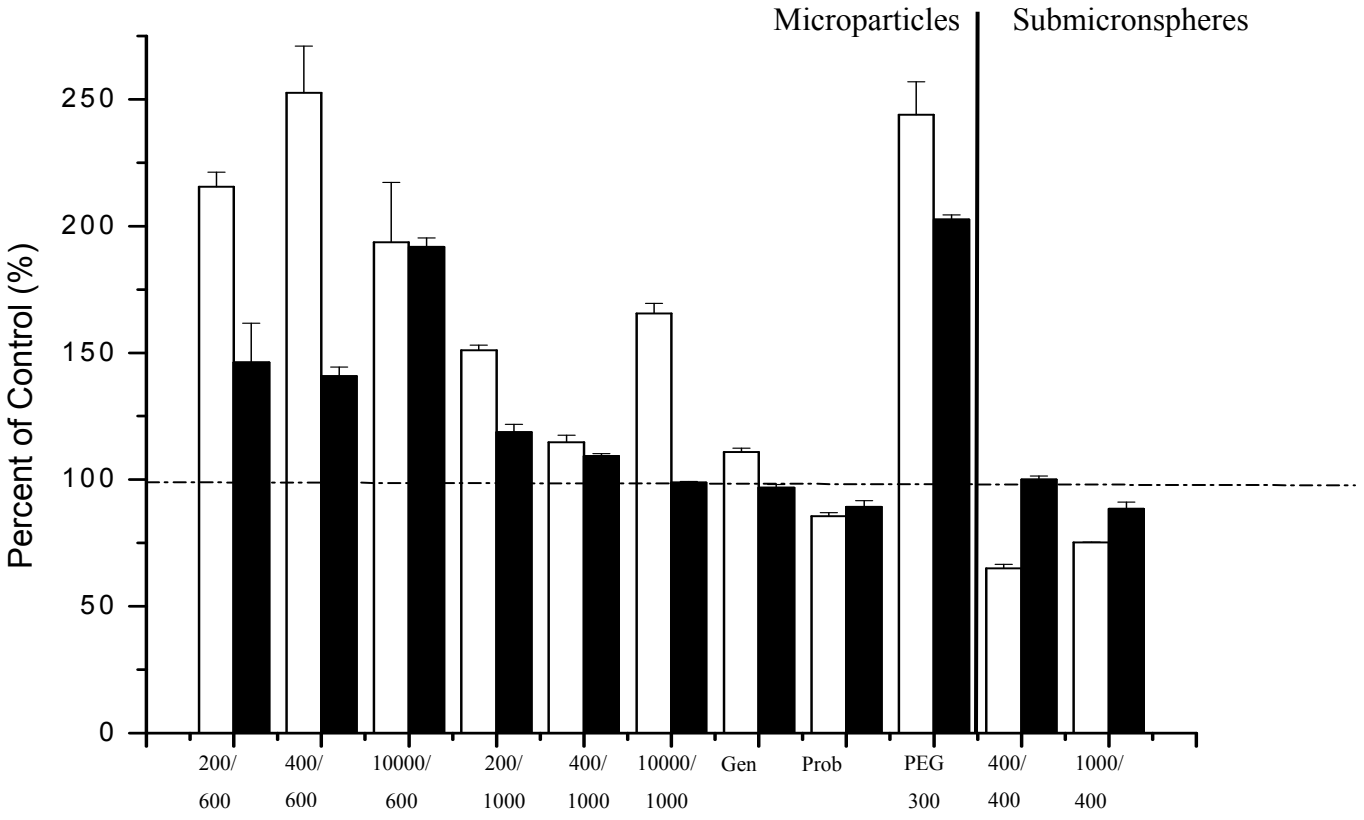

Figure 5.11: Transport of fluorescein sodium salt in the presence of various morphologies of PEG and compared to known inhibitors at 37 °C in the □apical to basolateral direction and the ■ basolateral to apical direction. The convention used to name the hydrogels was the PEGMA MW / PEDGDMA MW (g/mol). All hydrogels were added at a concentration of 10 mg/mL. Genistein was added at a concentration of 37 μM while probenecid at 100 μM. The lineal PEG 300 was added at a concentration of 20% (v/v). The passage number was in the rage of 40-60.

It appears that the transport enhancement conferred by the PEG hydrogel is due to interactions at the surface level and the availability of the tethered chains to provide these interactions. It is possible that hydrogels with longer crosslinker chains might have reduced tethered chain mobility due to entanglements. This phenomenon can also be observed in the release profile of fluorescein sodium salt (figure 4.9) where the hydrogels with the crosslinker length of PEGDMA 1000 g/mol showed a reduction on the release of the model drug.

The transport enhancement is increased with increasing tethered chain length, with the exception of the PEGMA 1000/ PEGDMA 600 morphology. However, as explained earlier in the manuscript this morphology suffers from serious steric hindrance constraints that alter the availability of the tethered chains. This behavior suggests that the tethered chain is the responsible for the transport enhancement. These tethered chain length effects are consistent with experiments done using pluronic block copolymers (poly(ethylene oxide)-*block*-poly(propylene oxide)-*block*-poly(ethylene oxide) $EO_{m/2}$-PO_n-$EO_{m/2}$ (38, 39)). These polymers enhanced the transport of MDR and MRP substrates as evidenced by studies performed on MDR/MRP overexpressing and underexpressing cell lines (33, 38-52). Furthermore, the effect was strongly dependent on the molecular structure of the copolymer, in particular the length of the EO (hydrophilic chain) and PO (hydrophobic chain). Lipophilic polymers with intermediate PO chain lengths had the most effect (43). Another factor that strongly influenced is the concentration of the polymer

during the experiments with low concentrations producing the greatest effect (38, 43). Evidence also suggests that these polymers are internalized in the cell and interact with internal organelles such as the mitochondria, thus interfering with the metabolism and reducing the internal ATP levels. Internal ATP was reduced as low as 50%. Since drug resistance is an ATP dependent process it is hypothesized that this may be crucial in the inhibitory effects of these polymers (40, 44, 46, 48). Finally, the polymers increased the membrane fluidity, than in turn may affect the conformation of the drug resistance proteins. The theory presented is that the mechanism of action of Pluronic copolymers is a two fold effect of ATP depletion and membrane fluidization (39, 40, 44, 46, 47, 49). However, due to the crosslinked nature of the hydrogels and their particle size, internalization of the polymer and interactions with the mitochondria are not possible. Membrane fluidization effects cannot be discarded at this point and will be further discussed in chapter 6.

To further investigate the effect of these hydrogels on the MRP pumps, experiments were performed at 4 °C and are summarized in figure 5.12. At this low temperature, the cellular metabolism is low enough that the active transport effects are negligible. No effects were observed for all the PEG hydrogels. This is further evidence that some type of active transport phenomenon is occurring with the hydrogels, most likely MRP inhibition. Effects at 4 °C were only observed for the lineal PEG-300 morphology, which suggests that the inhibition mechanisms of these two morphologies might be different.

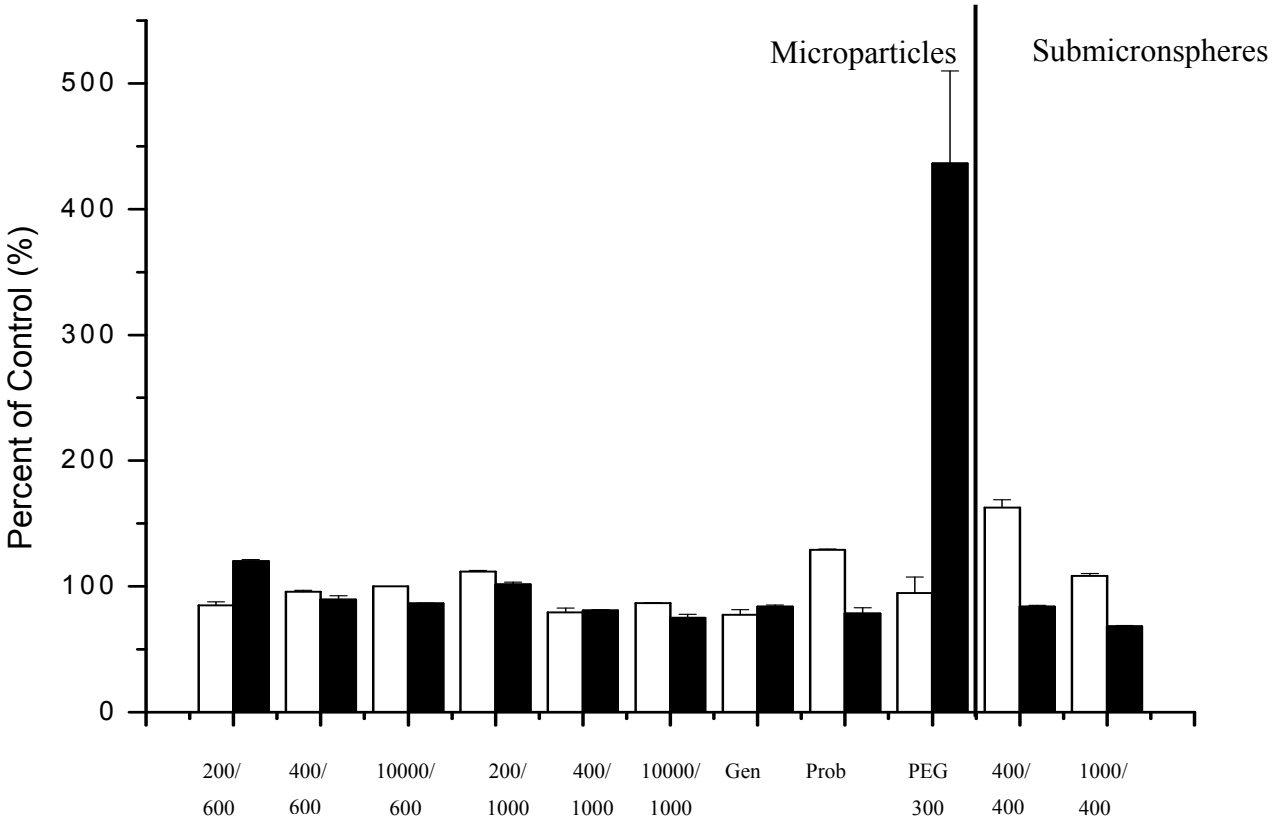

Figure 5.12: Transport of fluorescein sodium salt in the presence of various morphologies of PEG and compared to known inhibitors at 4 °C in the □ apical to basolateral direction and the ■ basolateral to apical direction. The convention used to name the hydrogels was the PEGMA MW / PEDGDMA MW (g/mol). All hydrogels were added at a concentration of 10 mg/mL. Genistein was added at a concentration of 37 μM while probenecid at 100 μM. The lineal PEG 300 was added at a concentration of 20% (v/v). The passage number was in a rage of 40-60.

It is possible for the lineal PEG morphology to be internalized in the cell and interact with the mitochondria as previously observed for pluronic block co-polymers (40). The fact that the hydrogels show no effect at the low temperature suggests that although membrane fluidity might play a role other mechanisms may be involved.

As compared to known inhibitors genistein and probenecid, all the hydrogels demonstrated a better permeability enhancement. The permeability enhancement of the known inhibitors genistein and probenecid observed in our laboratory is lower than that observed by other investigators. It is important to note that probenecid exhibited a fluorescein permeability deficit instead of an increase. Fluorescein is considered a non-specific substrate of MRP, affinity has been reported to be an MRP1, MRP2, and MRP5 substrate (37),(53, 54). Probenecid is also considered a non-specific inhibitor of MRP, inhibition mechanisms haven attributed to MRP1, MRP2, MRP4, and MRP5 (37, 55). It is important to note that both fluorescein and probenecid interact with proteins that are present in the apical and the basolateral membrane. There is a possibility that competitive interaction might be occurring. The relative expression of these transporters on Caco-2 cells has been previously reported and suggest that they are present at the following relative concentrations MRP2>MRP6>MRP4>MRP3>MRP1=MRP5 (7). Interestingly, fluorescein has also been reported to be a substrate of organic anion transporters (OAT) (53, 56) (an influx receptor). Probenecid has been reported to reduce the

permeability of fluorescein across primary porcine tubular cells as a result of OAT inhibition (56). Caco-2 cells also expresses several OAT transporters (6), which is a possible explanation for the reduction in transport. Another factor that might be taking place is increased cellular retention of the fluorescein sodium salt (commonly observed in probenecid inhibition) (57, 58) which would result in a reduced permeability. Genistein was also reported as to increase the flux of MRP substrates by Versantvoort (59). As compared to probenecid, genistein has been considered a more potent inhibitor according to [^{3}H] bis (pivaloxymethyl) -9-(2-phosphonylmethoxyethyl) adenine efflux (bis (POM) PMEA) studies on the microglia cell line (MLS-9) (60). In this study produced a 60% reduction of bis(POM)PMEA efflux as compared to 10% reduction by probenecid. However, it is important to note that the genistein concentration used in that study (200μM) is significantly higher than our concentration (37 μM). The genistein concentration used in this study was selected as the IC_{50} concentration reported elsewhere (61). It is important to note that direct comparison of the performance of inhibitors is a difficult task. There are many factors regarding cell culture as well as the diverse variations in protocol that are encountered in the literature. In order to do direct comparison experiments must be replicated in equal circumstances.

As compared to the lineal morphology counterpart PEG 300, also reported as MDR1 inhibitor, the hydrogels of the shorter crosslinker length showed a similar permeability enhancement effect. This is important because the hydrogels due to their crosslinked nature have less mobility and are less

likely to interact with the cell membrane (i.e. the integral proteins). The effects of lineal PEG morphologies of varying lengths have previously been studied. PEG of low chain lengths (PEG-4, PEG-8, PEG-20, PEG-75, PEG-150, PEG-200) did not show a transport enhancement of MDR1 substrates, however the concentrations (0.5% (w/v)) at which these experiments were performed were low as compared to other investigators (13, 62, 63). PEGs of chain lengths of 300 and 400g/mol have shown a transport enhancement of MDR1 substrates at concentrations as low as 1% (w/v) (13, 63, 64), no studies have been performed on MRP substrates. Our results show that PEG 300 has an inhibitory effect on MRP substrates as well. The effect of PEG 400 was observed whether the excipient was added at the basal or the apical side of the experiment, suggesting internalization of the polymer in accordance to Batrakova's findings (40, 44, 46, 64). Transport experiments at 4 °C seem to suggest that inhibition due to PEG 300 is due to a physical effect like membrane fluidization. Increases in membrane fluidity were corroborated for cells treated with PEG-300 (63). However, there appeared to be no correlation between membrane fluidity effects and MDR inhibition. Concentrations as low as 2.5% (v/v) produced an inhibition effect, while membrane fluidity changes were not observable until the concentrations reached 15% (v/v) (63). Results like these indicate that the effect of membrane fluidization and MDR inhibition merits further examination. There appears to be some kind of physical interaction between the lineal PEG morphology and the Caco-2 cells that is contributing to the transport enhancement of MRP substrates. Even tough,

these comparison are based on effects observed on the MDR1 protein is important to note that PEG based morphologies have been showed to interact with both MRPs and MDR1 proteins.

Submicron PEG hydrogel microspheres were synthesized to investigate the effects of increasing the surface area (i.e. interactions). Transport results of figure 5.11 demonstrate that the submicron spheres behavior is significantly lower than that from the crushed microparticles. The small particle size of the submicron sphere allows for Brownian movement of the polymer, which can result in a reduced direct interaction of the hydrogel with the cell membranes. Since the expected interaction mechanism from these hydrogel and the MRP proteins is occurring at the surface level, the difference in motion and contact between the polymer and the cell could result in a reduced response.

To summarize PEG-rich hydrogels provided a significant transport enhancement of the MRP substrate fluorescein sodium salt. This transport enhancement appears to be dependent on the hydrogel structure with both the crosslinker length and the tethered chain showing effects. However, the effect of the crosslinker length appears to be mostly due to structural parameters of the hydrogel rather to direct interaction with the MRP proteins. Experiments at the low temperature of 4 °C seem to confirm that the transport enhancement effects are due to some type of active transporter interaction, most likely the MRP proteins. Finally, these hydrogel appear to be more potent than the known inhibitors probenecid and verpamil, but similarly potent than the lineal morphology PEG-300. This evidence is sufficient to support the theory that

these hydrogels are good candidates for controlled drug delivery devices aimed at the inhibition of the MRP proteins.

Transport effects on the MDR1 substrate Rhodamine 123

Once that it was demonstrated that PEG-rich hydrogel have inhibitory effects on the MRP proteins, the next step was to evaluate their role with MDR1 proteins. At this point, the hydrogels that were evaluated were narrowed down to five and the studied variables to two (the length of the tethered chain and the particle size). The advantage of working with MDR1 proteins as opposed to MRP proteins is that these are located only in the apical side of the cell membrane, which simplifies the data analysis. They are also better understood and more data is available in the literature for comparison purposes.

The PEG-rich hydrogels were analyzed for possible effects involving the multidrug resistance protein MDR1. The fluorescent dye and MDR1 substrate Rhodamine-123 was selected (9). The transport effects were studied as function of the concentration of the hydrogel suspensions. Concentration dependent experiments were used to investigate the possibility that competitive mechanism were present. Due to the multiplicity of location of the MRP and the complexity of that system, those experiments were not performed on the fluorescein sodium salt system. As summarized in figure 5.13, transport enhancement shows a concentration dependency on the transport enhancement of Rhodamine 123 suggesting an active transporter interaction, with the MDR1 pump.

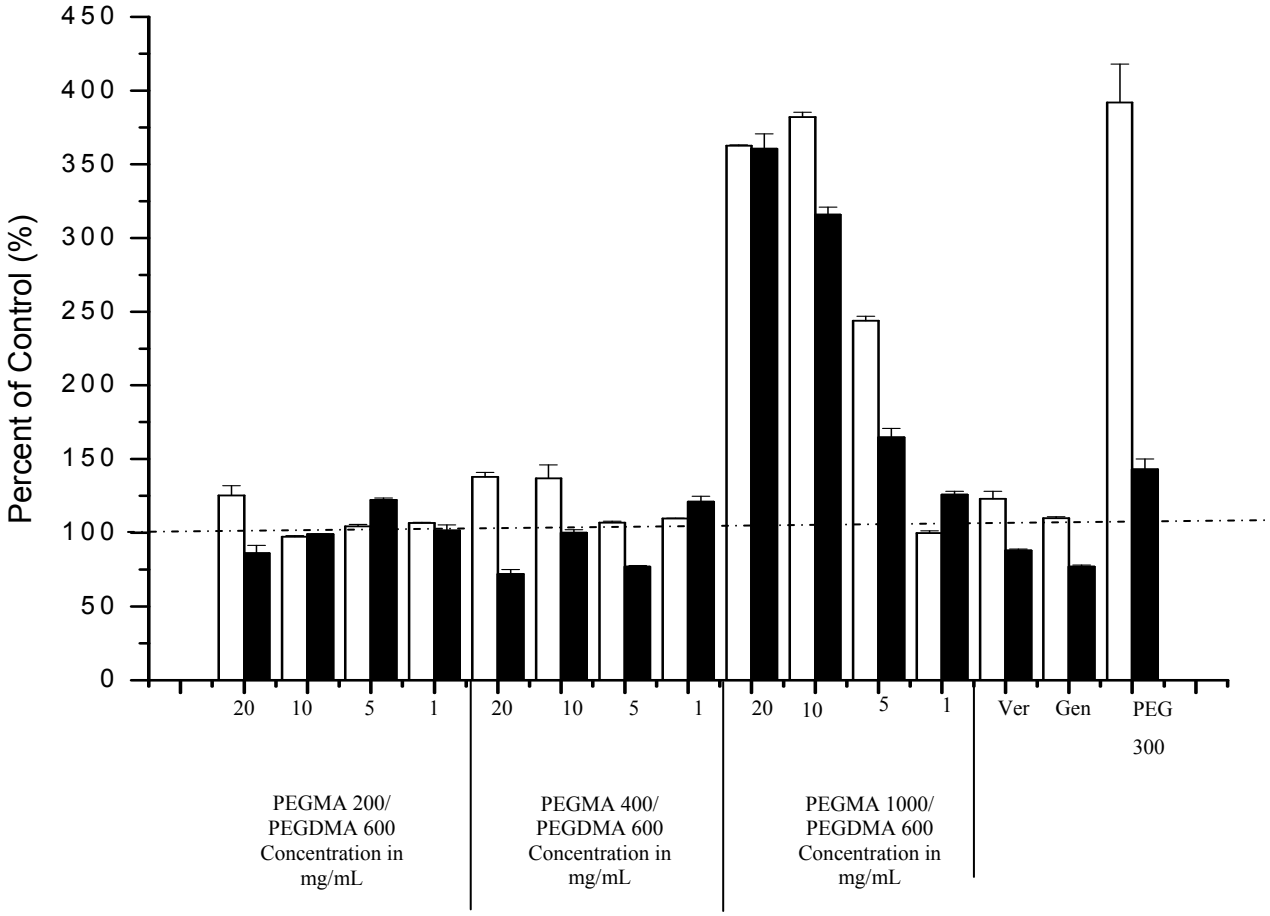

Figure 5.13: Transport of rhodamine 123 in the presence of various morphologies of PEG and compared to known inhibitors at 37 °C in the □ apical to basolateral direction and the ■ basolateral to apical direction. The convention used to name the hydrogels was the PEGMA MW / PEDGDMA MW (g/mol). Genistein was added at a concentration of 37 μM while verapamil at 100 μM. The lineal PEG 300 was added at a concentration of 20% (v/v). The passage number was in a rage of 40-60.

These results correlate well with previous data using PEG lineal polymer of 300 g/mol molecular weight where a concentration dependent enhancement was also observed (63). The PEG concentration was varied from 2.5 to 20 % with an apparently lineal correlation between concentration and transport enhancement. This lineal correlation between the concentration and transport enhancement seems to indicate that a possible competitive effect between the hydrogel and the substrate might be present. There is evidence in the literature that suggests that these polymers might be substrates of the multidrug resistance proteins. Zhang and coworkers demonstrated that 51-52% of intracellular poly(ethylene glycol)-block-polylactic acid nanoparticles were effluxed by mouse primary hepatocytes after saturation uptake was achieved at 750-1000 μg/mL concentrations. Also treatment of Kunming mice with these nanoparticle resulted in an increased expression of a variety of ABC proteins, especially MRP5 and MRP8. The results suggested an active efflux of the nanoparticles by ABC transporters, in particular MRP8. Even though this evidence is referenced for MRP8 interaction it is important to note that PEG based morphologies have been showed to interact with both MRPs and MDR1 proteins (41, 45).

It is also interesting to note that the permeability enhancement in the AB direction is usually greater in magnitude than that in the BA direction. This is typical behavior of MDR1 inhibition, the AB permeation increases while the BA permeation decrease until they are both equalized (this is known as efflux

ratio). At this point total inhibition was achieved. The fact that this behavior was observed serves as further evidence that the transport enhancement was most likely due to MDR1 inhibition.

Another important factor to consider is that the hydrogels here synthesized are composed of PEG tethered chains of increasing molecular weight (200, 400, and 1000 g/mol). There appears to be a correlation between the length of the tethered chain and the transport enhancement of rhodamine 123. This suggests that these tethered chains are playing an intricate role on the inhibition of the MDR1 protein. These findings correlate well with the results for the MRP inhibition of fluorescein sodium salt and previous studies on Pluronic block copolymers, as stated earlier. Again these findings seem to suggest an intimate contact interaction between the PEG tethered chain and the MDR1 protein. It is interesting to note that the PEGMA 1000/ PEGDMA 600 morphology demonstrated a higher inhibitory potency for the MDR1 substrate rhodamine 123 as compared to the MRP substrate fluorescein sodium salt. These two proteins differ significantly on their structure, active sites, and folding activities (65). Most notably, the MRP proteins are quite larger than the MDR1 (190 vs. 170 kDa and 5 extra transmembrane domains), since the expected interaction between the PEG hydrogel and the MDR proteins is expected to occur at the surface level, it is possible that the large size of the MRP proteins could act as an obstacle for proper hydrogel-protein interaction.

In order to attempt to increase the effect of the hydrogels as compared to the lineal morphology the effect of increasing the surface area (i.e. interactions) by reducing the particle size of the hydrogels was investigated. For this purpose hydrogel submicronspheres were synthesized. The crosslinker used for the submicron spheres differs from the one used for the crushed microparticles, because the 600 g/mol crosslinker yielded transparent submicron spheres and they were difficult to analyze with the available equipment. Figure 5.14 shows that the particle size reduction has no effect on the transport enhancement of rhodamine 123. Again, it can be concluded that these hydrogels are acting due to some intimate contact at the surface level of the cell membrane. The submicron sphere dispersions could provide a reduction in direct contact due to the Brownian motion of the particles.

As compared to the known inhibitors verapamil and genistein, again the hydrogels showed better enhancement. Another metric often used to evaluate MDR1 inhibition is the efflux ratio. This is defined as the ratio between the BA and the AB permeabilities, this metric is useful due to the polarized location of MDR1. A reduction in efflux ratio denotes partial inhibition; an efflux ratio of unity denotes total inhibition. The calculated efflux ratio for these experiments is summarized in table 5.3. As can be observed, the efflux ratio in the verapamil experiment for the controls was calculated as 1.93, while cells that were exposed to verapamil demonstrated and efflux ratio of 1.35. The results demonstrate a partial inhibition of MDR1 due to verapamil interaction. Other investigators have observed similar results (66, 67).

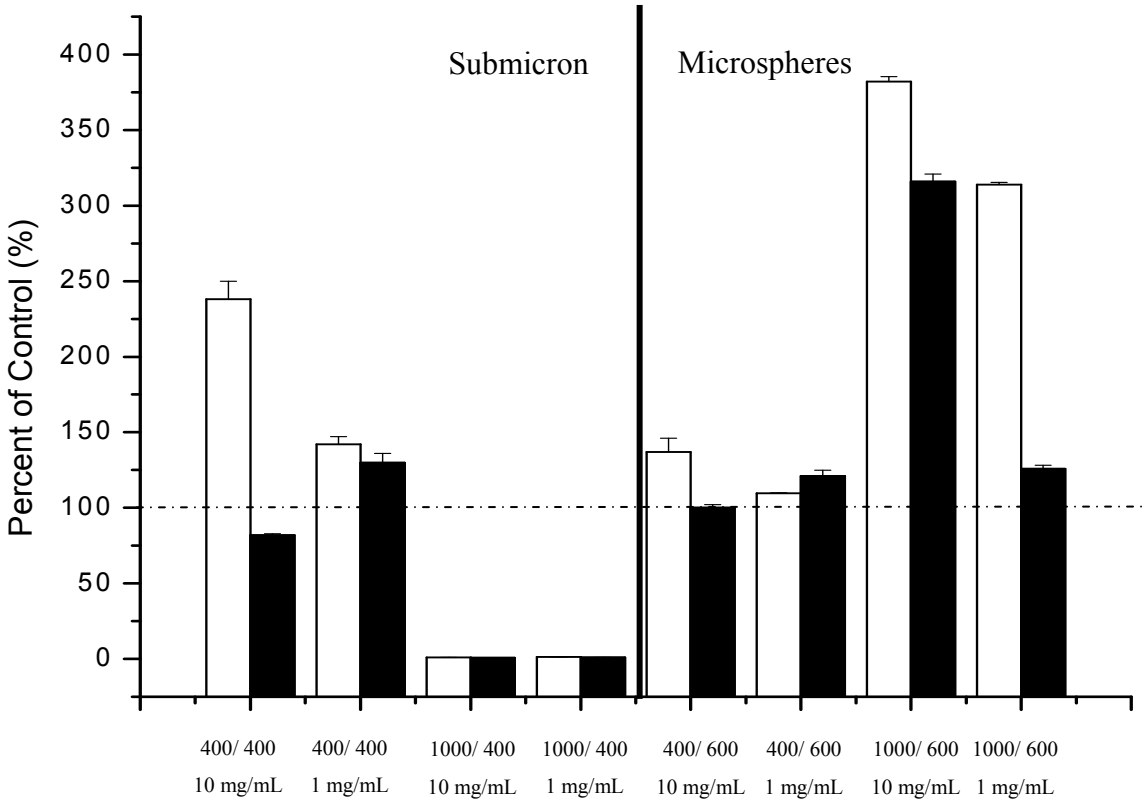

Figure 5.14: Effect of particle size on the transport of rhodamine 123 in the presence of various morphologies of PEG at 37 °C in the □ apical to basolateral direction and the ■ basolateral to apical direction. The convention used to name the hydrogels was the PEGMA MW / PEDGDMA MW (g/mol). The particle size of the microparticles ranged from 90-106 μm, while that of the submicron spheres ranged from 128-525 nm. The passage number was in a rage of 50-60.

For example, in a study of the Rhodamine 123 transport across Caco-2 cells in contact with methoxypolyethylene glycol-*block*-polycaprolactone amphiphilic diblock copolymers, verapamil was used for comparison and the AB transport enhancement was of 1.02; and the BA transport was reduced by 0.39 as compared to control. More importantly the efflux ratio was reduced from 3.20 to1.15 for a 95% inhibition (68). Also, in a study of methadone as an inhibitor of rhodamine-123 transport, verapamil was again used as a comparison basis. In those experiments, the AB transport was reduced to 0.75, and the BA transport was reduced to 0.06. Finally, the efflux ratio was reduced from 45 to 3.3 for 94% (67). However, these experiments were done on days 16-20 of culture. At this point, the cell integrity is not completely mature and cells tend to be more permeable. This can account for differences in the experiments. Our experiments showed a 75% inhibition by verapamil that is significantly lower that the one observed by other investigators. Again, it is important to note that the relative expression of the efflux pumps may play a significant role on the inhibition effect. The flavonoid, genistein has been shown to inhibit the Rhodamine 123 efflux from BALB/c-3T3 mouse fibroblast cells by 42% (69) which is significantly lower that the 28% observed during our experiments. As a word of caution it is important to keep in mind that direct comparison between laboratories is a difficult task. There are multiple variables both during cell culture and transport experiments that affect the permeability results as was very well reviewed by Volpe (70). These numbers are presented only to

provide a sense of the current developments regarding these particular inhibitors.

Table 5.3: Calculated efflux ratio for the inhibition of MDR1 calculated as the effect in transport of Rhodamine 123 at 100 μM through Caco-2 cells in the prescence and absence of several inhibitors.

Inhibitor	P_{app} BA/P_{app} AB (control)	P_{app} BA/P_{app} AB (experimental)
PEGMA 200/ PEGDMA 600 20 mg/mL	1.57+/- 0.07	1.087 +/- 0.08
PEGMA 200/ PEGDMA 600 10 mg/mL	1.31 +/- 0.01	1.33 +/- 0.002
PEGMA 200/ PEGDMA 600 5 mg/mL	1.02 +/- 0.04	1.19 +/- 0.05
PEGMA 200/ PEGDMA 600 1 mg/mL	1.05 +/- 0.03	1.00 +/- 0.05
PEGMA 400/ PEGDMA 600 20 mg/mL	2.18 +/- 0.17	1.14 +/- 0.02
PEGMA 400/ PEGDMA 600 10 mg/mL	1.20 +/- 0.04	0.87 +/- 0.04
PEGMA 400/ PEGDMA 600 5 mg/mL	1.55+/- 0.08	1.12 +/- 0.06
PEGMA 400/ PEGDMA 600 1 mg/mL	1.49 +/- 0.06	1.09 +/- 0.04
PEGMA 1000/ PEGDMA 600 20 mg/mL	1.44 +/- 0.05	0.90 +/- 0.01
PEGMA 1000/ PEGDMA 600 10 mg/mL	1.35 +/- 0.07	0.85 +/- 0.02
PEGMA 1000/ PEGDMA 600 5 mg/mL	1.24 +/- 0.08	0.84 +/- 0.02
PEGMA 1000/ PEGDMA 600 1 mg/mL	0.72 +/- 0.05	0.91 +/- 0.04
Verapail 100 μM	1.93 +/- 0.05	1.35+/- 0.06
Genistein 37 μM	2.17 +/- 0.09	1.55 +/- 0.01
PEG 300 20% (v/v)	2.53 +/- 0.15	0.92 +/- 0.05
PEGMA 400/ PEGDMA 400 10 mg/mL	1.44 +/- 0.005	0.49 +/- 0.01
PEGMA 400/ PEGDMA 400 1 mg/mL	0.84 +/- 0.04	0.76 +/- 0.02
PEGMA 1000/ PEGDMA 400 10 mg/mL	1.23 +/- 0.12	0.76 +/- 0.02
PEGMA 1000/ PEGDMA 400 1 mg/mL	1.15 +/- 0.05	0.86 +/- 0.02

5.5 Conclusions

Poly(ethylene glycol) hydrogels were designed for controlled drug delivery of MDR and MRP substrates. These devices would be capable of enhancing drug absorption by the inhibition of these pumps. During the previous chapter, it was detailed how these hydrogels are good candidates for drug delivery applications due to their swelling abilities and the relaxation controlled mechanism of diffusion. In this chapter it is clearly observed that these hydrogel are able to enhance the transport of both the MRP and MDR efflux pumps substrates. Data also appears to indicate that this transport enhancement is most likely due to some type of interaction with these pumps. The concentration dependent data for the MDR1 substrate rhodamine 123 appears to indicate that the interaction mechanism might be competitive. Relatively speaking the transport enhancement properties of the hydrogels was significantly more potent than those of the known inhibitors probenecid, verapamil and genistein. Although the transport enhancement inhibition of the hydrogels was similar to that of the lineal morphology PEG 300 it is important to stress that the lineal morphology is not suitable for controlled drug delivery applications.

The transport enhancement appears to depend mostly on the length of the PEG tethered chain with intermediate lengths providing the best results. However, the increased surface area of they hydrogel does not appear to indicate that this leads to an increase in transport enhancement, which may

indicate that that some type of external interaction may be contributing to the transport enhancement. Previous authors have suggested that the inhibition of polyethoxylated structures is due to membrane fluidity enhancement. This membrane fluidity changes may lead to perturbations in the conformational changes that the proteins must endure to confer efflux. It may also lead to a more leaky membrane and therefore enhanced transport. This is certainly a possible mechanism of action for the PEG hydrogels and an avenue that will be further explored during the next chapter.

5.6 References

1. K. L. Audus, R. L. Bartel, I. J. Hidalgo, and R. T. Borchardt. The Use of Cultured Epithelial and Endothelial Cells for Drug Transport and Metabolism Studies. *Pharmaceutical Research* **7**: 435-451 (1990).
2. C. Bailey, P. Bryla, and A. W. Maick. The Use of the Intestinal Epithelial Cell Culture Model, Caco-2 in Pharmaceutical Development. *Advanced Drug Delivery Reviews* **22**: 85-103 (1996).
3. P. Artursson. Cell Culture as Models for Drug Absorption Across Intestinal Mucosa. *Critical Reviews in Therapeutic Drug Carrier Systems* **8**: 305-330. (1991).
4. P. Artursson, P. K., and K. Luthman. Caco-2 Monolayers in Experimental and Theoretical Predictions of Drug Tranport. *Advanced Drug Delivery Reviews* **46**: 27-43 (2001).
5. L. Gan, C. Eads, T. Niederer, A. Bridgers, S. Yanni, P. Hsyu, F. J. Pritchard, and D. Thakker. Use of Caco-2 Cells as an in Vitro Intestinal Absorption and Metabolism Model. *Drug Development and Industrial Pharmacy* **20**: 615-631 (1994).
6. C. Hilgendorf, G. Ahlin, A. Seithel, P. Artursson, A.-L. Ungell, and J. Karlsson. Expression of 36 drug transporter genes in human intestine, liver, kidney, and organotypic cell lines. *Drug Metabolism and Disposition* **35**: 1333-1340 (2007).
7. H. M. Prime-Chapman, R. A. Fearn, A. E. Cooper, V. Moore, and B. H. Hirst. Differential Multidrug Resistance-Associated Protein 1 through 6 Isoform Expression and Function in Human Intestinal Epithelial Caco-2 Cells. *The Journal of Pharmacology and Experimental Therapeutics* **295**: 360–366 (2000).
8. K. B. Kostoand W. M. Deen. Hindered Convection of Macromolecules in Hydrogels. *Biophysical Jorunal* 277-286 (2005).
9. M. V. S. Varma, Y. Ashokraj, C. S. Dey, and R. Panchagnula. P-glycoprotein inhibitors and their screening: a perspective from bioavailability enhancement. *Pharmaceutical Research* **48**: 347-359 (2003).
10. M. Nerurkar, P. S. Burton, and R. T. Borchardt. The Use of Surfactants to Enhance the Permeability of Peptides Through Caco-2 Cells by Inhibition of an Apically Polarized Efflux System. *Pharmaceutical Research* **13**: 528-534 (1996).
11. P. K. Dudeja, K. M. Anderson, J. S. Harris, L. Buckingham, and J. S. Coon. Reversal of Multidrug Resistance Phenotype by Surfactants: Relationship to Membrane Lipid Fluidity. *Archives of Biochemistry and Biophysics* **319**: 309-315 (1995).
12. B. D. Rege, J. P. Y. Kao, and J. E. Polli. Effects of nonionic surfactants on membrane transporters in Caco-2 cell monolayers. *European Journal of Pharmaceutical Sciences* **16**: 237-246 (2002).

13. E. D. Hugger, Novak, B. L., Burton, P. S., Audus, K. L., Borchardt, R. T. A Comparison of Commonly Used Polyethoxylated Pharmaceutical Excipients on Their Ability to Inhibit P-glycoprotein Activity In Vitro. *Journal of Pharmaceutical Science* **91**: 1991-2002 (2002).
14. C.-H. Choi. ABC transporters as multidrug resistance mechanisms and the development of chemosensitizers for their reversal. *Cancer Cell International* **5**: 30 (2005).
15. A. E. Senior, M. K. Al-Shawi, and I. L. Urbatsch. The catalytic cycle of P-glycoprotein. *FEBS Letters* **377**: 285-289 (1995).
16. J. W. Kimball. *Biology*, Addison Wesley Publishing Company, Boston, MA, 1994.
17. M. Mackay, I. Williamson, and J. Hastewell. (A) Cell Biology of Epithelia. *Advanced Drug Delivery Reviews* **7**: 313-338 (1991).
18. J. Swan. Online Anatomy & Physiology Resources.
19. B. Alberts, A. Johnson, J. Lewis, M. Raff, K. Roberts, and P. Walter. *Molecular Biology of the cell*, Garland Science, New York, NY, 2002.
20. H. N. Nellans. Mechanisms of Peptide and Protein Absorption (1) Paracellular intestinal transport: modulation of absorption. *Advanced Drug Delivery Reviews* **7**: 339-366 (1991).
21. L. A. Lapierre. The Molecular Structure of the Tight Junction. *Advanced Drug Delivery Reviews* **41**: 255-264. (2000).
22. G. Barry. Structure, Biochemistry and Assembly of Epithelial Tight Junctions. *American Journal of Physiology* **253**: C749-C758 (1987).
23. F. Lacaz-Viera, J. M. M., P. Farshori, and B. Kachar. Calcium Site Specificity: Early Ca2+ related Tight Junction Events. *Journal of General Biology* **110 0**: 727-74 (1997).
24. B. M. Denkerand S. K. Nigam. Molecular Structure and Assembly of the Tight Junction. *American Journal of Physiology* **274**: F1-F9 (1998).
25. F. Lacaz-Viera, M. M. M. Jaeger, P. Farshori, and B. Kachar. Small Synthetic Peptides Homologous to Segments of the First External Loop of Occludin Impair Tight Junction Resealing. *Journal of Membrane Biology* **168**: 289-297 (1999).
26. Y. H. Tai, J. Flick, S. A. Levine, J. L. Madara, G. W. G. Sharp, and M. Donowitz. Regulation of Tight Junction Resistance in T84 Monolayers by Elevation in Intracellular Ca2+: A Protein Kinase C Effect. *Journal of Membrane Biology* **150**: 71-79 (1996).
27. P. Farshoriand B. Kachar. Redistribution and Phosphorylation of Occludin During Opening and Resealing of Tight Junctions in Cultured Epithelial Cells. *Journal of Membrane Biology* **170**: 147-156 (1999).
28. J. R. Turner, B. K. Rill, S. L. Carlson, D. Carnes, R. Kerner, R. J. Mrsny, and J. L. Madara. Physiological Regulation of Epithelial Tight Junctions is Associated with Myosin Light-Chain Phosphorylation. *American Journal of Physiology* **273**: C1378-C1385. (1997).
29. R. Taharand L. K. Basco. Molecular Epidemiology of Malaria in Cameroon. XXVI. Twelve-Year In Vitro and Molecular Surveillance of Pyrimethamine Resistance and Experimental Studies to Modulate

Pyrimethamine Resistance. *American Journal of Tropical Medicine and Hygene* **77**: 221-227 (2007).
30. J. N. Cogburn, M. G. Donovan, and C. S. Schasteen. A Model of Human Small Intestinal Absorptive cells. 1. Transport Barrier. *Pharmaceutical Research* **8**: 210-216 (1991).
31. A. Adson, P. S. Burton, T. J. Raub, C. L. Barsuhn, K. L. Audus, and N. F. H. Ho. Passive Diffusion of Weak Organic Electrolytes Across Caco-2 Cell Monolayers: Uncoupling the Contributions of Hydrodynamic, Transcellular, and Paracellular Barriers. J. Pharm. Sci., 84 (1995) 1197-1204. *Journal of Pharmeutical Science* **84**: 1197-1204 (1995).
32. J. Karlsoonand P. Artursson. A method for the detrmination of cellular permeability coefficients and aqueous boundary layer thickness in monolayers of intestinal epitelial (Caco-2) cells grown in permeable filter chambers. *International Journal of Pharmaceutics* **71**: 55-64 (1991).
33. D. W. Miller, Bratakovaand K. E. V., A. V. Inhibition of Multidrug Resistance Associated Protein (MRP) Functional Activity with Pluronic Block Copolymers. *Pharmaceutical Research* **16**: 396-401 (1999).
34. R. W. Glenny, S. Bernard, and M. Brinkley. Validation of fluorescent labeled microspheres for measurement of regional organ perfusion. *Journal of Applied Physiology* **74**: (1993).
35. H. Sato, J. R. Kusel, and J. Thornhill. Excretion of fluorescent substrates of mammalian multidrug resistance-associated protein (MRP) in the Schistosoma mansoni excretory system. *Parasitology* **128**: 43-52 (2004).
36. L. M. S. Chan, S. Lowes, and B. H. Hirst. The ABCs of Drug Transport in Intestine and Liver: Efflux Proteins Limiting Drug Absorption and Bioavailability. *European Journal of Pharmaceutical Sciences* **21**: 25-51 (2004).
37. W. Lo¨scherand H. Potschka. Blood-Brain Barrier Active Efflux Transporters: ATP-Binding Cassette Gene Family. *NeuroRx: The Journal of the American Society for Experimental NeuroTherapeutics* **Vol. 2**: 86–98 (2005).
38. E. V. Batrakova, S. Lee, S. Li, A. Venne, V. Alakhov, and A. V. Kabanov. Fundamental Relationships Between the Composition of Pluronic Block Copolymers and Their Hypersensitization Effect in MDR Cancer Cells. *Pharmaceutical Research* **16**: 1373-1379 (1999).
39. A. V. Kabanov, E. V. Batrakova, and V. Y. Alakhov. Pluronic block copolymers for overcoming drug resistance in cancer. *Advanced Drug Delivery Reviews* **54**: 759–779 (2002).
40. E. Batrakova, S. Li, W. Elmquist, D. Miller, V. Alakhov, and A. Kabanov. Mechanism of sensitization of MDR cancer cells by Pluronic block copolymers: Selective energy depletion. *British Journal of Cancer* **85**: 1987–1997 (2001).
41. E. V. Batrakova, H. Han, V. Yu, D. W. Miller, and A. V. Kabanov. Effects of Pluronic Block Copolymers on Drug Absorption in Caco-2 Cell Monolayers. *Pharmaceutical Research* **15**: 850-855 (1998).

42. E. V. Batrakova, S. Li, V. Y. Alakhov, W. F. Elmquist, D. W. Miller, and A. V. Kabanov. Sensitization of Cells Overexpressing Multidrug-Resistant Proteins by Pluronic P85. *Pharmaceutical Research* **20**: 1581-1590 (2003).
43. E. V. Batrakova, S. Li, V. Y. Alakhov, D. W. Miller, and A. V. Kabanov. Optimal Structure Requirements for Pluronic Block Copolymers in Modifying P-glycoprotein Drug Efflux Transporter Activity in Bovine Brain Microvessel Endothelial Cells. *The Journal of Pharmacology and Experimental Therapeutics* **304**: 845-854 (2003).
44. E. V. Batrakova, S. Li, Y. Li, V. Y. Alakhov, and A. V. Kabanov. Effect of Pluronic P85 on ATPase Activity of Drug Efflux Transporters. *Pharmaceutical Research* **21**: 2226-2233 (2004).
45. E. V. Batrakova, S. Li, D. W. Miller, and A. V. Kabanov. Pluronic P85 Increases Permeability of a Broad Spectrum of Drugs in Polarized BBMEC and Caco-2 Cell Monolayer. *Pharmaceutical Research* **16**: 1366-1372 (1999).
46. E. V. Batrakova, S. Li, S. V. Vinogradov, V. Y. Alakhov, Donald W. Miller, and A. V. Kabanov. Mechanism of Pluronic Effect on P-Glycoprotein Efflux System in Blood-Brain Barrier: Contributions of Energy Depletion and Membrane Fluidization. *The Journal of Pharmacology and Experimental Therapeutics* **299**: 483-493 (2001).
47. E. V. Batrakova, S. V. Vinogradov, S. M. Robinson, M. L. Niehoff, W. A. Banks, and A. V. Kabanov. Polypeptide Point Modifications with Fatty Acid and Amphiphilic Block Copolymers for Enhanced Brain Delivery. *Bioconjugate Chemistry* **16**: 793-802 (2005).
48. A. V. Kabanov, E. V. Batrakova, and V. Y. Alakhov. A n essential relationship between ATP depletion and chemosensitizing activity of Pluronic block copolymers. *Journal of Controlled Release* **91**: 75–83 (2003).
49. A. V. Kabanov, E. V. Batrakova, and D. W. Miller. Pluronic block copolymers as modulators of drug efflux transporter activity in the blood–brain barrier. *Advanced Drug Delivery Reviews* **55**: 151–164 (2003).
50. T. Minkoa, E. V. Batrakova, S. Li, Y. Li, R. I. Pakunlua, V. Y. Alakhov, and A. V. Kabanov. Pluronic block copolymers alter apoptotic signal transduction of doxorubicin in drug-resistant cancer cells. *Journal of Controlled Release* **105**: 269–278 (2005).
51. S. Vinogradov, E. Batrakova, and A. Kabanov. Poly(ethylene glycol)-polyethyleneimine NanoGel™ particles: novel drug delivery systems for antisense oligonucleotides. *Colloids and Surfaces B-Biointerfaces* **16**: 291-304. (1999).
52. S. S. Vinogradov, T. K. Bronich, and A. V. Kabanov. Nanosized cationic hydrogels for drug delivery: preparation, properties and interactions with cells. *Advanced Drug Delivery Reviews* **54**: 135-147 (2002).
53. B. T. Hawkins, S. M. Ocheltree, K. M. Norwood, and R. D. Egleton. Decreased blood-brain barrier permeability to fluorescein in streptozotocin-treated rats. *Neuroscience Letters* **411**: 1–5 (2007).

54. S. Notenboom, A. C. Wouterse, B. Peters, L. H. Kuik, Suzanne Heemskerk, F. G. M. Russel, and R. Masereeuw. Increased Apical Insertion of the Multidrug Resistance Protein2 (MRP2/ABCC2) in Renal Proximal Tubules following Gentamicin Exposure. *The Journal of Pharmacology and Experimental Therapeutics* **318**: 1194–1202 (2006).
55. C. J. Endres, P. Hsiao, F. S. Chung, and J. D. Unadkat. The Role of Transporters in Drug Interactions. *European Journal of Pharmaceutical Sciences* **27**: 501-517 (2006).
56. S. Philipp, G. Heike, and B. Juergen. Primary porcine proximal tubular cells as a model for transepithelial drug transport in human kidney. *European Journal of Pharmaceutical Sciences* **28**: 141-154 (2006).
57. H. Sun, D. W. Miller, and W. F. Elmquist. Effect of Probenecid on Fluorescein Transport in the Central Nervous System Using In Vitro and In Vivo Models. *Pharmaceutical Research* **18**: 1542-1549 (2001).
58. H. Chanteux, F. V. Bambeke, M.-P. Mingeot-Leclercq, and P. M. Tulkens. Accumulation and Oriented Transport of Ampicillin in Caco02 Cells from Its Pivaloyloxymethylester Prodrug, Pivampicillin. *Antimicobial Agents and Chemotherapy* **49**: 1279-1288 (2005).
59. C. Versantvoort, T. Rhodes, and P. Twentyman. Acceleration of MRP associated efflux of Rhodamine 123 by genistein and related compounds. *British Journal of Cancer* **74**: 1949-54 (1996).
60. S. Dallas, L. Schlichter, and R. Bendayan. Multidrug Resistance Protein (MRP) 4- and MRP 5-Mediated Efflux of 9-(2-Phosphonylmethoxyethyl)adenine by Microglia. *Journal of Pharmacology And Experimental Therapeutics* **309**: Vol. 309, No. 3 (2004).
61. S. Zhang, X. Yang, and M. E. Morris. Combined Effects of Multiple Flavonoids on Breast Cancer Resistance Protein (ABCG2)- Mediated Transport. *Pharmaceutical Research* **21**: 1263-1274 (2004).
62. S. W. Wang, J. Monagle, C. McNulty, D. Putnam, and H. Chen. Determination of P-glycoprotein Inhibition Excipients and Their Combinations Using an Integrated High-Throughput Process. *Journal of Pharmaceutical Sciences* **93**: 2755-2767 (2004).
63. E. D. Hugger, K. L. Audus, and R. T. Borchardt. Effects of Poly(ethylene glycol) on Efflux Transporter Activity in Caco-2 Cell Monolayers. *Journal of Pharmaceutical Science* **91**: 1980-1990 (2002).
64. B. M. Johnson, W. N. Charman, and C. J. H. Porter. An In Vitro Examination of the Impact of Polyethylene Glycol 400, Pluronic P85, and Vitamin E d-a-Tocopheryl Polyethylene Glycol 1000 Succinate on PGlycoprotein Efflux and Enterocyte-Based Metabolism in Excised Rat Intestine. *AAPS PharmSci* **4**: 1-13 (2002).
65. D. R. Hipfner, R. G. Deeley, and S. P. C. Cole. Structural, mechanistic and clinical aspects of MRP1. *Biochimica et Biophysica Acta* **1461**: 359-376 (1999).
66. J. Zastre, J. Jackson, M. Bajwa, R. Liggins, F. Iqbal, and H. Burta. Enhanced cellular accumulation of a P-glycoprotein substrate, rhodamine-123, by caco-2 cells using low molecular weight

methoxypolyethylene glycol-block-polycaprolactone diblock copolymers. *European Journal of Pharmaceutics and Biopharmaceutics* **54**: 299–309 (2002).
67. E. Stömer, M. D. Perloff, L. L. v. Moltke, and D. J. Greenblatt. Methadone Inhibits Rhodamine 123 Transport in Caco-2 Cells. *Drug Metabolism and Disposition* **29**: 954–956 (2001).
68. J. Zastre, J. Jackson, and H. Burt. Evidence for Modulation of P-glycoprotein–Mediated Efflux by Methoxypolyethylene Glycol-block-PolycaprolactoneAmphiphilic Diblock Copolymers. *Pharmaceutical Research* **21**: 1489-1497 (2004).
69. A. F. Castroand G. A. Altenberg. Inhibition of Drug Transport by Genistein in Multidrug-Resistant Cells Expressing P-Glycoprotein. *Biochemical Pharmacology* **53**: 89-93 (1997).
70. D. A. Volpe. Variability in Caco-2 and MDCK Cell-Based Intestinal Permeability Assays. *Journal of Pharmaceutical Science* **97**: 712-725 (2008).

6.0 Membrane Fluidity Assessment using Confocal Laser Scanning Microscopy

6.1 Introduction

The plasma membrane is essential for cell function; it encloses the cell, defines its boundaries, and maintains the differences between the cytosol and the extracellular environment. It is composed of a lipid bilayer and protein molecules, held together by noncovalent interactions as observed in figure 6.1 (1, 2). The lipid molecules that are present in the cell membrane are called phospholipids and they are amphipathic (they have a polar end and a non-polar end) as can be observed in figure 6.2. Due to their cylindrical shape and amphipatic nature, the phospholipids tend to spontaneously arrange themselves into bilayers. The mechanism for their self-arrangement is governed by thermodynamics. If the lipids are dispersed in water, the adjacent water molecules will reorganize themselves into ice-like cages that surround the hydrophobic molecules. This reorganization causes an increase in the free energy. In order to reduce the energy, the hydrophopic tails form clusters with the intention of affecting the smallest amount of water molecules as possible (2).

As a consequence, the plasma membrane is not a static entity rather is in constant movement, this is known as the Fluid Mosaic Model (1, 2). It was around 1970 that scientist first recognized that the individual phospholipids are able to diffuse freely within the lipid bilayers. These studies were first performed in artificial lipid layers.

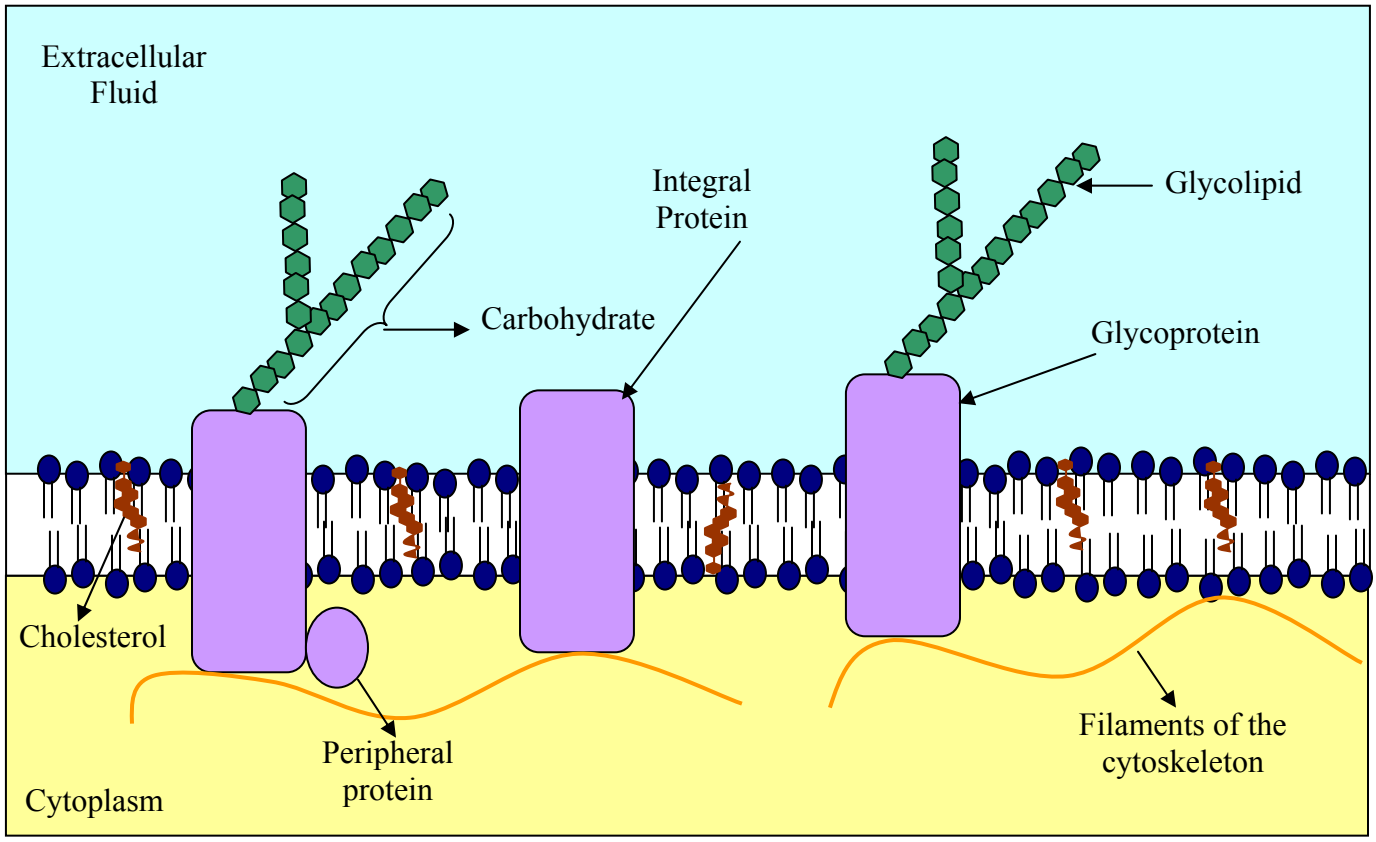

Figure 6.1: Schematical representation of the plasma membrane and its componets. The membrane is composed of a phospholipid bilayer and protein molecules (3).

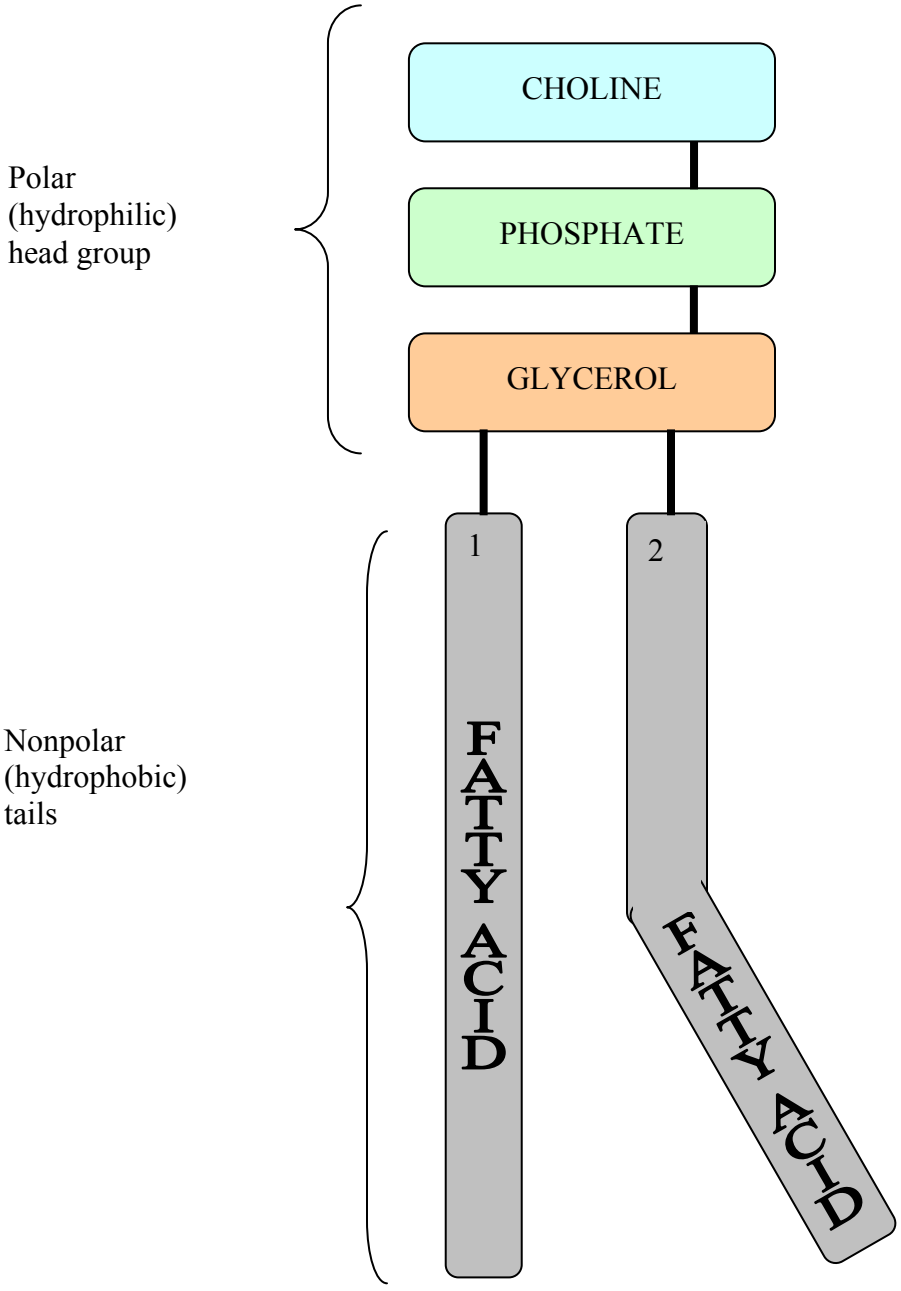

Figure 6.2: Schematic representation that describes the composition of a phospolipid molecule (2).

There are two types of preparations for these layers. The first one is the spherical vesicles called liposomes. These vesicles vary in size from about 25 nm to 1 μm depending on how they are produced. They are also named differently according to their size, small unilamellar vesicles (SUV) (up to 90 nm), large unilamellar vesicles (LUV) (around 500 nm), and giant unilamellar vesicles (GUV) (around 12500 nm) (4). The second are planar bilayers, called black membranes that are formed across a hole in a partition between two aqueous compartments.

In general, there are three different types of phospholipid movements that can occur. The first one, is lateral diffusion, it is the sideways movement and place exchange of the lipids with a monolayer. This event is very fast and occurs frequently (about 10^7 times per second) (2). The second is flip-flop, which is the migration of one phospholipid from one monolayer (leaflet) to the other. This event is very slow and occurs rarely (once a month for one individual molecule). The last one is spinning, in which the lipids are able to rotate very rapidly along their axis. These events are summarized in figure 6.3. The fluidity of the plasma membrane also depends on external factors such as temperature and composition. Lower temperatures will produce stiffer membranes. Therefore, the membrane will change state from a liquid to a crystalline (or gel) state as the temperature is lowered. Changing the composition of the hydrophobic tails to shorter or unsaturated chains lowers the phase transition temperature.

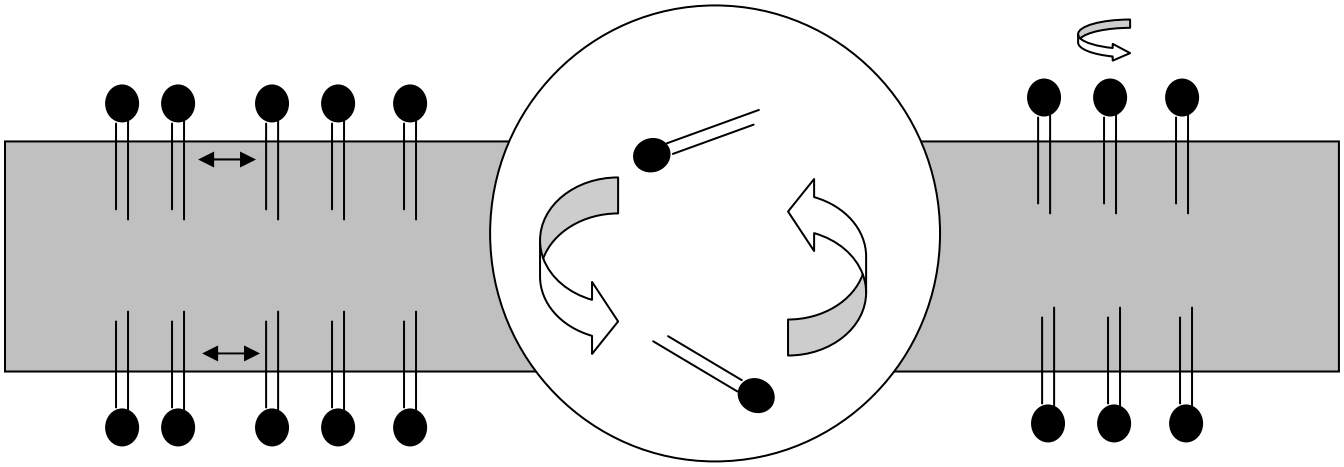

(A) Lateral Movement

(B) Flip-Flop

(C) Spinning

Figure 6.3: Schematical representation of the different types of movements that phospholipids are able to initiate, (A) lateral diffusion, (B) flip-flop, and (C) spinning (5).

Shorter chain length reduces the tendency of the hydrophobic tails to interact with one another while the kinks produced in unsaturated tails makes them more difficult to pack together. Also, the addition of other compounds such as glycolipids and cholesterol has effects on the membrane fluidity. Eucaryotic plasma membranes contain large amounts of cholesterol, typically up to one molecule for every phospholipid molecule. The rigid steroid ring structure of cholesterol tends to interact with the hydrocarbon chains of the phospholipids and immobilize them. Cholesterol also prevents the hydrocarbon chains from coming together and crystallizing and makes the membrane less deformable.

A change in membrane fluidity has been attributed as the mechanism responsible for MDR1 inhibition conferred by polyethoxylated compounds. It is hypothesized that these molecules interact with the plasma membrane making them more fluid and therefore more permeable. In order to explore this hypothesis, it was important to perform studies in membrane fluidity that could latter be compared to the transport effects and observe possible correlations.

6.2 Background

6.2.1 Methods to measure membrane fluidity

There are three known methods to measure the fluidity of the plasma membrane. The first one is fluorescence anisotropy. It is based on the principle of photo selective excitation of fluorophores by polarized light. In an isotropic solution, the fluorophores are randomly oriented. If this solution is

excited with a polarized light only those who are parallel to the excitation vector will be energized. This will result in a partially oriented population of fluorescence emission (6). Therefore, fluorescence anisotropy can be defined as (6, 7):

$$R = \frac{I_{par} - I_{per}}{I_{par} + 2I_{per}} \qquad [6.1]$$

where I_{par} and I_{per} are the emission fluorescence intensity parallel and perpendicular to the plane of excitement.

The spatial movement of the flurophores has a negative effect on the anisotropy, therefore, fluorescence anisotropy has been deemed as the inverse of membrane fluidity. That is that an increase in anisotropy means a reduction in membrane fluidity and vice versa. The advantage of this method is that is fairly simple and the equations involved for the calculation are simple as well and no approximations are required. On the down side, not all fluorescent spectrophotometers have capabilities to analyze polarized light. Also, this technique is best suited for vesicles and cells that are on suspension and not all systems are suitable for this type of analysis. Like for example, adherent cells like Caco-2 (7). Researchers that have used this technique on adherent cells, usually put them in suspension in order to perform the analysis. Caution must be taken when analyzing the results because the properties of adherent cells in suspension may vary from those in their native form. However, it is important

to note that its use on adherent cells has been previously reported (8). In this case a special setup was used using a epifluorescence microscope.

For this technique there are various fluorescent probes that are commonly employed. The most popular ones used for this application are 1-(4-trimethylammoniumphenyl)-6-phenyl-1,3,5 hexatiene p-toluenesulfonate (TMA-DPH) and 1,6-Diphenyl-1,3,5 hexatriene (DPH). These are largely sensitive to only the angular reorientation of lipid acyl chains. This motion does not necessarily correlate with other dynamic processes such as lateral diffusion (9). These probes are often used because the orientation of the fluorophophore within the bilayer is somewhat constrained. DPH orients itself parallel to the lipid chain, while TMA-DPH orients itself parallel to the membrane surface (10).

The second method is electron spin resonance (ESR). It is a technique similar to nuclear magnetic resonance, but electron spins are excited instead of atomic nuclei spins. The method can be applied by varying the photon frequency incident to the sample while keeping the magnetic field constant or vice versa. Usually the latter one is used. The increase in magnetic field causes the gap in the electron spin energy state to widen until it matches the energy of the microwaves. At this point, the unpaired electrons can move between the two states and since there are typically more electrons in the lower state this causes energy absorption. This energy is monitored and converted to spectrum (11). For membrane fluidity experiments, the phospholipids are usually marked with a spin-labeling probe like 5-doxyl stearic acid, these markers usually have a group like NO^{-} that has an unpaired electron making it

suitable for ESR experiments. The advantage of this technique is that all three phospholipid movements can be analyzed. The disadvantage is that it is a complicated method and has large uncertainties.

The last method is fluorescence recovery after photobleaching (FRAP). This technique requires the labeling of the phospholipids with a fluorescent probe. At time zero a small (usually circular) area is permanently bleached. Due to the fast and constant lateral movement of the phospholipids, the area will regain fluorescence at least partially. Therefore, the fluorescent intensity of the bleached area is monitored with time as described in figure 6.4. The time required for fluorescence recovery is directly related to the membrane fluidity.

These experiments are usually carried out in a confocal laser scanning microscope (CLSM) coupled with acousto-optic tunable filters (AOTF) which allows the polarization of the laser beam and it's filtering to a specific region within the visual field. Confocal laser scanning microscopy (CLSM) has become an invaluable tool in biology research. Marvin Minsky originally developed it in the 1950's, but it was not until the 1980 when it became commercially available (12). During LSCM a coherent light emmited by a laser (excitation source) is reflect by a dichromatic mirror and scanned across a specimen in a defined focal plane. S mixture of emitted fluorescence and reflected laser light is recollected by the objective. The beam splitter separates the light allowing the laser light to pass through and reflecting the emitted light to the detector. Before reaching the detector the emitted light must pass a pinhole that is located exactly at the confocal point. Therefore, only emitted

light that passes through the focal point reaches the detector, which translates into high quality images. The emitted light signal is usually collected in a photomultiplier tube (PMT) that transforms the light signal into an electrical one.

It is called laser scanning because the image is constructed one point at a time. The focal point of the lens can be varied and therefore digital three-dimensional images of the specimen can be constructed. Also, since CLSMs are coupled to a computer, time series experiments are also possible. The principles of CLSM are summarized in figure 6.5.

During FRAP experiments the phospholipids are labeled with a fluorescent probe that has high affinity for them; like for example {6-[N-(7-nitrobenz-2-oxa-1,3-diazol-4-yl)amino)hexanoyl]sphingosyl phosphocholine} (NBD - C6 -sphingomyelin) or 1,1'- dioctadecyl- 3,3,3',3'-tetramethylindocarbocyanine perchlorate (DiI-C18). The advantage of this technique is that is fairly simple and it also allows the analysis of the lateral movement of integral proteins. The disadvantage is that care must be taken during image acquisition to avoid misinterpretation of the results.

Due to the ease of experimentation and availability of the equipment, fluorescence recovery after photobleaching (FRAP) was selected to conduct the membrane fluidity experiments. FRAP also, offers several advantages over fluoresce anisotropy, which is also an easy to implement technique. FRAP is conveniently limited to adherent cells, like Caco-2. Also, there is no controversy regarding the interpretation of the results and its relationship to lateral diffusion.

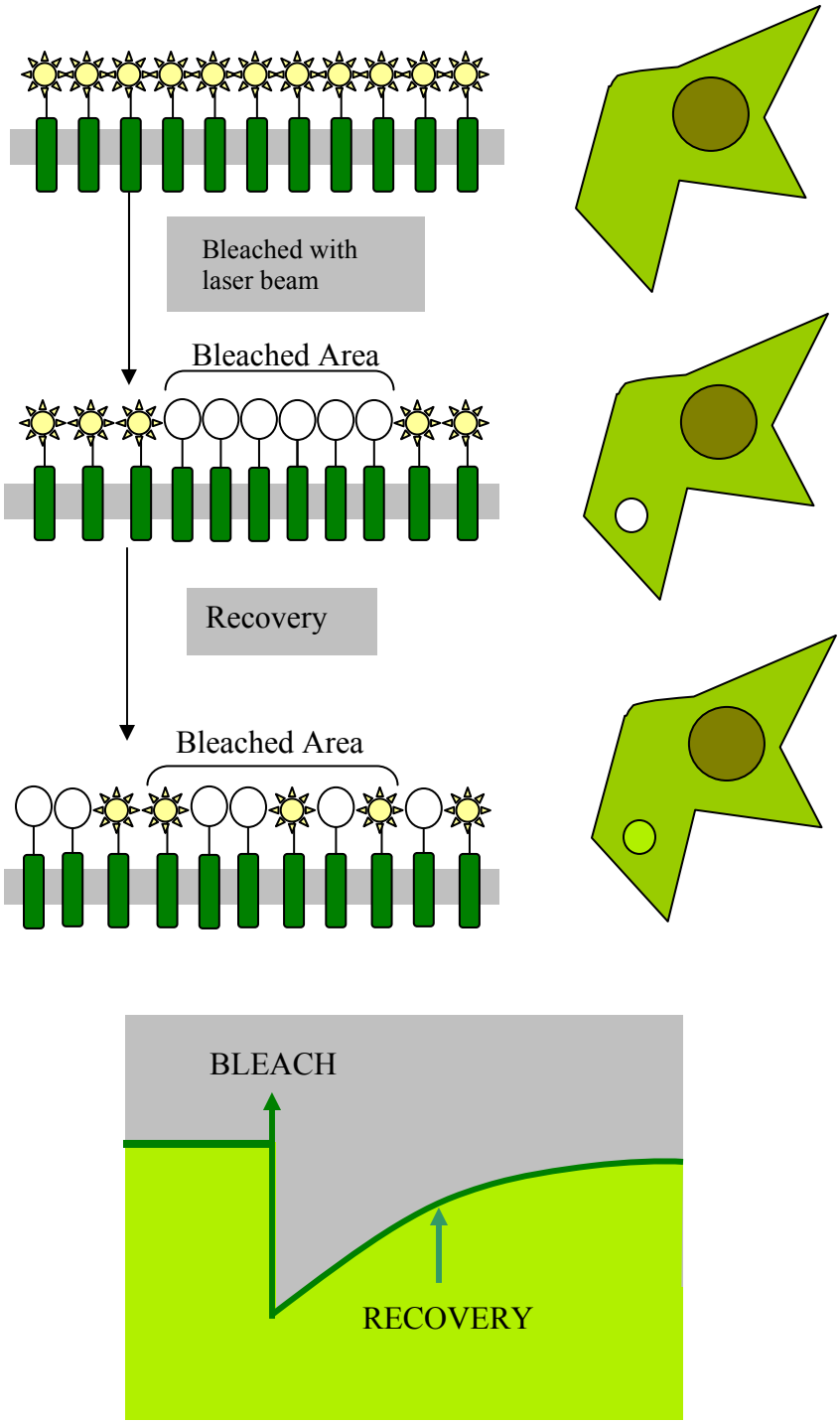

Figure 6.4: Schematic representation of a fluorescence recovery after photobleaching (FRAP) experiment (2).

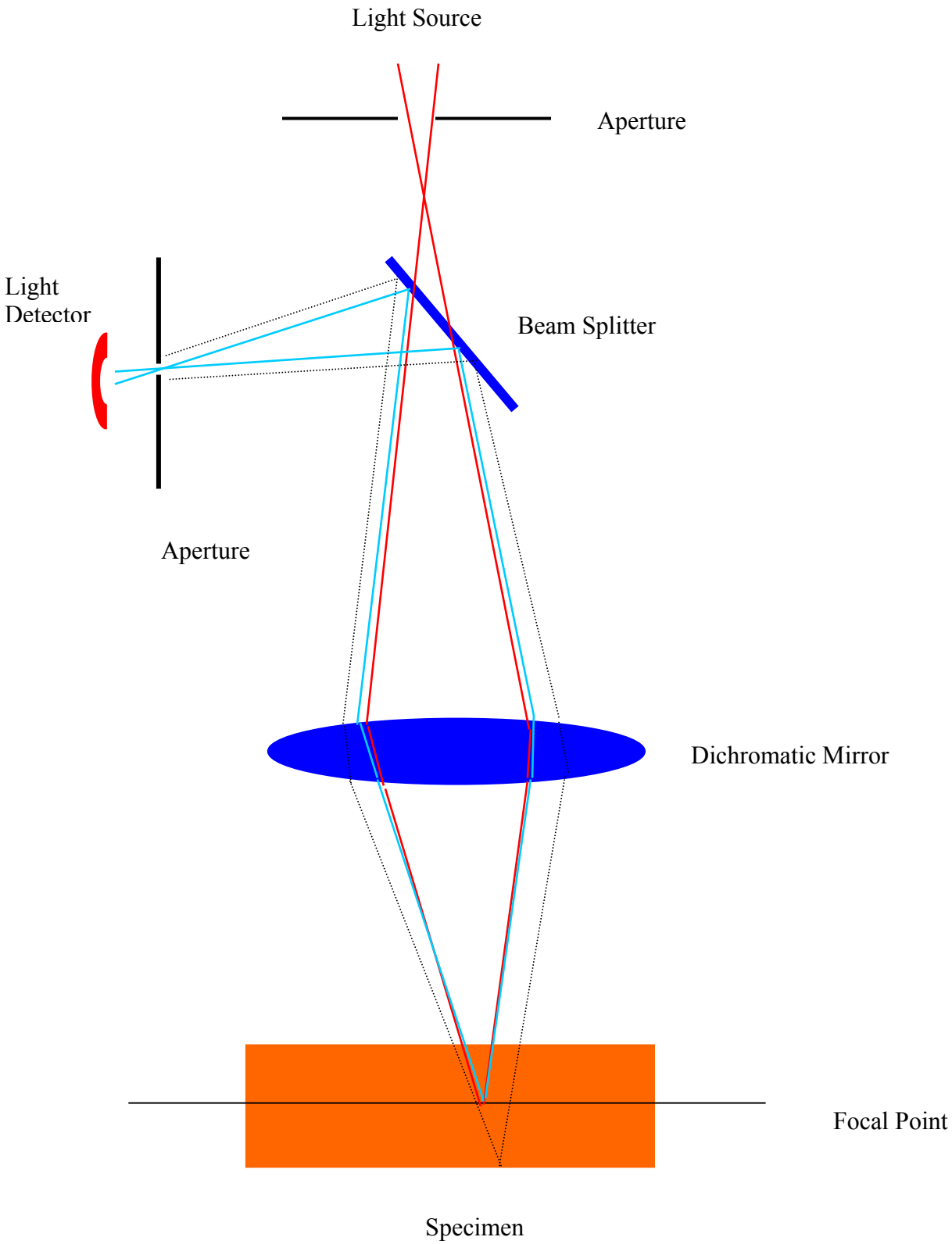

Figure 6.5: Schematic representation of the optical pathway of a confocal laser scanning microscope (LSCM) (12).

6.2.1 Previous Work

The aforementioned techniques have been extensively used in the literature to study membrane fluidity effects both in natural and artificial membranes. Most of them have been used to interpret the connection between membrane fluidity and MDR1 and MRP inhibition. The following is just a brief example of some of the citations found in the literature regarding the use of these techniques in connection with MDR1 and MRP inhibition or the effect of poly(ethylene glycol) on the microviscosity of membrane bilayers.

Various researchers have used to study the membrane fluidity effects associated to the lateral movement of the phospholipids including its relationship to MDR1 and MRP inhibition. Hugger used this technique to study the effects of lineal PEG-300 on the membrane fluidity of Caco-2 cells and its relationship to MDR1(13). Batrakova, employed this technique to examine the effects of several morphologies of pluronic block copolymers in bovine brain microvessel endothelial cells (BBMEC) and its relationship to MDR1 inhibition as well (14). Both researchers found a direct relationship between membrane fluidity and MDR1 inhibition. On a related investigation, Hashizaki employed this technique to study the effects of poly(ethylene glycol) of diverse chain molecular weights on PEG-lipid liposomes (15). In this study the membrane fluidity of the bilayer liposome membranes was not significantly changed by the addition of the distearoyl phosphatidylethanolamines covalently bonded to PEG.

Electron spinning resonance has been used by several investigators to study the membrane fluidity of lipid bilayers. For example, Collnot studied the membrane fluidity effects of tocopheryl polyethylene glycol succinate (TPGS, vitamin E) on Caco-2 cells and its relationship to MDR1 inhibition; where no correlation was found between inhibition and membrane fluidity (16). Van der Bergh used it to study the elasticity of vesicles formed from octaoxyethylenelaurate-ester (PEG-8-L), sucrose laurate-ester (L-595), and cholesterol sulfate (CS) (17). Beckman studied the membrane fluidity effects of PEG and PEG conjugated catalase and dismutase on porcine aortic endothelial cells to verify possible effects of PEG on increase permeabilization of the enzymes (18).

FRAP has been extensively used in the literature to track the lateral movement of phospholipids and lipid vesicles. Lalchev studied the effect of lineal PEG of molecular weight 400 g/mol on the fluidity of microscopic thin liquid films composed of phosphatidylcholine and using DiI-C18 as the marker (19). In this study, the diffusion coefficient was found to depend on the distance between foam films and film type. They concluded that the FRAP technique is a useful tool to investigate lateral mobility. Wojcieszyn used the technique to examine the mechanism by which poly(ethylene glycol) promotes cell fusion (20). Lund used it to investigate the effect of fish oil on the membrane fluidity of erythrocytes and its relationship to human health (21).

6.2.3 Mathematical Analysis of FRAP experiments

To employ the FRAP technique; it is prudent to fully understand the theory involved in the mathematical interpretation of the results. This problem was first studied by Axelrod in 1976 (22). He proposed a theoretical model based on the lateral diffusion of the unbleached fluorophore from a circular region. The model also assumes that the bleaching of a fluorophore is irreversible and follows first order kinetics with a rate constant αI(r). Therefore, the time dependent change in concentration of an unbleached fluorophore at a position r and time t, C(r,t) can be written as:

$$\frac{dC(r,t)}{dt} = -\alpha I(r)C(r,t) \qquad [6.2]$$

where I(r) is the bleaching intensity. Hence for a bleaching pulse that last a time T, the fluorophore concentration profile at the beginning of the recovery phase (t=0) is given by:

$$C(r,t) = C_0 \exp[-\alpha t I(r)] \qquad [6.3]$$

where C_0 is the uniform initial concentration of the fluorophore. The amount of bleaching induced is given by:

$$K \equiv \alpha T I(0) \qquad [6.4]$$

For a Gaussian circular disc profile I(r) is given by:

$$I(r) = \begin{cases} P_0 / \pi w^2 & r \le w \\ 0 & r > w \end{cases} \qquad [6.5]$$

where P_0 is the intensity of the laser beam and w is the radius of the circular region. Finally the differential equation that describes this phenomenon is given by (22, 23):

$$\frac{\partial C(r,t)}{\partial t} = D\left[\frac{\partial^2}{\partial r^2} + \frac{1}{r}\frac{\partial}{\partial r}\right]C(r,t) - V_0\left[\frac{\partial C(r,t)}{\partial x}\right] \qquad [6.6]$$

where D is the diffusion coefficient and V_0 is the velocity of the flow in the x direction. The boundary conditions for this problem are $C(\infty,t) = C_0$ and C(r,0) is given by (42). It is often convenient to present the fluorescence recovery data in fractional form as follows:

$$f(t) \equiv \left[F(t) - F(0)\right] \Big/ \left[F(\infty) - F(0)\right] \qquad [6.7]$$

where F (0) is the fluorescence intensity immediately after photobleaching, F (∞) is the fluorescence intensity once recovery has been completed and F (t) is the fluorescence intensity at any given time t that is given by:

$$F(t) = (q/A)\int I(r)C(r,t)d^2r \qquad [6.8]$$

where q is the product of all the quantum efficiencies of light absorption, emission and detection, A is the attenuation factor of the beam during recovery observation and C(r,t) is the solution to (45).

Therefore, the solution to [6.8] can be found by combining [6.7] and [6.6] for the specific case of pure isotropic diffusion on a circular region:

$$f(t) = 1 - \frac{\tau_D}{t}\exp\left(-\frac{2\tau_D}{t}\right)\left[I_0\left(\frac{2\tau_D}{t}\right) + I_1\left(\frac{2\tau_D}{t}\right)\right] + 2\sum_{k=0}^{\infty}\frac{(-1)^k(2k+2)!(k+1)!}{(k!)^2[(k+2)!]^2}\left(\frac{\tau_D}{t}\right)^{k+2} \qquad [6.9]$$

where I_0 and I_1 are the modified Bessel equations of the first kind, $\tau_D=w^2/4D$ is the characteristic diffusion time, and D is the diffusion coefficient.

However, this equation has a singularity a time equals zero, which is inconvenient for numerical work, and impractical for diffusion analysis especially at short time regimes ($t<0.1\tau_D$). To overcome this situation, Soumpasis decided to revisit the problem in order to simplify the equation and eliminate the singularity (24). The approach was to change the problem from monitoring the diffusion of unbleached molecules into the region to examine the bleached molecules out of the region. The analysis takes into consideration that the total amount of molecules remains constant.

$$C(r,t)+C^*(r,t)=C_0 \qquad [6.10]$$

where C (r,t) is the concentration of unbleached molecules, C^* is the concentration of bleached molecules and C_0 is the total concentration of molecules. The result of modifying the molecules that are being monitored is that the boundary conditions for (45) change as described below:

$$\begin{aligned} &C^*(\infty,t)=0 \\ &and \\ &C^*(r,0)=\begin{cases} C_0(1-\exp-K) & r\le w \\ 0 & r>w \end{cases} \end{aligned} \qquad [6.11]$$

The solution to [6.8] using the boundary conditions described in [6.11] and combining [6.6] and [6.7] is as follows:

$$f(t)=\exp\left(-\frac{2\tau_D}{t}\right)\left[I_0\left(\frac{2\tau_D}{t}\right)+I_1\left(\frac{2\tau_D}{t}\right)\right]. \qquad [6.12]$$

The resulting equation is much simpler and has no singularity problems at time equals zero.

However, numerous simplifications are required to obtain [6.12]. For example, the model assumes full recovery, which is rarely observed. Therefore, the fitting of analytical data is not always the best. To solve this problem several phenomenological models have emerged. Among them one of the most frequently used is Salmons' perturbation-relaxation model described below (25).

$$F(t) = F(0) + \left[F(\infty) - F(0)(1 - e^{-kt})\right] \qquad [6.13]$$

where k is the constant that describes the rate of recovery. This model assumes that the fluorescence intensity at a time t is dominated by two distinct events: (i) perturbation (i.e. bleaching), and (ii) relaxation (i.e. recovery) as described below:

$$F_k(t) = F_k(\text{perturbation}) + F_k(\text{relaxation}) \qquad [6.14]$$

These events are assumed to follow simple first order kinetics, therefore the predominant differential equation is as follows:

$$\frac{dF}{dt} = kF \qquad [6.15]$$

The boundary condition for the perturbation event is that at t=0, F=F(0), while the boundary condition for the relaxation event is that at t=∞, F=F(∞). These two differential equations are coupled and are assumed to posses the same rate constant k, giving rise to [6.13].

The time required to reach half of the recovery is defined as:

$$t_{1/2} = \frac{\ln 2}{k} \qquad [6.16]$$

This equation can then be coupled with Axelrod's half time approximation in order to calculate the diffusion coefficient (D) as follows:

$$t_{1/2} = \frac{w^2}{4D} \qquad [6.17]$$

Other parameters that are important for the analysis of fluoresce recovery experiments are the mobile fraction (M), that describes the fraction of the probe that is available for diffusion and the bleaching percent (B) that describes the fraction of the probe that was bleached and are defined below:

$$M = \frac{F(\infty) - F(0)}{F_0 - F(0)} \qquad [6.18]$$

where F_0 is the fluorescence intensity before photobleaching; and

$$B = \left[1 - \frac{F(0)}{F_0}\right] \times 100 \qquad [6.19]$$

6.3 Experimental

6.3.1 Materials

The monomer poly(ethylene)glycol monomethacrylate (PEGMA) with PEG chains of 400 and 1000 g/mol, the cross linker poly(ethylene) glycol dimetachrylate (PEGDMA) with chains of 400 g/mol, and the lineal poly(ethylene glycol) with molecular weight of 300 g/mol (PEG-300) were purchased from Polysciences, Inc (Warrington, PA). The photo-initiator, 1-hydroxyciclohexyl phenyl ketone, the gelatin, the hexanol, and the Hank's balanced salt solution (HBSS) (pH = 7.4) were obtained from Sigma Aldrich Co. (Milwaukee, WI). The phospholipid probe CM(DiI) a chloromethylbenzamide derivative of DiI was obtained from Molecular Probes (Carlsbad, CA). Finally, the solvent, ethanol was purchased from Fisher Scientific (Hampton, NH), and used as received. The Nunc Labtek II chambered coverglasses were purchased from Fisher Scientific as well.

The Caco-2 cell line (HBT-37) was purchased from the American Type Culture Collection (Manassas, VA). Dulbecco's modified eagle's medium (DMEM) was obtained from Sigma-Aldrich (St Louis, MO), supplemented with fetal bovine serum, and L-glutamine from Life Technologies, and penicillin/strepromycin antibiotics from Sigma-Aldrich (St Louis, MO).

6.3.2 Methods

Submicronsphere sythesis

Synthesized according to the methods described in section 4.3.2.

Caco-2 cell staining with the fluorescent probe CMDiI

Prior to cell passage the Nunc Labtek chambered coverglasses (2 wells) were pretreated with a 1mg/mL gelatin solution to promote cell adhesion. The gelatin solution was prepared by mixing gelatin and deionized water at a 1mg/mL proportion. The gelatin/water mixture was then sterilized by autoclaving at 121 °C and 20 psi. Next, a 2mL portion of the gelatin solution was transferred to each well of the chambered coverslips. The coverglasses were then transferred to a 4 °C atmosphere and let stand for 2 to 24 hours. Finally, the gelatin solution was then removed by aspiration; and Caco –2 cells were seeded at a concentration of 3,000 cells/cm^2.

The cells were maintained in a humid atmosphere of 5% CO_2 in air for four days with no medium change. At this point, the medium was removed and replaced with a 25 μM solution of CM-DiI in HBSS. The cells were allowed to stand for 2 minutes at 37 °C followed by 8 minutes at 4 °. The cells were then washed twice with HBSS and maintained on HBSS until the FRAP experiment could commence.

Fluorescence Recovery after Photobleaching using a Confocal Laser Scanning Microscope

Immediately after staining with CMDiI, the cells were transferred to the Confocal laser scanning microscope facilities. HBSS was then replaced with the appropriate experimental solution. These solutions consisted of either polymer dispersions at a concentration of 10 or 1 mg/mL, the lineal PEG-300 morphology at a concentration of 20% (v/v), or the known fluidizer hexanol at a concentration of 10 mM. Immediately, the cells were then observed on a FluoView system FV300 mounted on a Olympus IX71 (Olympus, Center Valley, PA) using a 100X 1.4 NA (numerical aperture) objective. The CM-DiI probe was excited using a 543 nm He-Ne laser and emission was observed using a 605 BP filter. Images were taken at 256x256 pixel resolution from a clip scan of 40x40 pixels. These conditions result in an image acquisition speed of 78 ms/image. A region of interest (ROI) area of 1 μm of diameter was selected using the REX (region of excitement) tool. This area was corroborated to belong to the plasma membrane by analyzing both the Nomarski and the fluorescence images. The time series were composed of 5 images taken at 20% laser intensity (initial), followed by 1,195 images at 100% laser intensity (bleaching) and completed by 800 images at 20% laser intensity (recovery). All experiments were performed at ambient temperature. The fluorescence intensity as a function of time data was then saved in a separate file for later analysis using the equations discussed in section 6.2.1.

Statistics

Experimental data was analyzed using the 95% confidence interval using the Microsoft Excel Analysis Tool Pack package.

6.4 Results and Discussion

Transport experiments of an MDR1 substrate (Rhodamine 123) and an MRP substrate (Fluorescein sodium salt) demonstrated that poly(ethylene glycol) hydrogels provided a transport enhancement of these substrates. Further experimentation at diverse temperatures and concentrations appeared to indicate that the transport enhancement is most likely due to an inhibition of the MDR1 and MRP pump by some type of interaction with the hydrogels. Previous researchers have suggested that a possible mechanism of action for surfactants and amphiphilic molecules like PEG is a membrane fluidization effect. Due to the amphiphatic nature of both pluronic copolymers and PEG its comparison to surfactants is undeniable. To this point, only polyethoxylated surfactants like Vitamin E TPGS, Nonidet P-40, Triton X-100, Cremophor EL and Tween 80 have been proven to have inhibition effects of MDR1 as well as an increase in membrane fluidity (13, 26-31). It has been proposed that changes in the membrane fluidity caused by surfactants as the mechanism of inhibition of the MDR efflux systems. This effect may alter the protein conformation changes that occur during substrate efflux. It may also render the

plasma membrane more permeable, thus enhancing transport. Nonpolyethoxylated surfactants like the zwitterionic surfactant 3-[(3-cholamidopropyl) dimethylammonio]-1-propanesulfonate (CHAPS), Octylglucoside, Hecamegh and Poloxamer 188 do not present MDR inhibition effects (29, 30). Therefore, this possible scenario needed to be further evaluated.

Fluorescence recovery after photobleaching (FRAP) was selected as the technique to use to test the effect of diverse poly(ethylene glycol) morphologies on the membrane fluidity of Caco-2 cells. FRAP is a visual technique that involves the staining of the cell membrane with an appropriate fluorescent probe. Therefore, the first order of business was to choose an adequate probe. The first attempt was with NBD-C6-sphingomyelin. This probe was tested at various concentrations up to 30 μM. However, we experienced problems with the signal obtained from the microscope; also the probe would tend to photobleach before imaging was completed. This was probably due to the low extinction coefficient of the probe (22,000 (10)). It was decided at his point to change the fluorescent marker to CM-DiI a chloromethylbenzamido derivative of DiI. This marker has the advantage that is more soluble in water than DiI. It also possesses a higher extinction coefficient at 134,000 (10). Even tough the extinction coefficient of DiI is considered high, it is still capable of undergoing photobleaching and FRAP experiments have been done using this probe (19).

Once the probe was selected, the next step was to establish the working concentration for the staining of the cells. For FRAP experiments, the cells are

usually marked at fairly high concentrations. A high marker concentration allows the user to use low laser potency during the experiment to minimize bleaching due to the numerous images acquired during the experiment. Typically, a laser power of less than 30% is recommended. Although, the concentration should not be too high that will cause the PMT to saturate. Again, various concentrations were tested up to 50 μM, optimum conditions were detected at 25 μM.

FRAP experiments were initially tested on confluent cells. However, at this condition the staining of the cell membrane was poor at best. It was noticed that only cells that were on small clusters, usually far from the cell monolayer were the ones being stained (mostly the corners). From these observations, it was hypothesized that the probe required a high surface area in order to penetrate the plasma membrane. To take this factor into account, the cell density was lowered by reducing the cell density from 10,000 to 3,000 cells/cm^2. The time of incubation was also reduced from 7 days to 4 days. These changes greatly improved the staining of the plasma membrane with nearly 90% of the cells stained partially or completely. However, due to the low cell density and the poor adherence properties of the cells on a glass substrate we experienced problems with cell attachment. Before experimentation, the coverslip was observed and adequate population of cells was present. After the staining procedure (which required 4 sets of washes with HBSS), almost no cells were present. The Caco-2 cells are adherent cells that depended on their neighbors to establish good support. Once the cell density was considerably

lowered, the cell adhesion was reduced as well. To make matters worse the cells were seeded on glass coverslips, and glass has very poor adherence properties due to its smooth surface and the lack of functional groups. However, glass was needed due to its optical properties and its availability at very thin films. In order to improve cell adhesion, the glass coverglasses were pretreated with cell adhesion promoters. Two substances were tested Collagen IV and Gelatin; both materials had similar positive results. Gelatin was chosen because the pretreatment procedure was less labor intensive.

Once the staining procedure was well established, the confocal laser scanning microscope FRAP experiments were optimized. First, the appropriate excitement laser and emission filters needed to be chosen. The fluorescent data of the probe stated that the excitation maximum is observed at 553 nm and the emission maximum is 570 nm. There were two excitation laser guns that were near the excitation maximum of the probe. The first one was the 488 nm Ar laser (red light) and the second one was the 543 nm He-Ne laser (green light). The He-Ne laser was chosen because it provided a better signal. The chosen filter was the 605 BP that takes in wavelengths between 575-630 nm, close enough to the emission maximum of the probe. An example of Caco-2 cell stained with CM-DiI as observed in the LSCM is observed in figure 6.6.

Next, the image acquisition speed needed to be established. The process of the lateral movement of the phospholipids and images were needed at frequency ranging in the milliseconds per image.

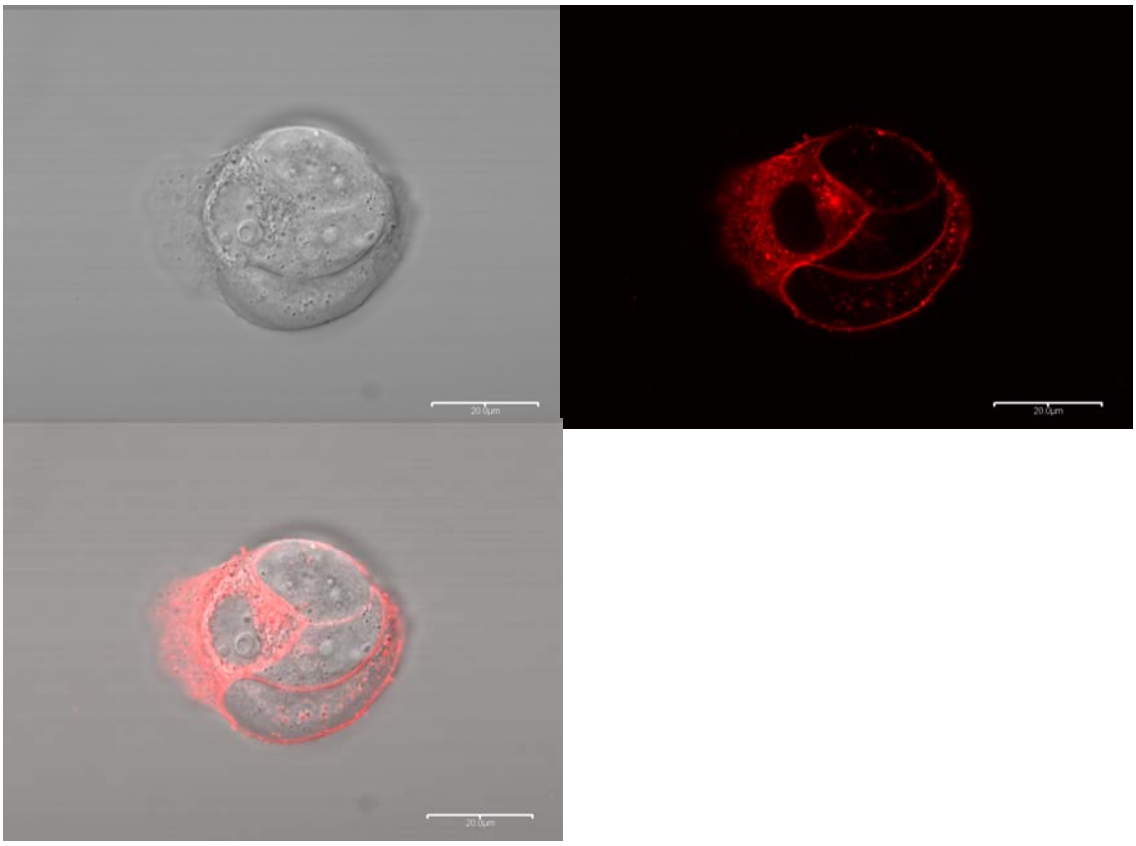

Figure 6.6: Cao-2 stainned with 25 μM CM-DiI solution and observed on a FluoView FV 300 system mounted on a Olympus IX71 laser scanning confocal microscope.

After consultation with the Olympus technical team, the image resolution was lowered to 256x256 pixels and a clip scan of the image of a 40x40 pixel size was taken. These conditions allowed us to achieve an image acquisition speed of 78ms/image. Last, the time series conditions needed to be set.

The first attempt included 500 images total (5 initial, 395 for photobleaching and 100 for recovery) at this conditions almost no photobleaching was observed. The total of images acquired was then elevated to 800 (5 initial, 595 phobleaching and 200 for recovery), again almost no photobleaching was observed. Finally, the time series was set to 2000 images (5 initial, 1195 phobleaching and 800 recovery). With these conditions photobleaching was among the required parameters (greater than 50%) and the recovery curve had acceptable mobility fractions (greater than 25%).

Finally, after all experimental conditions were well established, the data analysis procedure needed to be validated. As was discussed in section 6.2.2, there are several mathematical methods available in the literature to analyze FRAP experiments, of these methods, the Soumpasis fundamental model and the Salmon phenomological model were chosen for further analysis. The raw data was tabulated into an Excel worksheet and the time series were adjusted so that time =0 corresponded to the first recovery data point. Another column was added that contained the estimated fluorescence intensity according to the models (Soumpasis and Salmon). Finally, the parameters of the model were adjusted using the least square methods using the Excel's solver tool. For the Soumpasis model an initial estimate for F(0), F(∞), and τ_D were provided, then

the sum of difference squares was minimized by changing these three parameters. For the Salmon model, and initial estimate for F(0), F(∞), and k were provided and the same procedure of the Soumpasis model was followed. For all the data sets tested (16% of total data), the Salmon model provided a better fit of the experimental data (as observed in the example provided in figure 6.7). This is probably due to the fact that this fundamental model assumes full recovery of the fluorescence. However, full recovery was not observed in the experimental trials. At best, the mobility fraction (an indicator of the recovery percent) was 60%. Therefore, the Salmon model was chosen to analyze the FRAP experiments.

The membrane fluidity effects of two PEG hydrogels (PEGMA 400/ PEGDMA 400 and PEGMA 1000/ PEGDMA 400) were evaluated as a function of concentration. These effects were compared to the lineal morphology PEG 300 at a concentration of 20% (v/v) previously reported to confer an increase fluidity effect (13, 26) and to the known fluidizer hexanol at a concentration of 10mM (32). The results show (please refer to figure 6.8) that neither PEG morphology is statistically different to the control group. However, there it is a statistical difference between the diffusion coefficients at the 10 and the 1 mg/mL concentrations for both morphologies ($P<0.05$). This observation correlates well with Hugger that also observed a concentration dependence on membrane fluidity (13).

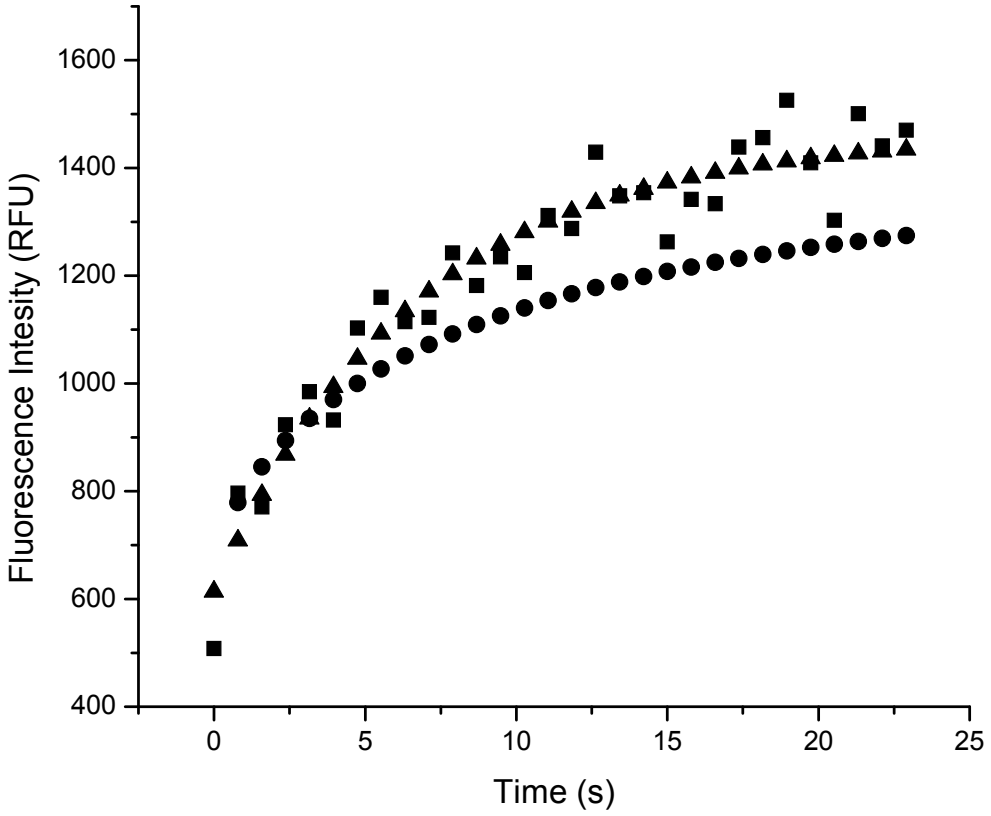

Figure 6.7: Fluorescence recovery profile after photobleaching (FRAP) of Caco-2 cells stained with CM-DiI at 25 μM concentration and ambient temperature. The raw data ■ was fitted according to the Soumpasis model ● and the Salmon model ▲. Each data point represents one time series point as read by the FluoView FV 300 system mounted on a Olympus IX71 laser scanning confocal microscope.

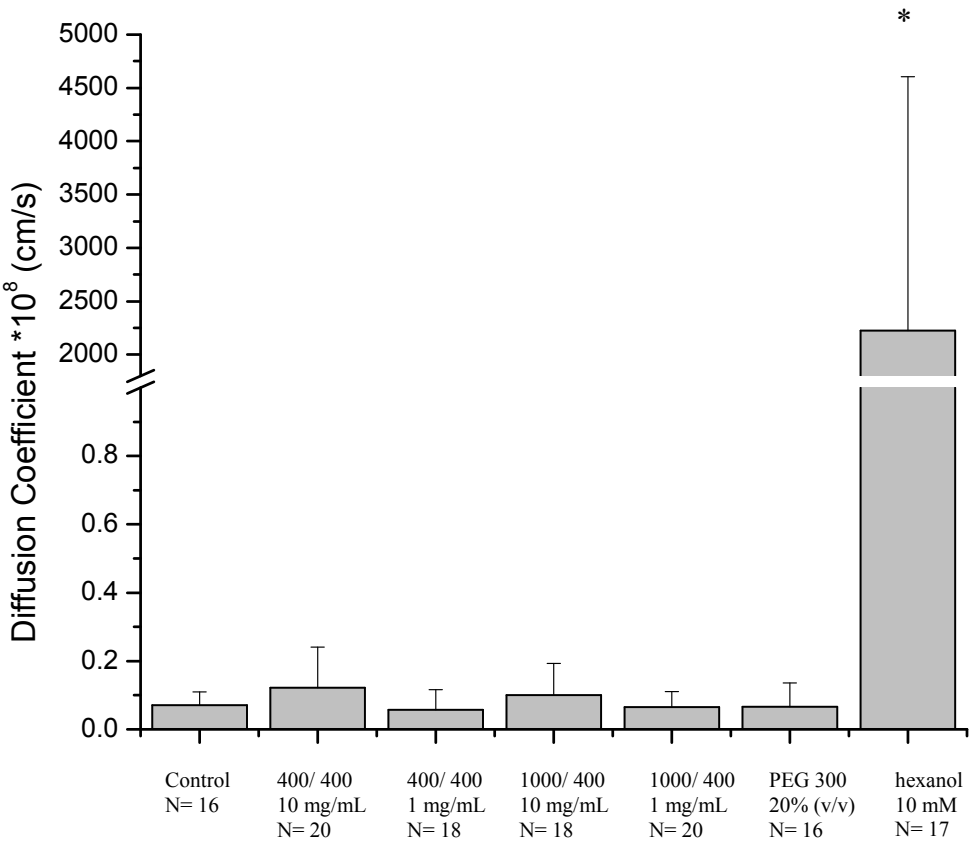

Figure 6.8: Effects of PEGMA 400/ PEGDMA 400 and PEGMA 1000/ PEGDMA 400 hydrogels on the membrane fluidity of Caco-2 cells stained with CM-DiI at 25 μM. The effects were studied as a function of concentration and compared to the lineal morphology PEG 300 20% (v/v) and the known fluidizer hexanol 10 mM. Membrane fluidity was analyzed with FRAP using FluoView system FV300 mounted on a Olympus IX71 (Olympus, Center Valley, PA). The 1 μm ROI was selected from a 40x40 pixel clip scan of an image obtained with a 100x 1.4 NA objective at a 254x254 pixel resolution.

In general, the membrane fluidity effect does not appear to correlate well with the transport effects. This appears to correlate well with previous observations in which membrane fluidity effects low PEG 300 concentrations (>2.5% (v/v)) were able to confer MDR1 inhibitory effects, while larger concentrations (>15% (v/v)) were needed before membrane fluidity effects could be observed (13). Also, other investigators have failed to observe a direct correlation between an increase in membrane fluidity and transport enhancement of MDR1 substrates. For example, Collnot (16) reported that membrane fluidity is not the mechanism for MDR1 inhibition induced by TPGS because membrane fluidity changes were observed only at concentration 100 times higher than the ones needed for transport enhancement. However, a correlation between ATPase activity and inhibitory effect was found. Contrary to the expected results, Dudeja reported a reduction of membrane fluidity coupled with an increase in MDR1 substrate transport (28). A possible explanation for these observations is that although membrane fluidity might be an important factor during MDR1 inhibition, other mechanisms might be present as well.

Finally, the validation of the membrane fluidity effects observed for both PEG-300 and hexanol can not be directly assessed because FRAP experiments with these excipients on Caco-2 cells were not found in the literature. With regards to hexanol, Ismaili observed a ~7% reduction in fluorescence anisotropy (increase in membrane fluidity) on the human epithelial

cell line Hep-2 (Epidermoid carcinoma) (32) at a 5 mM concentration. Ingram observed that a 7.8 mM hexanol concentration produced anisotropy drops of up to –0.0121 units on *Escherichia coli* cultures (33). A remarkable increase in diffusion coefficient with hexanol 10 mM was observed in this study, which serves as a confirmation that the FRAP procedure is capable of detecting changes in membrane fluidity. Finally, with regard to PEG-300 Hugger observed an increase in anisotropy from 0.280 (control) to 0.298 (PEG 300 at 20% (v/v)), which will translate into a reduction in membrane fluidity. This study observed no statistical difference between the PEG-300 morphology and the control. It is possible that the fluorescence anisotropy technique is more sensitive to changes in the membrane fluidity, than FRAP.

6.4 Conclusions

Poly(ethylene glycol) hydrogels were shown to have inhibitory effects on MDR1 and MRP efflux pumps. However, the mechanism of action for these effects was unknown. Several researchers have suggested that amphiphilic substances such as surfactants and PEG may confer efflux pump inhibition trough a membrane fluidization mechanism. This theory was tested using fluorescence recovery after photobleaching. As expected the results showed that the hydrogel produced a concentration dependent membrane fluidization effect. However, this effect could not be directly correlated to MDR1 and MRP inhibition because the trends in membrane fluidization and ABC transporter inhibition differed considerably. Therefore, it can be concluded that membrane

fluidity is an important factor during the inhibition of diverse ABC transporters, but at this point other mechanisms cannot be ruled out.

6.6 References

1. J. W. Kimball. *Biology*, Addison Wesley Publishing Company, Boston, MA, 1994.
2. B. Alberts, A. Johnson, J. Lewis, M. Raff, K. Roberts, and P. Walter. *Molecular Biology of the cell*, Garland Science, New York, NY, 2002.
3. G. Geibel. The Cell Membrane, 2008.
4. E. Feitosaand P. C. A. Barreleiro. *Surface and Colloid Science*, Springer, Berlin / Heidelberg, 2004.
5. K. Simmons. Membrane Structure and Function, Vol. 2008, 2002.
6. L. BR. Use of fluorescent probes to monitor molecular order and motions within liposome bilayers. *Chemistry and Physics of Lipids* **64**: 99-116. (1993).
7. C. A. Royer. Approaches to Teaching Fluorescence Spectroscopy. *Biophysical Journal* **68**: 1191-1195 (1995).
8. J. A. Dixand A. S. Verkman. Mapping of fluorescence anisotropy in living cells by ratio imaging: Application to cytoplasmic viscosity. *Biophysical Jorunal* **57**: 231-240 (1990).
9. K. AM, D. P, K. RD, P. WJ, and M. ED. The lack of relationship between fluorescence polarization and lateral diffusion in biological membranes. *Biochim Biophys Acta* **649**: 471-80. (1981).
10. R. P. Hauglandand M. T. Z. Spence. *The Handbook — A Guide to Fluorescent Probes and Labeling Technologies*, Invitrogen Corp, 2005.
11. J. A. Weil, J. R. Bolton, and J. E. Wertz. *Electron paramagnetic resonance: elementary theory and practical applications*, New York: Wiley, 1994.
12. N. S. Claxton, T. J. Fellers, and M. W. Davidson. Laser Scanning Confocal Microscopy, The Florida State University, Tallahassee, FL.
13. E. D. Hugger, K. L. Audus, and R. T. Borchardt. Effects of Poly(ethylene glycol) on Efflux Transporter Activity in Caco-2 Cell Monolayers. *Journal of Pharmaceutical Science* **91**: 1980-1990 (2002).
14. E. V. Batrakova, S. Li, V. Y. Alakhov, D. W. Miller, and A. V. Kabanov. Optimal Structure Requirements for Pluronic Block Copolymers in Modifying P-glycoprotein Drug Efflux Transporter Activity in Bovine Brain Microvessel Endothelial Cells. *The Journal of Pharmacology and Experimental Therapeutics* **304**: 845-854 (2003).
15. K. Hashizaki, H. Taguchi, C. Itoh, H. Sakai, M. Abe, Y. Saito, and N. Ogawa. Effects of Poly(ethylene glycol) (PEG) Chain Length of PEG-Lipid on the Permeability of Liposomal Bilayer Membranes. *Chemical and Pharmaceutical Bulletin* **51**: 815—820 (2003).

16. E.-M. Collnot, C. Baldes, M. F. Wempe, R. Kappl, J. Huttermann, J. A. Hyatt, K. J. Edgar, U. F. Schaefer, and C.-M. Lehr. Mechanism of Inhibition of P-Glycoprotein Mediated Efflux by Vitamin E TPGS: Influence on ATPase Activity and Membrane Fluidity. *Molecular Pharmaceutics* **4**: 465-474.
17. B. A. I. v. d. Bergh, P. W. Wertzb, H. E. Jungingera, and J. A. Bouwstra. Elasticity of vesicles assessed by electron spin resonance, electron microscopy and extrusion measurements. *International Journal of Pharmaceutics* **217**: 13-24 (2001).
18. J. S. Beckman, J. Robert L. Minor, C. W. Whiten, J. E. Repinell, G. M. Rosenil, and B. A. Freeman. Superoxide Dismutase and Catalase Conjugated to Polyethylene Glycol Increases Endothelial Enzyme Activity and Oxidant Resistance. *The Journal of Biological Chemistry* **263**: 6884-6892 (1988).
19. Z. Lalchev, R. Todorov, H. Ishida, and H. Nakazawa. Lateral mobility of phospholipid molecules in thin liquid films. *European Biophysics Journal* **23**: 433-438 (1995).
20. J. W. Wojcieszyn, R. A. Schlegel, K. Lumley-Sapanski, and K. A. Jacobson. Studies on the Mechanism of Polyethylene Glycol-Mediated Cell Fusion Using Fluorescent Membrane and Cytoplasmic Probes. *The Journal of Cell Biology* **96**: 151-159 (1983).
21. E. K. Lund, L. J. Harvey, S. Ladha, D. C. Clark, and I. T. Johnson. Effects of Dietary Fish Oil Supplementation on the Phospholipid Composition and Fluidity of Cell Membranes from Human Volunteers. *Annals of Nutrition & Metabolism* **43**: 290-300 (1999).
22. D. Axelrod, D. E. Koppel, J. Schlessinger, E. Elson, and W. W. Webb. Mobility Measurement by Analysis of Fluorescence Photobleaching Recovery Kinetics. *Biophysical Jourmal* **16**: 1055-1069 (1976).
23. U. Kubitscheck, P. Wedeldnd, and R. Peters. Lateral Diffusion Measurement at High Spatial Resolution by Scanning Microphotolysis in a Confocal Microscope. *Biophysical Jourmal* **67**: 948-956 (1994).
24. D. M. Soumpasis. Theoretical Analysis of Fluorescence Photobleaching Recovery Experiments. *Biophysical Journal* **41**: 95-97 (1983).
25. E. D. Salmon, R. J. Leslie, W. M. Saxton, M. L. Karow, and J. R. Mclntosh. Spindle Microtubule Dynamics in Sea Urchin Embryos: Analysis Using a Fluorescein-labeled Tubulin and Measurements of Fluorescence Redistribution after Laser Photobleaching. *The Journal of Cell Biology* **99**: 2165-2174 (1984).
26. E. D. Hugger, Novak, B. L., Burton, P. S., Audus, K. L., Borchardt, R. T. A Comparison of Commonly Used Polyethoxylated Pharmaceutical Excipients on Their Ability to Inhibit P-glycoprotein Activity In Vitro. *Journal of Pharmaceutical Science* **91**: 1991-2002 (2002).
27. M. Nerurkar, P. S. Burton, and R. T. Borchardt. The Use of Surfactants to Enhance the Permeability of Peptides Through Caco-2 Cells by Inhibition of an Apically Polarized Efflux System. *Pharmaceutical Research* **13**: 528-534 (1996).

28. P. K. Dudeja, K. M. Anderson, J. S. Harris, L. Buckingham, and J. S. Coon. Reversal of Multidrug Resistance Phenotype by Surfactants: Relationship to Membrane Lipid Fluidity. *Archives of Biochemistry and Biophysics* **319**: 309-315 (1995).
29. K. Bogman, Y. Zysset, L. Degen, G. Hopfgartner, H. Gutmann, J. Alsenz, and J. Drewe. P-glycoprotein and surfactants: Effect on intestinal talinolol absorption. *Clinical Pharmacology & Therapeutics* **77**: 24-32 (2005).
30. T. Zordan-Nudo, V. Ling, Z. Liu, and E. Georges. Effects of nonionic detergents on P-glycoprotein drug binding and reversal of multidrug resistance. *Cancer Research* **53**: 5994-6000 (1993).
31. D. Woodcock, S. Jefferson, M. Linsenmeyer, P. Crowther, G. Chojnowski, B. Williams, and I. Bertoncello. Reversal of the multidrug resistance phenotype with cremophor EL, a common vehicle for water-insoluble vitamins and drugs. *Cancer Research* **50**: 4199-4203 (1990).
32. A. Ismaili, J. B. Meddings, S. Ratnam, and P. M. Sherman. Modulation of host cell membrane fluidity: a novel mechanism for preventing bacterial adhesion. *American Journal of Physiology- Gastrointestinal and Liver Physiology* **277**: 201-208 (1999).
33. L. Ingram and N. S. Vreeland. Differential Effects of Ethanol and Hexanol on the Escherichia coli Cell Envelopet. *Journal of Bacteriology* **144**: 481-488 (1980).

7.0 Conclusions and Recommendations

The main objective of this work was to evaluate the effects of poly(ethylene glycol) rich hydrogels on the transport of MDR1 and MRP substrates for future use in controlled drug delivery applications. Three variables of control on the design of the hydrogels were evaluated (1) the length of the PEG tethered chain, (2) the length of the crosslinker, and (3) the particle size. From the results obtained several conclusions can be drawn.

Regarding the effects of the molecular structure of the hydrogel network, it affected the properties of the hydrogel network. Particullary, the tethered chain length appears to play an important role in the hydrogel behavior. This observation appears to be observed in numerous properties of the hydrogel including the swelling ratio, correlation length, partition coefficient, release of model substrate and transport of MDR1 and MRP substrates.

The results also indicated that, the PEG-based hydrogel microparticles were found to greatly enhance the transport of MRP and MDR1 model sustrates when compared to controls and known inhibitors. Experiments at the low 4 ºC temperature demonstrated no transport enhacement, which seems to indicate that transport enhancement is due to some type of active transport interaction, most likely MDR1 and MRP efflux pumps. The transport enhancement also appeared to be concentration dependent, which might be an indication of a competitive action.

Contrary to the expected results, the particle size (i.e. surface area) does not appear to enhance the inhibition effects suggesting an indirect interaction.

A possible mechanim of action for the PEG based hydrogels that was explored was the possibility of a fluidization effect. The PEG-hydrogels provided no statistically significant change in membrane fluidity, implying that membrane fluidity changes is not an important aspect of the inhibition process. Furthermore, no direct correlation between membrane fluidity and transport enhancement was found, therefore other mechanism might be present.

In conclusion, these hydrogel systems have shown their capacity to enhance the transport of model substrate, which makes them potential candidates for controlled drug delivery of MRP and MDR substrates.

The main objective was to establish if poly(ethylene glycol) hydrogels have transport enhancement effects on MDR and MRP substrates and asses its possible use for controlled drug delivery. This objective was completed and their effect was corroborated using two different substrates and comparing the effects to known inhibitors and to lineal morphologies of PEG. However, from this research, questions arise that give foot to new research avenues, specially concerning the mechanism of action of the hydrogel. Therefore, this work cannot be completed without recommendations for future research.

The Caco-2 cell line is excellent cell line to establish if MDR1 or MRP inhibition is present. However in order to study the problem with more detail it is recommended that other cell lines will be used. These cell lines are selected to express only one ABC transporter at higher concentrations therefore they provide flexibility for other types of experiments to be performed. Some examples of these cell lines include: the human breast carcinoma cell line

MCF-7 (low endogenous expression) and its analog MCF-7/ADR (doxorubicin selected with high P-gp expression), the human nasopharinx carcinoma cell line KB (low endogenous expression) and its analog KBv (vinblastine selected with high P-gp expression), the porcine kidney cells LLC-PK1 (no endogenous P-gp expression) and its analog LLC-MDR1 (transfected with the MDR1 gene), the human umbilical vein endothelial cells HVECs (no P-gp expression), the murine myoblast cell line C2C12 (no P-gp expression) (1), the leukemia cell lines HL60/AR and H69/AR (MRP overexpressing) (2), the Madin Darby canin kidney MDCKII-MRP1 or - -MRP2 (tranfected with MRP1 and MRP2 genes respectively), and the human lung carcinoma cell line COR-L23 (low endogenous MRP expression) and its analogy COR-L23/R (doxorubicin selected for MRP1 overexpression) (3). However, if cells with different expression levels of these protein are used the protein expression should be verified by Western Blot or other appropriate analysis

Exploring the mechanism of action of these hydrogels and their possible interaction with the MDR1 and MRP proteins goes beyond the scope of this investigation. Given the fact that this research provides evidence to support that these hydrogels have inhibitory effects on these proteins this is an important aspect that should be pursued in the near future. This investigation would most likely need the incorporation of personel with expertise in molecular biology that could provide an insight at the complex interactions between the integral proteins and the hydrogel. Among possible mechanisms that could be

present are the ATPase reduction and ATP depletion that have been shown to contribute to the inhibition on other polyethoxylated compounds.

Finally, animal experimentation (most likely wild type and MDR knock out mice) to study the pharmacokinetics and pharmacodynamic effects of adding the ABC transporter inhibition to the administration of a known drug should be considered. Cancer chemotherapy such as doxorubicin or vinblastin, which are well known in the literature, are possible starting points.

7.1 References

1. E. Batrakova, S. Li, W. Elmquist, D. Miller, V. Alakhov, and A. Kabanov. Mechanism of sensitization of MDR cancer cells by Pluronic block copolymers: Selective energy depletion. *British Journal of Cancer* **85**: 1987–1997 (2001).
2. T. Tsuruo, H. Iida, S. Tsukagoshi, and Y. Sakurai. Overcoming of Vincristine Resistance in P388 Leukemia in Vivo and in Vitro through Enhanced Cytotoxicity of Vincristine and Vinblastine by Verapamil. *Cancer Research* **41**: 1967-1972 (1981).
3. E. V. Batrakova, S. Li, V. Y. Alakhov, W. F. Elmquist, D. W. Miller, and A. V. Kabanov. Sensitization of Cells Overexpressing Multidrug-Resistant Proteins by Pluronic P85. *Pharmaceutical Research* **20**: 1581-1590 (2003).

APPENDIX I

Raw data for transport experiments of fluorescein sodium salt and rhodamine 123 across Caco-2 cell monolayers

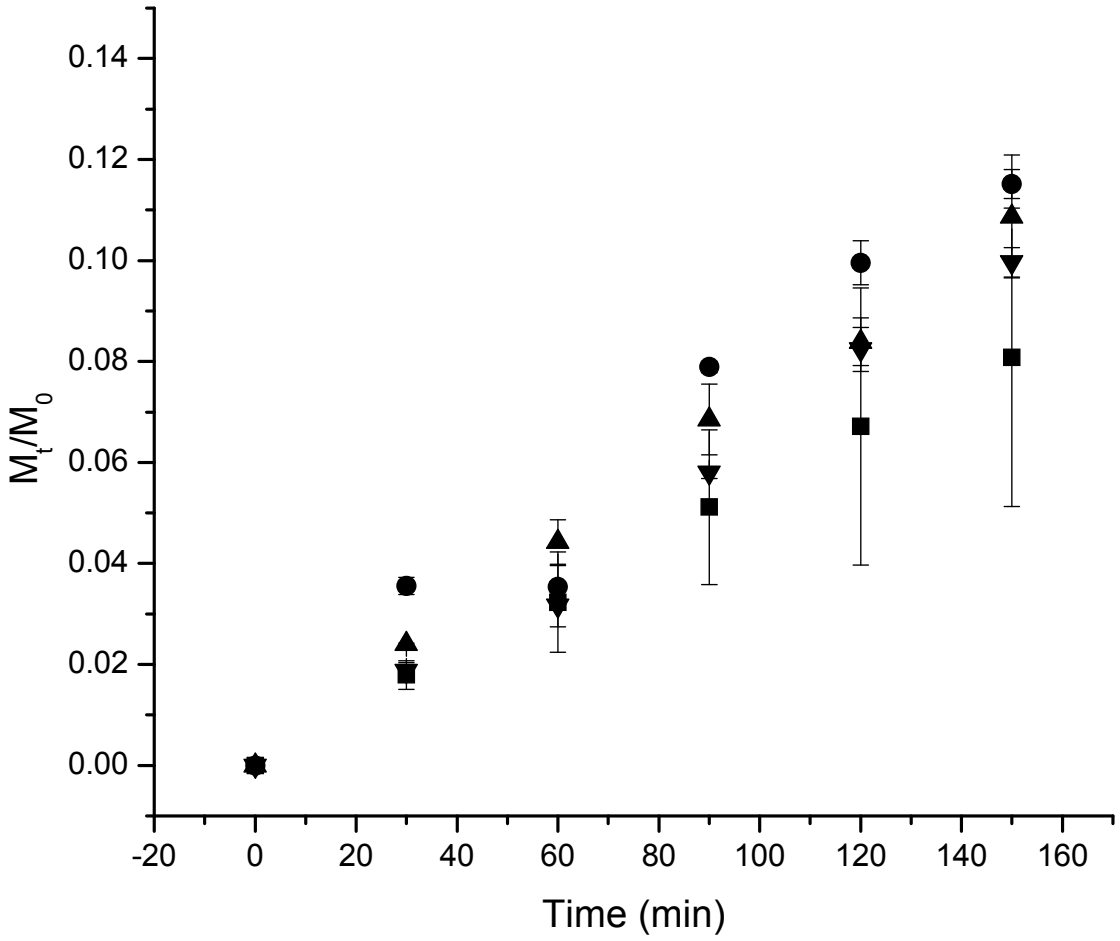

Effect of PEGMA 200/ PEGDMA 1000 at a concentration of 10 mg/mL on the transport of fluorescein sodium salt across Caco-2 cell monolayers at 37 °C. Transport on the AB direction for control (no hydrogel) ■, AB direction experimental (hydrogel) ●, BA direction control ▲, BA direction experimental ▼. Each data point represents the average of three experiments, passage number 24. Each data point represents an average of 3 experiments ± one standard deviation.

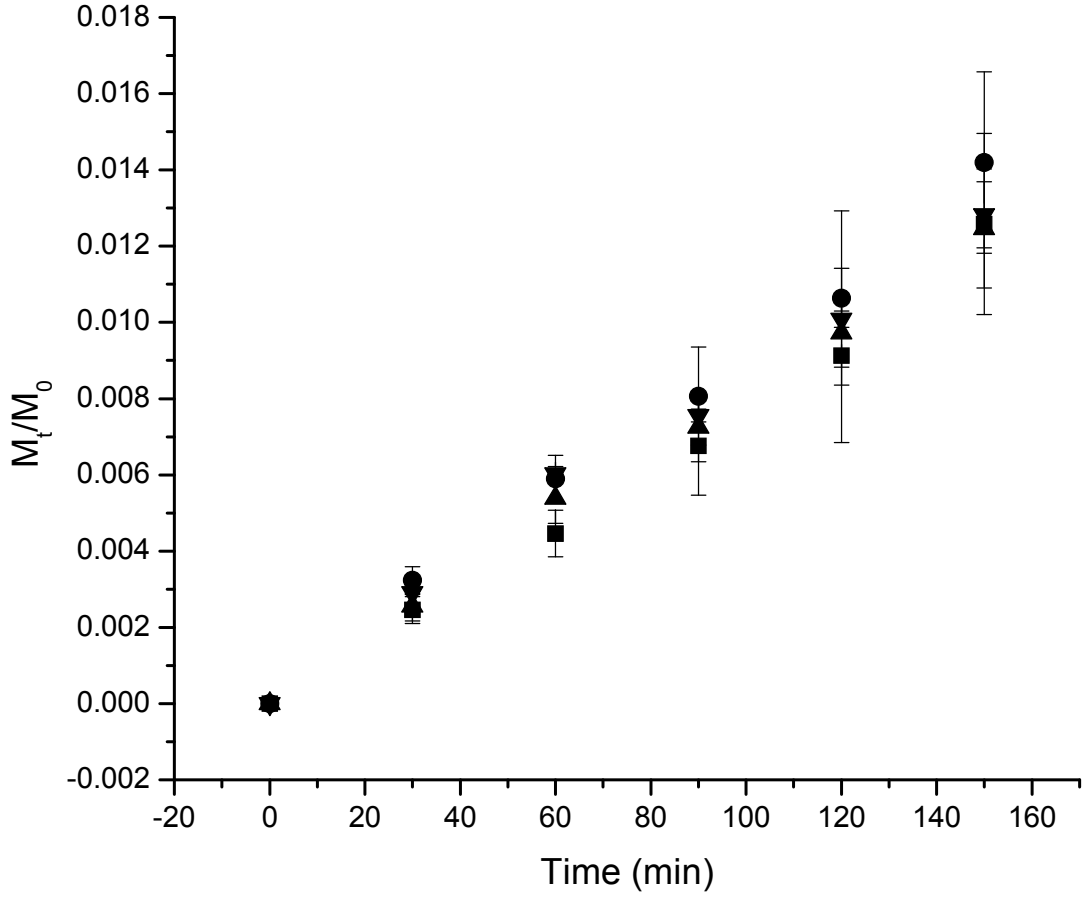

Effect of PEGMA 200/ PEGDMA 1000 at a concentration of 10 mg/mL on the transport of fluorescein sodium salt across Caco-2 cell monolayers at 4 °C. Transport on the AB direction for control (no hydrogel) ■,AB direction experimental (hydrogel) ●, BA direction control ▲, BA direction experimental ▼. Each data point represents the average of three experiments, passage number 29. Each data point represents an average of 3 experiments ± one standard deviation.

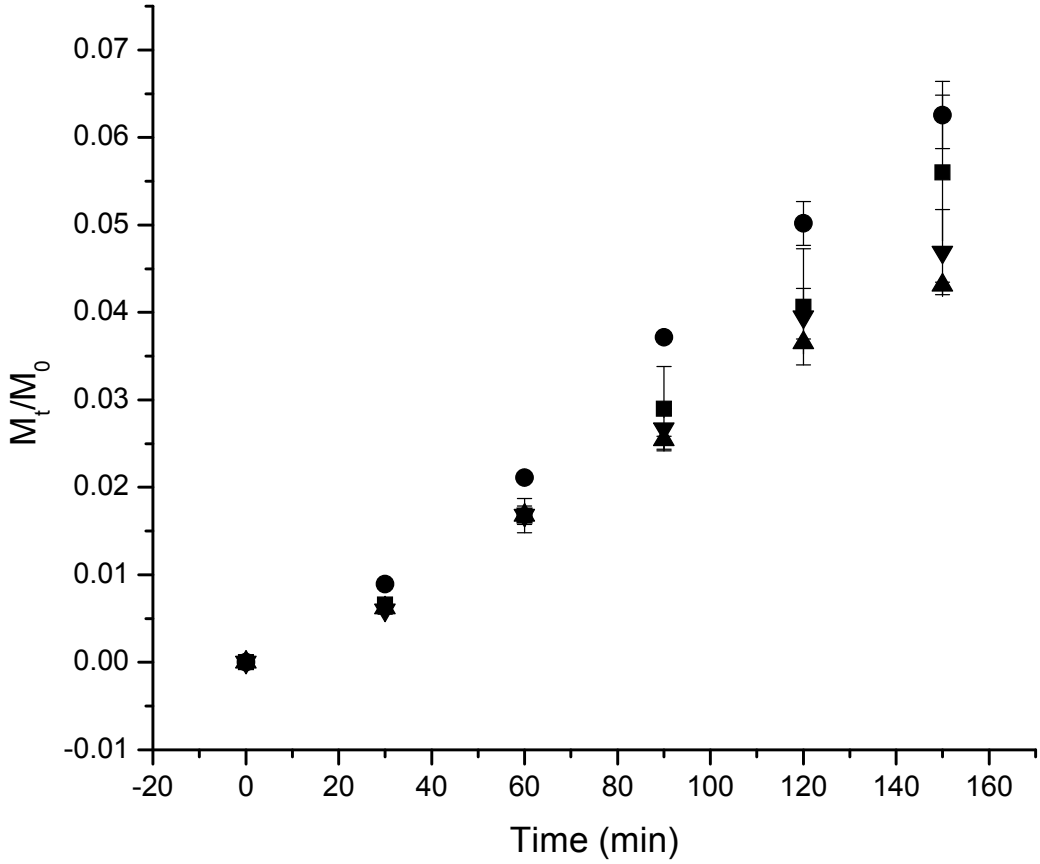

Effect of PEGMA 400/ PEGDMA 1000 at a concentration of 10 mg/mL on the transport of fluorescein sodium salt across Caco-2 cell monolayers at 37 °C. Transport on the AB direction for control (no hydrogel) ■,AB direction experimental (hydrogel) ●, BA direction control ▲,BA direction experimental ▼. Each data point represents the average of three experiments, passage number 24. Each data point represents an average of 3 experiments ± one standard deviation.

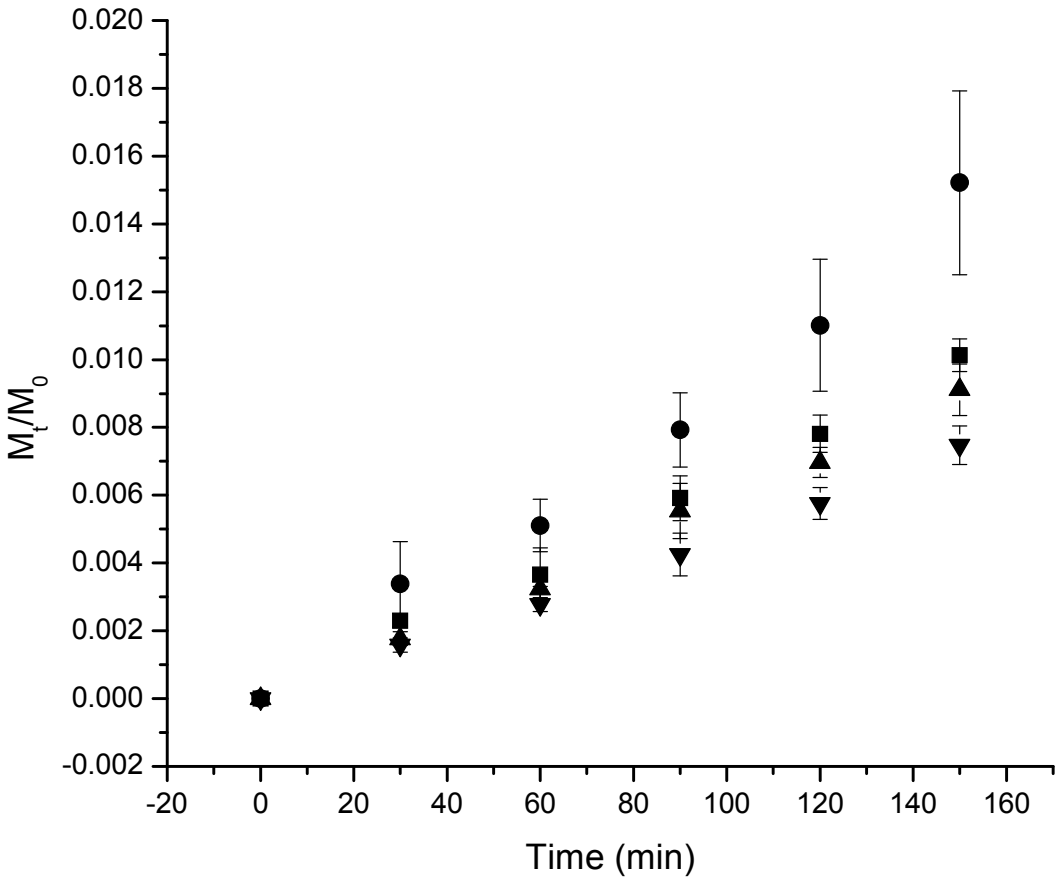

Effect of PEGMA 400/ PEGDMA 1000 at a concentration of 10 mg/mL on the transport of fluorescein sodium salt across Caco-2 cell monolayers at 4°C. Transport on the AB direction for control (no hydrogel) ■,AB direction experimental (hydrogel) ●,BA direction control ▲,BA direction experimental ▼. Each data point represents the average of three experiments, passage number 25. Each data point represents an average of 3 experiments ± one standard deviation.

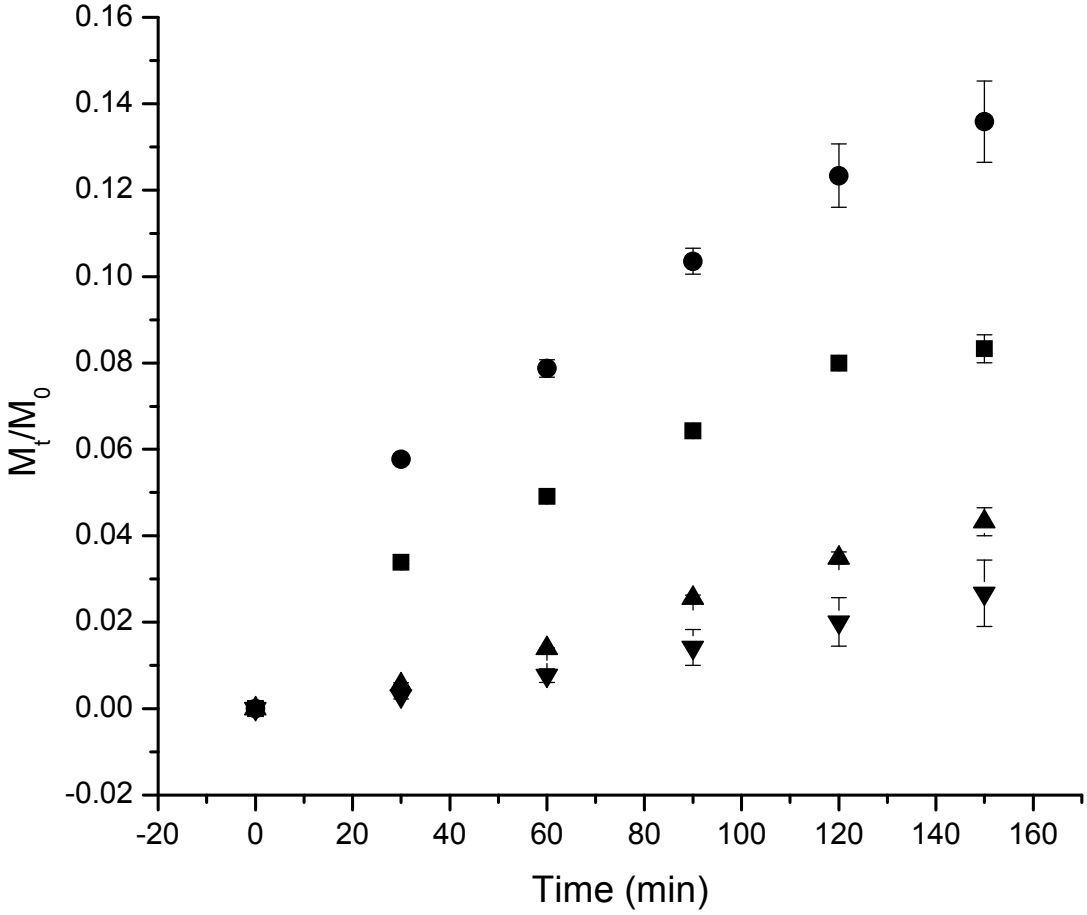

Effect of PEGMA 1000/ PEGDMA 1000 at a concentration of 10 mg/mL on the transport of fluorescein sodium salt across Caco-2 cell monolayers at 37°C. Transport on the AB direction for control (no hydrogel) ■, AB direction experimental (hydrogel) ●, BA direction control ▲, BA direction experimental ▼. Each data point represents the average of three experiments, passage number 26. Each data point represents an average of 3 experiments ± one standard deviation.

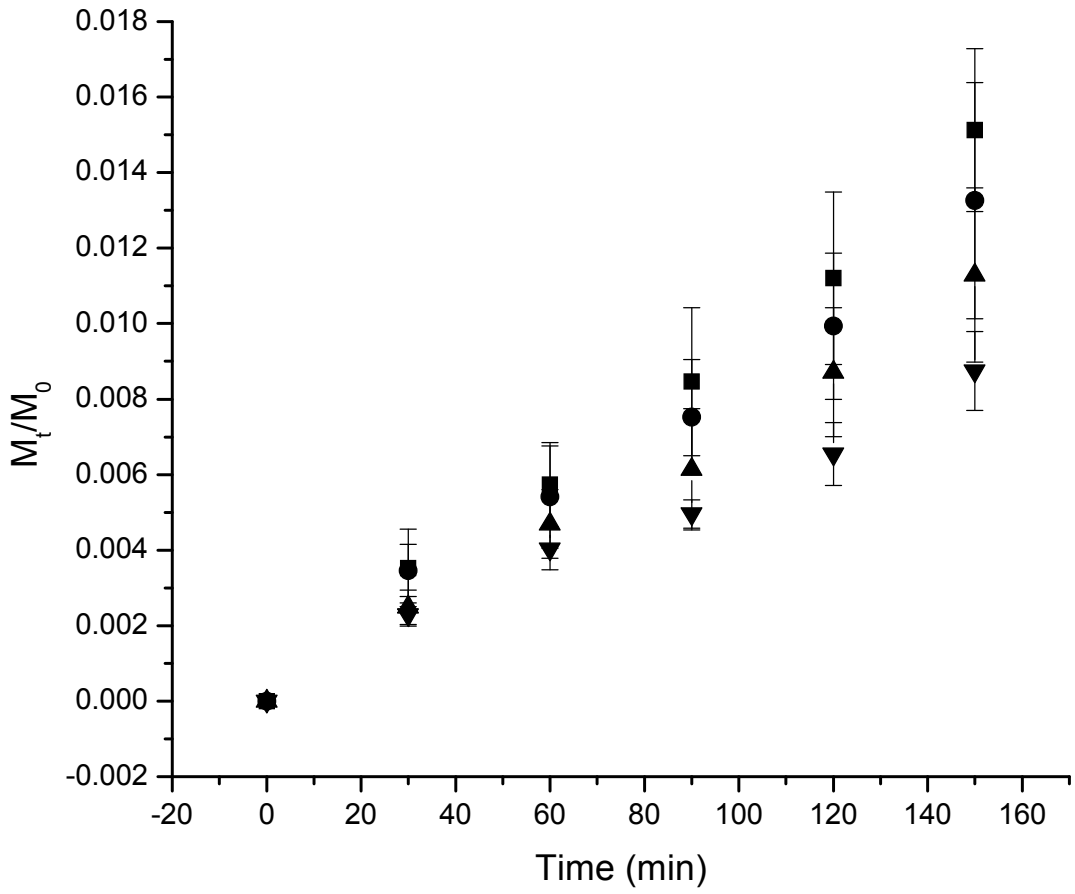

Effect of PEGMA 1000/ PEGDMA 1000 at a concentration of 10 mg/mL on the transport of fluorescein sodium salt across Caco-2 cell monolayers at 4°C. Transport on the AB direction for control (no hydrogel) ■,AB direction experimental (hydrogel) ●,BA direction control ▲,BA direction experimental ▼. Each data point represents the average of three experiments, passage number 28. Each data point represents an average of 3 experiments ± one standard deviation.

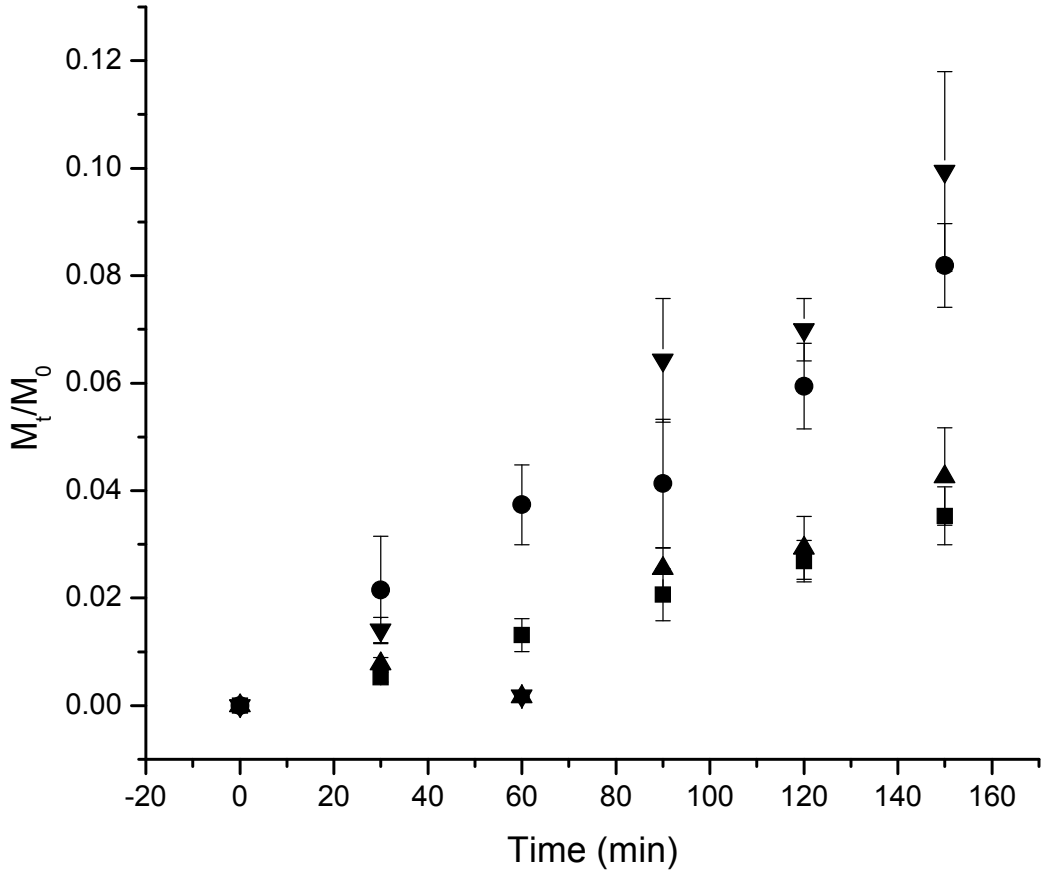

Effect of PEGMA 200/ PEGDMA 600 at a concentration of 10 mg/mL on the transport of fluorescein sodium salt across Caco-2 cell monolayers at 37°C. Transport on the AB direction for control (no hydrogel) ■,AB direction experimental (hydrogel) ●,BA direction control ▲,BA direction experimental ▼. Each data point represents the average of three experiments, passage number 66. Each data point represents an average of 3 experiments ± one standard deviation.

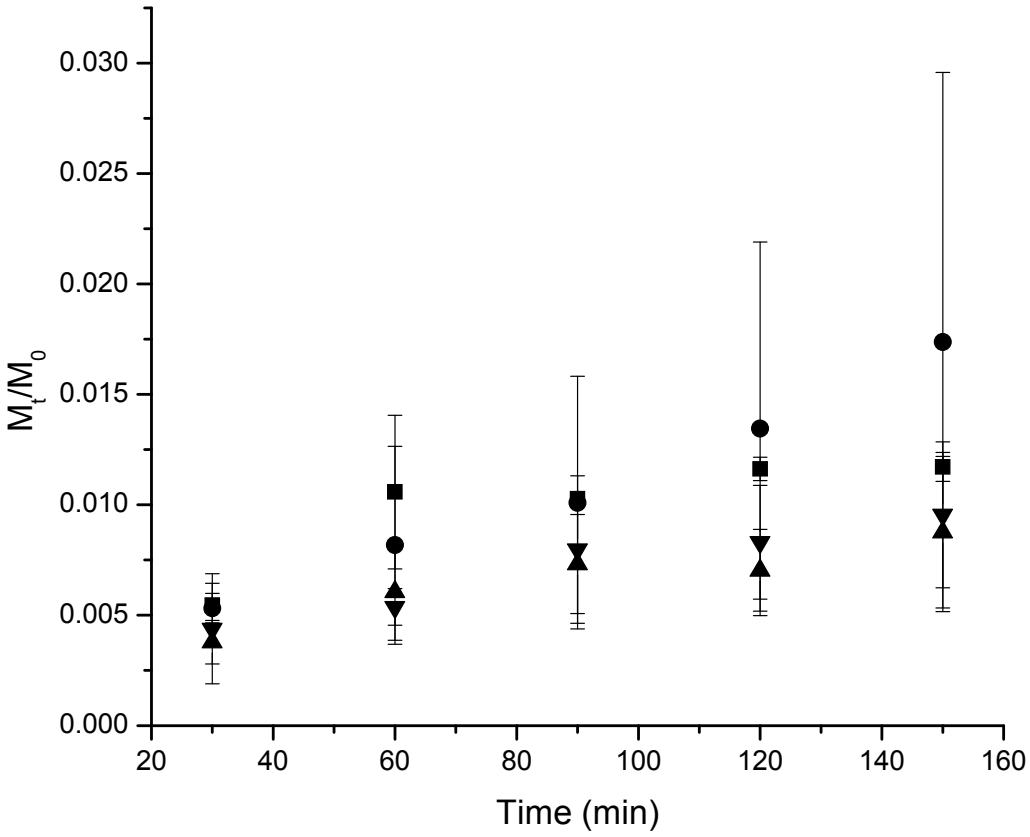

Effect of PEGMA 200/ PEGDMA 600 at a concentration of 10 mg/mL on the transport of fluorescein sodium salt across Caco-2 cell monolayers at 4°C. Transport on the AB direction for control (no hydrogel) ■,AB direction experimental (hydrogel) ●,BA direction control ▲,BA direction experimental ▼. Each data point represents the average of three experiments, passage number 50. Each data point represents an average of 3 experiments ± one standard deviation.

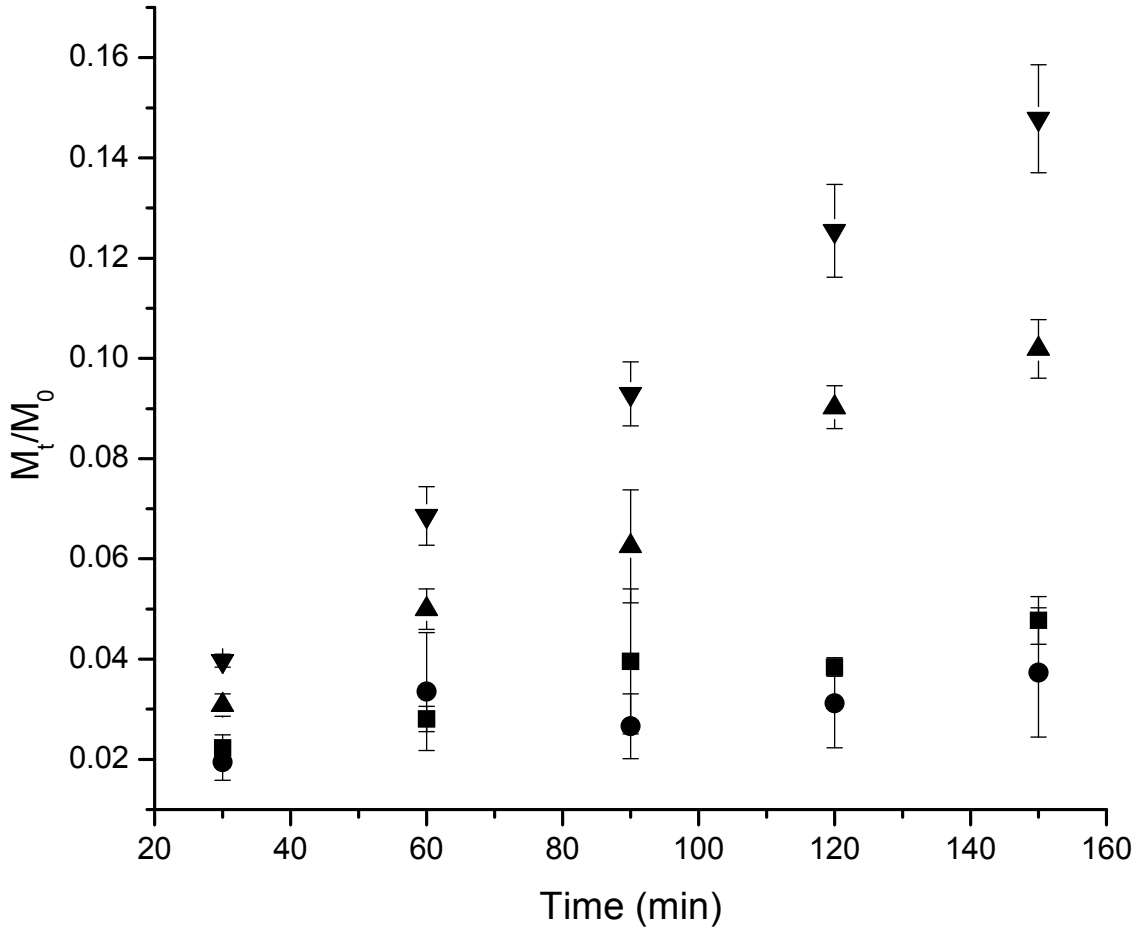

Effect of PEGMA 400/ PEGDMA 600 at a concentration of 10 mg/mL on the transport of fluorescein sodium salt across Caco-2 cell monolayers at 37°C. Transport on the AB direction for control (no hydrogel) ■,AB direction experimental (hydrogel) ●,BA direction control ▲,BA direction experimental ▼. Each data point represents the average of three experiments, passage number 42. Each data point represents an average of 3 experiments ± one standard deviation.

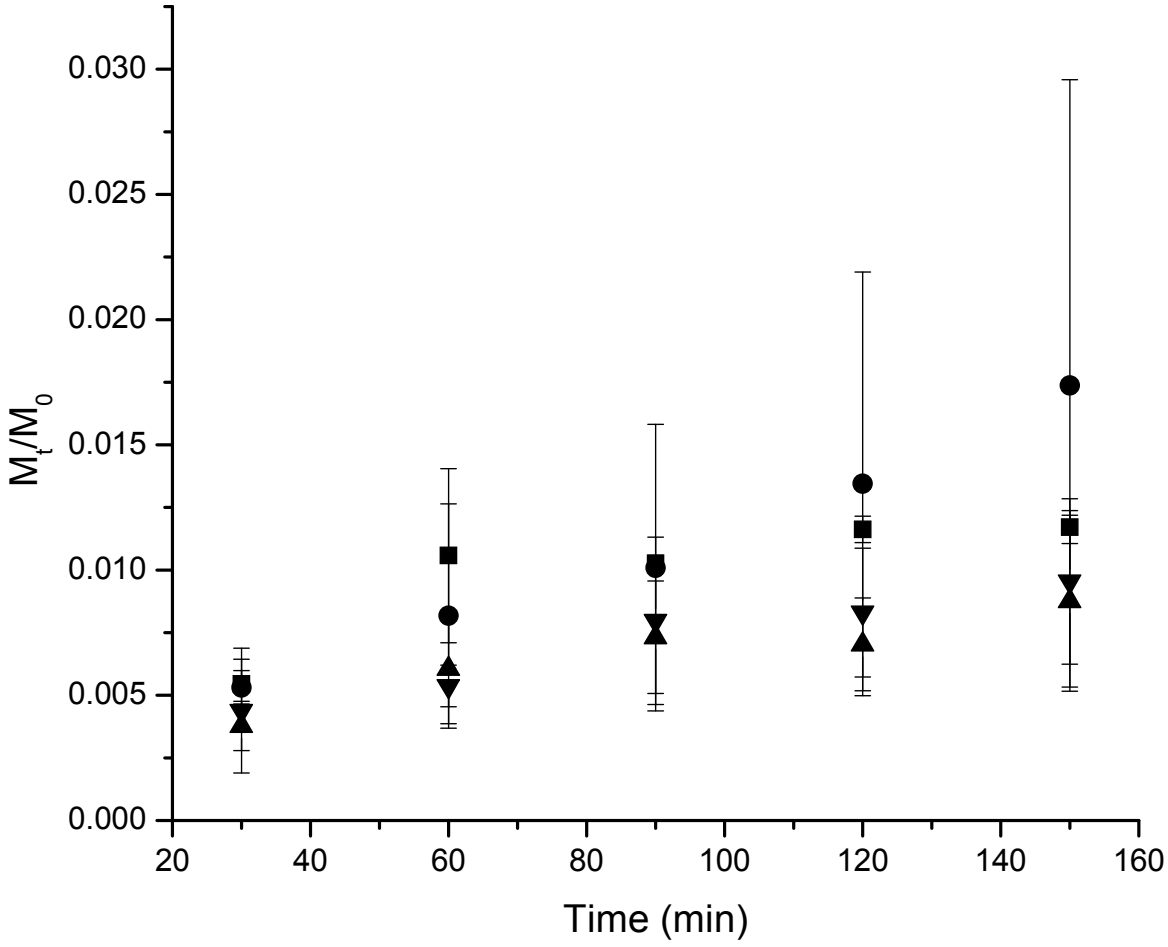

Effect of PEGMA 400/ PEGDMA 600 at a concentration of 10 mg/mL on the transport of fluorescein sodium salt across Caco-2 cell monolayers at 37°C. Transport on the AB direction for control (no hydrogel) ■,AB direction experimental (hydrogel) ●, BA direction control ▲, BA direction experimental ▼. Each data point represents the average of three experiments, passage number 55. Each data point represents an average of 3 experiments ± one standard deviation.

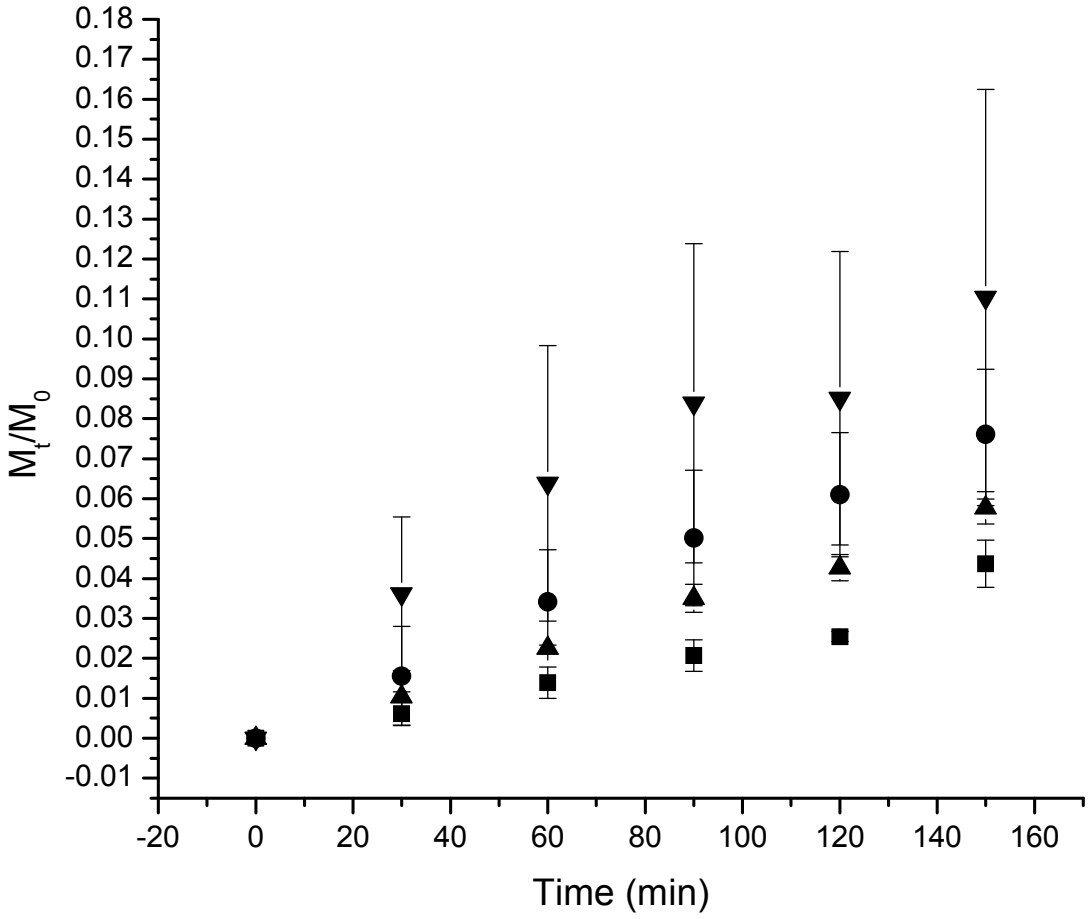

Effect of PEGMA 1000/ PEGDMA 600 at a concentration of 10 mg/mL on the transport of fluorescein sodium salt across Caco-2 cell monolayers at 37°C. Transport on the AB direction for control (no hydrogel) ■,AB direction experimental (hydrogel) ●, BA direction control ▲, BA direction experimental ▼. Each data point represents the average of three experiments, passage number 66. Each data point represents an average of 3 experiments ± one standard deviation.

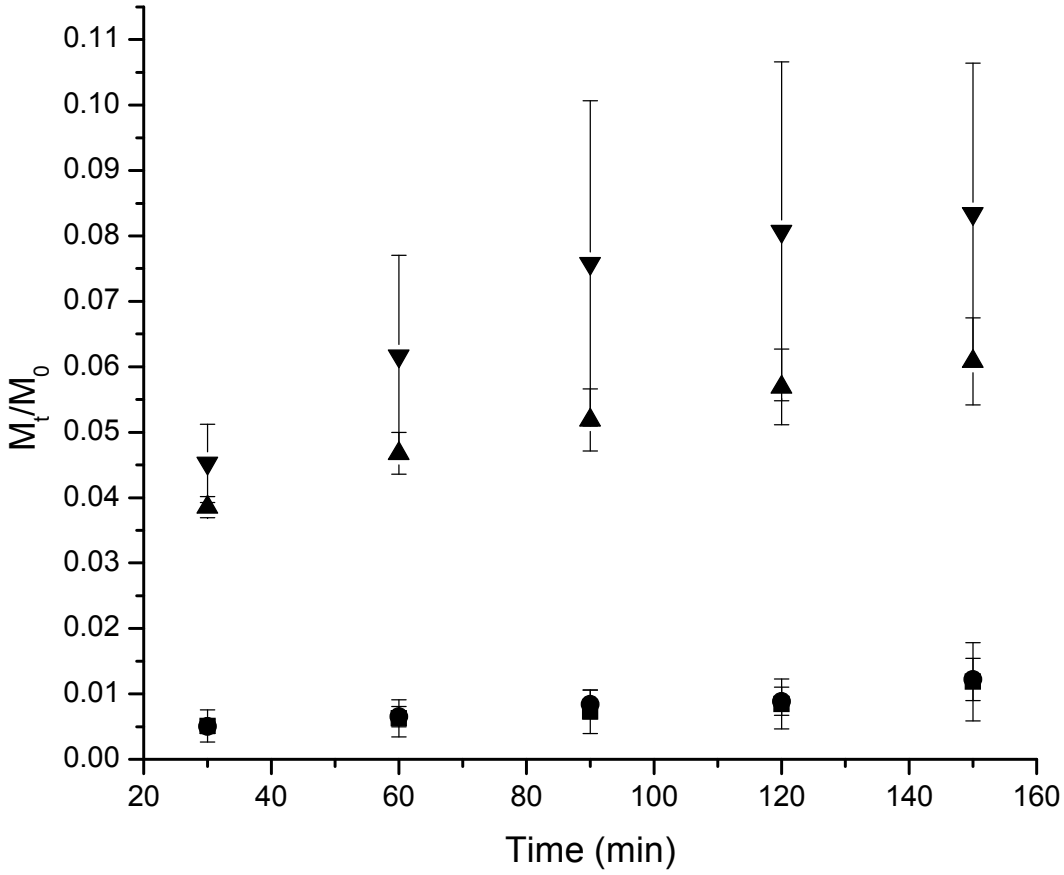

Effect of PEGMA 1000/ PEGDMA 600 at a concentration of 10 mg/mL on the transport of fluorescein sodium salt across Caco-2 cell monolayers at 4°C. Transport on the AB direction for control (no hydrogel) ■,AB direction experimental (hydrogel) ●, BA direction control ▲, BA direction experimental ▼. Each data point represents the average of three experiments, passage number 53. Each data point represents an average of 3 experiments ± one standard deviation.

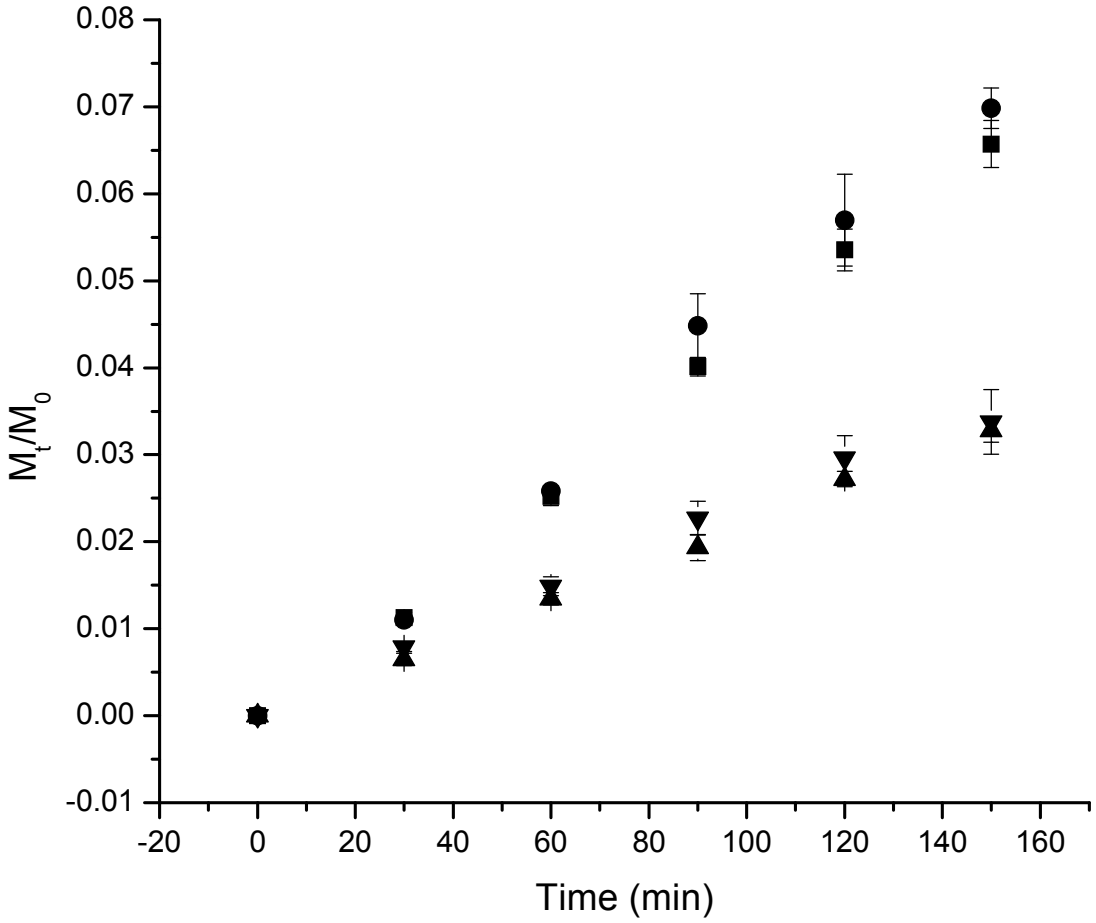

Effect of genistein at a concentration of 37 μM on the transport of fluorescein sodium salt across Caco-2 cell monolayers at 37°C. Transport on the AB direction for control (no hydrogel) ■,AB direction experimental (hydrogel) ●, BA direction control ▲, BA direction experimental ▼. Each data point represents the average of three experiments, passage number 41. Each data point represents an average of 3 experiments ± one standard deviation.

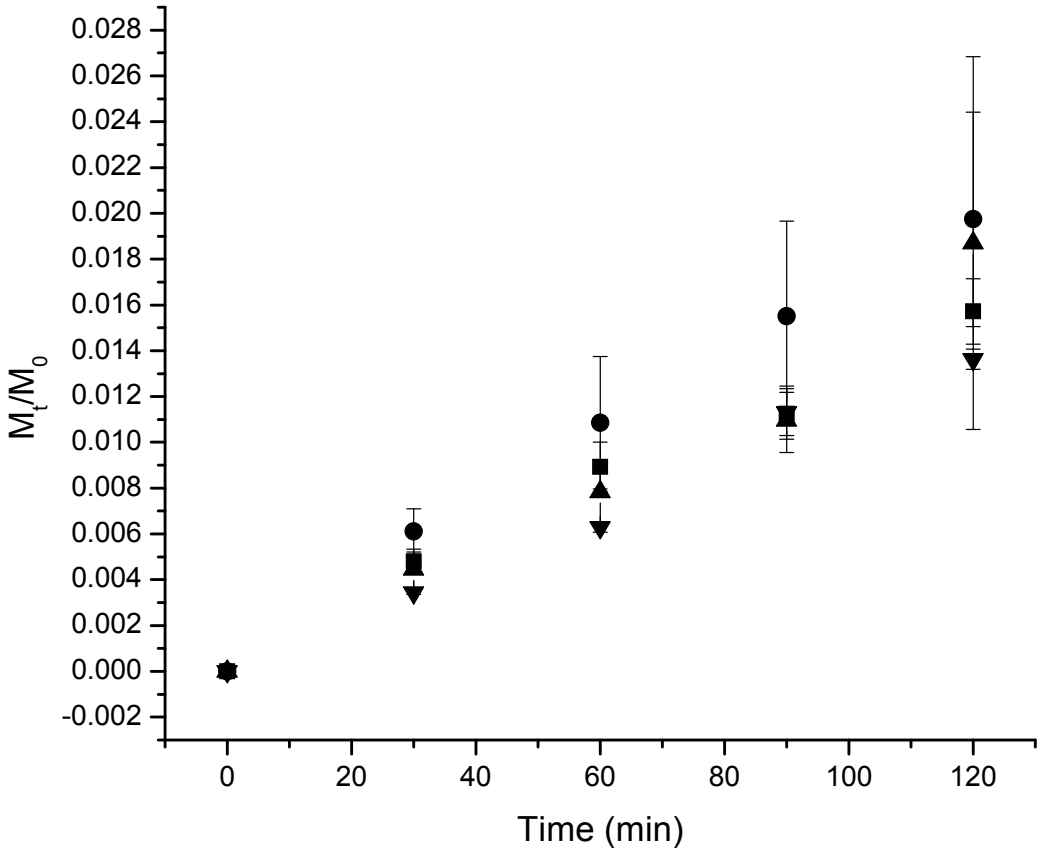

Effect of genistein at a concentration of 37 μM on the transport of fluorescein sodium salt across Caco-2 cell monolayers at 4°C. Transport on the AB direction for control (no hydrogel) ■,AB direction experimental (hydrogel) ●, BA direction control ▲, BA direction experimental ▼. Each data point represents the average of three experiments, passage number 50. Each data point represents an average of 3 experiments ± one standard deviation.

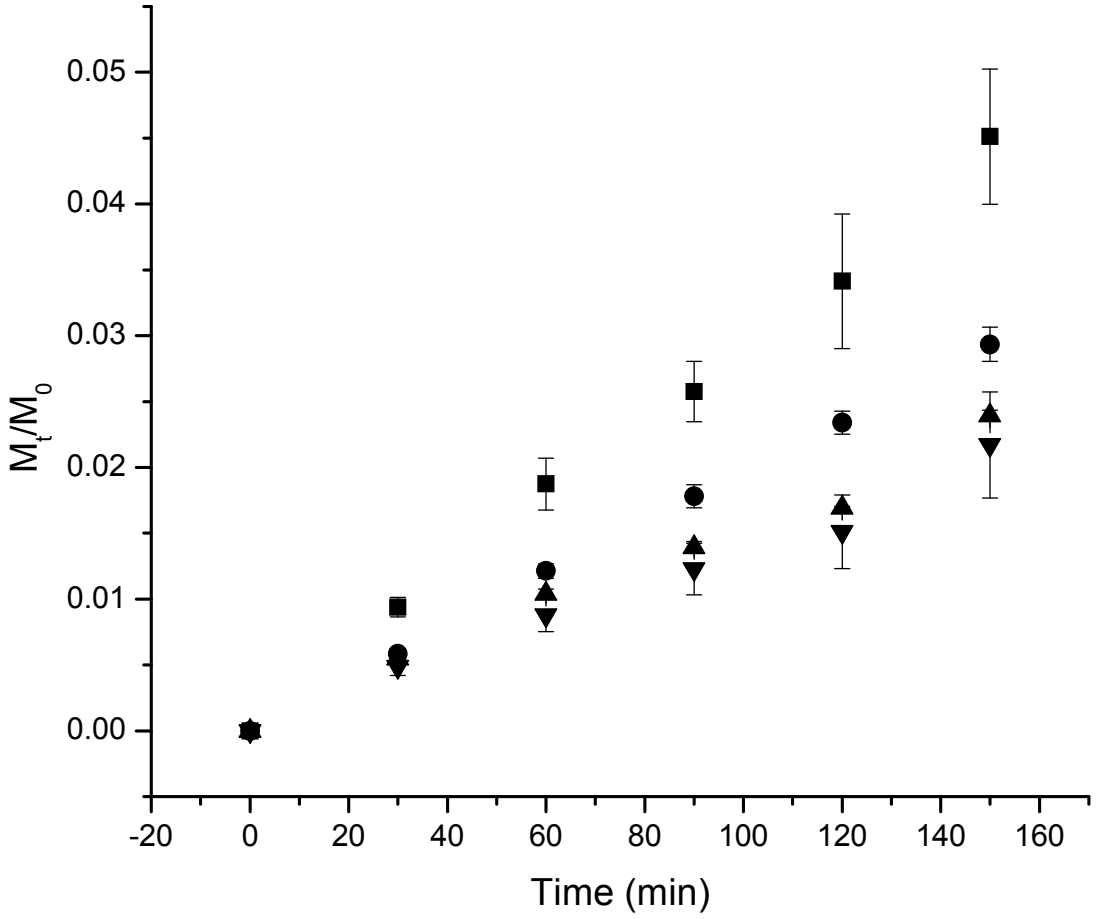

Effect of probenecid at a concentration of 100 μM on the transport of fluorescein sodium salt across Caco-2 cell monolayers at 37°C. Transport on the AB direction for control (no hydrogel) ■,AB direction experimental (hydrogel) ●, BA direction control ▲, BA direction experimental ▼. Each data point represents the average of three experiments, passage number 41. Each data point represents an average of 3 experiments ± one standard deviation.

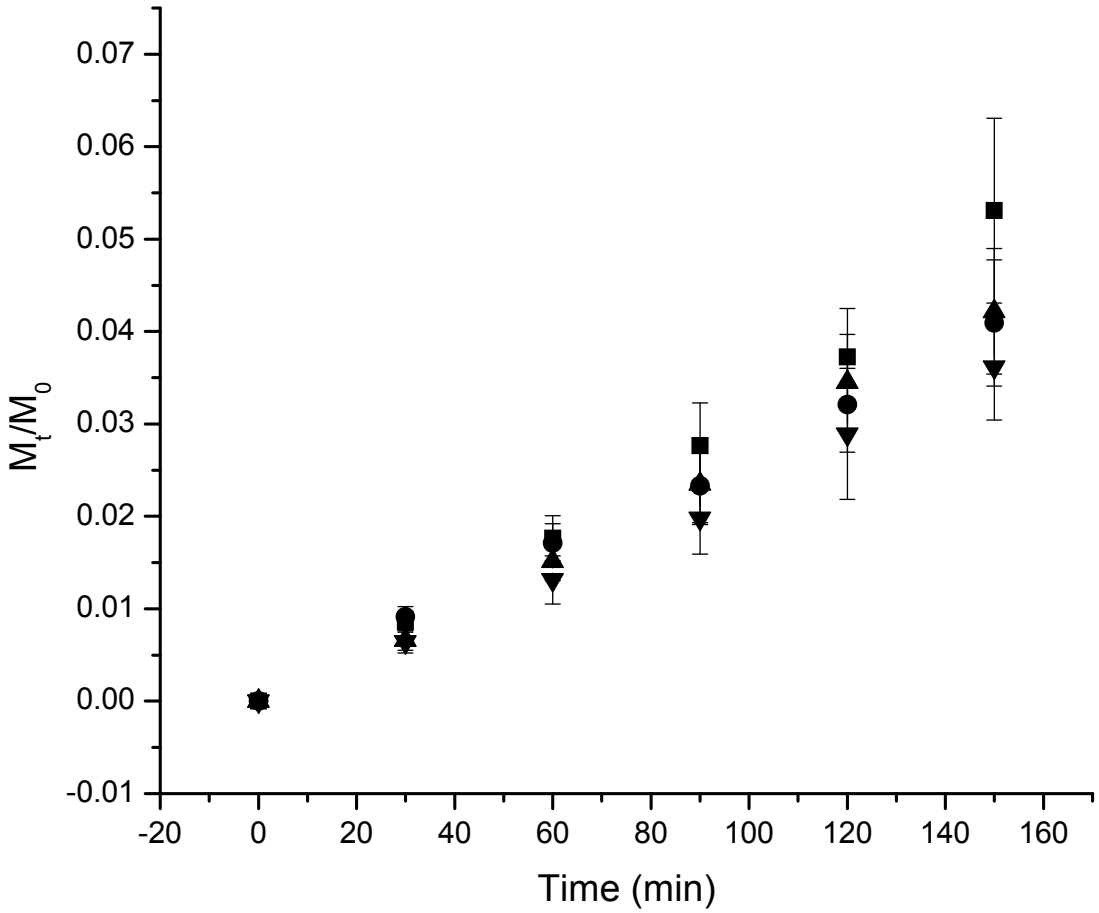

Effect of probenecid at a concentration of 100 μM on the transport of fluorescein sodium salt across Caco-2 cell monolayers at 4°C. Transport on the AB direction for control (no hydrogel) ■,AB direction experimental (hydrogel) ●, BA direction control ▲, BA direction experimental ▼. Each data point represents the average of three experiments, passage number 50. Each data point represents an average of 3 experiments ± one standard deviation.

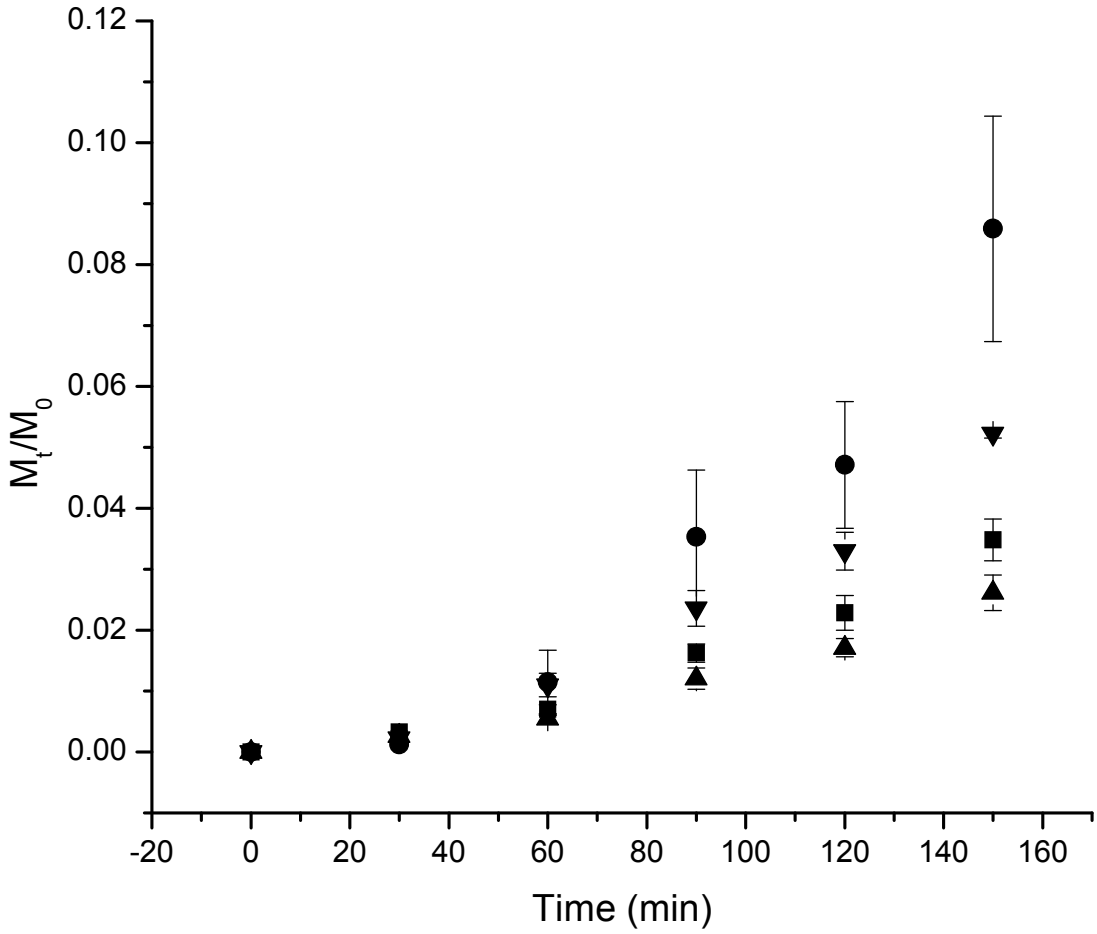

Effect of lineal PEG-300 morphology at a concentration of 20% (v/v) on the transport of fluorescein sodium salt across Caco-2 cell monolayers at 37°C. Transport on the AB direction for control (no hydrogel) ■, AB direction experimental (hydrogel) ●, BA direction control ▲, BA direction experimental ▼. Each data point represents the average of three experiments, passage number 33. Each data point represents an average of 3 experiments ± one standard deviation.

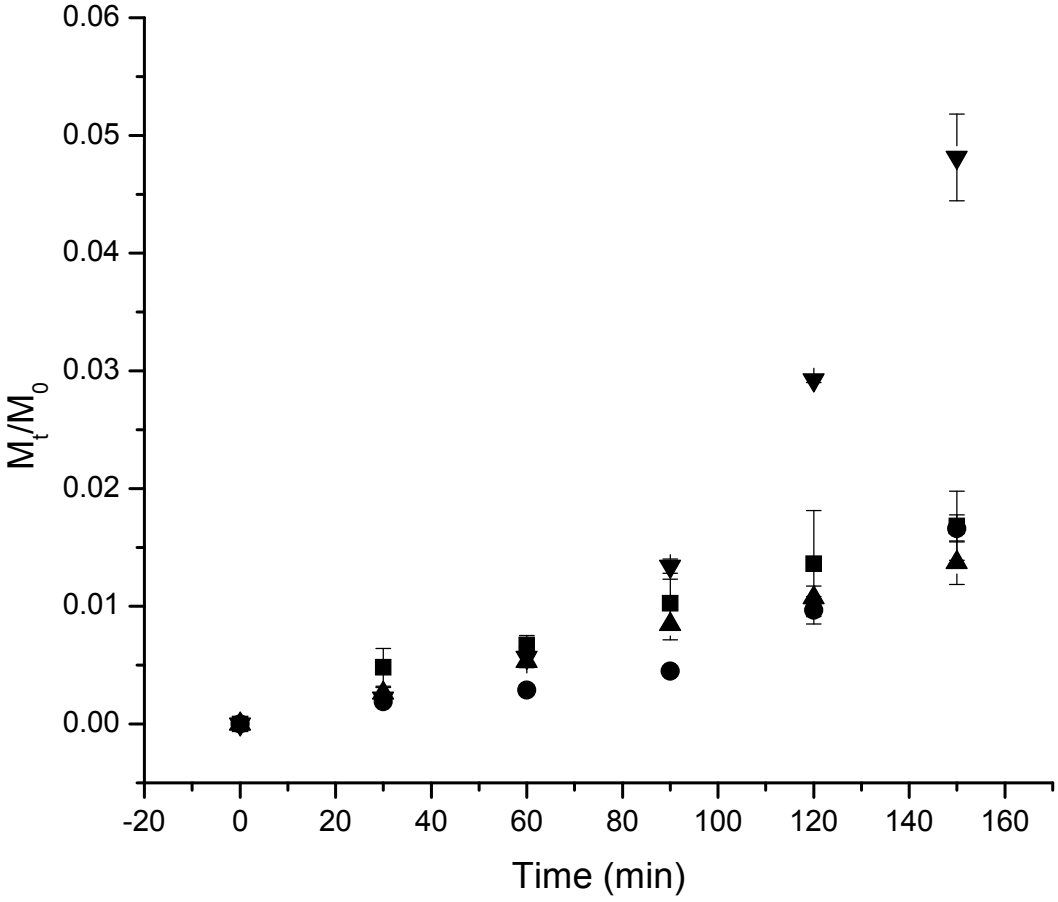

Effect of lineal PEG-300 morphology at a concentration of 20% (v/v) on the transport of fluorescein sodium salt across Caco-2 cell monolayers at 4°C. Transport on the AB direction for control (no hydrogel) ■, AB direction experimental (hydrogel) ●, BA direction control ▲, BA direction experimental ▼. Each data point represents the average of three experiments, passage number 59. Each data point represents an average of 3 experiments ± one standard deviation.

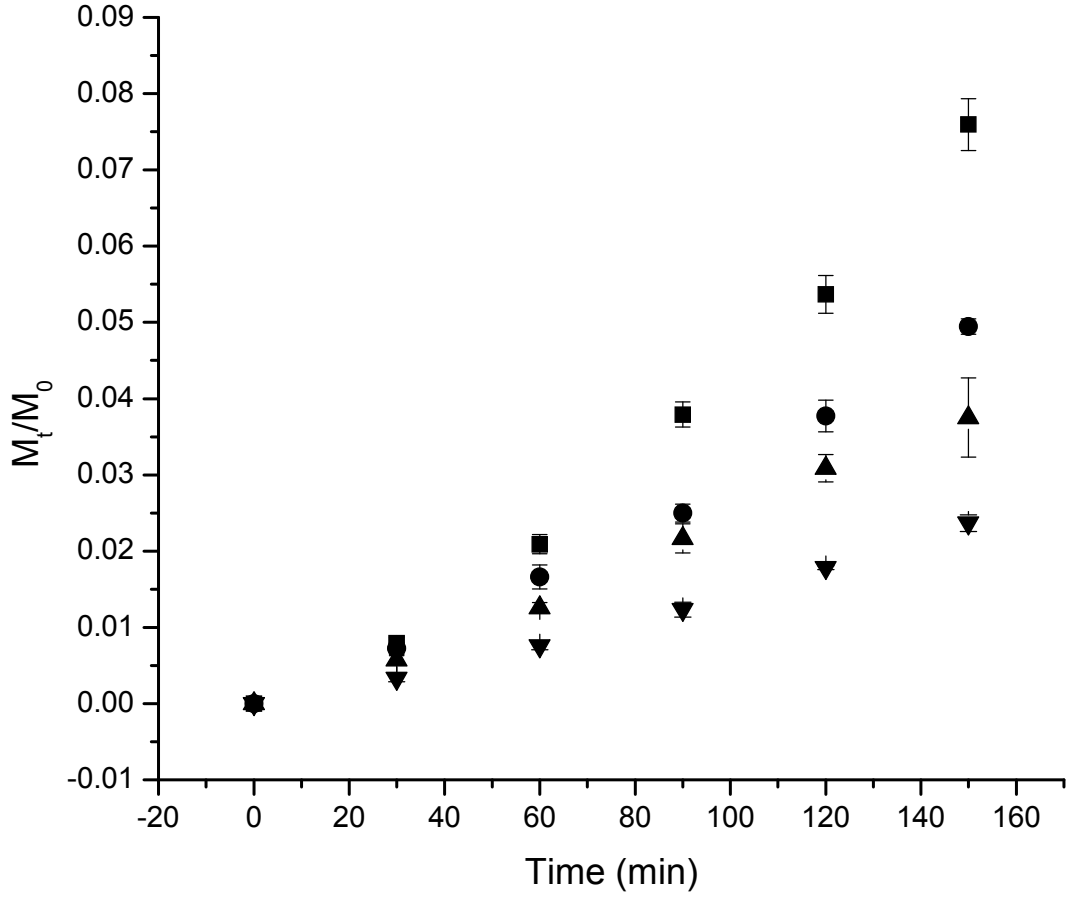

Effect of PEGMA 400/ PEGDMA 400 at a concentration of 10 mg/mL on the transport of fluorescein sodium salt across Caco-2 cell monolayers at 37°C. Transport on the AB direction for control (no hydrogel) ■, AB direction experimental (hydrogel) ●, BA direction control ▲, BA direction experimental ▼. Each data point represents the average of three experiments, passage number 51. Each data point represents an average of 3 experiments ± one standard deviation.

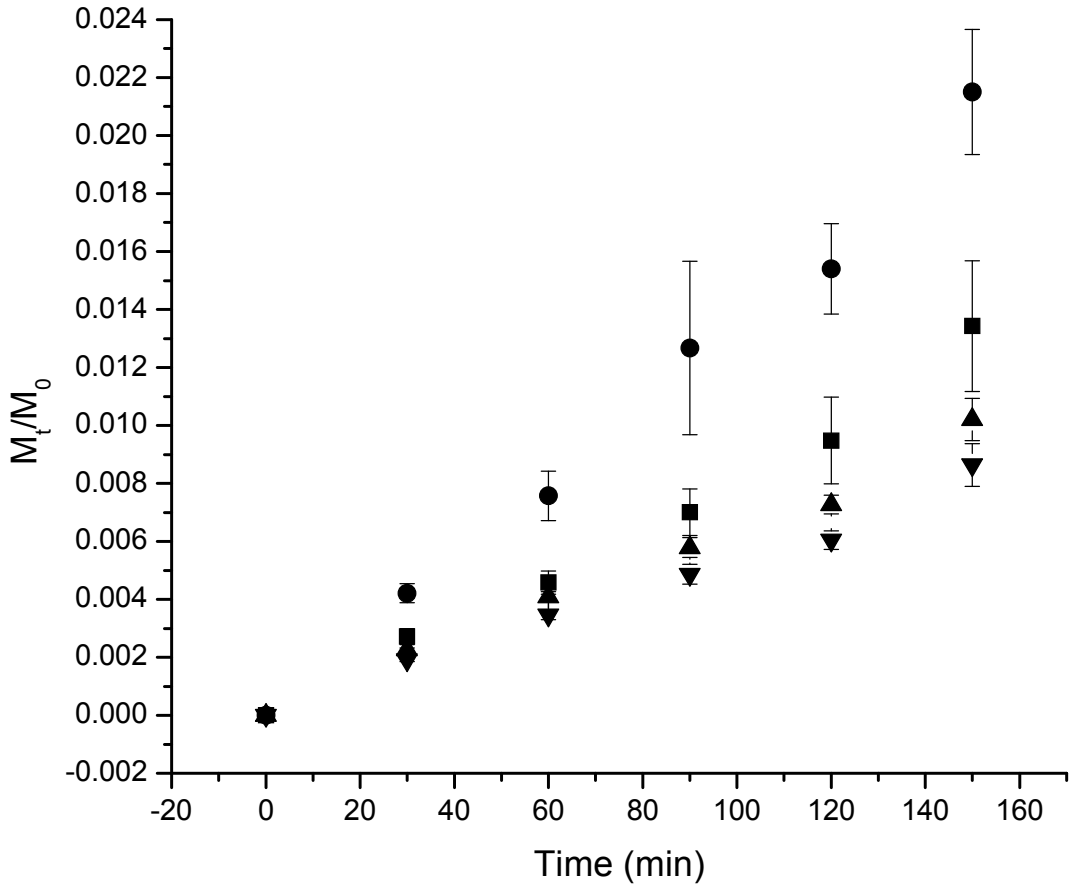

Effect of PEGMA 400/ PEGDMA 400 at a concentration of 10 mg/mL on the transport of fluorescein sodium salt across Caco-2 cell monolayers at 4°C. Transport on the AB direction for control (no hydrogel) ■, AB direction experimental (hydrogel) ●, BA direction control ▲, BA direction experimental ▼. Each data point represents the average of three experiments, passage number 51. Each data point represents an average of 3 experiments ± one standard deviation.

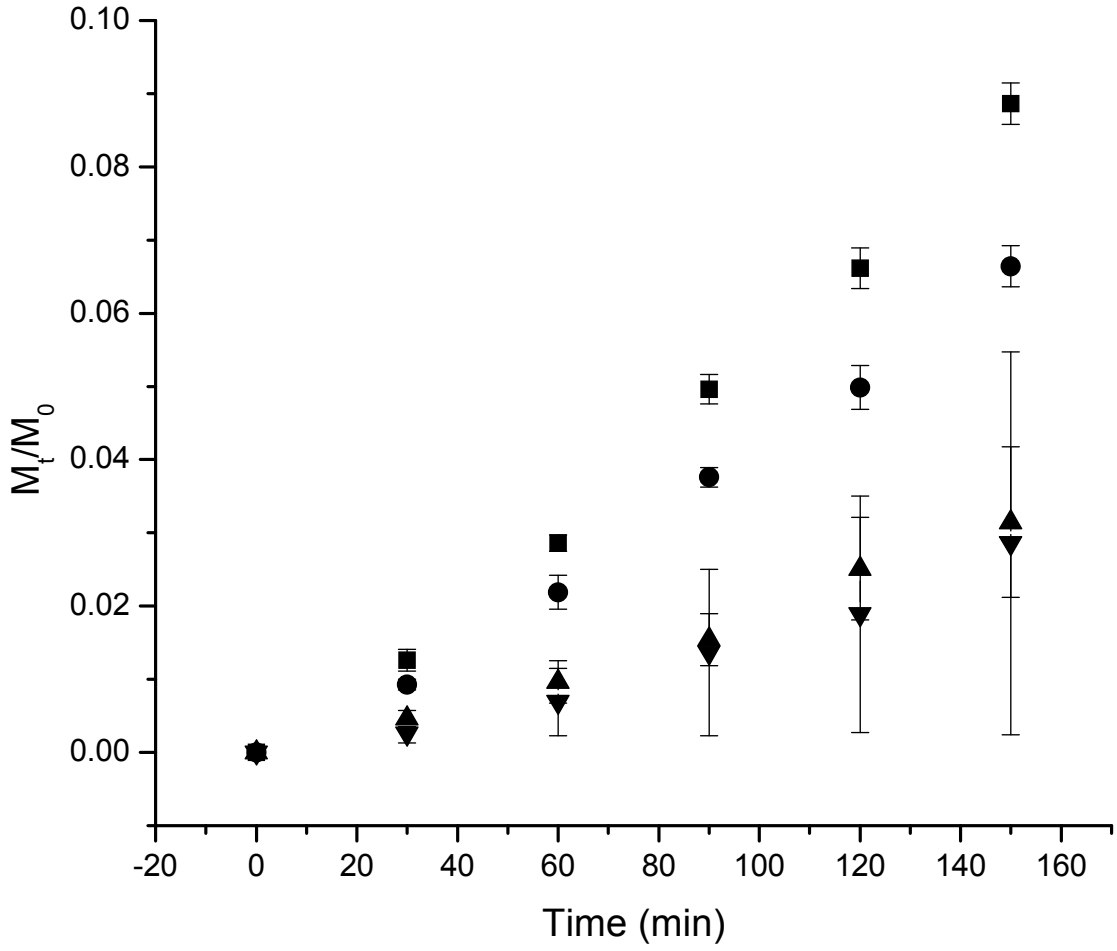

Effect of PEGMA 1000/ PEGDMA 400 at a concentration of 10 mg/mL on the transport of fluorescein sodium salt across Caco-2 cell monolayers at 37°C. Transport on the AB direction for control (no hydrogel) ■,AB direction experimental (hydrogel) ●, BA direction control ▲, BA direction experimental ▼. Each data point represents the average of three experiments, passage number 51. Each data point represents an average of 3 experiments ± one standard deviation.

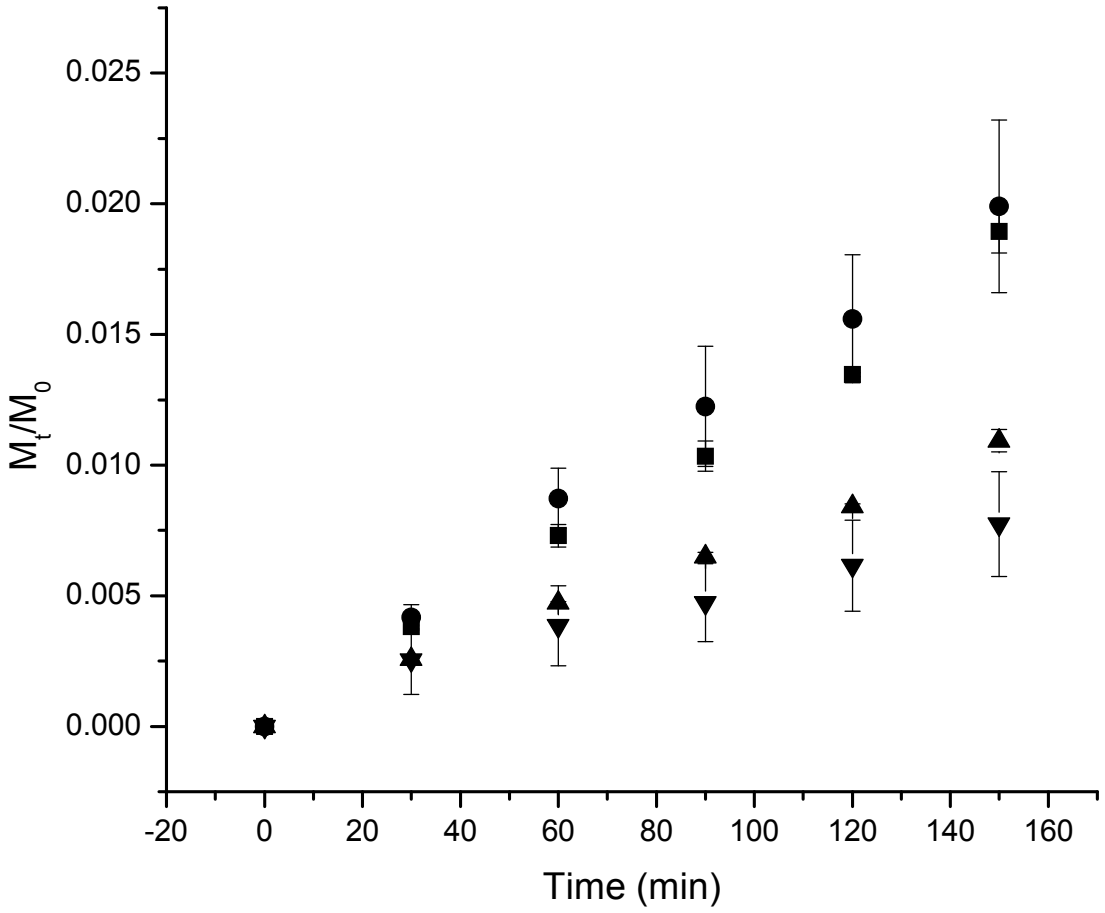

Effect of PEGMA 1000/ PEGDMA 400 at a concentration of 10 mg/mL on the transport of fluorescein sodium salt across Caco-2 cell monolayers at 4°C. Transport on the AB direction for control (no hydrogel) ■, AB direction experimental (hydrogel) ●, BA direction control ▲, BA direction experimental ▼. Each data point represents the average of three experiments, passage number 51. Each data point represents an average of 3 experiments ± one standard deviation.

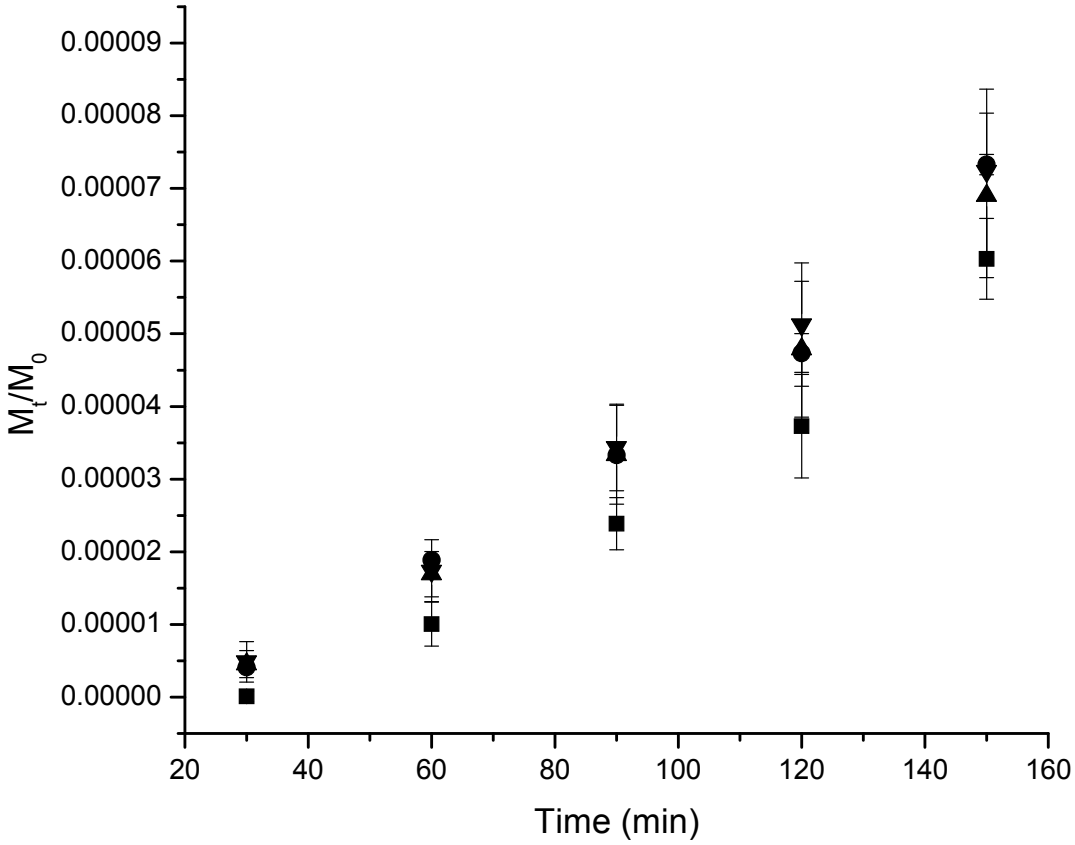

Effect of PEGMA 200/ PEGDMA 600 at a concentration of 20 mg/mL on the transport of rhodamine 123 across Caco-2 cell monolayers at 37°C. Transport on the AB direction for control (no hydrogel) ■, AB direction experimental (hydrogel) ●, BA direction control ▲, BA direction experimental ▼. Each data point represents the average of three experiments, passage number 37. Each data point represents an average of 3 experiments ± one standard deviation.

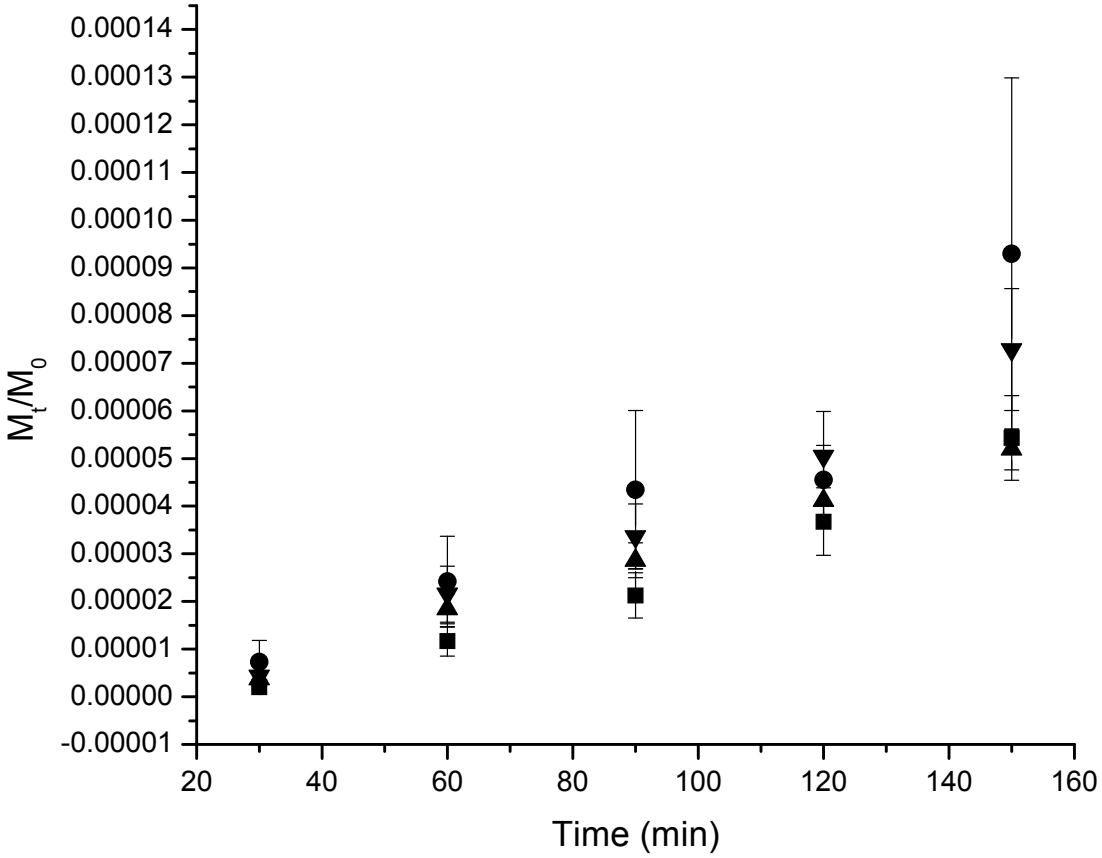

Effect of PEGMA 200/ PEGDMA 600 at a concentration of 10 mg/mL on the transport of rhodamine 123 across Caco-2 cell monolayers at 37°C. Transport on the AB direction for control (no hydrogel) ■, AB direction experimental (hydrogel) ●, BA direction control ▲, BA direction experimental ▼. Each data point represents the average of three experiments, passage number 37. Each data point represents an average of 3 experiments ± one standard deviation.

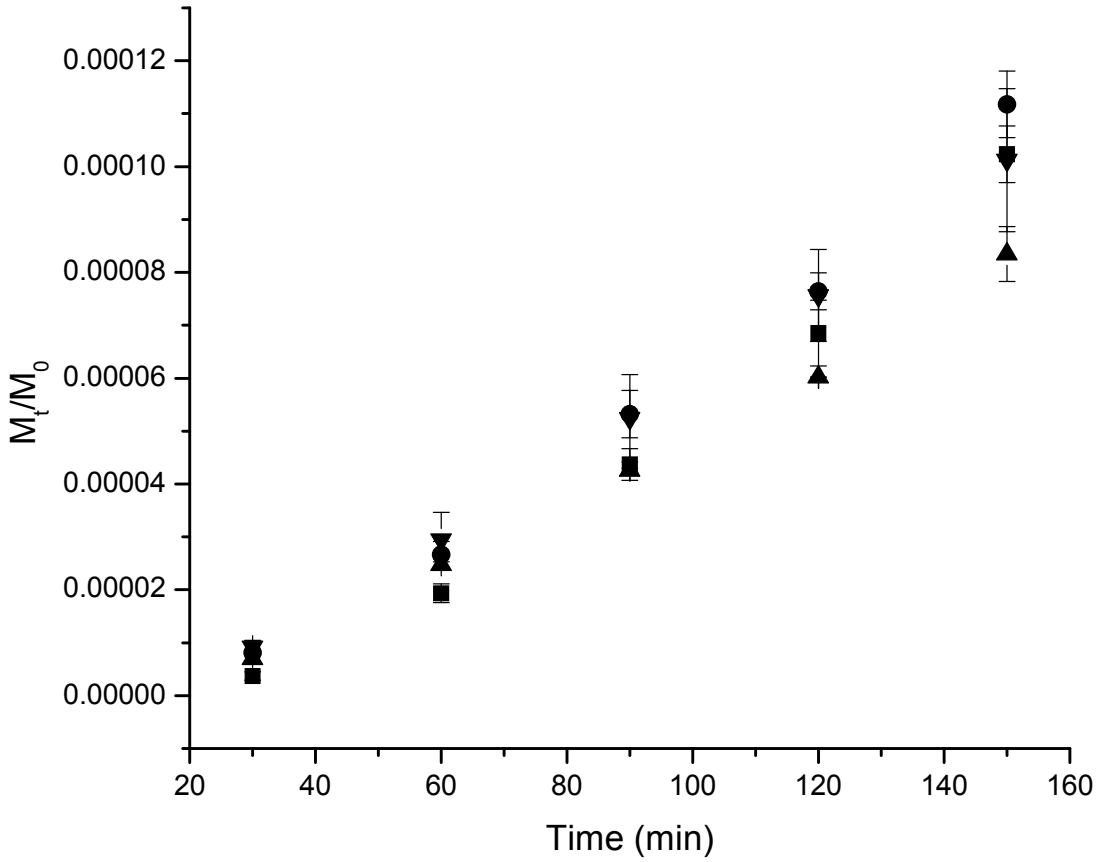

Effect of PEGMA 200/ PEGDMA 600 at a concentration of 5 mg/mL on the transport of rhodamine 123 across Caco-2 cell monolayers at 37°C. Transport on the AB direction for control (no hydrogel) ■, AB direction experimental (hydrogel) ●, BA direction control ▲, BA direction experimental ▼. Each data point represents the average of three experiments, passage number 37. Each data point represents an average of 3 experiments ± one standard deviation.

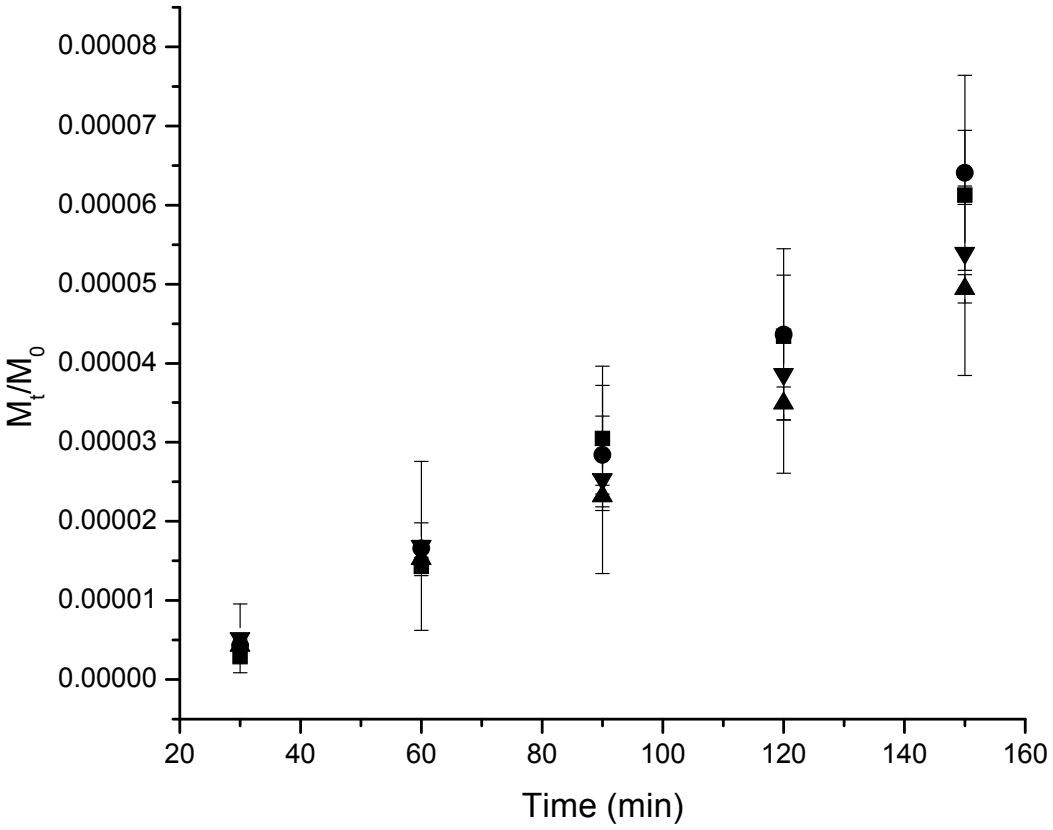

Effect of PEGMA 200/ PEGDMA 600 at a concentration of 1 mg/mL on the transport of rhodamine 123 across Caco-2 cell monolayers at 37°C. Transport on the AB direction for control (no hydrogel) ■, AB direction experimental (hydrogel) ●, BA direction control ▲, BA direction experimental ▼. Each data point represents the average of three experiments, passage number 37. Each data point represents an average of 3 experiments ± one standard deviation.

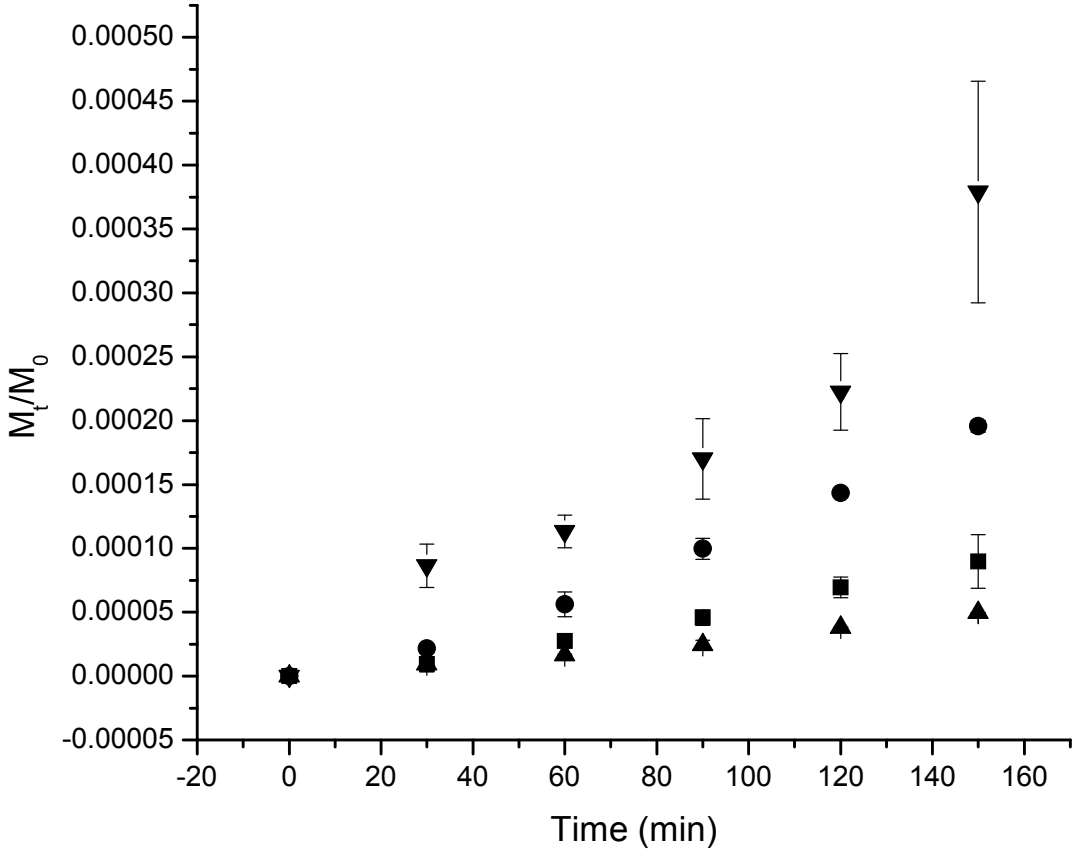

Effect of PEGMA 400/ PEGDMA 600 at a concentration of 20 mg/mL on the transport of rhodamine 123 across Caco-2 cell monolayers at 37°C. Transport on the AB direction for control (no hydrogel) ■, AB direction experimental (hydrogel) ●, BA direction control ▲, BA direction experimental ▼. Each data point represents the average of three experiments, passage number 32. Each data point represents an average of 3 experiments ± one standard deviation.

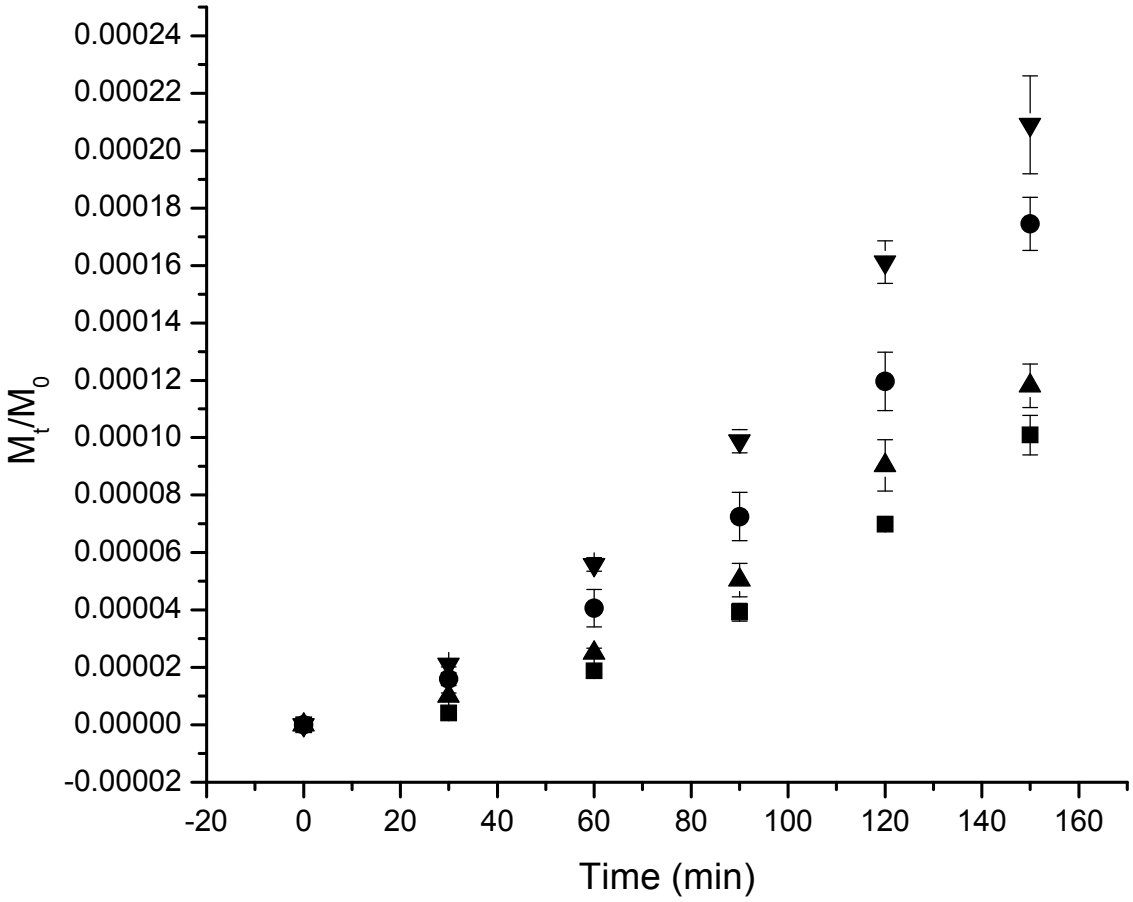

Effect of PEGMA 400/ PEGDMA 600 at a concentration of 10 mg/mL on the transport of rhodamine 123 across Caco-2 cell monolayers at 37°C. Transport on the AB direction for control (no hydrogel) ■, AB direction experimental (hydrogel) ●, BA direction control ▲, BA direction experimental ▼. Each data point represents the average of three experiments, passage number 32. Each data point represents an average of 3 experiments ± one standard deviation.

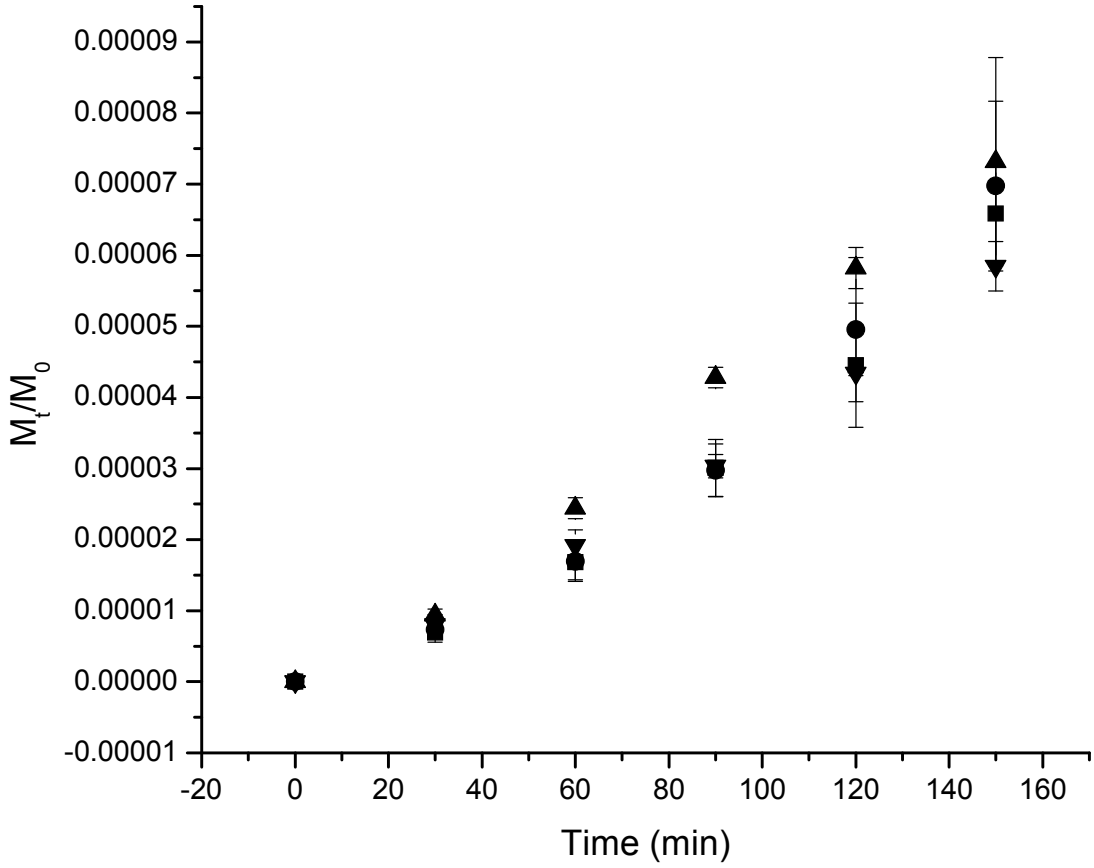

Effect of PEGMA 400/ PEGDMA 600 at a concentration of 5 mg/mL on the transport of rhodamine 123 across Caco-2 cell monolayers at 37°C. Transport on the AB direction for control (no hydrogel) ■, AB direction experimental (hydrogel) ●, BA direction control ▲, BA direction experimental ▼. Each data point represents the average of three experiments, passage number 32. Each data point represents an average of 3 experiments ± one standard deviation.

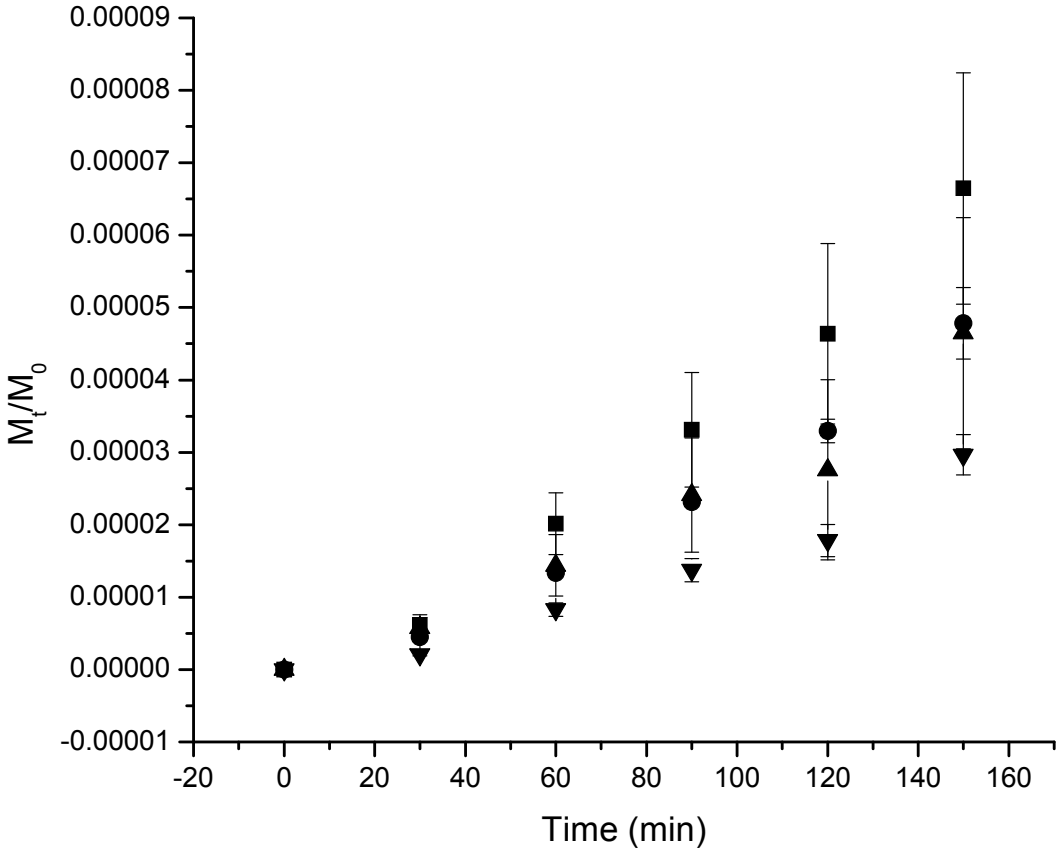

Effect of PEGMA 400/ PEGDMA 600 at a concentration of 1 mg/mL on the transport of rhodamine 123 across Caco-2 cell monolayers at 37°C. Transport on the AB direction for control (no hydrogel) ■, AB direction experimental (hydrogel) ●, BA direction control ▲, BA direction experimental ▼. Each data point represents the average of three experiments, passage number 38. Each data point represents an average of 3 experiments ± one standard deviation.

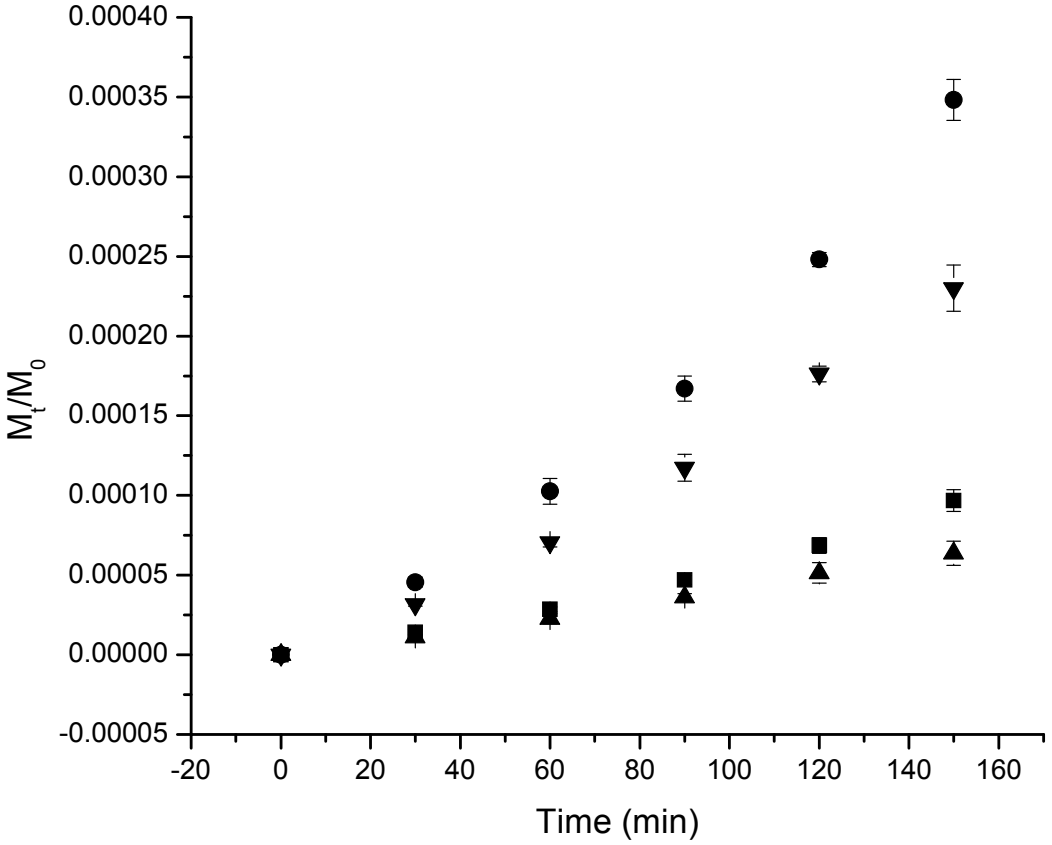

Effect of PEGMA 1000/ PEGDMA 600 at a concentration of 20 mg/mL on the transport of rhodamine 123 across Caco-2 cell monolayers at 37°C. Transport on the AB direction for control (no hydrogel) ■, AB direction experimental (hydrogel) ●, BA direction control ▲, BA direction experimental ▼. Each data point represents the average of three experiments, passage number 62. Each data point represents an average of 3 experiments ± one standard deviation.

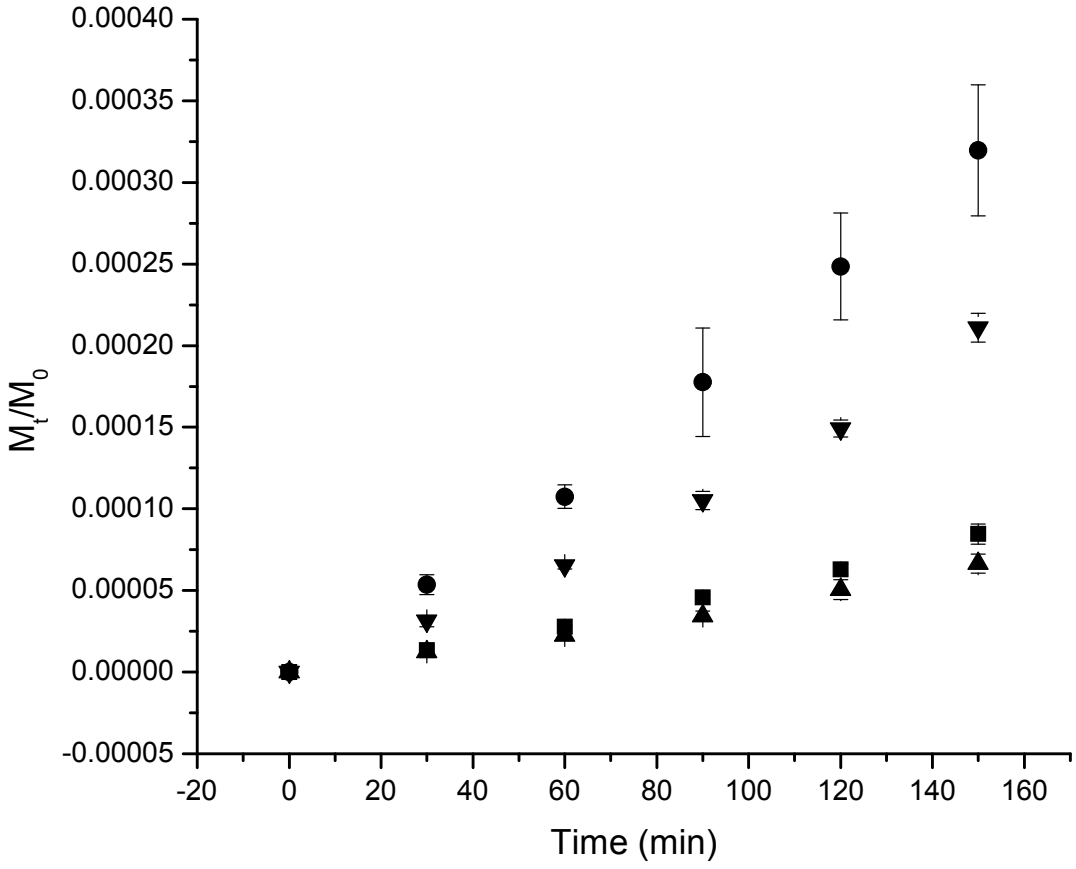

Effect of PEGMA 1000/ PEGDMA 600 at a concentration of 10 mg/mL on the transport of rhodamine 123 across Caco-2 cell monolayers at 37°C. Transport on the AB direction for control (no hydrogel) ■, AB direction experimental (hydrogel) ●, BA direction control ▲, BA direction experimental ▼. Each data point represents the average of three experiments, passage number 62. Each data point represents an average of 3 experiments ± one standard deviation.

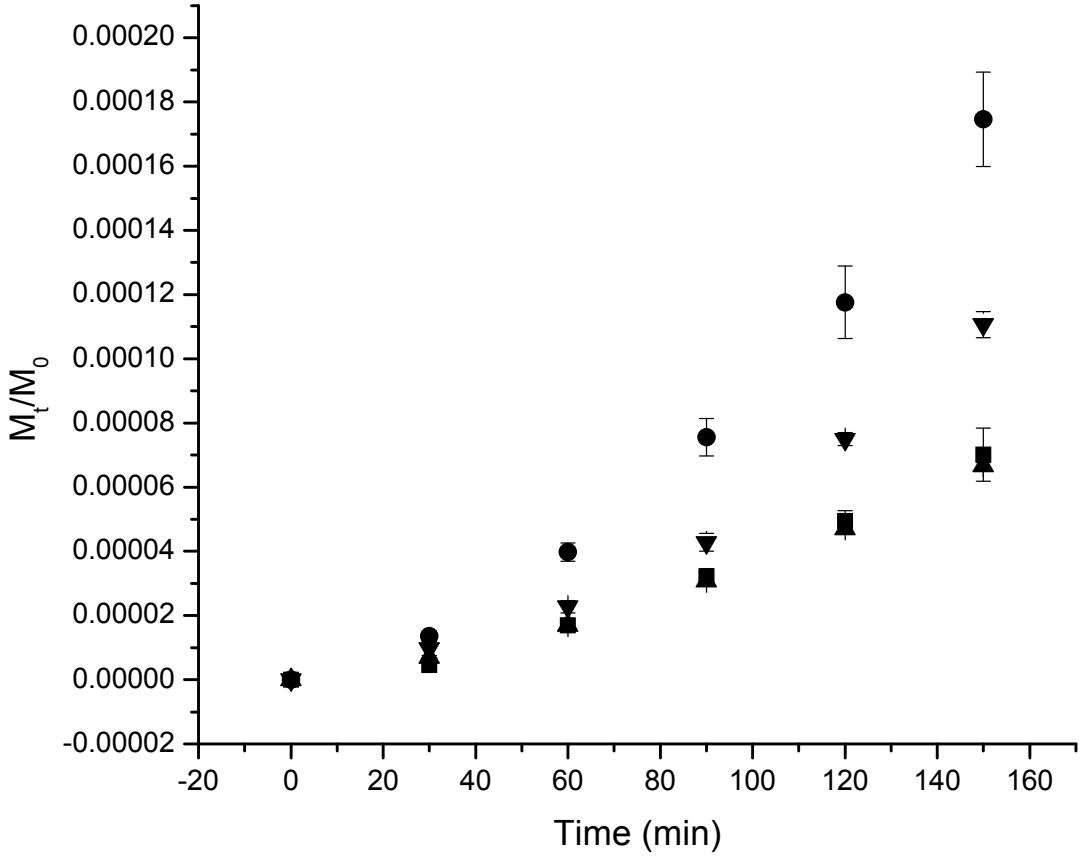

Effect of PEGMA 1000/ PEGDMA 600 at a concentration of 5 mg/mL on the transport of rhodamine 123 across Caco-2 cell monolayers at 37°C. Transport on the AB direction for control (no hydrogel) ■, AB direction experimental (hydrogel) ●, BA direction control ▲, BA direction experimental ▼. Each data point represents the average of three experiments, passage number 62. Each data point represents an average of 3 experiments ± one standard deviation.

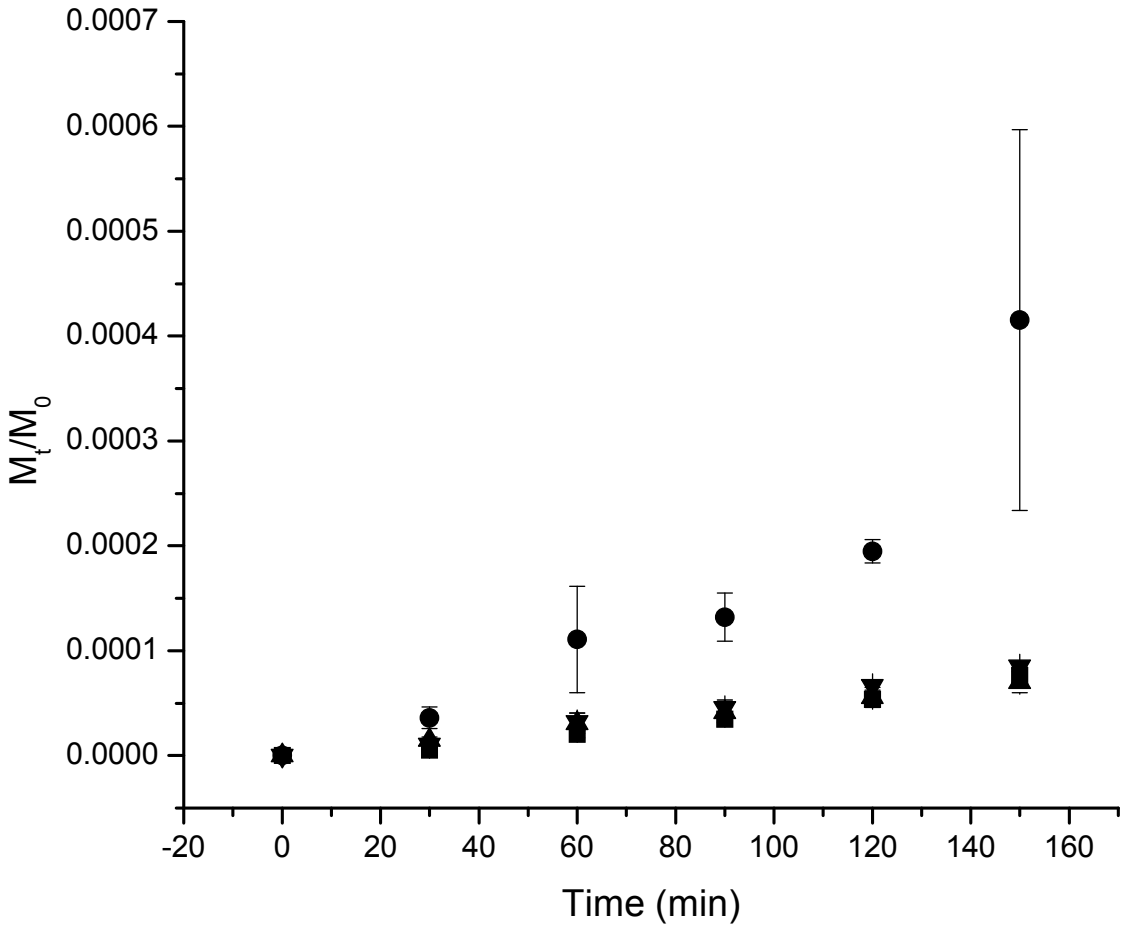

Effect of PEGMA 1000/ PEGDMA 600 at a concentration of 1 mg/mL on the transport of rhodamine 123 across Caco-2 cell monolayers at 37°C. Transport on the AB direction for control (no hydrogel) ■, AB direction experimental (hydrogel) ●, BA direction control ▲, BA direction experimental ▼. Each data point represents the average of three experiments, passage number 62. Each data point represents an average of 3 experiments ± one standard deviation.

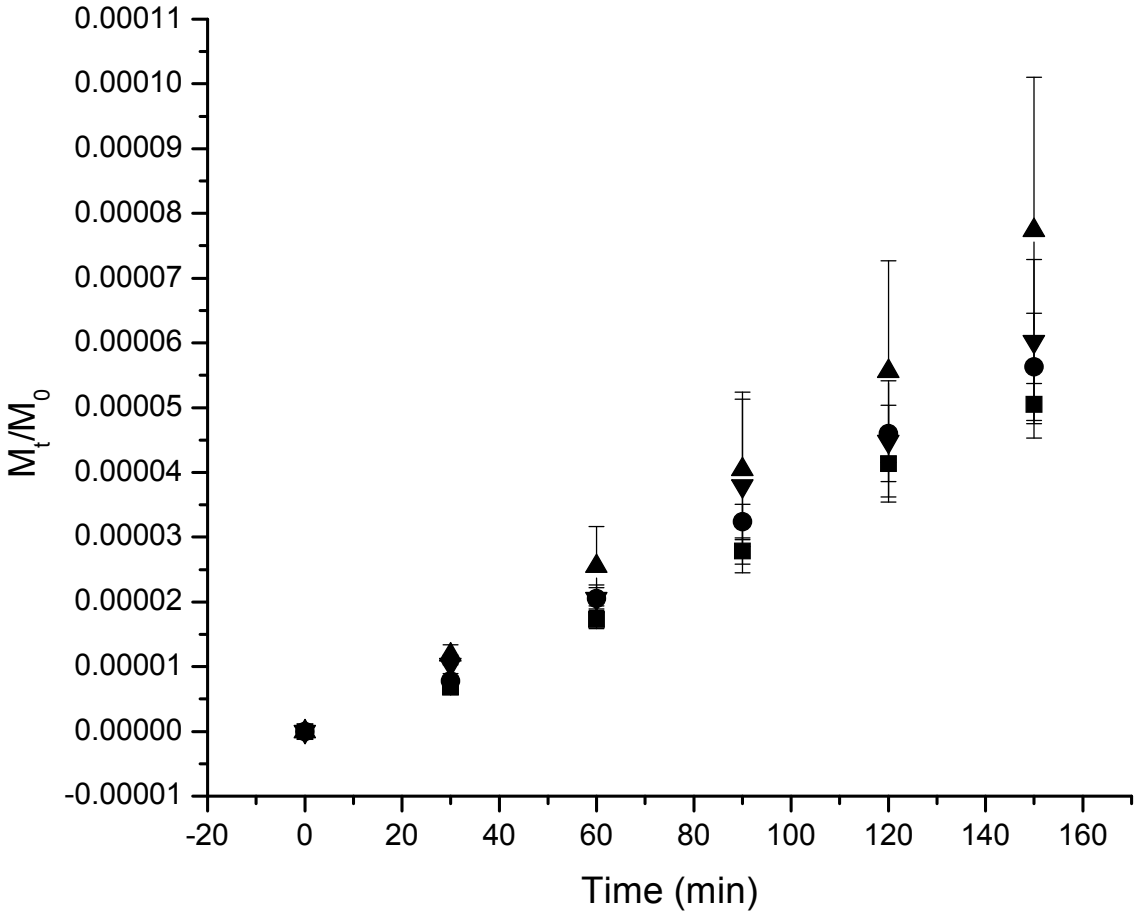

Effect of genistein at a concentration of 37 μM on the transport of rhodamine 123 across Caco-2 cell monolayers at 37°C. Transport on the AB direction for control (no hydrogel) ■, AB direction experimental (hydrogel) ●, BA direction control ▲, BA direction experimental ▼. Each data point represents the average of three experiments, passage number 39. Each data point represents an average of 3 experiments ± one standard deviation.

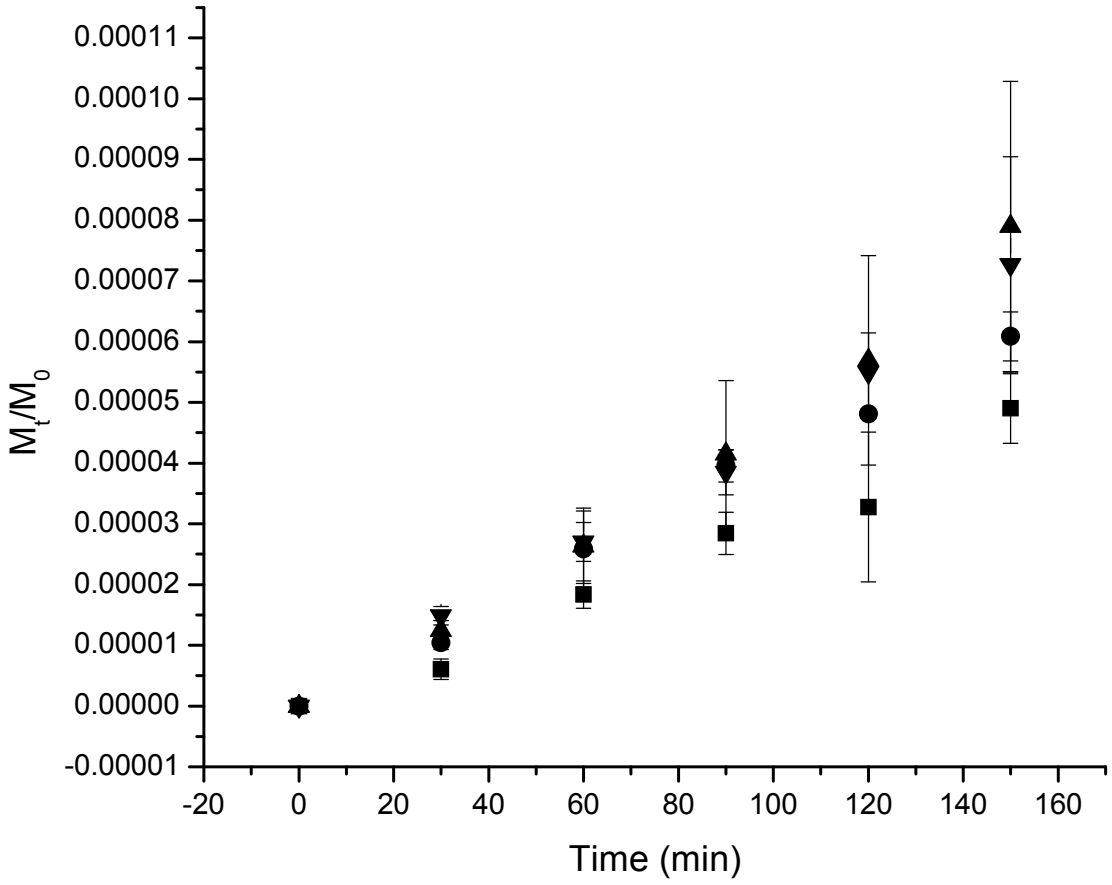

Effect of verapamil at a concentration of 100 μM on the transport of rhodamine 123 across Caco-2 cell monolayers at 37°C. Transport on the AB direction for control (no hydrogel) ■, AB direction experimental (hydrogel) ●, BA direction control ▲, BA direction experimental ▼. Each data point represents the average of three experiments, passage number 39. Each data point represents an average of 3 experiments ± one standard deviation.

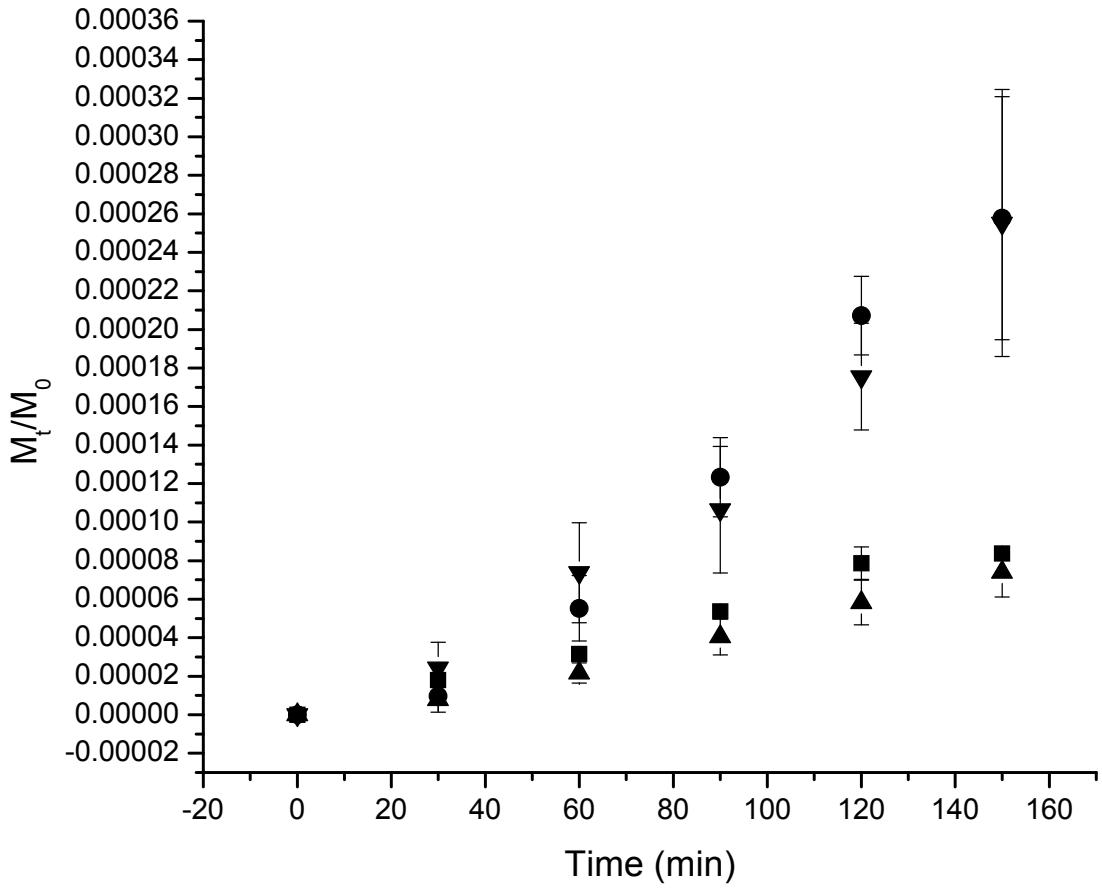

Effect of lineal PEG 300 at a concentration of 20% (v/v) on the transport of rhodamine 123 across Caco-2 cell monolayers at 37°C. Transport on the AB direction for control (no hydrogel) ■, AB direction experimental (hydrogel) ●, BA direction control ▲, BA direction experimental ▼. Each data point represents the average of three experiments, passage number 39. Each data point represents an average of 3 experiments ± one standard deviation.

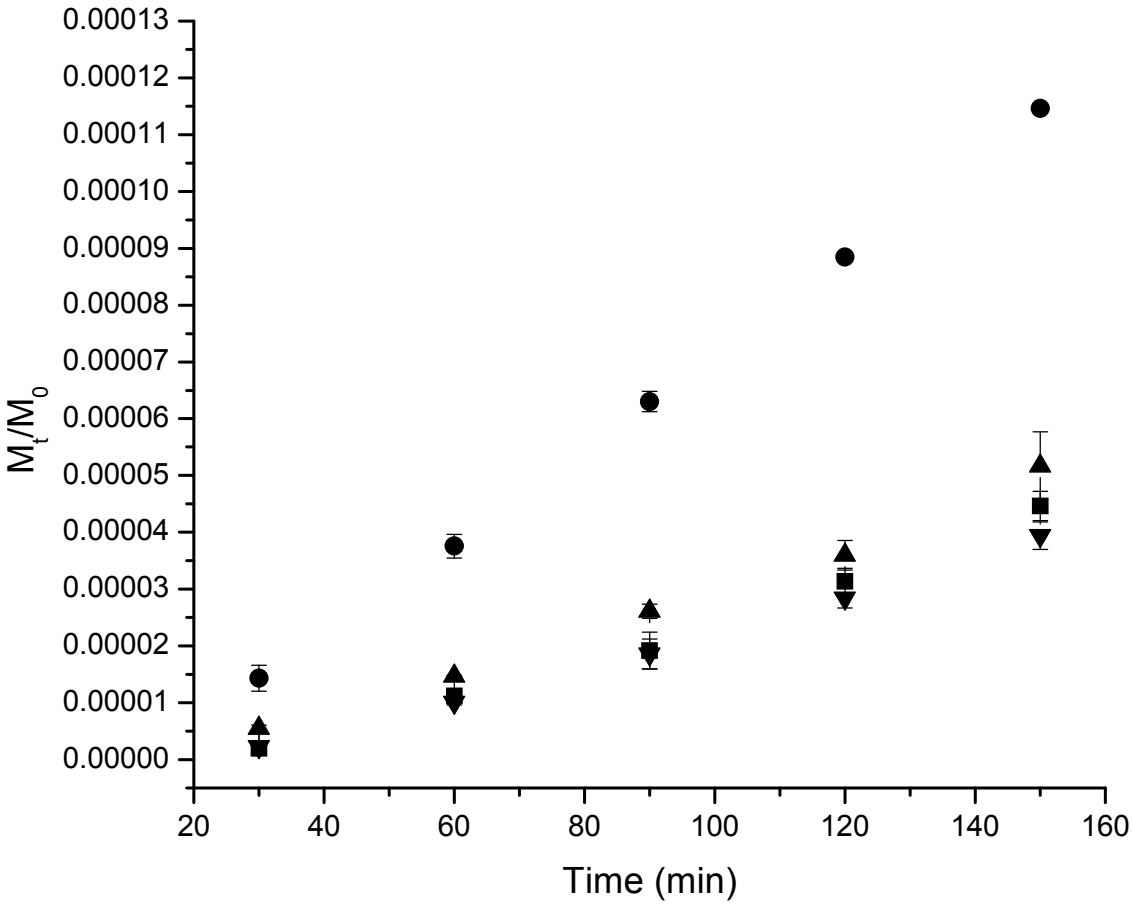

Effect of PEGMA 400/ PEGDMA 400 at a concentration of 10 mg/mL on the transport of rhodamine 123 across Caco-2 cell monolayers at 37°C. Transport on the AB direction for control (no hydrogel) ■, AB direction experimental (hydrogel) ●, BA direction control ▲, BA direction experimental ▼. Each data point represents the average of three experiments, passage number 44. Each data point represents an average of 3 experiments ± one standard deviation.

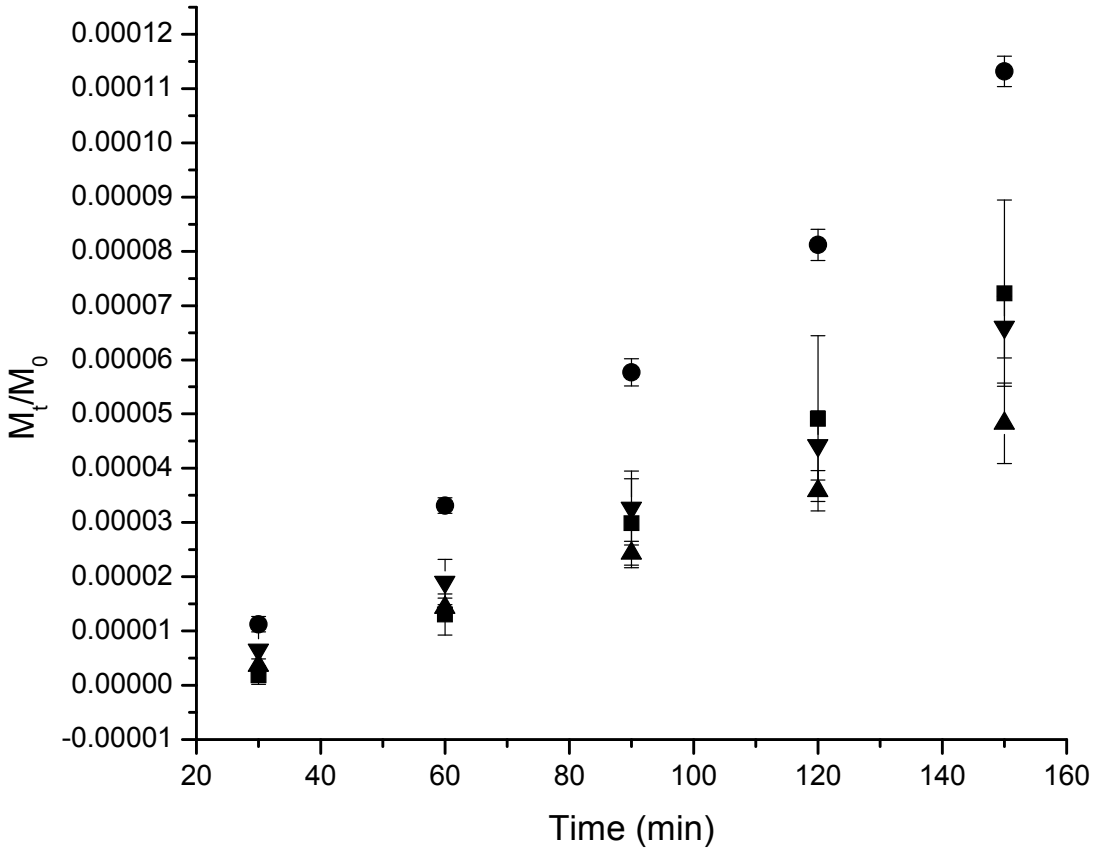

Effect of PEGMA 400/ PEGDMA 400 at a concentration of 1 mg/mL on the transport of rhodamine 123 across Caco-2 cell monolayers at 37°C. Transport on the AB direction for control (no hydrogel) ■, AB direction experimental (hydrogel) ●, BA direction control ▲, BA direction experimental ▼. Each data point represents the average of three experiments, passage number 44. Each data point represents an average of 3 experiments ± one standard deviation.

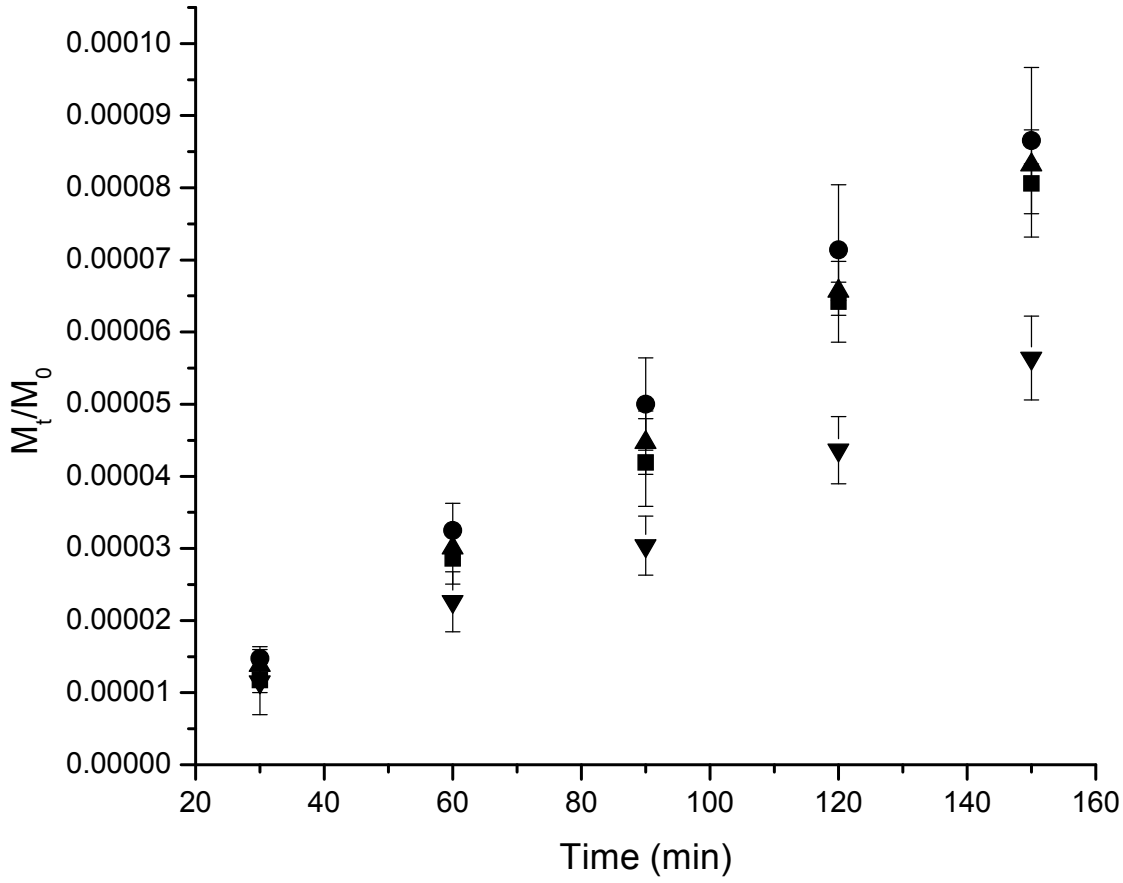

Effect of PEGMA 1000/ PEGDMA 400 at a concentration of 10 mg/mL on the transport of rhodamine 123 across Caco-2 cell monolayers at 37°C. Transport on the AB direction for control (no hydrogel) ■, AB direction experimental (hydrogel) ●, BA direction control ▲, BA direction experimental ▼. Each data point represents the average of three experiments, passage number 45. Each data point represents an average of 3 experiments ± one standard deviation.

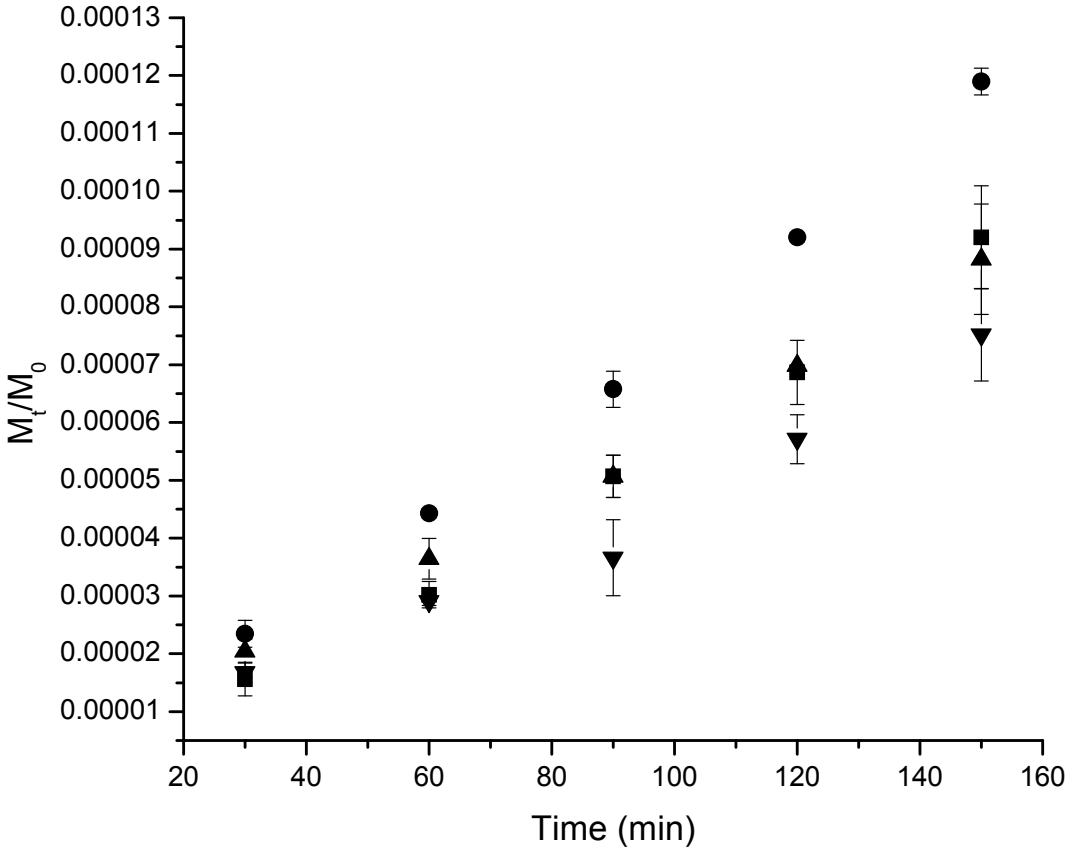

Effect of PEGMA 1000/ PEGDMA 400 at a concentration of 1 mg/mL on the transport of rhodamine 123 across Caco-2 cell monolayers at 37°C. Transport on the AB direction for control (no hydrogel) ■, AB direction experimental (hydrogel) ●, BA direction control ▲, BA direction experimental ▼. Each data point represents the average of three experiments, passage number 45. Each data point represents an average of 3 experiments ± one standard deviation.

APPENDIX II
Raw data for Fluorescence Recovery after Photobleaching Experiments

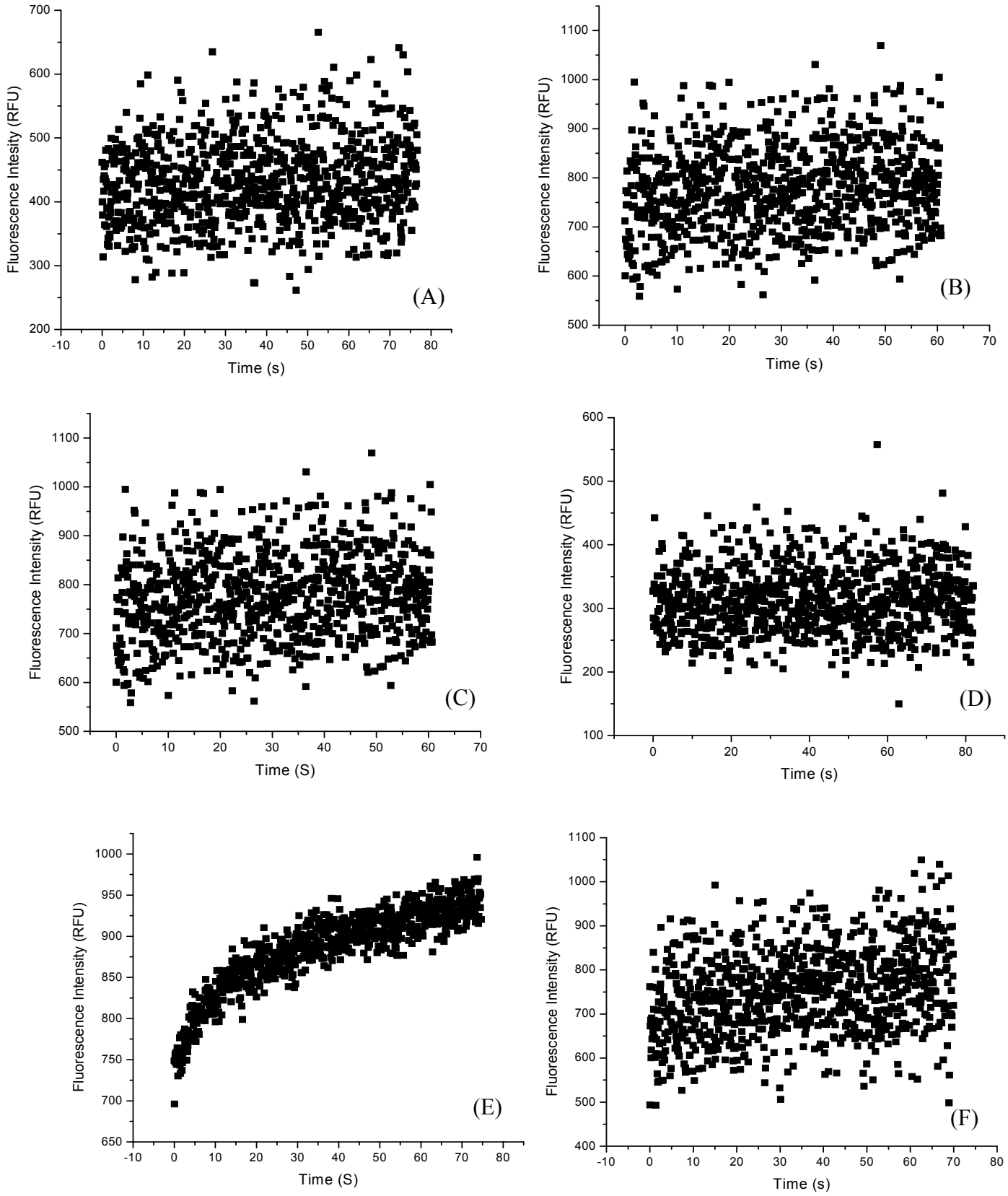

Figure 1: Fluorescence recovery after photobleaching (FRAP) raw data for control experiments 1-6 (A-F).

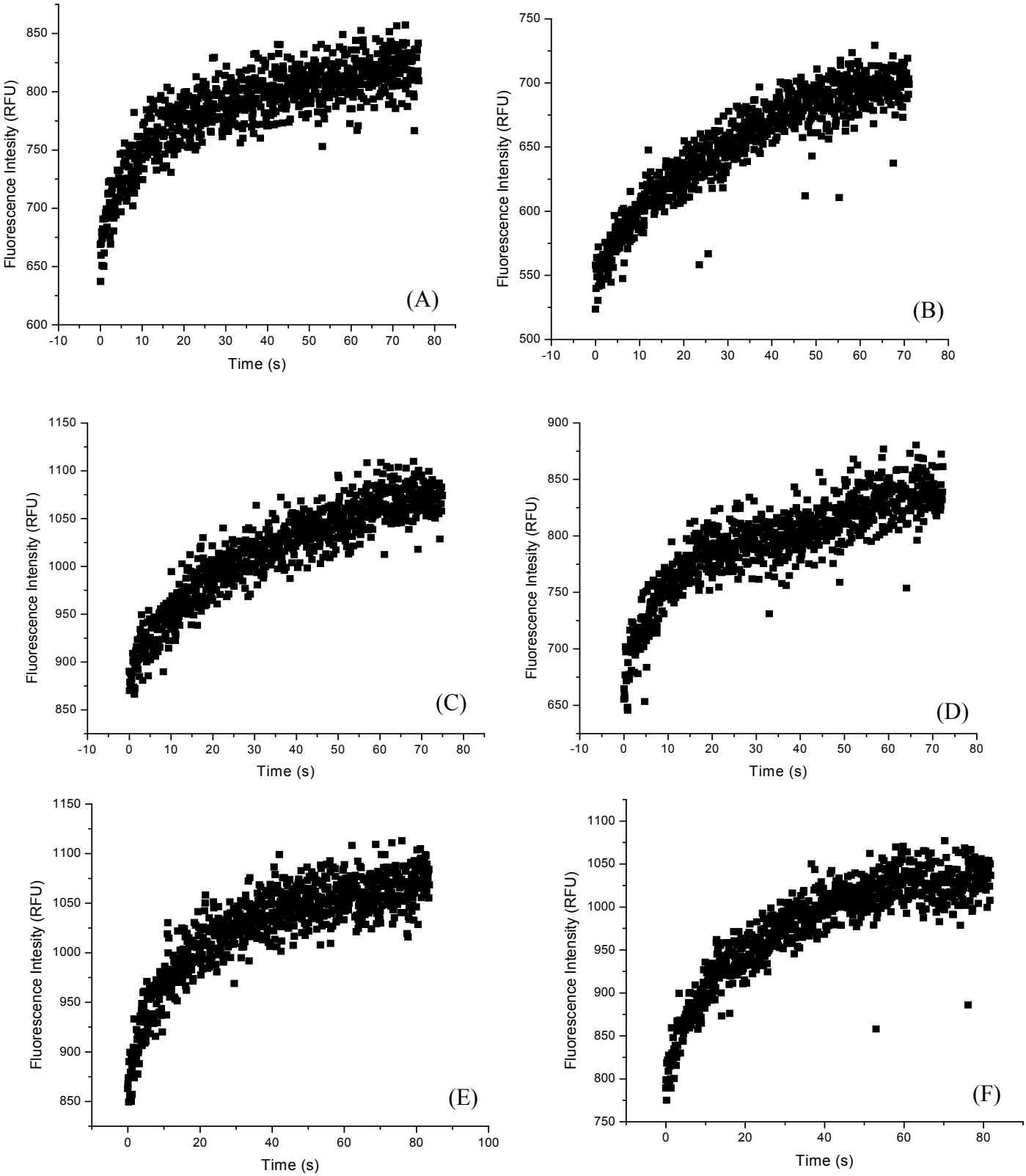

Figure 2: Fluorescence recovery after photobleaching (FRAP) raw data for control experiments 7-12 (A-F).

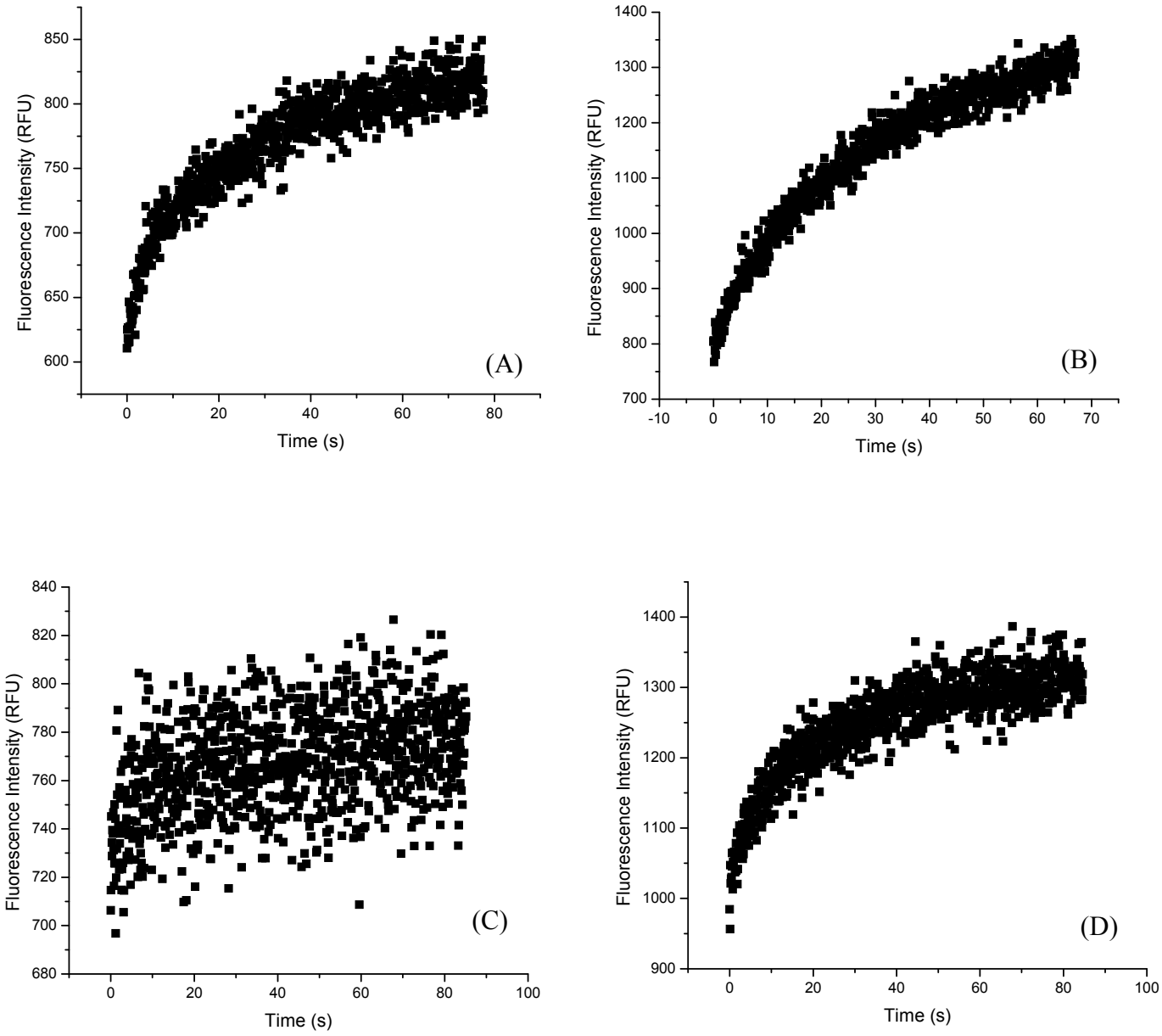

Figure 3: Fluorescence recovery after photobleaching (FRAP) raw data for control experiments 13-16 (A-D).

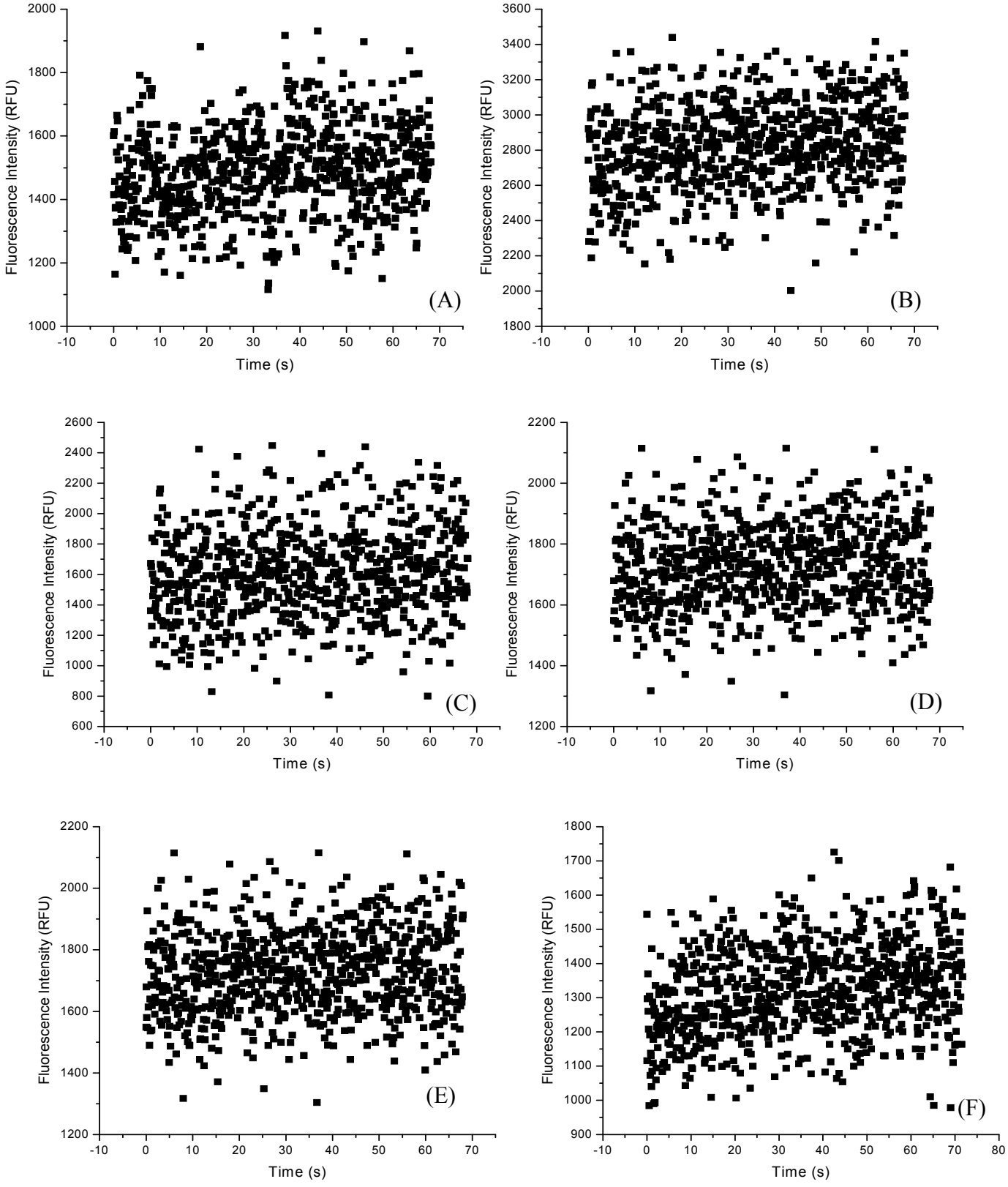

Figure 4: Fluorescence recovery after photobleaching (FRAP) raw data for PEGMA 400/ PEGDMA 400 10 mg/mL experiments 1-6 (A-F).

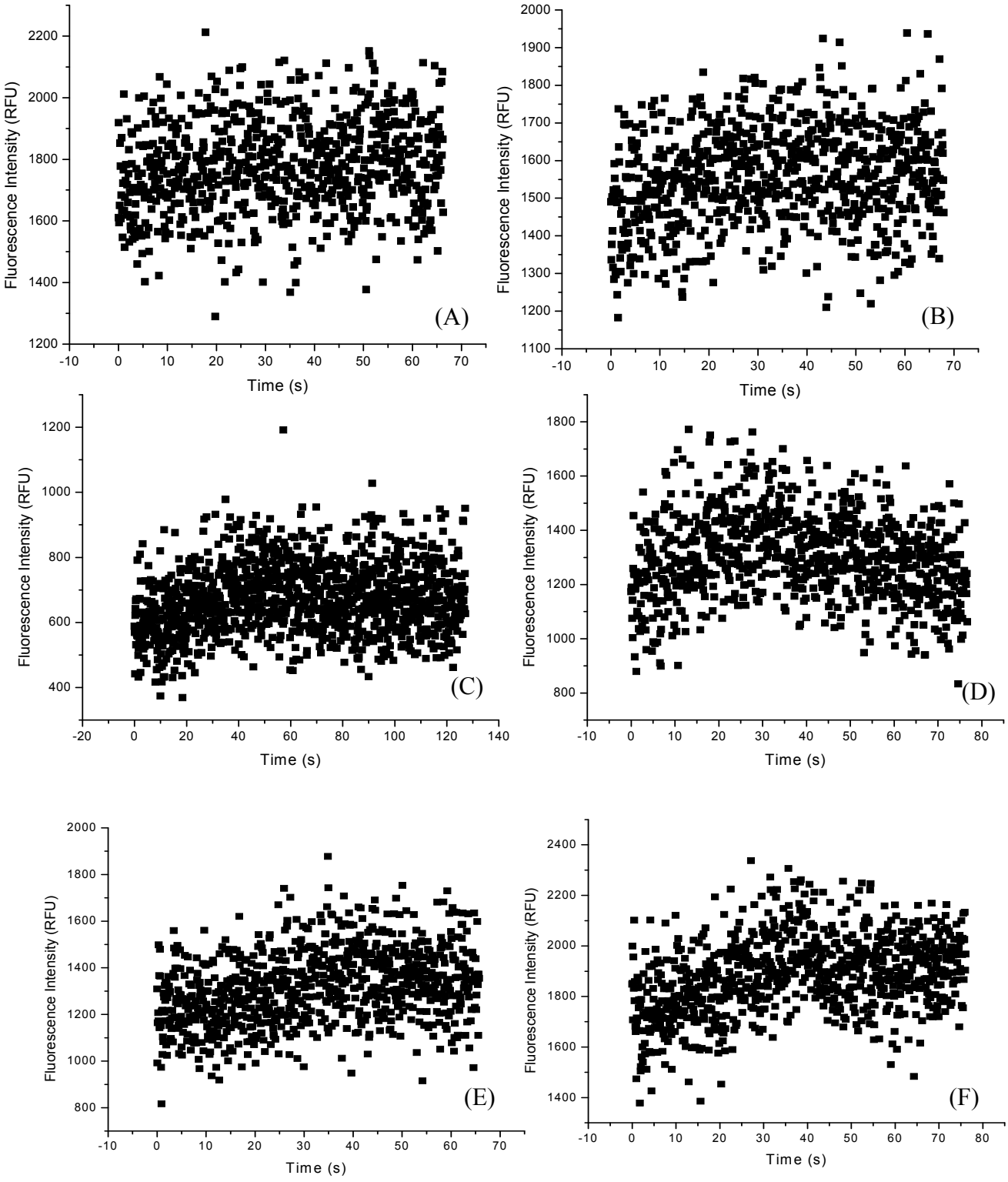

Figure 5: Fluorescence recovery after photobleaching (FRAP) raw data for PEGMA 400/ PEGDMA 400 10 mg/mL experiments 7-12 (A-F).

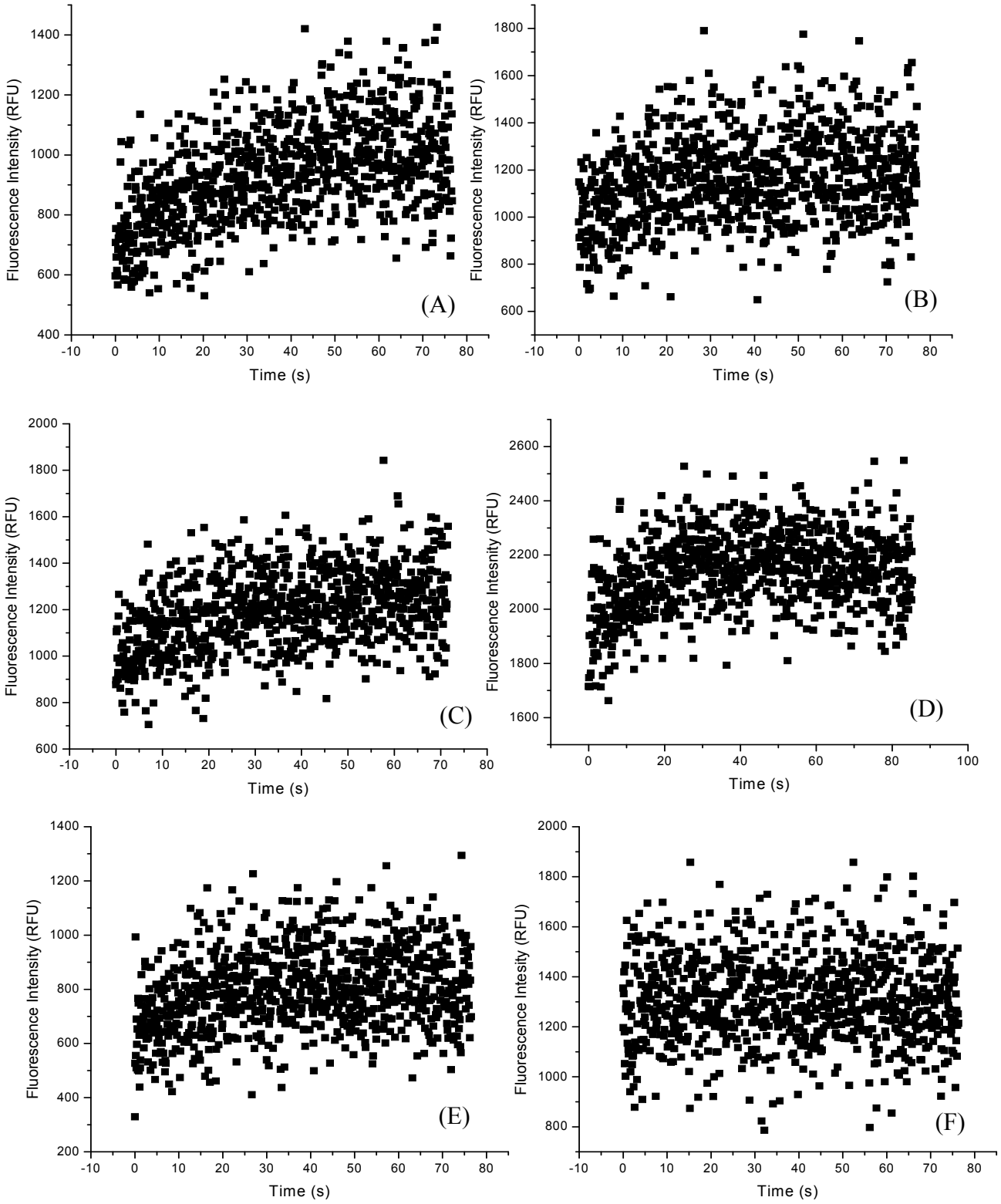

Figure 6: Fluorescence recovery after photobleaching (FRAP) raw data for PEGMA 400/ PEGDMA 400 10 mg/mL experiments 13-18 (A-F).

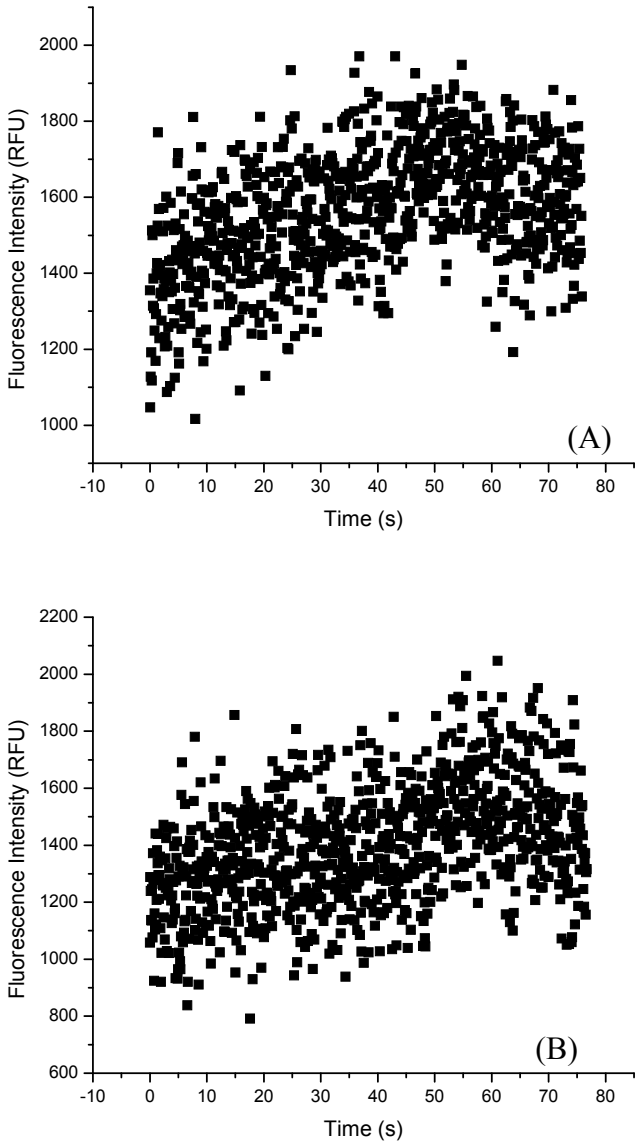

Figure 7: Fluorescence recovery after photobleaching (FRAP) raw data for PEGMA 400/ PEGDMA 400 10 mg/mL experiments 19-20 (A-B).

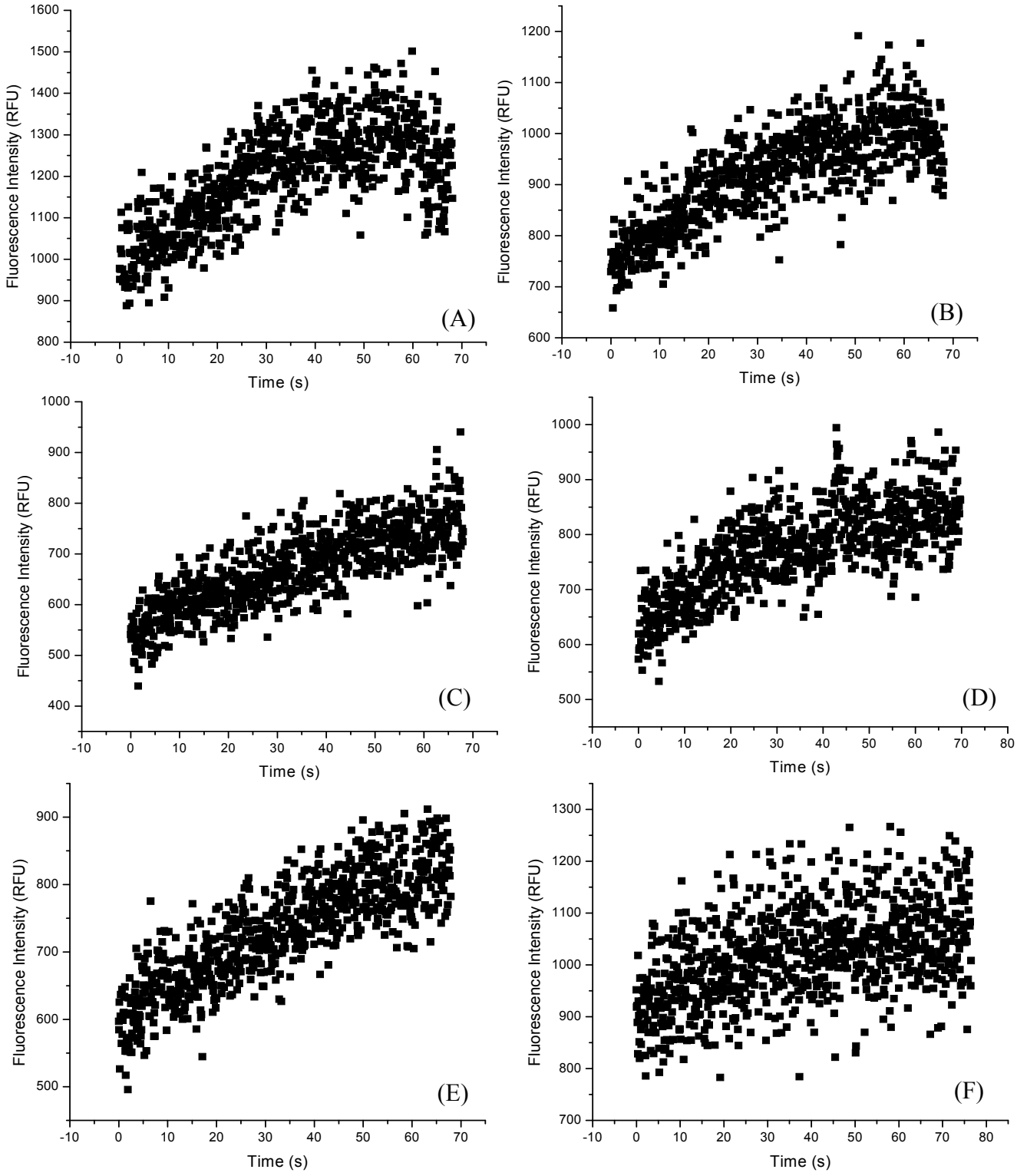

Figure 8: Fluorescence recovery after photobleaching (FRAP) raw data for PEGMA 400/ PEGDMA 400 1 mg/mL experiments 1-6 (A-F).

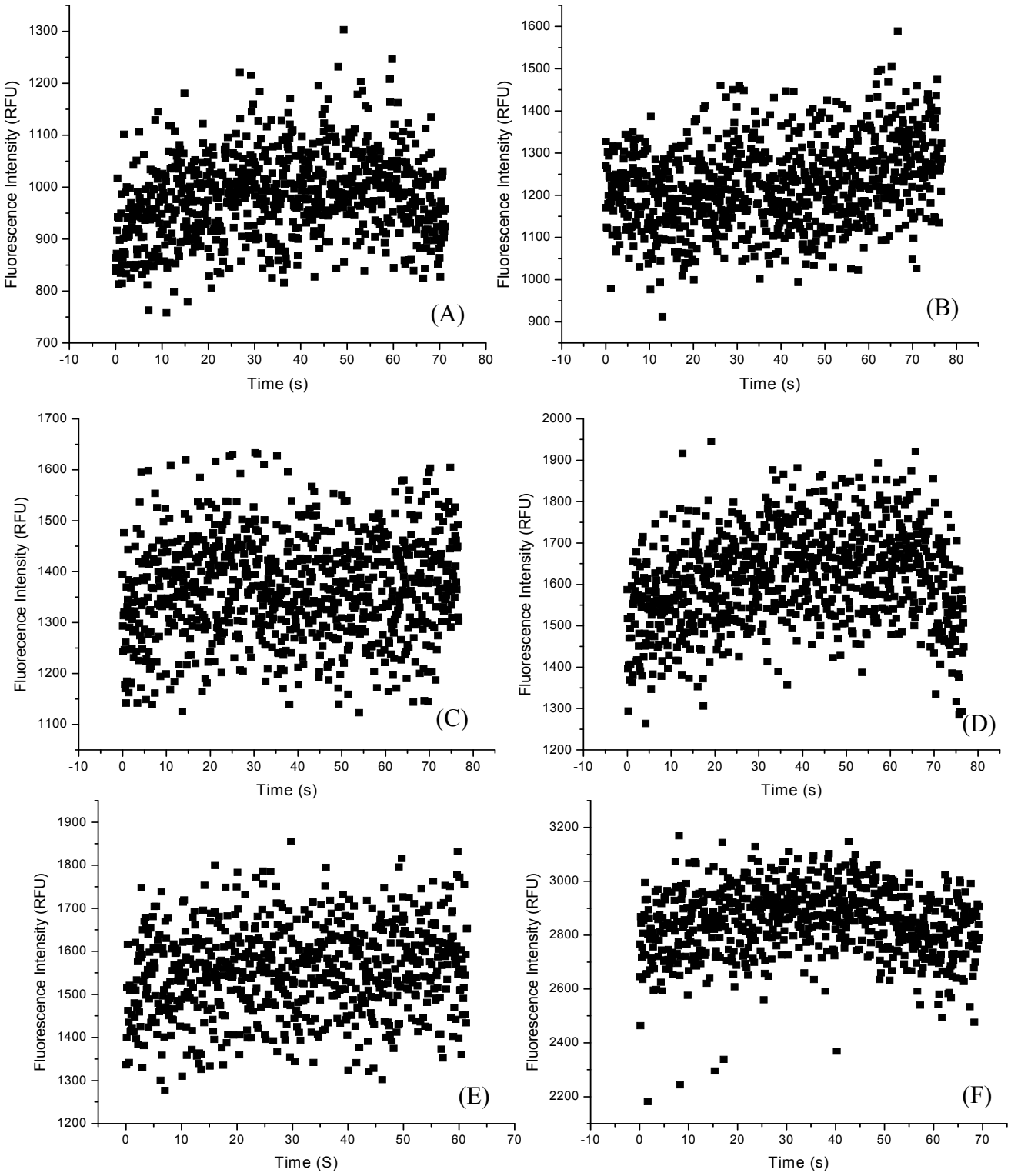

Figure 9: Fluorescence recovery after photobleaching (FRAP) raw data for PEGMA 400/ PEGDMA 400 1 mg/mL experiments 7-12 (A-F).

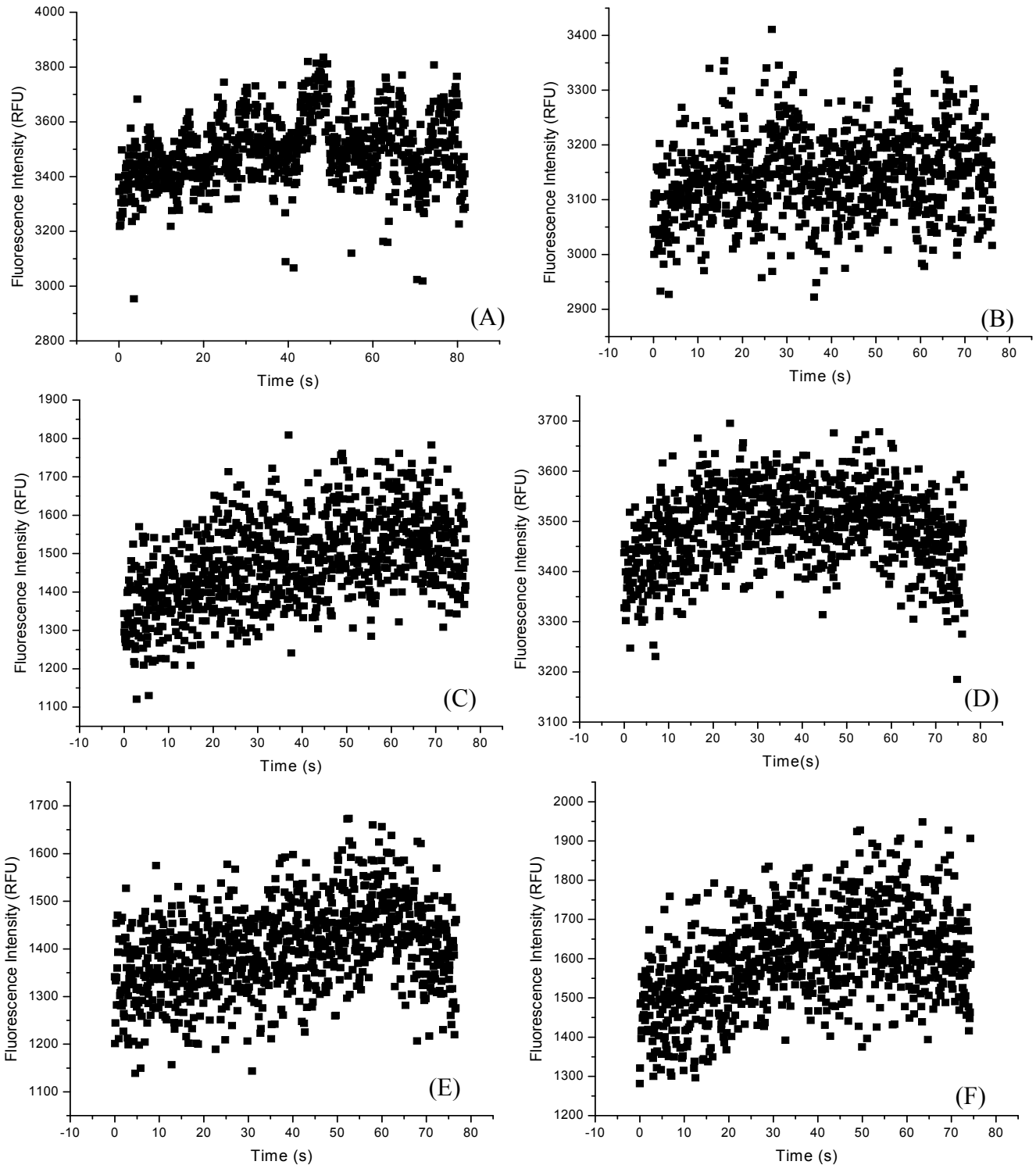

Figure 10: Fluorescence recovery after photobleaching (FRAP) raw data for PEGMA 400/ PEGDMA 400 1 mg/mL experiments 13-18 (A-F).

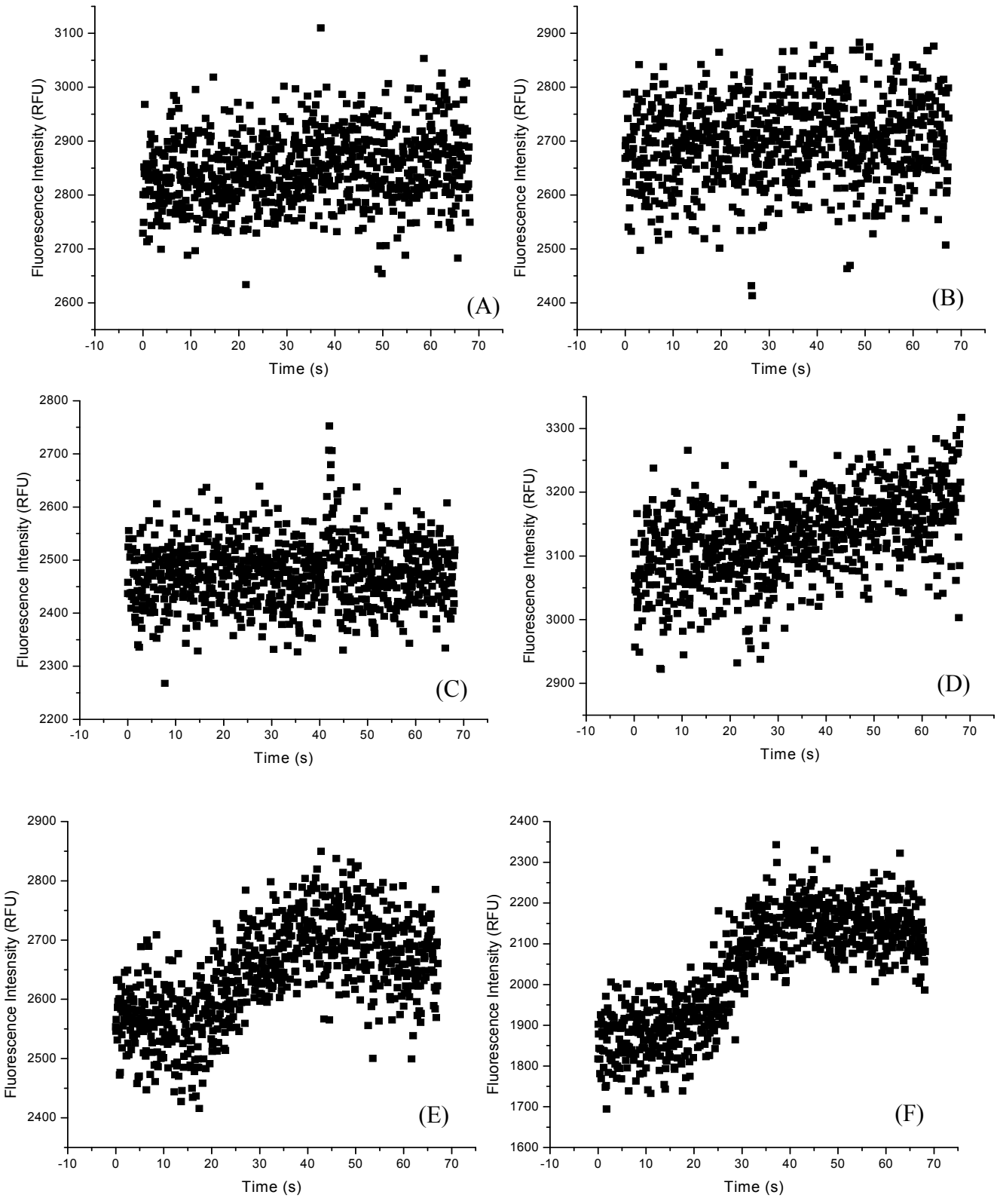

Figure 11: Fluorescence recovery after photobleaching (FRAP) raw data for PEGMA 1000/ PEGDMA 400 10 mg/mL experiments 1-6 (A-F).

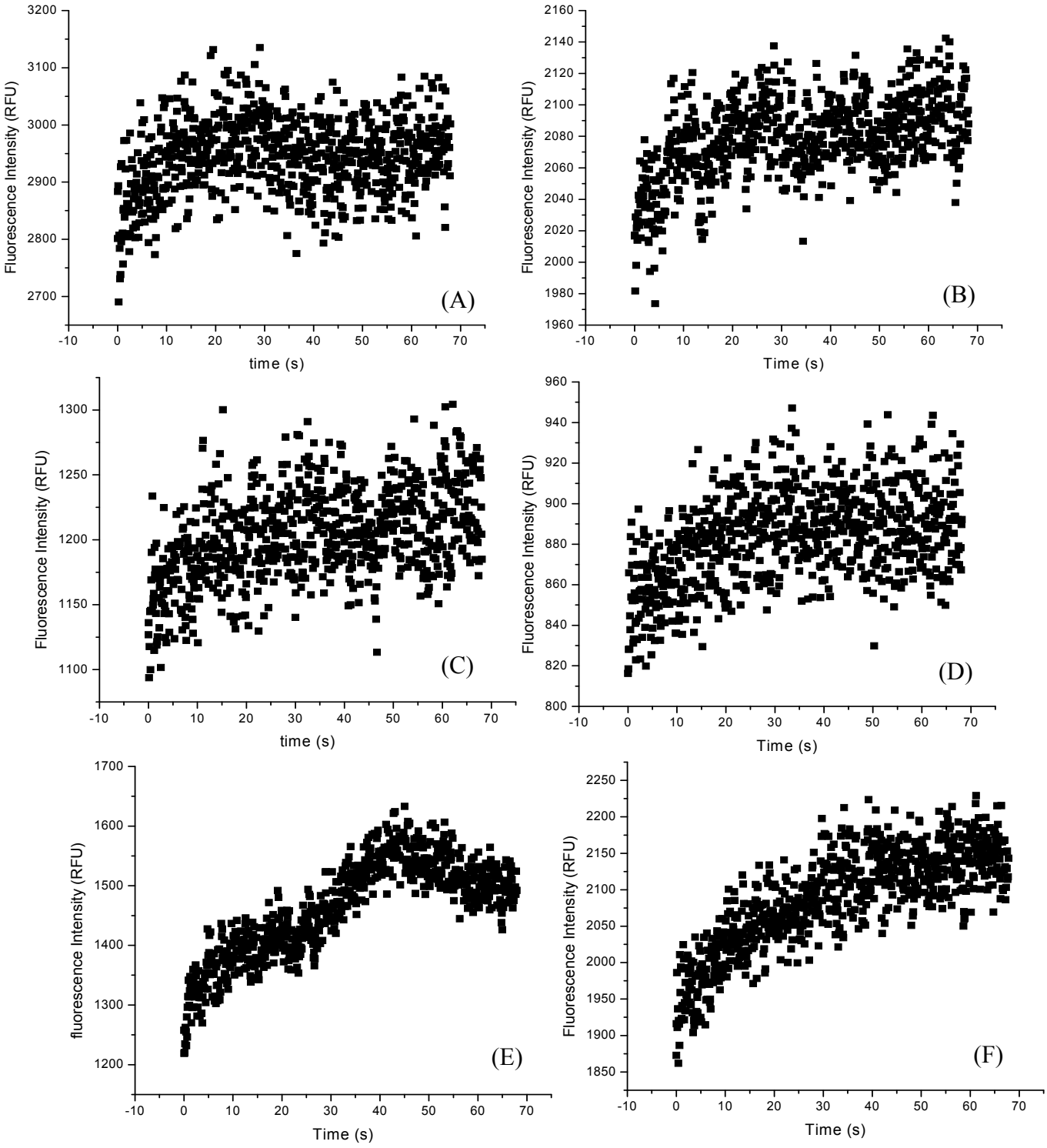

Figure 12: Fluorescence recovery after photobleaching (FRAP) raw data for PEGMA 1000/ PEGDMA 400 10 mg/mL experiments 7-12 (A-F).

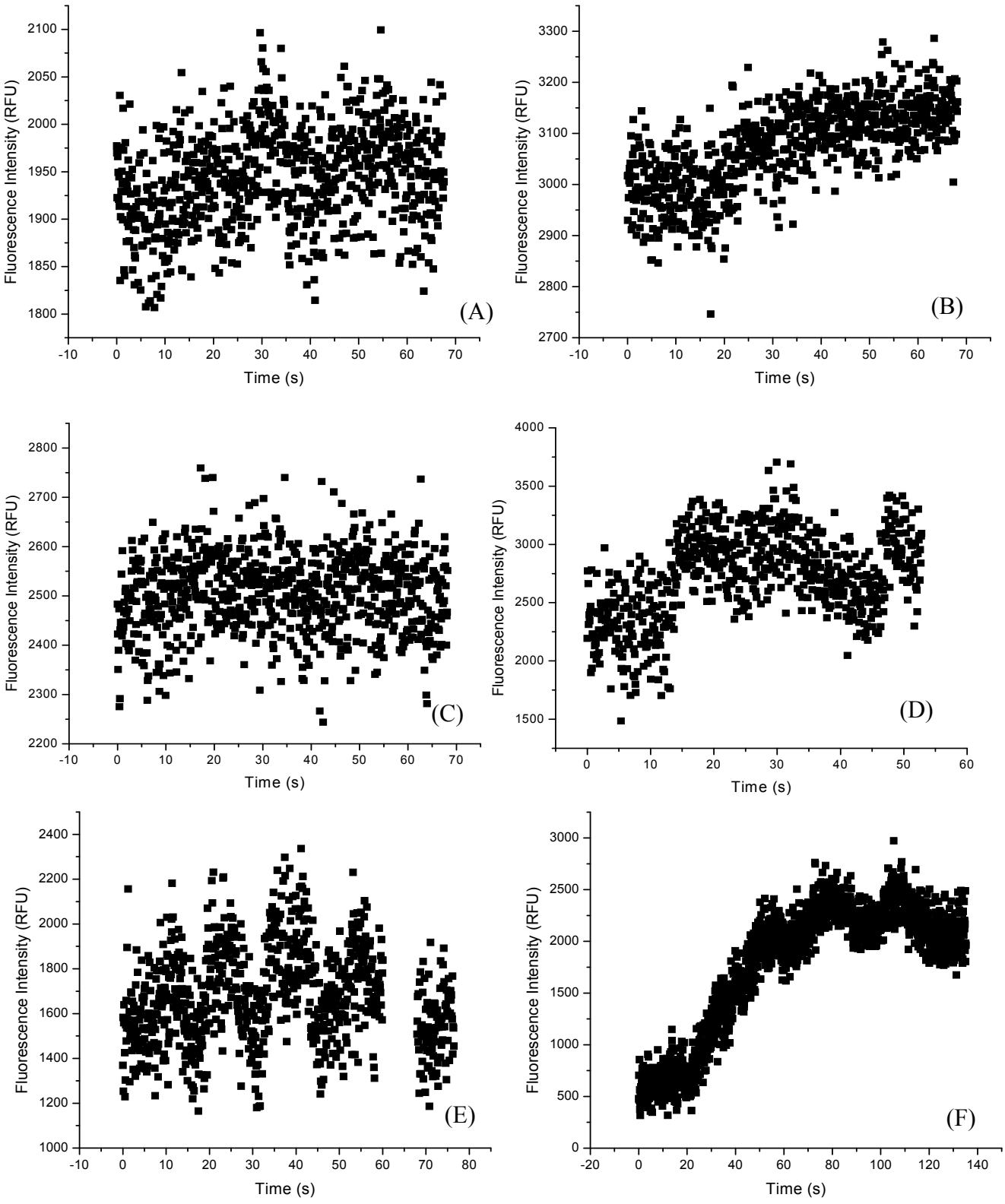

Figure 13: Fluorescence recovery after photobleaching (FRAP) raw data for PEGMA 1000/ PEGDMA 400 10 mg/mL experiments 13-18 (A-F).

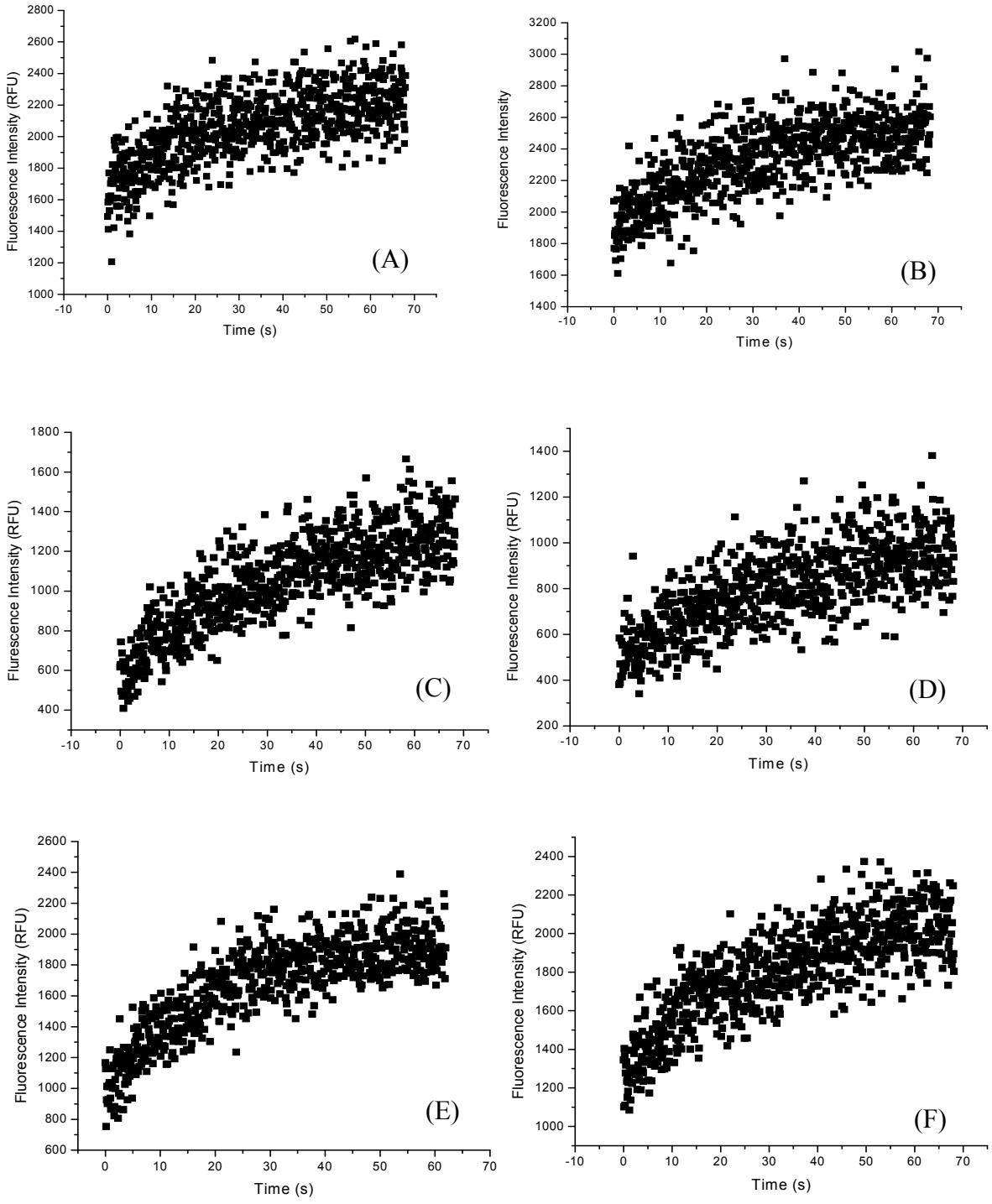

Figure 14: Fluorescence recovery after photobleaching (FRAP) raw data for PEGMA 1000/ PEGDMA 400 1 mg/mL experiments 1-6 (A-F).

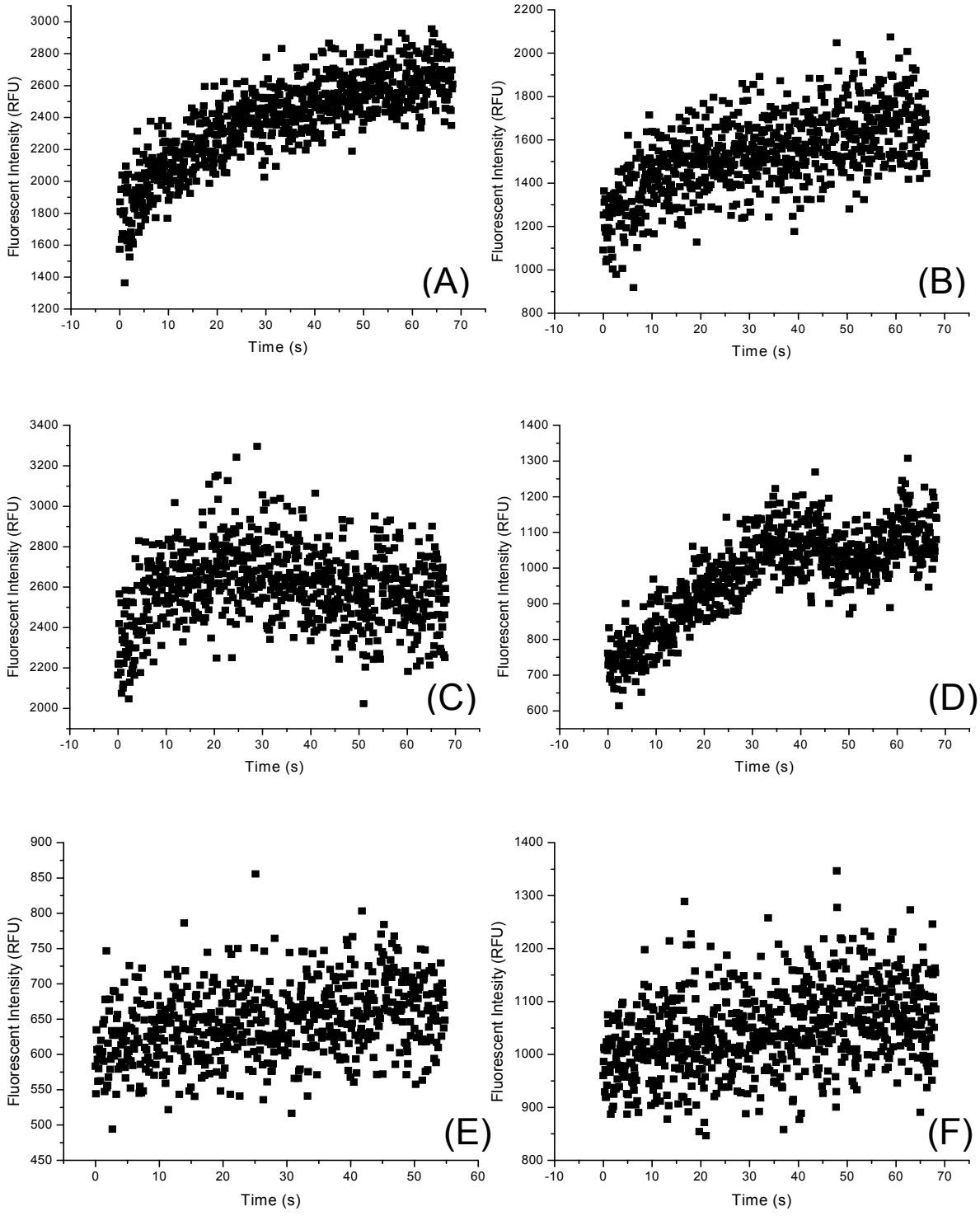

Figure 15: Fluorescence recovery after photobleaching (FRAP) raw data for PEGMA 1000/ PEGDMA 400 1 mg/mL experiments 7-12 (A-F).

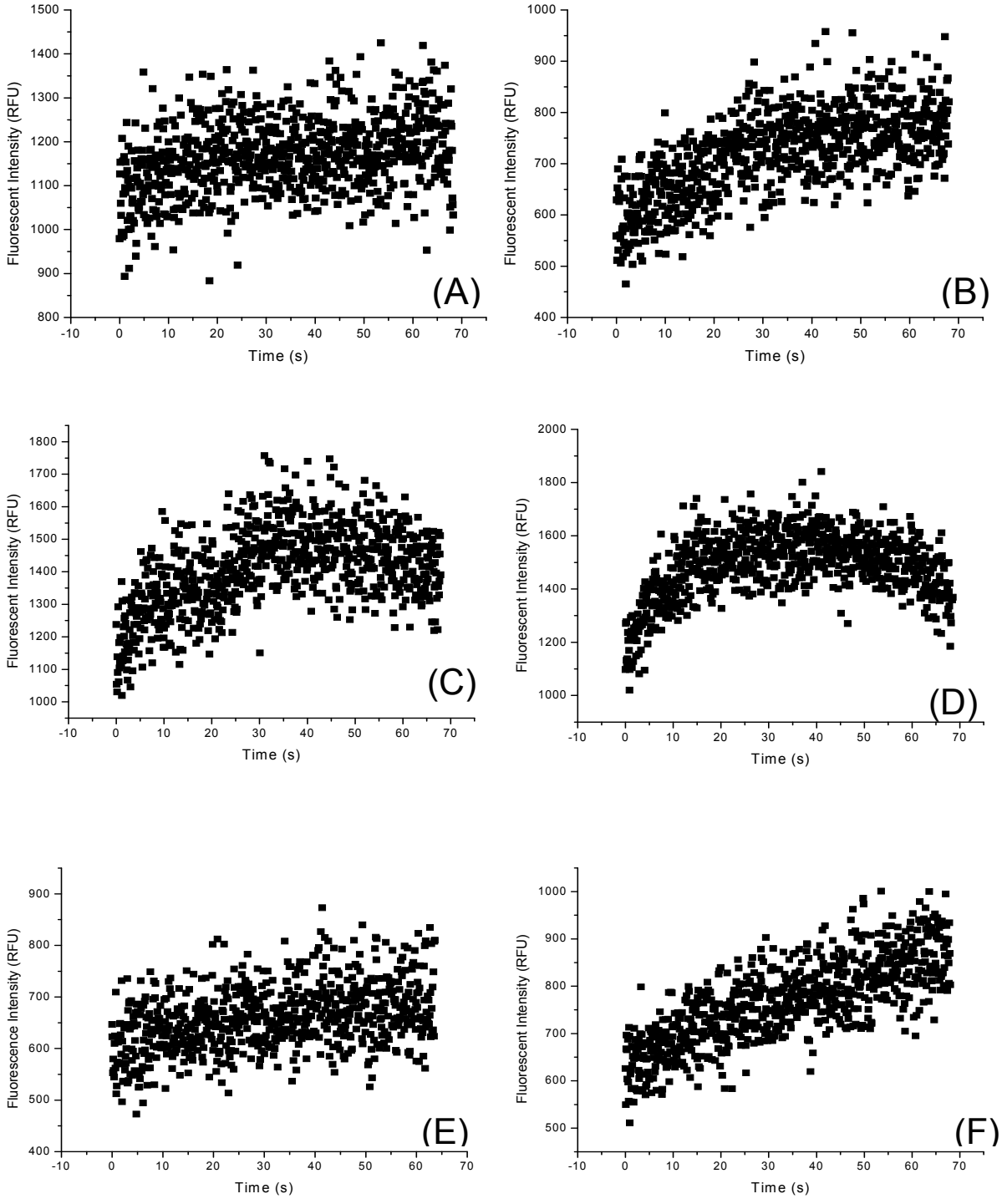

Figure 16: Fluorescence recovery after photobleaching (FRAP) raw data for PEGMA 1000/ PEGDMA 400 1 mg/mL experiments 13-18 (A-F).

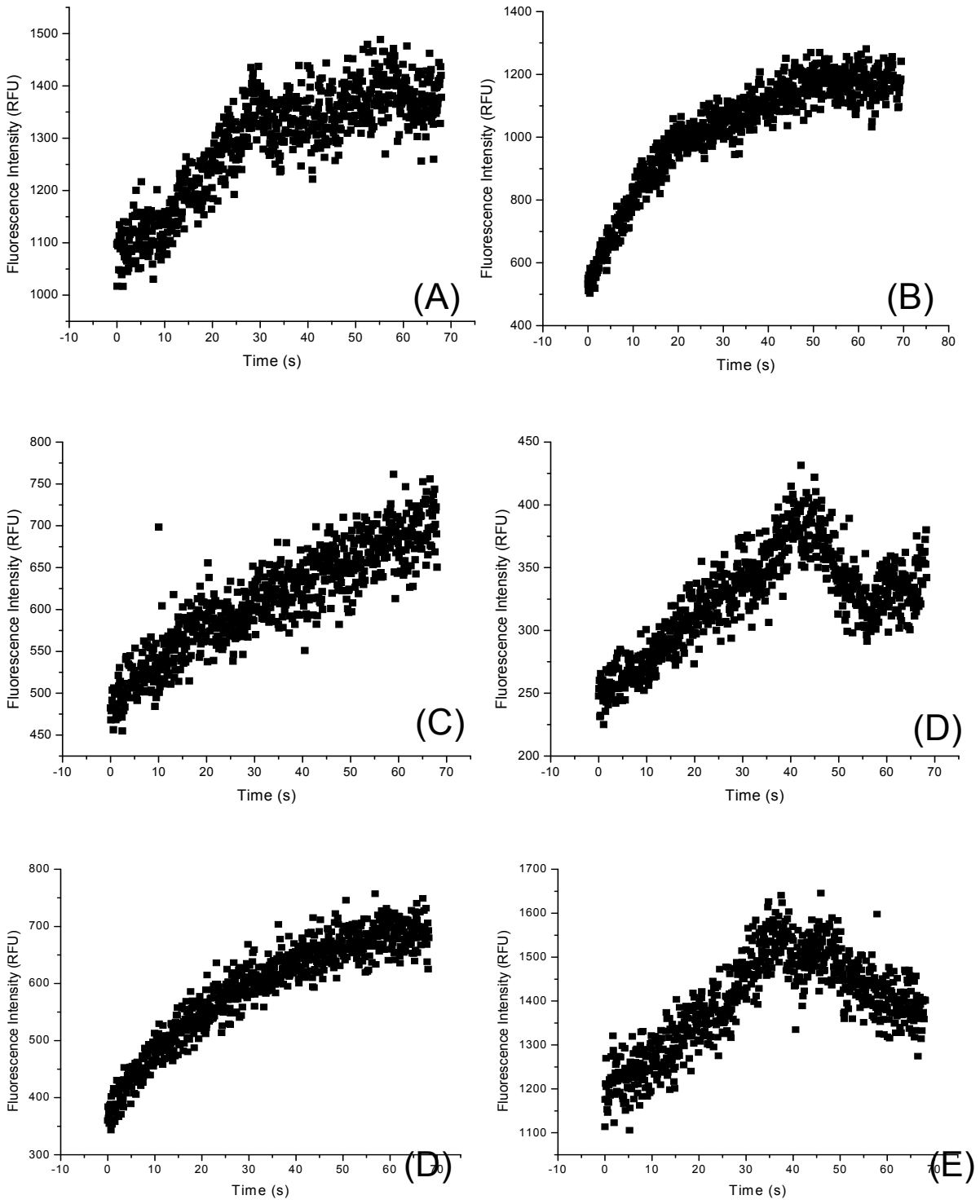

Figure 17: Fluorescence recovery after photobleaching (FRAP) raw data for PEG-300 20% (v/v) experiments 1-6 (A-F).

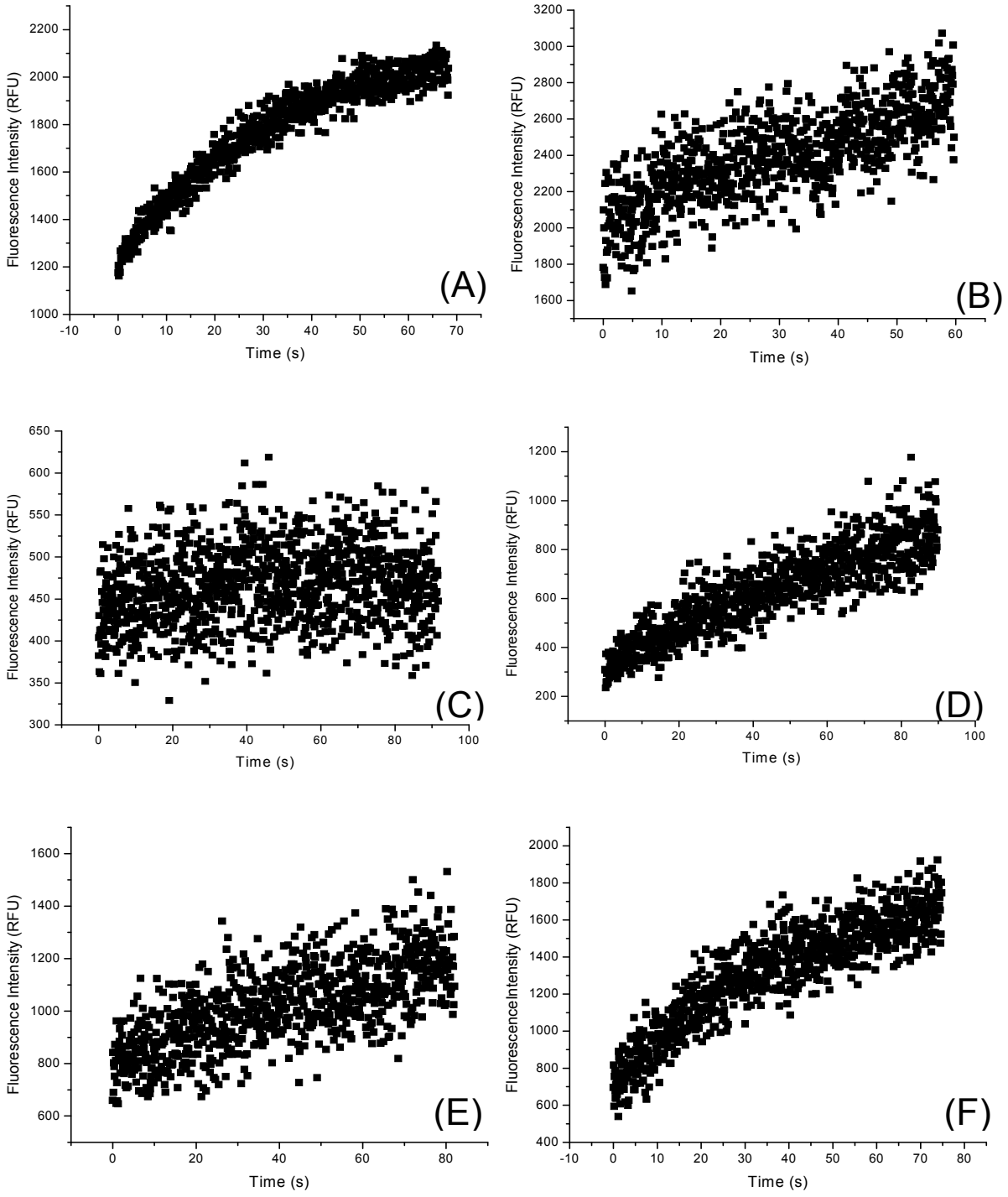

Figure 18: Fluorescence recovery after photobleaching (FRAP) raw data for PEG-300 20% (v/v) experiments 7-12 (A-F).

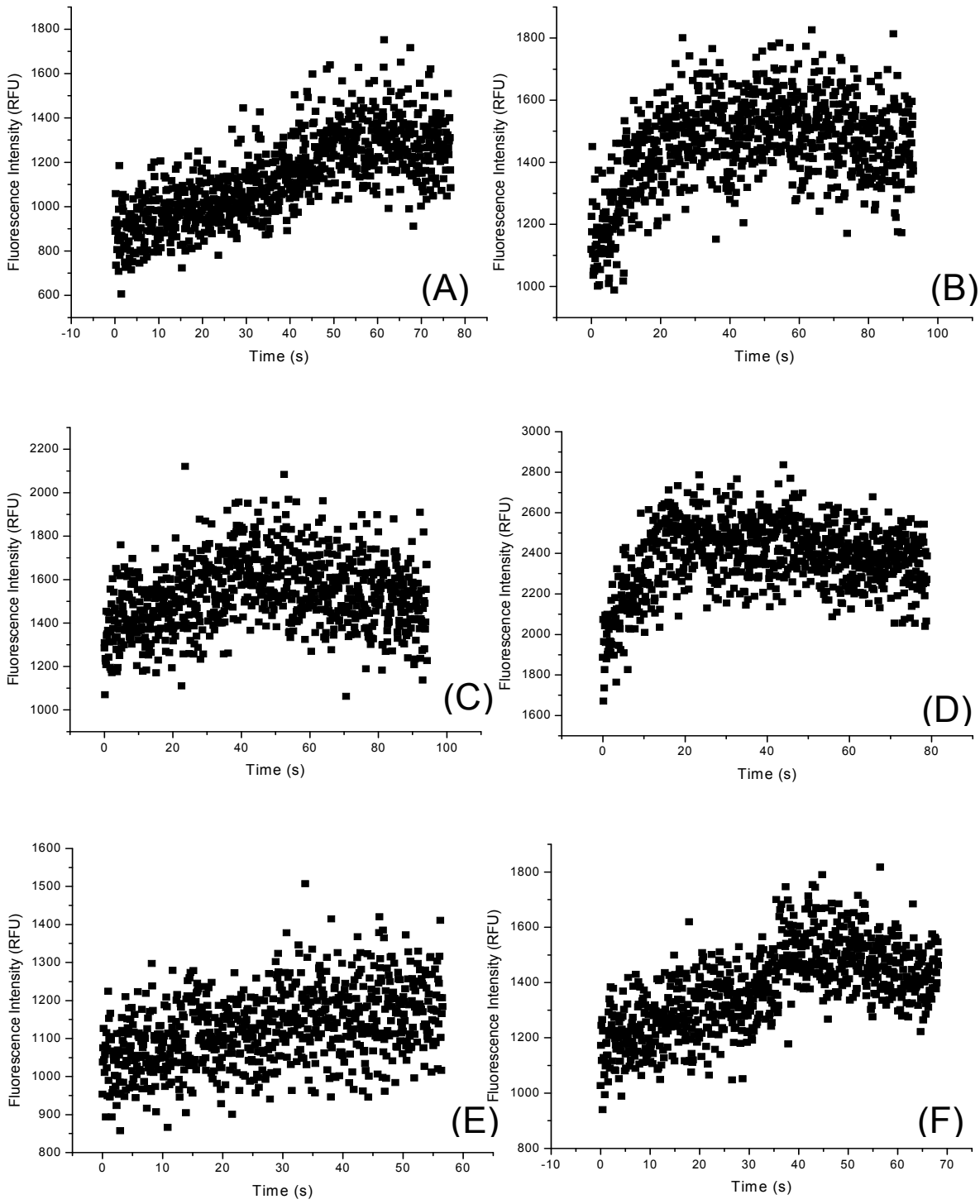

Figure 19: Fluorescence recovery after photobleaching (FRAP) raw data for PEG-300 20% (v/v) experiments 13-18 (A-F).

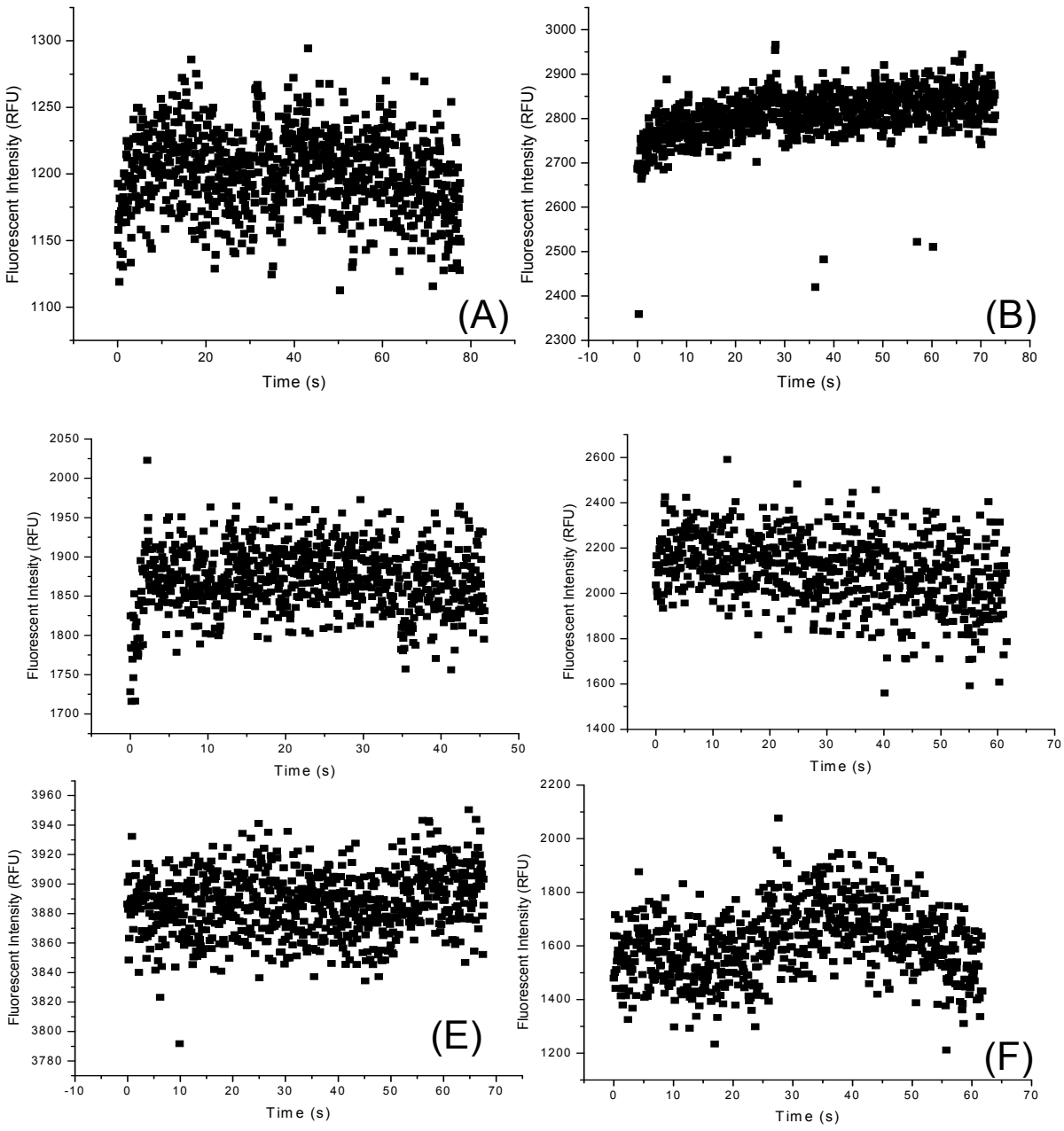

Figure 20: Fluorescence recovery after photobleaching (FRAP) raw data for hexanol 20mM experiments 1-6 (A-F).

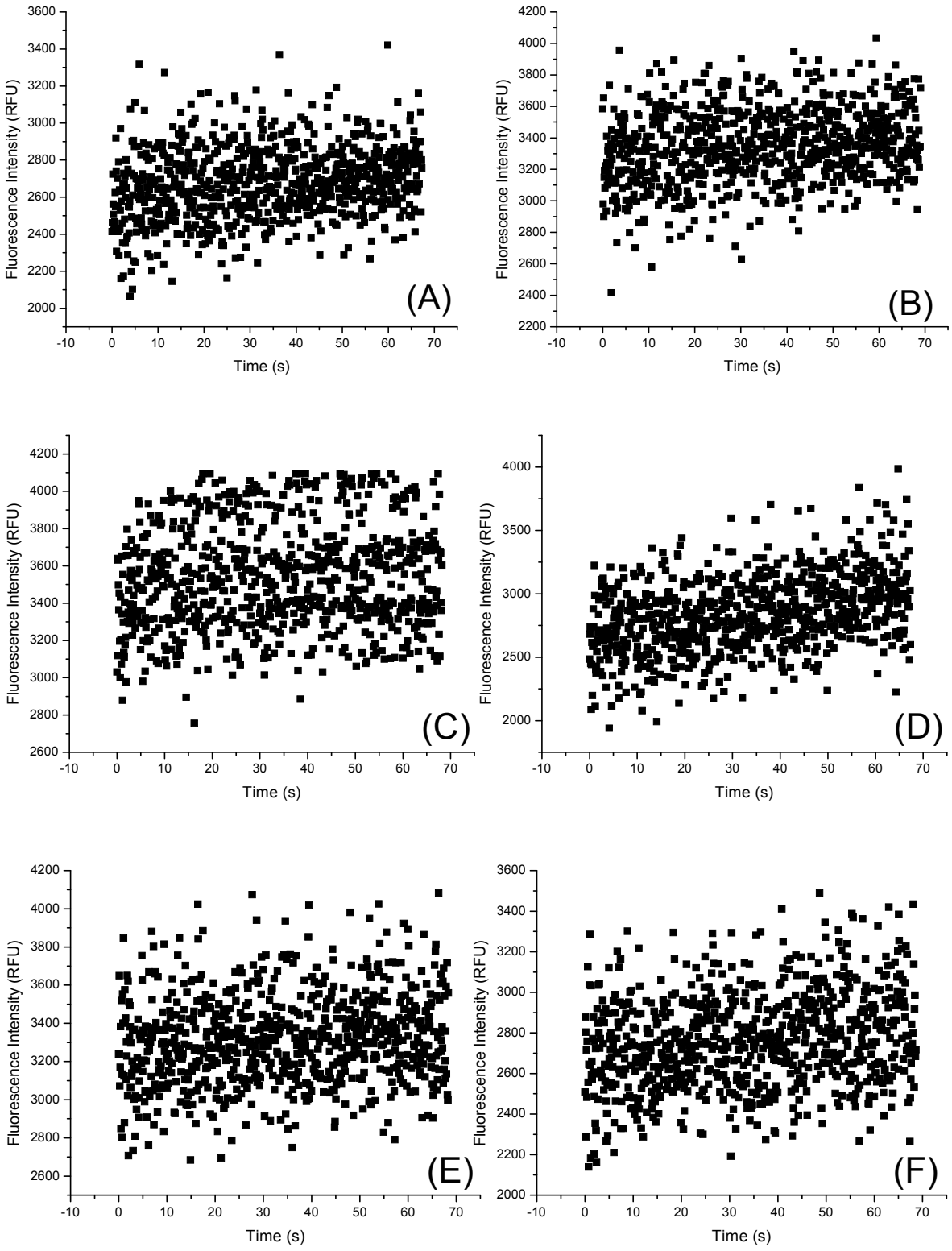

Figure 21: Fluorescence recovery after photobleaching (FRAP) raw data for hexanol 20mM experiments 7-12 (A-F).

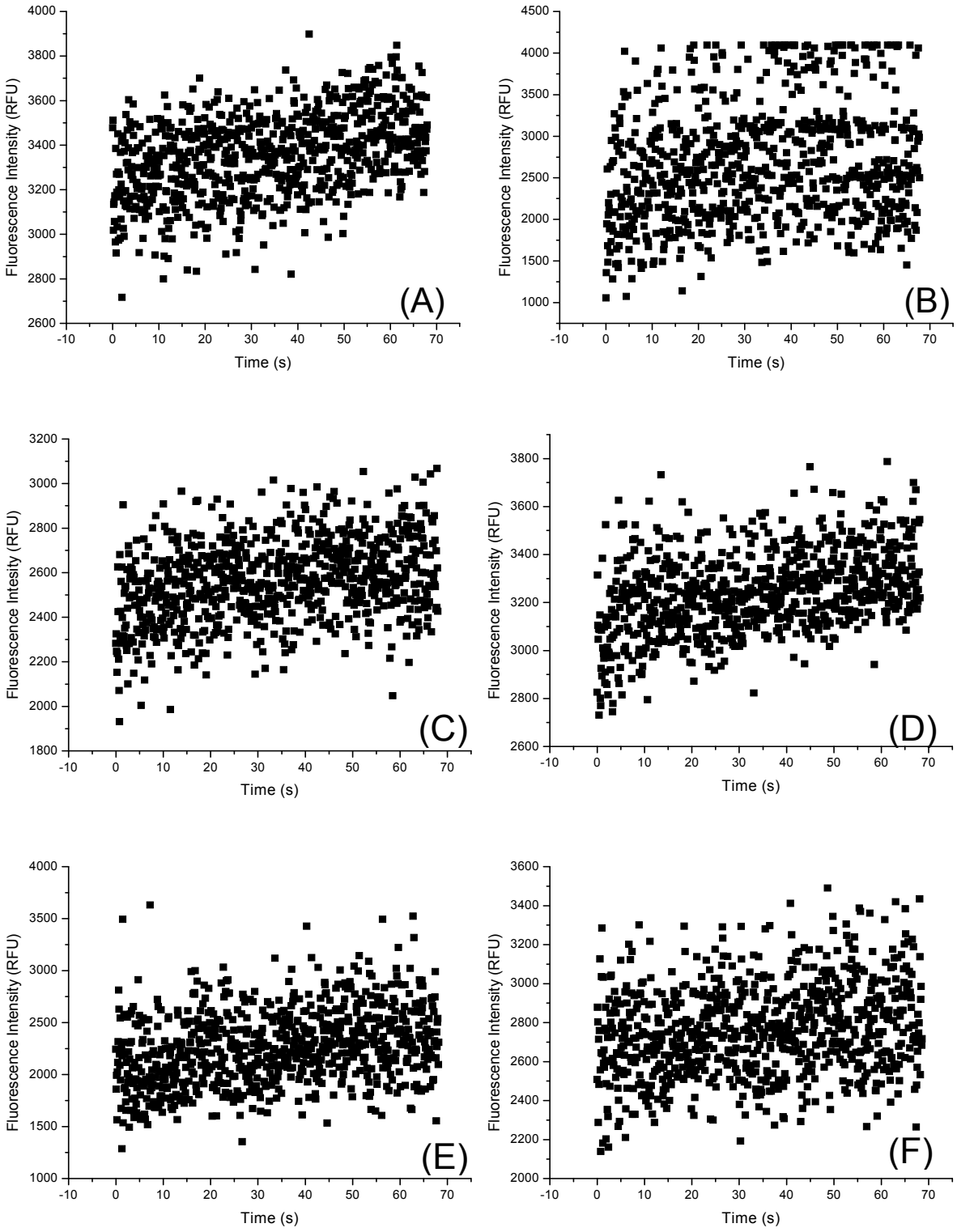

Figure 22: Fluorescence recovery after photobleaching (FRAP) raw data for hexanol 20mM experiments 13-18 (A-F).